

**Factors contributing to artemisinin resistance  
in *Plasmodium falciparum* parasites**

**Dissertation with the aim of achieving a doctoral degree at the Faculty of  
Mathematics, Informatics and Natural Sciences**

Department of Biology  
of the University of Hamburg

submitted by

**Sabine Schmidt**

2021 in Hamburg

Day of oral defense: 24. September 2021

The following evaluators recommend the admission of the dissertation:

Dr. Tobias Spielmann

Prof. Dr. Tim-Wolf Gilberger

## **Eidesstattliche Versicherung**

Hiermit erkläre ich an Eides statt, dass ich die vorliegende Dissertationsschrift selbst verfasst und keine anderen als die angegebenen Quellen und Hilfsmittel benutzt habe.

Ort, Datum

Sabine Schmidt

## Language certificate

I am a native speaker, have read the present PhD thesis and hereby confirm that it complies with the rules of the English language.

Name: CHERRELLE DACON 

Date: 07/12/2021

Location: MARYLAND, UNITED STATES

## Summary

*Plasmodium falciparum* is a unicellular protozoan parasite transmitted by the bite of an infected female *Anopheles* mosquito. Of the five human-infecting *Plasmodium* species, *P. falciparum* is the most virulent. Although malaria is preventable and curable, in 2019 almost half of the world's population was still at risk to suffer from malaria with the highest risk seen in sub-Saharan Africa. To date, the most effective treatment for uncomplicated *P. falciparum* malaria recommended by the WHO is the artemisinin-based combination therapy (ACT), combining a short-acting artemisinin derivative (ART) with a longer-acting partner drug. In 2008, artemisinin (ART) resistant parasites were reported for the first time. This resistance was detected in Cambodia and manifested as a delayed parasite clearance after ART treatment in malaria patients. Thereafter, ART resistance spread across the entire Southeast Asian subcontinent. For a long time, the African continent seemed to be unaffected by ART resistant strains, but in 2020 low prevalent ART resistant *P. falciparum* strains were also reported for Rwanda, Tanzania, and Uganda. Since Africa carries the largest malaria burden, affecting mostly children under the age of five and pregnant women, resistance to the most effective drug would be devastating.

In 2014, mutations in the *PfKelch13* protein propeller domain were identified as a molecular marker for ART resistance and demonstrated to be responsible for a reduced susceptibility of young ring stage parasites to ART. The resistance can be measured *in vitro* using a ring-stage survival assay (RSA). Several studies revealed that besides *PfKelch13*, mutations in other genes can cause ART resistance, suggesting that also *PfKelch13*-independent resistance mechanisms exist. Using a novel dimerization-induced quantitative BioID (DiQ-BioID) approach, a new cellular compartment, where *PfKelch13* is located, was defined. In this thesis proteins of this compartment were analyzed. Upon partial inactivation of either *PfKelch13* itself or of essential *Kelch13* compartment members (*PfAP-2 $\mu$* , *PfEps15*, *PfUBP1*, *PfKIC7*), parasites became resistant to ART, indicating that they are involved of ART resistance in *P. falciparum*. In addition, two further hits from the DiQ-BioID, *PfMCA2* and *PfMyosinF*, were analyzed in this work. Co-localization experiments confirmed that *PfMCA2* is indeed part of the *Kelch13* compartment but is also localized to additional foci in the periphery of the parasite cell. A mutation, leading to a premature stop codon at amino acid position 1344 of *PfMCA2* rendered parasites resistant to ART when it was introduced in 3D7 parasites, confirming a role of *PfMCA2* in ART resistance. While the SNP, leading to this pre-mature stop, was detected in African *Plasmodium* strains in patient field samples, this SNP only seemed to co-occur with another mutation in the same codon, resulting in an

amino acid change rather than a stop. This indicated that this SNP is not relevant for ART resistance in the field.

Performing co-localization experiments with *PfMyosinF* demonstrated that this protein is also part of the Kelch13 compartment, although fully overlapping signals were only observed for ~14% of the *PfMyosinF* foci and overall, *PfMyosinF* was mostly found in close association to *PfKelch13* positive structures rather than fully overlapping. Myosins are part of the actomyosin motor to generate movement of cellular components. Inhibition of actin-polymerization by Cytochalasin D treatment caused the dissociation of *PfMyosinF* and *PfKelch13* positive structures in *P. falciparum* in trophozoite stage parasites, indicating that the association of both proteins - or the structures they are contained in - is actin-dependent. Furthermore, although mislocalization of *PfMyosinF* by knock sideways was only partially successful, this nevertheless significantly reduced parasite growth, suggesting that *PfMyosinF* is important for *Plasmodium* blood stage development. However, this partial inactivation of *PfMyosinF* did not render parasites resistant to ART as determined by RSA. Additionally, it was observed in this work that *PfMyosinF* is located in proximity of phosphatidylinositol-3-phosphate positive structures in the parasite cell, suggesting it is proximal to endosomal structures. Finally, partial inactivation reduced uptake of hemoglobin into the parasite's food vacuole. Overall, these findings indicate a role of *PfMyosinF* in hemoglobin endocytosis, similar to Kelch13 compartment proteins.

As this and previous work indicated that Kelch13 compartment proteins are all involved in the same pathway that can influence the susceptibility of the parasite to ART, it was in a next step tested whether non-synonymous single nucleotide polymorphisms (SNPs) in these genes could also mediate ART resistance in the field. As few *PfKelch13* mutations were so far reported from Africa, one focus was set on SNPs in African isolates to assess if they might have gone unnoticed, as most previous studies focused on *pfkelch13*. For this part of the work, different approaches were used. One approach was based on the simultaneous introduction of multiple non-synonymous mutations in one genomic locus of the 3D7 laboratory isolate, using the selection-linked integration system (SLI), creating mutation pools. In total, 125 mutations in eight different genes (*pfkic1* (PF3D7\_0606000), *pfkic2* (PF3D7\_1227700), *pfkic4* (PF3D7\_1246300), *pfkic5* (PF3D7\_1138700), *pfkic7* (PF3D7\_0813000), *pfkic9* (PF3D7\_1442400), *pfmyosinF* (PF3D7\_1329100), *pfubp1* (PF3D7\_0104300)) were tested with this method. These experiments showed that none of the included mutations changed parasite susceptibility to ART. In a second approach, non-synonymous mutations that either were mentioned in the literature or were detected by sequencing the DNA of a potentially resistant *P. falciparum* field isolate obtained during the 'Fever without Source' study in Ghana, were tested individually. In total, 11 non-

synonymous mutations in five different genes were tested, including mutations in *pfkelch13* itself. This revealed that two mutations of *pfkelch13* (leading to amino acid change V520A and V589I) and one mutation of *pfubp1* (leading to amino acid change R3138H) conferred a reduced susceptibility to ART upon introduction into the 3D7 parasite genome, while one mutation found in *pfap-2α* (leading to amino acid change H817P) decreased ART susceptibility but did not reach the threshold of 1% survival in RSA to define it as a resistance mutation. All of the other tested mutations, including in *pfeps15* and *pfmyosinF*, did not result in ART resistance.

Additionally, confocal microscopy of ART resistant parasites was performed to follow up the growth of the parasites after an ART pulse in an RSA. This work indicated that either ART treatment delayed parasite development after the drug pulse, or that a subset of more slowly growing parasites survived. Conducting consecutive RSA with the already resistant C580Y mutant parasites rendered these parasites even more resistant (K13<sup>C580Y\_29th</sup>). When the *PfKelch13* protein level of these highly ART resistant K13<sup>C580Y\_29th</sup> parasites was compared to *PfKelch13* wild type, unselected resistant C580Y parasites and the mildly resistant V520A parasites, the K13<sup>C580Y\_29th</sup> parasites displayed the lowest protein amount. This correlated inversely with the parasite survival rate in RSA. Competitive growth assays performed with different *PfKelch13* mutant lines revealed that the ART resistant C580Y mutant had the highest fitness cost, while the moderate resistant V520A mutant had a similar fitness compared to *PfKelch13* wild type parasites. These results suggest that there is also a correlation between the degree of ART resistance and the level of fitness of the parasite. Hence, lower *PfKelch13* levels result in lower fitness but higher resistance.

Altogether, this work provided further evidence that *PfKelch13* and its compartment members are important for a pathway relevant for ART resistance. Mutations, either detected in *PfKelch13* or the compartment members, reduced parasite susceptibility to the drug. The mutation tested in *PfUBP1* demonstrated that resistance exists in the field that is independent of changes in *PfKelch13*. This may indicate that further diagnostic markers for ART resistance exist in the field. Furthermore, this work shows that there are mutations in *pfkelch13* found in African parasite isolates that influence *PfKelch13* protein levels as well as fitness of the parasite but to a more moderate level than the most prevalent mutation (C580Y) found in Southeast Asia. This data could help to understand the reason for the unequal spread of ART resistance in different areas of the world.

## Zusammenfassung

*Plasmodium falciparum* ist ein einzelliger, protozoischer Parasit, welcher durch den Stich einer infizierten weiblichen *Anopheles* Mücke übertragen wird. Unter insgesamt fünf humanpathogenen Plasmodien-Erregern ist *Plasmodium falciparum* die virulenteste Art. Obwohl die Krankheit Malaria durch vorbeugende Maßnahmen gut zu kontrollieren ist und effektive Medikamente zur Behandlung einer Infektion erhältlich sind, stellt die parasitäre Erkrankung auch im Jahr 2019 eines der größten Gesundheitsprobleme weltweit dar. Ungefähr die Hälfte der Gesamtbevölkerung der Erde ist dem Risiko einer Infektion ausgesetzt, wobei Afrika südlich der Sahara am stärksten betroffen ist. Das wirksamste, von der WHO empfohlene Medikament zur Behandlung einer Malariaerkrankung ist die Artemisinin-basierte Kombinationstherapie (ACT). Hierbei werden ein kurzlebiges Artemisinin-Derivat und ein langfristig wirkendes Partnermedikament kombiniert. Erste Resistenzen gegenüber Artemisinin wurden im Jahr 2008 in Kambodscha beobachtet. Diese äußerten sich in einer verlangsamten Eliminierung des Parasiten im Blut. In den darauffolgenden Jahren verbreitete sich die Resistenz über den gesamten südostasiatischen Subkontinent. Für lange Zeit schien der afrikanische Kontinent von Artemisinin-Resistenz verschont zu bleiben, allerdings wurden auch hier im Jahr 2020 die ersten resistenten Plasmodien-Stämme in Ruanda, Tansania und Uganda detektiert. Da Afrika am stärksten von der Infektionskrankheit betroffen ist, und dort in den meisten Fällen Kinder im Alter bis fünf Jahre oder Schwangere schwer an Malaria erkranken, würde eine Medikamenten-Resistenz verheerende Auswirkungen haben.

Im Jahr 2014 konnte eine Mutation in der Propeller-Domäne des *PfKelch13* Proteins als molekularer Marker der Artemisinin Resistenz identifiziert werden und für eine reduzierte Sensitivität junger Ringstadien gegenüber Artemisinin verantwortlich gemacht werden. Diese Resistenz kann anhand eines sogenannten „ring-stage survival assays“ (RSA) *in vitro* gemessen werden. Einige Studien deuten darauf hin, dass es neben der durch *PfKelch13* vermittelten Resistenz eine *PfKelch13* unabhängige Form der Artemisinin-Resistenz gibt. Anhand einer neuentwickelten Methode, die auf einer quantitativen BioID basiert (DiQ-BioID), wurden verschiedenen Interaktionspartner des *PfKelch13* Proteins bestimmt, die ein bis dahin unbekanntes Zellkompartiment, in welchem *PfKelch13* lokalisiert ist, definieren. In der vorliegenden Arbeit wurden Proteine dieses Kompartiments analysiert. Durch die partielle Inhibierung des *PfKelch13* Proteins, aber auch der essenziellen Kompartimentproteine (*PfAP-2 $\mu$* , *PfEps15*, *PfUBP1*, *PfKIC7*), wurden die Parasiten resistent gegen Artemisinin, was darauf hindeutet, dass sie an einem Prozess beteiligt sind, der für den Resistenzmechanismus in *P. falciparum* wichtig ist. Zusätzlich wurden in dieser

Arbeit zwei bisher noch nicht untersuchte Kandidaten aus der DiQ-BioID, *PfMCA2* und *PfMyosinF*, genauer funktionell studiert. Co-Lokalisationsexperimente zeigten, dass *PfMCA2* tatsächlich Teil des Kelch13 Kompartiments ist, allerdings auch in anderen Foci in der Zellperipherie gefunden werden kann. Eine Mutation, die zu einem vorzeitigen Stopp an der Position 1344 in *PfMCA2* führte, resultierte darin, dass die Parasiten resistent gegenüber Artemisinin wurden. Dies bekräftigt, dass die Funktion von *PfMCA2* die Artemisininresistenz beeinflusst. Allerdings scheint diese Mutation, welche in afrikanischen Feldisolaten vorhanden ist, nur zusammen mit einer zweiten Mutation im selben Codon aufzutreten, wodurch es zu einem Aminosäureaustausch statt eines Stopps kommt und darauf hindeutet, dass diese Mutation daher für die Resistenz im Feld nicht relevant ist.

Co-Lokalisationsexperimente mit *PfMyosinF* zeigten, dass dieses Protein ebenfalls Teil des *PfKelch13* Kompartiments ist, obwohl komplett überlappende Signale nur in ~14% der *PfMyosinF* Foci beobachtet werden konnte und *PfMyosinF* meist nur in der näheren Umgebung zu *PfKelch13*-positiven Strukturen gefunden werden konnte, aber keine vollständige Überlappung zeigte. Myosine sind Teil des Actomyosinmotors, welcher Bewegung zellulärer Komponenten generiert. Inhibierung der Polymerisation von Aktinfilamenten durch Cytochalasin D führte zur Dissoziation von *PfMyosinF*- und *PfKelch13*-positiven Strukturen in Trophozitenstadien, was darauf hindeutet, dass die Interaktion beider Proteine (oder der durch diese Proteine definierten Strukturen) Aktin-abhängig ist. Desweiteren konnte anhand von Wachstumsexperimenten gezeigt werden, dass obwohl die Mislokalisierung von *PfMyosinF* durch das knock sideways-System nur partiell möglich war, diese partielle Inaktivierung das Wachstum der Blutstadien des Parasiten signifikant reduzierte. Allerdings resultierte eine partielle Inaktivierung von *PfMyosinF* nicht in Resistenz der Plasmodien gegenüber Artemisinin, was durch einen RSA getestet wurde. Zusätzlich konnte in dieser Arbeit gezeigt werden, dass *PfMyosinF* in der Nähe zu Phosphatidylinositol-3-phosphat-positiven Strukturen im Parasiten lokalisiert ist, was vermuten lässt, dass es sich in der Nähe zu endosomalen Strukturen befindet. Schließlich konnte gezeigt werden, dass die teilweise Inaktivierung von *PfMyosinF* zu einer reduzierten Aufnahme von Hämoglobin in die Fressvakuole des Parasiten führte. Zusammengefasst deuten die Ergebnisse darauf hin, dass *PfMyosinF* - ähnlich wie andere Kelch13 Kompartimentproteine - eine Rolle während der Endozytose von Hämoglobin spielt.

Da diese und vorherige Arbeiten gezeigt haben, dass die Kelch13 Kompartimentproteine am selben Prozess beteiligt sind, welcher auch die Sensitivität der Parasiten gegenüber Artemisinin beeinflusst, wurde in einem nächsten Schritt getestet, ob verschiedene nicht-synonyme Mutationen in diesen *PfKelch13*-Kompartimentproteinen Artemisinin-Resistenz

im Feld vermitteln. Da bisher nur wenige Mutationen in *pfkelch13* in Afrika festgestellt wurden, wurde ein spezieller Fokus auf afrikanische Varianten gerichtet, um zu untersuchen, ob diese übersehen wurden, da sich die meisten Studien bisher nur mit *pfkelch13* Mutationen befasst haben. Für diesen Teil der Arbeit wurden verschiedene Ansätze gewählt. Im ersten Ansatz wurden mehrere verschiedene nicht-synonyme Mutationen gleichzeitig über das SLI-System in einen genomischen Locus des 3D7 Laborstammes integriert und damit sogenannte Mutationspools erzeugt. Insgesamt wurden auf die Weise 125 Mutationen in acht verschiedenen Genen (*pfkic1* (PF3D7\_0606000), *pfkic2* (PF3D7\_1227700), *pfkic4* (PF3D7\_1246300), *pfkic5* (PF3D7\_1138700), *pfkic7* (PF3D7\_0813000), *pfkic9* (PF3D7\_1442400), *pfmyosinF* (PF3D7\_1329100), *pfubp1* (PF3D7\_0104300)) getestet. Die damit durchgeführten Versuche zeigten, dass keine der eingefügten Mutationen die Toleranz des Parasiten gegenüber Artemisinin verringert hat. Im zweiten Ansatz wurde verschiedenen nicht-synonyme Mutationen, die entweder in der Literatur erwähnt wurden, oder mittels Sequenzierung von Parasiten-DNA eines potenziell resistenten Stammes aus einem Patienten der „Fever without Source“-Studie in Ghana stammten, individuell getestet. Insgesamt wurden 11 verschiedene Mutationen in fünf Genen getestet, wobei auch Mutationen in *pfkelch13* selbst miteinbezogen wurden. Dabei konnten zwei *pfkelch13* Mutationen (resultieren in den folgenden Aminosäureaustauschen: V520A und V589I) und eine Mutation in *pfubp1* (resultiert im Aminosäureaustausch R3138H) identifiziert werden, die zu einer reduzierten Sensitivität gegenüber Artemisinin führten, wenn sie in 3D7 *P. falciparum* Genom eingebracht wurden, während eine Mutation in *pfap-2α* (resultiert im Aminosäureaustausch H817P) ebenfalls die Sensitivität gegenüber ART reduzierte, jedoch nicht den Grenzwert von 1% Überlebensrate im RSA überschritt (der Grenzwert um als Resistenz-vermittelnde Mutation bezeichnet zu werden). Keine der anderen getesteten Mutationen, einschließlich derer in den Kandidaten *pfeps15* und *pfmyosinF*, führten zu einer erhöhten Toleranz gegenüber Artemisinin.

Zusätzlich wurde ein RSA mit Artemisinin resistente Parasiten durchgeführt und die Entwicklung der Parasiten nach dem Artemisinin Puls mittels Konfokalmikroskopie nachverfolgt. Anhand der gewonnenen Daten konnte gezeigt werden, dass sich das Wachstum der Parasiten nach Artemisinin-Gabe verlangsamte bzw., dass ein generell verlangsamtes Wachstum einer Subpopulation an Parasiten ermöglichte, zu überleben. Desweiteren erreichten Artemisinin-resistente C580Y Parasiten ein noch höheres Resistenzlevel, wenn sie in einem konsekutiv durchgeführten RSA wiederholt mit dem Medikament behandelt wurden (K13<sup>C580Y\_29th</sup>). Die quantitative Bestimmung der PfKelch13-Menge dieser hochresistenten K13<sup>C580Y\_29th</sup> Parasiten ergab, dass sie im Vergleich zu PfKelch13-Wildtyp Parasiten, unselektionierten C580Y Parasiten und den moderat

resistenten V520A Mutanten die geringste Proteinmenge exprimierten. Dabei korrelierten die *PfKelch13*-Proteinmenge und das Artemisinin-Resistenzlevel im RSA invers miteinander. Kompetitive Wachstumsexperimente mit den verschiedenen *PfKelch13*-Mutanten zeigten, dass die Artemisinin resistente C580Y Mutation die höchsten Fitnesskosten verursachte, während die moderat-resistente V520A Mutante eine ähnliche Fitness aufwies wie die *PfKelch13* Wildtyp-Parasiten. Diese Ergebnisse deuteten darauf hin, dass auch das Artemisininresistenz-Level und die Fitness der Parasiten miteinander korrelieren. Demnach führt ein geringeres *PfKelch13*-Level zwar zu einer geringeren Fitness, dafür aber zu einer höheren Resistenz gegenüber Artemisinin.

Zusammengefasst konnten mit dieser Arbeit weitere Beweise dafür geliefert werden, dass *PfKelch13* und seine Kompartimentproteine wichtige Regulatoren eines Signalweges darstellen, der für die Artemisininresistenz wichtig ist. Mutationen in *PfKelch13* oder *Kelch13* Kompartimentproteinen resultierten in einer erhöhten Toleranz gegenüber Artemisinin. Dabei zeigt die Mutation in *PfUBP1*, dass Resistenz unabhängig von *PfKelch13* im Feld existiert. Zusätzlich zeigt diese Arbeit, dass in Afrika vorkommende Mutationen in *pfkelch13* sowohl das *PfKelch13* Proteinlevel als auch die Fitness der Parasiten auf eine moderatere Weise reduzieren, wenn dies mit der am häufigsten in Südostasien vorkommenden C580Y Variante verglichen wird. Diese Daten können dazu beitragen, die Ursachen der ungleichmäßigen Verbreitung von Artemisininresistenz in den verschiedenen Malaria-endemischen Regionen der Erde zu verstehen.

# Table of contents

<b>Summary</b>	<b>IV</b>
<b>Zusammenfassung</b>	<b>VII</b>
<b>List of Figures</b>	<b>XVII</b>
<b>List of Tables</b>	<b>XVIII</b>
<b>Abbreviations</b>	<b>XIX</b>
<b>1 Introduction.....</b>	<b>1</b>
1.1 Malaria – Key facts.....	1
1.1.1 Discovery and taxonomic classification of <i>Plasmodium</i> parasites.....	1
1.1.2 Epidemiology.....	1
1.1.3 Pathology .....	4
1.2 Biology of <i>Plasmodium</i> species.....	5
1.2.1 Life cycle of <i>P. falciparum</i> .....	5
1.2.1.1 Sexual reproduction in the mosquito vector .....	6
1.2.1.2 Asexual replication in the human liver.....	6
1.2.1.3 Asexual replication in human red blood cells .....	7
1.2.1.4 Development of sexual precursors in the human host.....	9
1.2.2 Surviving inside the host cell .....	10
1.2.2.1 Remodeling of the infected red blood cell .....	10
1.2.2.1.1 The parasitophorous vacuole .....	10
1.2.2.1.2 The tubovesicular network.....	11
1.2.2.1.3 The PTEX complex.....	11
1.2.2.1.4 The Maurer`s clefts.....	12
1.2.2.1.5 Knob structures at the erythrocyte surface are needed for parasite virulence.....	13
1.2.2.2 <i>Plasmodium</i> specific organelles.....	13
1.2.2.2.1 The apical organelles of the invasive stages .....	14
1.2.2.2.2 The apicoplast.....	15
1.2.2.2.3 The food vacuole.....	16
1.2.3 Malaria Prophylaxis and Treatment.....	17
1.3.1 Vector control and drug-based prevention of malaria .....	17
1.3.2 Vaccines .....	18
1.3.2.1 Pre-erythrocytic vaccines.....	18
1.3.2.2 Blood-stage vaccines.....	19
1.3.2.3 Transmission-blocking vaccines .....	20
1.3.3 Antimalarial drugs.....	21

1.3.3.1	Quinoline derivatives .....	22
1.3.3.2	Antifolates.....	22
1.3.3.3	Atovaquone .....	23
1.3.3.4	Artemisinin and its derivatives .....	23
1.4	Artemisinin resistance .....	24
1.4.1	Definition of ART resistance and current situation worldwide.....	24
1.4.2	Molecular markers of ART resistance.....	26
1.4.2.1	<i>PfKelch13</i> as molecular marker of ART resistance .....	26
1.4.2.2	<i>PfKelch13</i> independent mutations contributing to ART resistance .....	29
1.4.3	Mechanism of ART resistance.....	30
1.5	Aims of the present thesis .....	32
<b>2</b>	<b>Material.....</b>	<b>33</b>
2.1	Antibodies .....	33
2.1.1	Primary antibodies.....	33
2.1.2	Secondary antibodies.....	33
2.2	Bacteria and <i>Plasmodium</i> strains .....	33
2.3	Chemicals .....	34
2.4	DNA and protein ladders .....	36
2.5	Enzymes and polymerases .....	36
2.5.1	Restriction endonucleases .....	36
2.5.2	Polymerases .....	36
2.5.3	Oligonucleotides.....	36
2.6	Kits.....	37
2.7	Labware and disposables.....	37
2.8	Plasmids .....	38
2.9	Solutions, media, and buffer.....	38
2.9.1	Microbiological culture .....	38
2.9.2	Molecular biological buffers and solutions .....	39
2.9.3	Biochemical buffers and solutions .....	40
2.9.4	Cell biological buffers, media, and solutions ( <i>P. falciparum in vitro</i> culture).....	41
2.10	Technical devices.....	43
2.11	Bioinformatic tools and databases.....	45
2.12	Computer software.....	45
<b>3</b>	<b>Methods.....</b>	<b>46</b>
3.1	Molecular biological methods .....	46
3.1.1	Polymerase chain reaction (PCR) .....	46
3.1.2	Agarose gel electrophoresis (Garoff & Ansoerge, 1981).....	47
3.1.3	Clean-up of PCR product or digested plasmids .....	47
3.1.4	Enzymatic digestion of PCR products and plasmids.....	47

3.1.5	DNA ligation by Gibson assembly .....	48
3.1.6	Colony-PCR to screen bacterial clones .....	48
3.1.7	Sequencing of plasmids .....	49
3.1.8	DNA precipitation .....	49
3.1.9	Isolation of <i>P. falciparum</i> genomic DNA for integration check.....	50
3.1.10	Integration check using PCR .....	50
3.1.11	Sequencing of <i>P. falciparum</i> field isolates .....	51
3.2	Microbiological methods.....	52
3.2.1	Preparation of chemical competent <i>E. coli</i> bacteria (Hanahan, 1983).....	52
3.2.2	Transformation of chemical competent XL-10 gold <i>E. coli</i> .....	52
3.2.3	Overnight culture of transformed <i>E. coli</i> clone for plasmid purification .....	53
3.2.4	Freezing of <i>E. coli</i> culture .....	53
3.2.5	Plasmid purification (MINI and MIDI preparation) .....	53
3.3	Cell biological methods .....	54
3.3.1	Cultivation of <i>P. falciparum</i> (Trager & Jensen, 1976).....	54
3.3.2	Preparation of blood smears and Giemsa staining of parasite cultures.....	54
3.3.3	Freezing of <i>P. falciparum</i> culture for storage .....	55
3.3.4	Thawing of <i>P. falciparum</i> cryo-stabilates .....	55
3.3.5	Synchronization of asexual parasite culture.....	55
3.3.6	Transfection of <i>P. falciparum</i> parasites via electroporation.....	56
3.3.7	Selection of transgenic parasites via selection linked integration (SLI) .....	57
3.3.8	Saponin lysis of <i>P. falciparum</i> infected erythrocytes .....	58
3.3.9	Inactivation of parasite proteins by knock sideways system .....	58
3.3.10	Flow cytometry-based growth assay.....	59
3.3.11	<i>In vitro</i> ring-stage survival assay <sup>0-3h</sup> (RSA) .....	59
3.3.12	Consecutive <i>in vitro</i> ring-stage survival assay <sup>0-3h</sup> (RSA) .....	60
3.3.13	Bloated food vacuole assay.....	61
3.3.14	Cytochalasin D inhibitor treatment of <i>P. falciparum</i> .....	61
3.3.15	Parasite fitness assay .....	62
3.3.16	Measurement of protein amount by fluorescence intensity .....	62
3.4	Biochemical methods .....	63
3.4.1	Discontinuous SDS-polyacrylamide gel electrophoresis (SDS-PAGE).....	63
3.4.2	Western Blot analysis .....	63
3.4.3	Immunodetection of proteins .....	64
3.5	Microscopy.....	64
3.5.1	Live cell imaging.....	64
3.5.2	Confocal imaging of parasites following DHA pulse in standard <i>in vitro</i> RSA .....	65
3.5.3	Immunofluorescence assay (IFA) performed with acetone fixed cells.....	65

3.5.4	Immunofluorescence assay (IFA) performed with formaldehyde / glutaraldehyde-fixed cells .....	66
<b>4</b>	<b>Results .....</b>	<b>68</b>
4.1	Functional characterization of <i>PfMCA2</i> (PF3D7_1438400) .....	68
4.1.1	Localization of <i>PfMCA2</i> (PF3D7_1438400) .....	68
4.1.2	<i>PfMCA2</i> is part of the Kelch13 compartment .....	69
4.1.3	SNP found mainly in African field isolated leads to truncation of <i>PfMCA2</i> and renders parasite resistant to ART .....	72
4.1.4	<i>PfMCA2</i> <sup>Y1344Stop</sup> co-localizes with <i>PfKelch13</i> .....	74
4.2	Functional characterization of <i>PfMyosinF</i> (PF3D7_1329100, previously annotated as <i>PfMyosinC</i> ) .....	77
4.2.1	<i>PfMyosinF</i> is found in close proximity to the Kelch13 compartment .....	77
4.2.2	Cytochalasin D treatment causes dissociation of <i>PfMyosinF</i> and <i>PfKelch13</i> in trophozoites .....	82
4.3	<i>PfMyosinF</i> is important for parasite development .....	85
4.3.1	Inactivation of <i>PfMyosinF</i> leads to a reduced parasite growth .....	85
4.3.2	Inactivation of <i>PfMyosinF</i> does not influence survival of ring stage parasites under ART treatment .....	88
4.3.3	<i>PfMyosinF</i> is involved in hemoglobin uptake .....	89
4.3.4	Actin filaments accumulate close to <i>PfMyosinF</i> .....	91
4.3.5	Inactivation of <i>PfMyosinF</i> increases co-localization with PI3P-positive structures at the food vacuole .....	94
4.4	<i>PfKelch13</i> compartment members are involved in ART resistance .....	98
4.4.1	<i>PfKelch13</i> mediated ART resistance .....	98
4.4.2	<i>PfKelch13</i> -independent ART resistance .....	100
4.5	Mutations in Africa and generation of mutation pools .....	102
4.5.1	Selection of SNPs for mutation pools .....	102
4.5.2	<i>PfKIC1</i> (PF3D7_0606000) .....	106
4.5.3	<i>PfKIC2</i> (PF3D7_1227700) .....	108
4.5.4	<i>PfKIC4</i> (PF3D7_1246300) .....	109
4.5.5	<i>PfKIC5</i> (PF3D7_1138700) .....	112
4.5.6	<i>PfKIC7</i> (PF3D7_0813000) .....	114
4.5.7	<i>PfKIC9</i> (PF3D7_1442400) .....	115
4.5.8	<i>PfMyosinF</i> (PF3D7_1329100) .....	118
4.5.9	<i>PfUBP1</i> (PF3D7_0104300) .....	120
4.6	Non-synonymous SNPs tested individually on their contribution to ART resistance .....	122
4.6.1	Non-synonymous SNPs in <i>PfMyosinF</i> (PF3D7_1329100) do not influence ART resistance .....	122
4.6.2	Parasites with a SNP in <i>PfAP-2α</i> (PF3D7_0617100) show a very mild reduction in susceptibility to ART compared to 3D7 .....	123

4.6.3	Asian non-synonymous SNP identified in <i>PfEps15</i> (PF3D7_1025000) does not influence ART resistance .....	125
4.6.4	<i>PfUBP1</i> (PF3D7_0104300) SNP detected in Asia confers tolerance to ART .....	126
4.6.5	Two non-synonymous SNPs detected in <i>PfKelch13</i> (PF3D7_1343700) reduce ART susceptibility in <i>P. falciparum</i> .....	128
4.7	<i>K13<sup>C580Y</sup></i> parasites become more resistant to DHA after consecutively performed standard RSAs.....	130
4.7.1	ART resistant <i>K13<sup>C580Y</sup></i> parasites show reinvasion of fresh RBCs and less far development after DHA pulse .....	130
4.7.2	Consecutive cycles of standard RSA render <i>K13<sup>C580Y</sup></i> parasites even more resistant to ART .....	133
4.8	Non-synonymous SNPs of <i>pfkelch13</i> influence protein amount and parasite fitness .....	134
4.8.1	Non-synonymous SNPs causing ART resistance influence <i>PfKelch13</i> protein amount .....	134
4.8.2	Parasite fitness is influenced by different non-synonymous SNPs and negatively correlates with ART resistance .....	136
<b>5</b>	<b>Discussion .....</b>	<b>139</b>
5.1	<i>PfKelch13</i> -independent ART resistance.....	139
5.1.1	<i>PfMCA2</i> belongs to the Kelch13 compartment and truncated versions of the protein mediate ART resistance <i>in vitro</i> .....	139
5.1.2	<i>PfMyosinF</i> is an actin-associated protein that is part of the Kelch13 compartment and contributes to hemoglobin uptake in <i>P. falciparum</i> parasites .....	144
5.1.3	Other proteins besides <i>PfKelch13</i> influence ART resistance .....	149
5.2	<i>PfKelch13</i> -dependent ART resistance.....	151
5.2.1	Further mutations detected in the Kelch13 propeller domain of <i>PfKelch13</i> that mediate ART resistance .....	151
5.2.2	Does dormancy provide an explanation for ART resistance? .....	154
5.2.3	Fitness and <i>PfKelch13</i> protein levels vary in parasites with different <i>pfkelch13</i> mutations .....	156
<b>6</b>	<b>References .....</b>	<b>159</b>

<b>Danksagung</b>	<b>i</b>
<b>List of Publications</b>	<b>ii</b>
<b>Appendix</b>	<b>iii</b>
<b>Appendix A</b>	<b>iii</b>
<b>Appendix B</b>	<b>v</b>
<b>Appendix C</b>	<b>x</b>
<b>Appendix D</b>	<b>xx</b>
<b>Appendix E</b>	<b>xxiii</b>

<b>Appendix F</b>	<b>xxiii</b>
<b>Appendix G</b>	<b>xxv</b>
<b>Appendix H</b>	<b>xxviii</b>

## List of Figures

Figure 1) Global <i>P. falciparum</i> death rate in 2019.....	2
Figure 2) Life cycle of <i>P. falciparum</i> parasites.....	5
Figure 3) Invasion of the red blood cell.....	8
Figure 4) Asexual replication of <i>P. falciparum</i> inside the erythrocyte.....	9
Figure 5) Five stages of gametocytogenesis.....	10
Figure 6) Intracellular organelles of trophozoite stage and merozoite stage <i>Plasmodium</i> parasite.....	14
Figure 7) Vaccine targets of <i>Plasmodium</i> stages.....	21
Figure 8) Status of artemisinin resistance in 2014 and 2018.....	25
Figure 9) Protein structure of <i>PfKelch13</i> .....	27
Figure 10) Experimental procedure of standard <i>in vitro</i> RSA.....	28
Figure 11) <i>PfMCA2</i> (PF3D7_1438400) localizes close to food vacuole and vesicles.....	69
Figure 12) Relative localization of <i>PfMCA2</i> to <i>PfKelch13</i> .....	71
Figure 13) SNP (Y1344Stop) found in field isolates that when introduced into 3D7 leads to truncation of <i>PfMCA2</i> and renders parasite resistant to ART.....	73
Figure 14) Relative localization of <i>PfMCA2</i> <sup>Y1344Stop</sup> -GFP foci to <i>PfKelch13</i> .....	75
Figure 15) Localization of <i>PfMyosinF</i> compared to <i>PfKelch13</i> .....	79
Figure 16) Relative localization of <i>PfMyosinF</i> to <i>PfKelch13</i> .....	81
Figure 17) Cytochalasin D treatment leads to dissociation of <i>PfMyosinF</i> and <i>PfKelch13</i> foci in early and late trophozoites.....	85
Figure 18) <i>PfMyosinF</i> is important for parasite development.....	88
Figure 19) RSA of <i>MyosinF</i> <sup>wt</sup> -2x2+1xNLS parasites after partial inactivation of <i>PfMyosin</i> by knock sideways.....	89
Figure 20) Inactivation of <i>PfMyosinF</i> prevents hemoglobin uptake.....	91
Figure 21) Actin filaments accumulate next to <i>PfMyosinF</i> .....	93
Figure 22) Inactivation of <i>PfMyosinF</i> leads to increased co-localization with PI3P-positive structures (P40PX marker) at the food vacuole.....	96
Figure 23) RSA of <i>Kelch13</i> <sup>wt</sup> +3xNLS parasites after partial inactivation of <i>PfKelch13</i> by knock sideways.....	99
Figure 24) RSA of essential <i>PfKelch13</i> -compartment members after partial inactivation of respective candidate by knock sideways.....	101
Figure 25) Analysis of mutant <i>PfKIC1</i> (PF3D7_0606000).....	107
Figure 26) Analysis of mutant <i>PfKIC2</i> (PF3D7_1227700).....	109
Figure 27) Analysis of mutant <i>PfKIC4</i> (PF3D7_1246300).....	111
Figure 28) Analysis of mutant <i>PfKIC5</i> (PF3D7_1138700).....	113
Figure 29) Analysis of mutant <i>PfKIC7</i> (PF3D7_0813000).....	115
Figure 30) Analysis of mutant <i>PfKIC9</i> (PF3D7_1442400).....	117
Figure 31) Analysis of mutant <i>PfMyosinF</i> (PF3D7_1329100).....	119
Figure 32) Analysis of mutant <i>PfUBP1</i> (PF3D7_0104300).....	121
Figure 33) Individually tested SNPs of <i>pfmyosinF</i> .....	123
Figure 34) Individual tested SNP of <i>pfap-2α</i> .....	124
Figure 35) Individual tested SNP of <i>pfeps15</i> .....	125
Figure 36) <i>UBP1</i> <sup>R3138H</sup> renders parasite resistant to ART.....	127
Figure 37) <i>K13</i> <sup>V520A</sup> and <i>K13</i> <sup>V589I</sup> render parasites resistant to ART.....	129
Figure 38) <i>K13</i> <sup>C580Y</sup> parasites develop less far after DHA pulse.....	132
Figure 39) Consecutive cycles of standard RSA with DHA survivors render <i>K13</i> <sup>C580Y</sup> parasites more resistant over time.....	134
Figure 40) Resistance-causing non-synonymous SNPs reduce <i>PfKelch13</i> protein amount.....	136
Figure 41) Higher ART resistance level results in higher fitness cost.....	138

## List of Tables

Table 1) List of all SNPs collected for mutation pools of the candidate genes indicated.....	103
--	-----

## Abbreviations

aa	amino acid
ACT	artemisinin combination therapy
AMA1	apical membrane antigen 1
AQ	amodiaquine
ART	artemisinin and its derivatives
AS	artesunate
BSV	blood-stage vaccine
CSP	circumsporozoite protein
DAPI	4',6-Diamidin-2-phenylindol
DHA	dihydroartemisinin
DIC	differential interference contrast
DiQ-BioID	dimerization-induced quantitative BioID
DNA	deoxyribonucleic acid
DP	dihydroartemisinin-piperaquine
DV	digestive vacuole
EBL	erythrocyte binding-like
EMA	European Medicine Agency
EPM	erythrocyte plasma membrane
ER	endoplasmic reticulum
EXP2	exported protein 2
FV	food vacuole
GDV1	gametocyte development 1
GFP	green fluorescent protein
GMS	Greater Mekong Subregion
GWAS	genome wide association study
h	hour
HA	hemagglutinin
HDA2	histone deacetylase 2
HIV	human immunodeficiency viruses
HP1	heterochromatin protein 1
HRP	horseradish peroxidase
HSP101	heat shock protein 101
IFA	immunofluorescence assay
IMC	inner membrane complex

IRS	indoor residual spray
ITN	insecticide treated net
K13	Kelch13 protein
KAHRP	knob associated histidine-rich protein
kDa	kilodaltons
KIC	Kelch13 interaction candidates
KLHL	Kelch-like gene family
LLINs	long lasting insecticidal nets
LysoPC	Lysophosphatidylcholine
MAHRP1	Maurer`s cleft protein 1
MC	Maurer`s cleft
MQ	mefloquine
MSRP6	merozoite surface related protein 6
MW	molecular weight
NLS	nuclear localization signal
nM	nanomolar
PCR	polymerase chain reaction
PEV	pre-erythrocytic vaccine
PEXEL	<i>Plasmodium</i> export element
<i>Pf</i> AP-2 $\mu$	<i>P. falciparum</i> adaptor protein complex subunit mu
<i>Pf</i> CRT	<i>P. falciparum</i> chloroquine resistance transporter
<i>Pf</i> DPAP1	<i>P. falciparum</i> dipeptidyl aminopeptidase 1
<i>Pf</i> EMP1	<i>P. falciparum</i> erythrocyte membrane protein 1
<i>Pf</i> MCA2	<i>P. falciparum</i> metacaspase 2
<i>Pf</i> MDR1	<i>P. falciparum</i> multidrug resistance protein 1
<i>Pf</i> PI3K	<i>P. falciparum</i> phosphatidylinositol 3-kinase
<i>Pf</i> Rh	<i>P. falciparum</i> reticulocyte binding-like proteins
<i>Pf</i> RH5	<i>P. falciparum</i> reticulocyte binding protein homologue
<i>Pf</i> UBP1	<i>P. falciparum</i> ubiquitin carboxyl-terminal hydrolase 1
<i>Pf</i> VP1	<i>P. falciparum</i> V-type H(+)-translocating pyrophosphatase
PI3P	phosphatidylinositol 3-phosphate
PNEP	PEXEL negative exported protein
PPM	parasite plasma membrane
PTEX	<i>Plasmodium</i> translocon of exported proteins
PTP1	protein tyrosine phosphatase
PV	parasitophorous vacuole

PVM	parasitophorous vacuole membrane
RBC	red blood cell
RESA	ring-infected erythrocyte surface antigen
REX1	ring-exported protein 1
REX2	ring-exported protein 2
RFP	red fluorescent protein
RIMA	ring membrane antigen
RNA	ribonucleic acid
RON	rhoptry neck protein
RSA	ring-stage survival assay
SBP1	skeleton-binding protein 1
SEA	Southeast Asia
SLI	selection linked integration
SNP	single nucleotide polymorphism
SP	sulphadoxine-pyrimethamine
STEVOR	subtelomeric variant open reading frame
SUB	subtilisin-like serine protease
TBV	transmission blocking vaccine
TGD	targeted gene disruption
TRX2	thioredoxin 2
TSA	trophozoite-stage survival assay
TVN	tubovesicular network
UN	untreated nets
UPR	unfolded protein response
WHO	World Health Organization
WSV	whole sporozoite vaccine
wt	wild type

# 1 Introduction

## 1.1 Malaria – Key facts

### 1.1.1 Discovery and taxonomic classification of *Plasmodium* parasites

The French Alphonse Charles Laveran was garrisoned in 1878 as military doctor in Algeria where many soldiers were suffering from malaria, but at that time the origin of the disease was unknown. Laveran was very ambitious and persistently worked on elucidating the causal agent of this febrile disease and finally was the first to achieve the microscopical description of the protozoan parasite in the blood of infected soldiers (Alphonse Charles Laveran, 1881).

The organisms he described are obligate intracellular parasites whose motile invasive stages exhibit an evolutionary unique apical complex (Morrison, 2008) that serves as eponym of the phylum Apicomplexa (also known as Sporozoa). Together with dinoflagellates and ciliates, the Apicomplexans belong to the taxonomic group of the Alveolata (Gould *et al.*, 2008; Moore *et al.*, 2008; Yoon *et al.*, 2008). All Apicomplexans are characterized by a parasitic lifestyle and a wide range of animal species can be infected by these unicellular protists. The phylum itself is subclassified in four traditional groups, namely coccidians, gregarines, haemosporidian and piroplasmids (Adl *et al.*, 2005; Morrison, 2008). Covering more than 200 species, the genus *Plasmodium* belongs to the Apicomplexan subgroup of Haemosporidia (Danilewsky, 1885). Out of those five species, *Plasmodium falciparum*, *Plasmodium vivax*, *Plasmodium ovale*, *Plasmodium malariae* and *Plasmodium knowlesi*, are known to infect humans, while the other plasmodial species are capable of infecting birds, reptiles, or mammals (Martine Zilvermit & Daniel L. Hartl, 2014). Among the five human infecting species, *P. falciparum* is the most virulent.

### 1.1.2 Epidemiology

Although malaria is preventable and curable, still almost half of the world's population is at risk of this disease with 87 countries being malaria endemic. In 2019, the WHO reported an estimated 229 million clinical malaria episodes and 409 000 deaths, with the WHO African Region having the globally highest disease burden of 94% of reported deaths (Figure 1). In

general, the overall malaria burden declined since the year 2000 and several countries were declared as permanently malaria-free between 2000 and 2019 (WHO, 2020b).

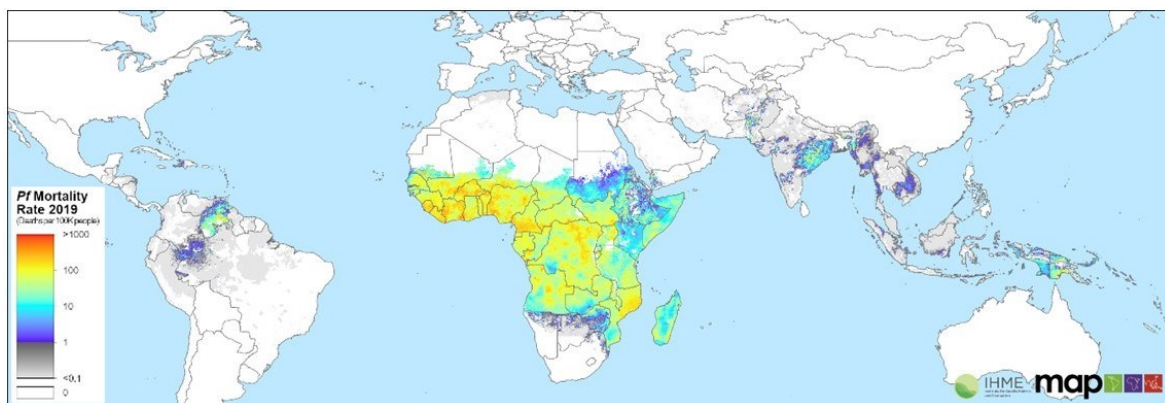


**Figure 1) Global *P. falciparum* death rate in 2019.** Death incidence due to malaria per 100K people of all ages is indicated in color code. Red color depicts countries with a high mortality rate due to malaria (deaths per 100K people), while grey marks countries with a low mortality rate. (MAP, 2021)

Malaria is endemic in tropical and subtropical areas, mostly in sub-Saharan Africa, but also in the WHO regions of South-East Asia (3% of global malaria deaths), Western Pacific, Eastern Mediterranean, and the Americas (WHO, 2020b). In general, pregnant women and children under the age of five years are the most vulnerable group, but also people with HIV / AIDS (Korenromp *et al.*, 2005) or with immunosuppression as well as travelers have an increased risk to develop severe pathology (Poumerol & Wilder-Smith, 2012).

Malaria is a rural and poverty-related febrile illness (Gallup & Sachs, 2001; Barat *et al.*, 2004). The disease is strongly influenced by climatic conditions, namely temperature, humidity, and rainfall patterns (Gilles, 1993). Climatic factors regulate the development and survival of the mosquito vector and at the same time influence the plasmodial development inside the insect. When temperatures fall below 16°C transmission of the parasite becomes very unlikely since the parasite stops its development and the mosquitoes pause their biting activity (Guerra *et al.*, 2008).

The protozoan parasite is transmitted by females of the *Anopheles* mosquito when taking a blood meal (Ross, 1898). The transmission capacity depends on different factors such as contact frequency between humans and infected insect vector, vector density in general, and feeding habits of the mosquitoes. Besides these parameters, the longevity of the mosquito plays an important role since the transmission frequency is increased when there is more time for the parasite to successfully complete its development inside the mosquito (Breman *et al.*, 2001).

In total, five different *Plasmodium* species are able to infect the human host. The most pathogenic species causing malaria is *P. falciparum* which frequently provokes a severe course of disease and is the reason for most of all malaria deaths. Regional distribution of this parasite species is limited by climatic factors since *P. falciparum* relies on temperatures above 20°C for its development and replication (Anderson & May, 1992; Colluzzi, 1999; Sachs & Malaney, 2002).

Outside the African continent *P. vivax* is the most frequent agent causing malaria. Its wider distribution is based on a lower dependency on temperature when compared to *P. falciparum* (Greenwood *et al.*, 2008; Gething *et al.*, 2012). A limiting issue for *P. vivax* is the restriction to young red blood cells (reticulocytes), leading to a finite maximal parasitemia which reduces the severity of the course of disease (Craik, 1920; HEGNER, 1938; Malleret *et al.*, 2015). *P. vivax* parasites are able to develop into dormant stages in the liver, called hypnozoites, and can persist for months or years in the liver of the patient (White, 2011a; Dembélé *et al.*, 2014). This adaptation is ideal in regions with seasonal transmission of malaria.

*P. ovale* is mainly distributed in tropical Western Africa. In rare instances it is also found in Indonesia, the Philippines, or Papua New Guinea (Kawamoto *et al.*, 1999; Collins & Jeffery, 2005). Similar to *P. vivax*, *P. ovale* infects reticulocytes and has the capacity to develop into dormant hypnozoites that remain in the liver, which can lead to a spontaneous malaria relapse after months.

The fourth *Plasmodium* parasite infecting humans is *P. malariae*. Contrary to *P. vivax* and *P. ovale*, this protozoan species does not generate dormant hypnozoites. Nevertheless, *P. malariae* is capable of remaining in the blood of immune patients over decades without causing symptoms. Co-infections of *P. malariae* and *P. falciparum* are frequent in endemic regions in Africa, but the infection with *P. malariae* often remains undetected until proper laboratory diagnostics are performed (Collins & Jeffery, 2007).

*P. knowlesi* is the fifth known *Plasmodium* species that can infect humans (Collins, 2012). Originally, it was described in macaques in Malaysia (Franchini, 1927), but experimental work demonstrated that *P. knowlesi* can also infect human beings (Knowles & Gupta, 1932). Recent findings show that the parasite is also naturally transmitted to humans (White, 2008a; Singh & Daneshvar, 2013), where it was often confused with *P. malariae* due to its morphological similarities (Singh *et al.*, 2004).

### 1.1.3 Pathology

While the development of the parasite inside the liver (see section 1.2.1.2) does not cause any clinical symptoms, the asexual replication of *Plasmodium* species in the erythrocytes is responsible for the symptoms of the disease (Schofield & Grau, 2005; Bartoloni & Zammarchi, 2012). Malaria, particularly if caused by *P. falciparum*, can present in two different ways: it can lead either to uncomplicated malaria or can progress to a severe form. The uncomplicated form of the disease is characterized by non-specific symptoms such as fever, chills, headache, cough, or diarrhea, often resulting in a misdiagnosis. In contrast, severe malaria leads to multiorgan damage, anemia, cerebral malaria, kidney failure, acidosis, or respiratory organ failure (Taylor *et al.*, 2012; Ashley *et al.*, 2018).

The distribution of severe malaria in different age groups in the population is influenced by the transmission rate of the parasite in the different regions. In areas with low transmission of parasite species (low endemicity settings), all ages are at risk of developing clinical symptoms since there is only a low level of immunity in the human population. In these settings, the clinical spectrum of severe malaria is predominated by cerebral malaria. In contrast, when the transmission rate is high (high endemicity settings), the immune system of people adapts to parasite exposure and a status of semi-immunity develops. In these high endemicity regions the constant exposure to parasites prevents severe malaria in adults that become semi-immune due to a history of multiple infections. In contrast, young children often suffer from a severe course of the disease (Cowman *et al.*, 2016).

Besides the transmission rate, severity of a malaria infection is also influenced by the age of the individuals per se, which is due to the maturation status of the immune system of the host. A severe clinical course is mainly present in non-immune children who suffer from symptoms such as severe anemia and hypoglycemia, while adults develop acute pulmonary oedema, kidney failure, jaundice, or cerebral malaria (Dondorp *et al.*, 2008).

The vulnerability for a severe malaria progress is also influenced by the interaction with other infectious diseases. The risk of complicated or severe malaria is intensified when an individual is infected simultaneously with HIV (Korenromp *et al.*, 2005). In contrast, it is assumed that a helminth co-infection shields the individual from severe malaria in some cases, but this seems to be specific for particular geographical sites and modulated by local malaria and helminth infection patterns (Hartgers & Yazdanbakhsh, 2006; Mwangi *et al.*, 2006).

## 1.2 Biology of *Plasmodium* species

### 1.2.1 Life cycle of *P. falciparum*

The life cycle of *P. falciparum* parasites includes the shuttling between two different host systems. It consists of the sexual reproduction within the *Anopheles* mosquito vector (section 1.2.1.1), asexual replications in the human host (section 1.2.1.2 and section 1.2.1.3) and the generation of sexual precursors, also in the human host (section 1.2.1.4). The asexual multiplication in the human host involves two separate phases, the liver stage (section 1.2.1.2), and the blood stage (section 1.2.1.3) (Figure 2).

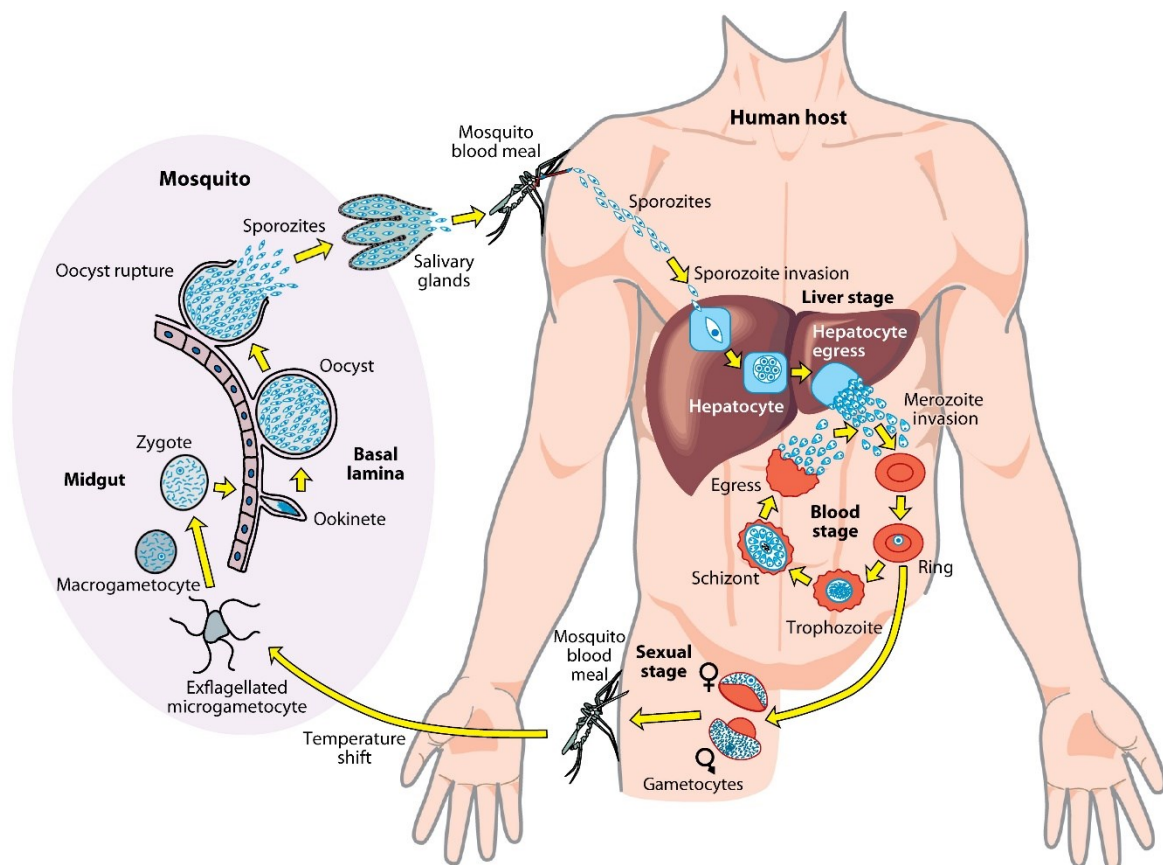


**Figure 2) Life cycle of *P. falciparum* parasites.** The life cycle of *Plasmodium* parasites includes the shuttling between two hosts, namely the invertebrate (female *Anopheles* mosquito) as well as the vertebrate host (human). During the blood meal of the female *Anopheles* mosquito sporozoites are injected into the human skin and migrate to the liver where the asexual replication inside hepatocytes begins. Mature merozoites are released into the blood stream, infect red blood cells, and start the asexual replication, running through ring, trophozoite and schizont stage. Upon rupture of the host cell up to 32 new daughter merozoites are released, each initiating a new replication round in red blood cells, a process that repeats every 48 hours. Some of the parasites differentiate into the sexual female and male gametocyte stage parasites and can be taken up by another female *Anopheles* mosquito during blood feeding. Inside the mosquito midgut, the parasite undergoes

sexual replication, producing the ookinete which translocates through the midgut wall, arresting in the mosquito midgut basal lamina. During this arrest, the ookinete matures into the oocysts, which results in the formation of sporozoites. The sporozoites are released into the mosquito hemolymph and migrate to the salivary glands where they are stored until the next blood meal of the *Anopheles* mosquito, closing the life cycle of the *Plasmodium* parasite. (Figure from (Boddey & Cowman, 2013))

#### 1.2.1.1 Sexual reproduction in the mosquito vector

The sporozoites, the parasite stage capable to infect the vertebrate host, are produced in a process called sporogony (Sinden, 2015). Sporogony starts, when the female *Anopheles* mosquito ingests the sexual precursor stages (gametocytes) of the *Plasmodium* parasite during a blood meal which then reach the mosquito midgut (Figure 2). In the midgut the male and female gametocytes are released from the infected red blood cell and differentiate into eight exflagellated motile microgametes (in case of the male gametocyte) and one macrogamete (in case of the female gametocyte), a process initiated by changes in temperature, pH and by the presence xanthurenic acid (Billker *et al.*, 1998; Billker *et al.*, 2000; Billker *et al.*, 2004). By fusion of a microgametes and a macrogamete, a zygote is produced, representing the only diploid parasite stage of the *Plasmodium* life cycle (Maccallum, 1897; Sinden *et al.*, 1976; Aikawa *et al.*, 1984). Subsequently, the fertilized zygote develops into a motile ookinete which travels through the epithelium of the midgut wall and differentiates into an oocyst. The oocyst asexually replicates and produces sporozoites. After oocyst rupture the sporozoites exit into the mosquito haemolymph (Sinden, 1974; Aly *et al.*, 2009). Through the haemolymph some sporozoites reach the salivary glands and can be injected into the human host during the next blood meal.

#### 1.2.1.2 Asexual replication in the human liver

The replication within the human host begins when the infectious stages of the sporozoites (section 1.2.1.1) are injected into the human skin during a blood meal of a female *Anopheles* mosquito (Medica & Sinnis, 2005; Prudêncio *et al.*, 2006) (Figure 2). Aided by their gliding motility they reach the human vasculature to enter the blood stream (Stewart & Vanderberg, 1988; Sultan *et al.*, 1997). Transported via the blood circulation, sporozoites reach the liver and - after crossing different types of host cells, including Kupffer cells or sinusoidal endothelial cells - they establish a productive hepatocyte infection (Mota *et al.*, 2001; Pradel & Frevert, 2001; Frevert *et al.*, 2006; Tavares *et al.*, 2013). This process of migrating through different cell types is called traversal and represents the starting point of the liver

stage. During invasion into the hepatocyte a parasitophorous vacuole (PV) is formed (Meis *et al.*, 1983). Inside this PV the parasite completes many rounds of asexual multiplication, resulting in the production of thousands of merozoites in a process termed schizogony. *P. vivax* or *P. ovale* also produce persistent dormant stages (hypnozoites) during this liver stage. These hypnozoites arrest early in liver development and remain silent up to years after which they activate and complete liver schizogony (Cogswell, 1992). The mature merozoites are packed into vesicles, called merozoites, and bud from the infected hepatocyte to be released into the bloodstream (Sturm, 2006). Upon rupture of the merozoites, the merozoites are released into the blood stream and invade red blood cells, initiating the erythrocyte cycle.

### 1.2.1.3 Asexual replication in human red blood cells

The invasion of erythrocytes into red blood cells is a process of multiple, highly orchestrated steps (Figure 3) (Gilson & Crabb, 2009; Riglar *et al.*, 2011; Weiss *et al.*, 2015). First, the merozoite attaches to the erythrocyte surface and reorientates its apical pole (harboring the secretory organelles that are needed for invasion (see section 1.2.2.2.1)), towards the red blood cell membrane. For the attachment to the erythrocyte surface different parasite proteins are required, including the erythrocyte-binding ligands (EBLs) and the *P. falciparum* reticulocyte binding protein-binding homologues (*PfRh*) (Rayner *et al.*, 2001; Gilberger *et al.*, 2003; Riglar *et al.*, 2011; Srinivasan *et al.*, 2011). During the second step, the parasite forms a tight junction between itself and the host cell. The active invasion process is powered by an actomyosin motor, during which the parasite forces itself into the erythrocyte (Keeley & Soldati, 2004; Baum *et al.*, 2006; Besteiro *et al.*, 2011; Riglar *et al.*, 2011). Simultaneously, the merozoite specific rhoptry organelles release their lipid-rich content to contribute - together with invaginated red blood cell membrane - to the formation of the parasitophorous vacuole membrane (PVM) that surrounds the parasite inside the host cell after invasion is complete (Cowman & Crabb, 2006). After successful invasion, the last step includes the resealing of erythrocyte membrane and red blood cell echinocytosis (Gilson & Crabb, 2009).

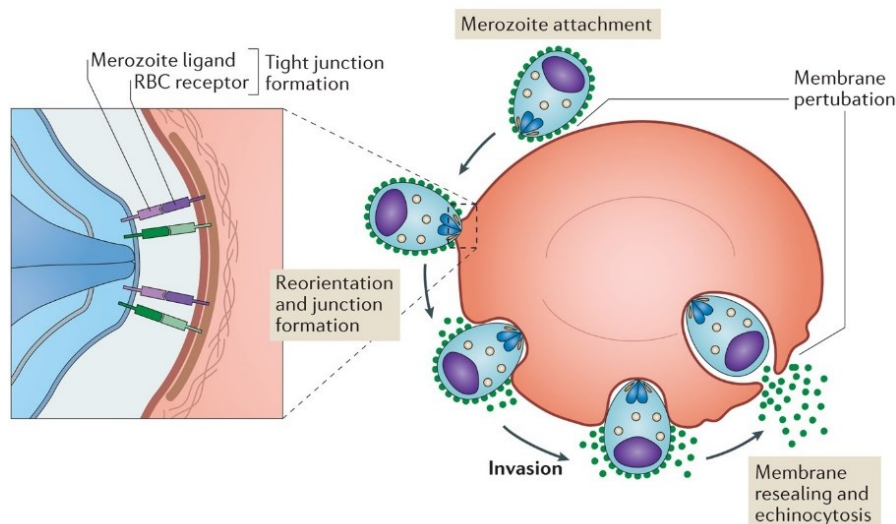


**Figure 3) Invasion of the red blood cell.** (Right) graphical representation of the different steps of invasion of the merozoite into a red blood cell. (left) enlargement of the apical end of the invading merozoite into the host cell. *Blue*, merozoite; *red*, red blood cell; *green*, merozoite surface proteins. (Niz *et al.*, 2017)

The asexual replication of *P. falciparum* parasite inside the red blood cell lasts 48 hours and during this process, the parasite runs through different stages (Figure 4). The development starts at the ring stage that is important for the parasite to establish itself in the host cell, for instance to install nutrient transport capacities at the host cell membrane. During this stage, the parasite is mobile in the red blood cell and switches between a circular disc shape and an amoeboid form (Grüring *et al.*, 2011). Host cell remodeling is a prominent process during the ring stage and is achieved by the export of many different parasite proteins into the red blood cell (see section 1.2.2.1). The ring stage is followed by the trophozoite stage during which the parasite settles at a stationary position in the host cell and the metabolism increases due to rapid growth of the parasite inside the red blood cell (Figure 4) (Grüring *et al.*, 2011). This results in a higher consumption of nutrients but also increases the need for space in the host cell. Thus, the uptake of host cell cytosol (mostly hemoglobin) is increased. This also leads to an increased formation of haemozoin, a degradation product of hemoglobin that becomes apparent in the parasite's food vacuole (FV) (the site where the hemoglobin is degraded). The trophozoite stage is followed by the schizont stage, where the parasite generates up to 32 new daughter cells (merozoites) within the same cell in a process termed schizogony. Upon rupture of the host cell, these merozoites are released into the blood stream and are able to invade new red blood cells.

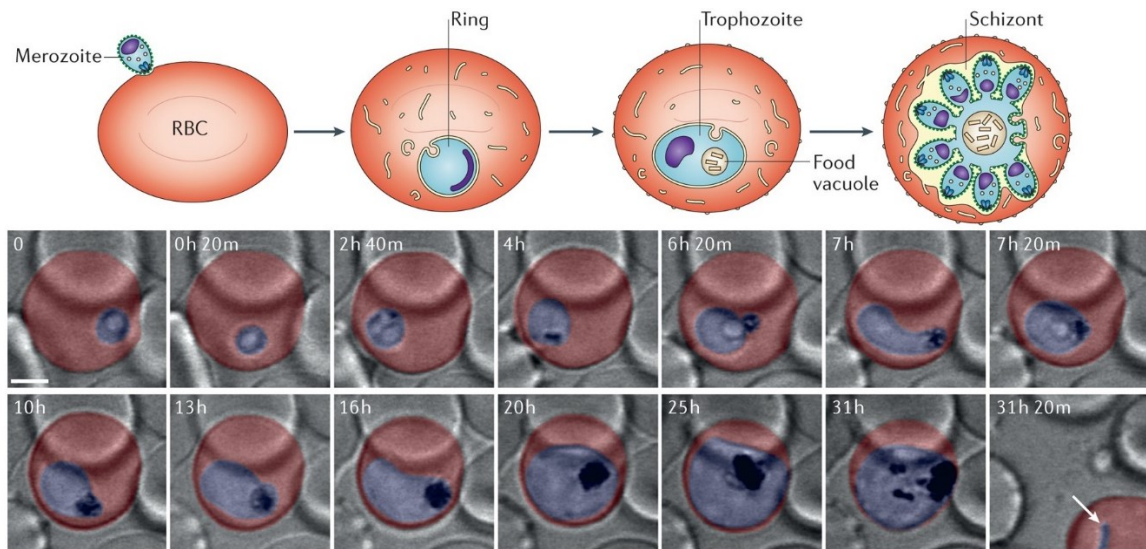


**Figure 4) Asexual replication of *P. falciparum* inside the erythrocyte.** (Top) Graph displays the different developmental stages of *P. falciparum* inside the host cell, including ring stage, trophozoite stage, schizont stage and merozoites. (Bottom) Confocal microscopy images showing selected single sections of a time lapse experiment of the intraerythrocytic development of a *P. falciparum* parasite. *Red*, marks the red blood cell (top and bottom panel). *Blue*, represents the parasite (top and bottom panel). *Black* shows hemozoin crystals accumulating in the parasite food vacuole (bottom panel). *White arrow* shows a newly invaded ring (bottom panel). (Niz *et al.*, 2017)

#### 1.2.1.4 Development of sexual precursors in the human host

During the repeated rounds of asexual replication inside the red blood cell, some parasites (~ 0.1 – 5%) enter sexual commitment and start the differentiation into gametocytes (Sinden, 1983). This process is called gametocytogenesis and consists of five different morphological stages (Figure 5). The maturation time is species dependent. For *P. falciparum* parasites the differentiation into mature gametocytes requires 9 – 12 days (Hawking *et al.*, 1971; Sinden *et al.*, 1978). It was suggested by different studies that differentiation of immature gametocytes takes place in the bone marrow and spleen, while the mature stages circulate in the blood (Farfour *et al.*, 2012; Aguilar *et al.*, 2014; Joice *et al.*, 2014; Lee *et al.*, 2018; Niz *et al.*, 2018; Obaldia *et al.*, 2018). Gametocytogenesis is regulated by the interplay of different genetic, epigenetic and environmental parameters. On a genetic level ApiAP2-G activates transcription to initiate sexual commitment and this is conserved across *Plasmodium* species (Kafsack *et al.*, 2014; Sinha *et al.*, 2014). Epigenetic silencing of *ap2-g* in asexual blood stage parasites is achieved by interaction of heterochromatin protein 1 (HP1) and the histone deacetylase 2 (HDA2) (Brancucci *et al.*, 2014; Coleman *et al.*, 2014). HP1 can be downregulated through the interaction of the perinuclear protein gametocyte development 1 (GDV1), resulting in the continued

transcription of the *ap2-g* locus (Eksi *et al.*, 2012; Filarsky *et al.*, 2018). The genetic and epigenetic factors are influenced by environmental parameters such as the level of human serum phospholipid lysophosphatidylcholine (LysoPC), all together regulating the differentiation into gametocytes (Brancucci *et al.*, 2017). When gametocytogenesis is completed, the mature gametocytes are present in the human blood stream for several days to increase the chances to be transmitted to an *Anopheles* mosquito (Smalley & Sinden, 1977; Gautret & Motard, 1999; Eichner *et al.*, 2001). When the gametocytes are ingested by the *Anopheles* vector during a blood meal, the *Plasmodium* life cycle is completed.

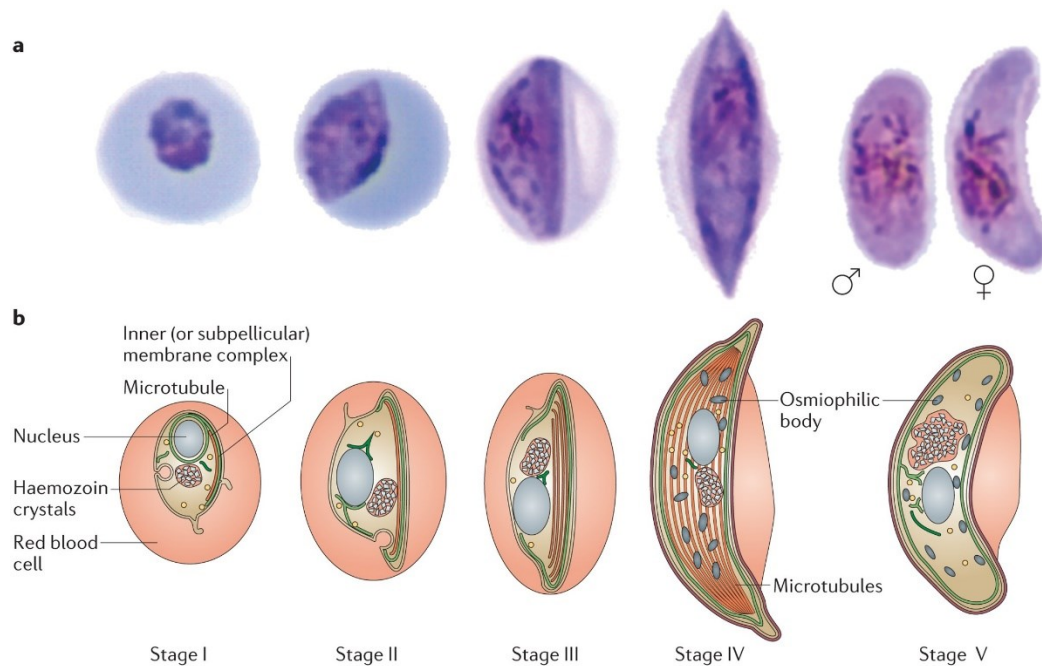


**Figure 5) Five stages of gametocytogenesis.** (A) The different gametocyte stages from Giemsa-stained smears. (B) Scheme showing the intracellular morphology of the different gametocyte stages during gametocytogenesis. (Josling & Llinás, 2015)

## 1.2.2 Surviving inside the host cell

### 1.2.2.1 Remodeling of the infected red blood cell

#### 1.2.2.1.1 The parasitophorous vacuole

The enucleated, metabolic inactive erythrocyte provides the perfect hiding place for the parasite to avoid clearance by the host immune system. Since red blood cells (RBCs) are

not able to present parasite antigens on their surface due to a lack of major histocompatibility complex class I and II, the infected cell remains undetected by the adaptive immune system. Inside the host cell, the parasite establishes the PV and resides inside this special compartment that is surrounded by the PVM, representing the interface between the parasite and the host cell cytoplasm. The PV in *P. falciparum* was described for the first time by *Ladda et al* in 1966 (*Ladda et al.*, 1966). During the entire intraerythrocytic development, the *Plasmodium* parasite replicates inside of the PV, while at the end of the asexual cycle the PVM and the RBC membrane are destroyed by the parasite to release the merozoites into the human blood stream (*Blackman & Carruthers*, 2013). The PVM serves as a barrier between the erythrocyte and the parasite and regulates the export of proteins and the uptake of nutrients (*Garnham et al.*, 1961; *Rudzinska et al.*, 1965; *Aikawa et al.*, 1966; *Aikawa*, 1971; *Seed et al.*, 1976). Only little is known about the function of the PV and PVM, but it is suggested that these structures are involved in protein folding and processing since different proteases and chaperons were identified in the PV (*Nyalwidhe & Lingelbach*, 2006; *Spielmann et al.*, 2012).

#### 1.2.2.1.2 The tubovesicular network

Several studies detected a loop-shaped structure, extending from the PVM and reaching into the erythrocyte cytoplasm, which is termed the tubovesicular network (*Kara et al.*, 1988; *Behari & Haldar*, 1994; *Elford et al.*, 1995; *Elford et al.*, 1997; *Grützke et al.*, 2014). The role of this structure is not fully defined but it is suggested to be important for nutrient uptake, or possibly is involved in lipid storage necessary for PVM expansion, or senses environmental changes in the erythrocyte cytosol (*Lauer et al.*, 1997; *Sherling & van Ooij*, 2016).

#### 1.2.2.1.3 The PTEX complex

Enveloped inside the PV, the parasite starts the remodeling of the RBC by exporting many different parasite proteins into the host cell to gain access to nutrients, alter the physical structures of the erythrocyte membrane, and enable cytoadhesion of the infected cell (*Sargeant et al.*, 2006; *Maier et al.*, 2008; *Haase & Koning-Ward*, 2010). Around 10% of the parasite proteome are exported from the *Plasmodium* parasite to the host RBC (*Koning-Ward et al.*, 2016). Protein export includes three subsequent steps and is mediated either via special export motifs (*Plasmodium* export element, PEXEL or host targeting, HT) that

are processed in the endoplasmic reticulum (ER) or functions without a PEXEL motif (PEXEL-negative exported proteins, PNEPs) (Hiller *et al.*, 2004; Marti *et al.*, 2004; Chang *et al.*, 2008; Osborne *et al.*, 2010; Russo *et al.*, 2010; Spielmann & Gilberger, 2010; Heiber *et al.*, 2013). After entry into the ER, the exported proteins pass through the secretory pathway, after which they cross the parasite plasma membrane (PPM) to reach the PV lumen. To cross the PVM, the exported proteins are translocated into the host cell by a parasite complex, called *Plasmodium* translocon of exported proteins (PTEX) (Koning-Ward *et al.*, 2009; Beck *et al.*, 2014; Elsworth *et al.*, 2014). This PTEX complex consists of five elements of which the AAA+ ATPase heat shock protein 101 (HSP101), the exported protein 2 (EXP2), and PTEX150 represent the core units (Koning-Ward *et al.*, 2009). Beside these three main components, the complex is supported by two accessory parts, thioredoxin 2 (TRX2) and PTEX88 which are dispensable for the parasite during the asexual blood stage replication (Matthews *et al.*, 2013; Matz *et al.*, 2013). After translocation through PTEX, the exported proteins either remain in the erythrocyte cytoplasm or are transported to different destinations in the host cell, such as the erythrocyte plasma membrane or membrane skeleton, or vesicular structures called Maurer's clefts that are important for protein sorting (Wickham *et al.*, 2001).

#### 1.2.2.1.4 The Maurer's clefts

Once the exported proteins reach the erythrocyte cytoplasm, the transport to the erythrocyte membrane is aided either by chaperone mediated complexes or the Maurer's clefts (MC) (Maier *et al.*, 2009). The Maurer's clefts are disk-shaped, single-membrane platforms that are believed to act as a sorting compartment inside the host cell (Lanzer *et al.*, 2006; Bhattacharjee *et al.*, 2008; Mundwiler-Pachlatko & Beck, 2013). The Maurer's clefts are built 2 – 4 hours after RBC invasion and are mobile in the host cell throughout ring stage development but become stationary during the transition to the trophozoite stage. Immobilization of the Maurer's clefts is achieved by tether-like structures or by actin filaments (Cyrklaff *et al.*, 2011; McMillan *et al.*, 2013). Starting from the first moment they become detectable, the number of Maurer's clefts remains constant across the asexual development (Hanssen *et al.*, 2008; Tilley *et al.*, 2008; Grüning *et al.*, 2011; McMillan *et al.*, 2013). Various studies revealed the presence of different integral and peripheral proteins at the Maurer's clefts, i.e. the membrane associated histidine -rich protein 1 (MAHRP1), the skeleton binding protein 1 (SBP1), the ring-exported protein 2 (REX2), and the merozoite surface related protein 6 (MSRP6) (Blisnick *et al.*, 2000; Spycher *et al.*, 2003; Spielmann *et*

*al.*, 2006; Heiber *et al.*, 2013). Beside these, one of the most prominent Maurer's clefts proteins is the ring exported protein 1 (REX1) which prevents stacking of the Maurer's clefts and is needed for the transfer of *Plasmodium falciparum* erythrocyte membrane protein 1 (PfEMP1), the main parasite virulence protein, to the host cell surface (McHugh *et al.*, 2015). Another important protein is the MC-associated PTP1 (PfEMP1 trafficking protein) that organizes the transfer of PfEMP1 and of STEVOR (subtelomeric variant open reading frame) to the erythrocyte surface (Kaviratne *et al.*, 2002; Przyborski *et al.*, 2005; Cyrklaff *et al.*, 2011).

#### 1.2.2.1.5 Knob structures at the erythrocyte surface are needed for parasite virulence

The knobs are surface elevations generated during trophozoite development via the accumulation of knobs-associated histidine-rich protein (KAHRP) and are connected to the erythrocyte cytoskeleton (Rug *et al.*, 2006; Watermeyer *et al.*, 2016). The surface antigens PfEMP1 and STEVOR are displayed at these knob structures present at the erythrocyte membrane (Kriek *et al.*, 2003; Tilley *et al.*, 2008). PfEMP1 mediates the cytoadhesion of the infected red blood cell to the endothelium, thus promoting sequestration to the human endothelium to avoid the elimination by the spleen (Kilejian, 1979; Baruch *et al.*, 1995). Most severe complications appear during *P. falciparum* infections due to this sequestration ability (Beeson & Brown, 2002; Miller *et al.*, 2002; Wassmer *et al.*, 2015; Plewes *et al.*, 2019). Besides this, due to the protein-export driven reorganization of the cytoskeleton and the generation of the cytoskeleton-anchored knob structures, the erythrocyte membrane becomes stabilized and inflexible, further enhancing trapping in small capillaries (Zhang *et al.*, 2015).

#### 1.2.2.2 *Plasmodium* specific organelles

*Plasmodium* parasites are unicellular eukaryotes and possess different organelles such as the endoplasmic reticulum (ER), a rudimentary Golgi apparatus, ribosomes, the apical organelles, and two organelles of endosymbiotic origin, the mitochondrion and a non-photosynthetic plastid called apicoplast (McFadden *et al.*, 1996; van Wye *et al.*, 1996; Bannister *et al.*, 2000; Bannister *et al.*, 2004; Struck *et al.*, 2005) (Figure 6).

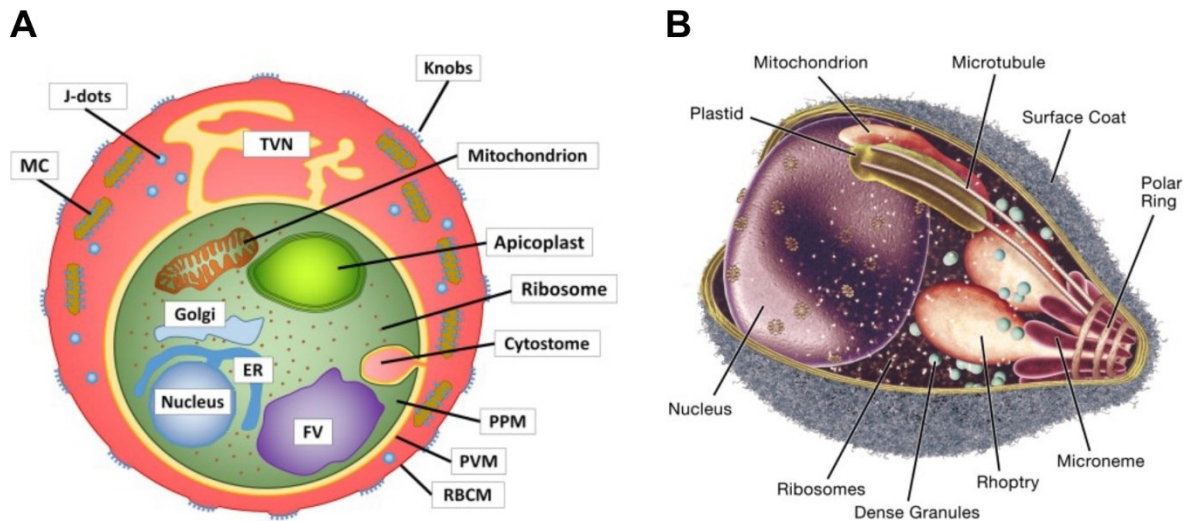


**Figure 6) Intracellular organelles of trophozoite stage and merozoite stage *Plasmodium* parasite.** (A) Scheme depicting the intracellular morphology of a trophozoite stage parasite. Different organelles are shown. MC, Maurer's clefts; TVN, tubovesicular network; ER, endoplasmic reticulum; FV, food vacuole; PPM, parasite plasma membrane; PVM, parasitophorous vacuole membrane; RBCM, red blood cell membrane. (B) Graph showing the different organelles of the invasive merozoite stage parasite. (modified from (Cowman & Crabb, 2006; Flammersfeld *et al.*, 2018))

#### 1.2.2.2.1 The apical organelles of the invasive stages

The life cycle of *Plasmodium* parasites is characterized by different invasive stages capable to invade the host cells, it develops in during different life cycle phases. To enable the invasion of the host cell, the parasites possess special essential apical organelles that are situated at the anterior end of the invasive stages. These include the rhoptries, micronemes and dense granules (Sam-Yellowe, 1996; Bannister *et al.*, 2000; Cowman & Crabb, 2002). The function and development of the apical organelles was initially investigated and characterized in *P. knowlesi*, mainly by electron microscopy (Bannister *et al.*, 1975; Aikawa *et al.*, 1978; Bannister *et al.*, 1986; Bannister & Mitchell, 1989; Torii *et al.*, 1989). The rhoptries are club-shaped elongated organelles (Bannister *et al.*, 2000). These organelles are present in pairs in the invasive stages and are filled with granular material. The secretion of their content, e.g. different rhoptry neck proteins (RONS) is essential for the invasion into the host cell (Alexander *et al.*, 2005; Lebrun *et al.*, 2005). In addition to proteins needed for invasion, the rhoptries also secrete proteins that are incorporated into the PVM during its formation (Sam-Yellowe *et al.*, 1988; Beckers *et al.*, 1994). The micronemes are also found at the apical end of the invasive stages. Like the rhoptries, they contain different types of

proteins involved in invasion, e.g. the apical membrane antigen 1 (AMA-1). For instance, the molecular interplay between RON2 and AMA-1 was shown to be a critical step of the invasion process (Lamarque *et al.*, 2011). The third component of the apical complex are the dense granules which are electron dense matrix granules (Aikawa *et al.*, 1990; Culvenor *et al.*, 1991; Trager *et al.*, 1992; Bannister *et al.*, 2000). In *P. falciparum* examples of dense granule proteins are the ring-infected erythrocyte surface antigen (RESA), ring membrane antigen (RIMA), and subtilisin-like serine proteases (SUBs) (Aikawa *et al.*, 1990; Culvenor *et al.*, 1991; Trager *et al.*, 1992; Blackman *et al.*, 1998). When the parasite invades the host erythrocyte, the content of the dense granules is released into the PV lumen (Preiser *et al.*, 2000; Blackman & Bannister, 2001).

#### 1.2.2.2.2 The apicoplast

Another *Plasmodium* specific organelle is the four membrane-bounded apicoplast that is found in most Apicomplexan parasites, such as *Plasmodium* and *Toxoplasma* but is lacking e.g. in *Cryptosporidium* (Zhu *et al.*, 2000). The apicoplast was acquired by endosymbiosis of a red algae (McFadden *et al.*, 1996). This organelle is of cylindrical shape that develops into a highly branched compartment in later *Plasmodium* parasite stages (Hopkins *et al.*, 1999; Waller *et al.*, 2000; Waller & McFadden, 2005). The apicoplast hosts different metabolic pathways, namely the biosynthesis of heme, type II fatty acids and isoprenoid precursors (Ralph *et al.*, 2004; Yu *et al.*, 2008; Vaughan *et al.*, 2009). However, during asexual replication in the erythrocyte only the isoprenoid precursor pathway is essential for parasite development (Yeh & DeRisi, 2011). Based on the fact that neither humans, nor animals possess a plastid, the apicoplast represents a very interesting target for drug development against apicomplexan causing diseases in humans and livestock. Electron and fluorescence microscopy analyses suggest a close association between the apicoplast and the mitochondrion in different erythrocytic stages (Aikawa, 1966; Hopkins *et al.*, 1999; Ralph *et al.*, 2004; Tonkin *et al.*, 2004). Both organelles, mitochondrion and apicoplast are not synthesized *de novo* during parasite replication but have to be replicated during growth and distributed between the daughter cells.

### 1.2.2.2.3 The food vacuole

The food vacuole (FV) or digestive vacuole (DV) is an acidic, lysosome-like organelle (Gluzman *et al.*, 1994; Francis *et al.*, 1997; Lazarus *et al.*, 2008; Abu Bakar *et al.*, 2010). The FV likely is present during the entire cycle of the parasite but is most easily detected by the accumulating hemozoin which becomes prominent in early trophozoite stage parasites in the blood phase (Abu Bakar *et al.*, 2010; Grüring *et al.*, 2011). The main function of the FV is the degradation of hemoglobin which also requires heme and oxygen radical detoxification, and the FV also has functions in the storage of non-degradable biomolecules, the modulation of intracellular ion homeostasis of the host erythrocyte, and peptide and amino acid transport (Goldberg *et al.*, 1990; Olliaro & Goldberg, 1995; Staines *et al.*, 2001; Krugliak *et al.*, 2002; Lew *et al.*, 2004). Since it plays a central role in the metabolism of the parasite, it serves as a main target for many antimalarial drugs. Host cell cytosol is taken up via the cytostome, a structure that is formed through the invagination of the PPM and the PVM (Aikawa *et al.*, 1966; Langreth *et al.*, 1978; Slomianny, 1990; Goldberg, 1993). When the parasite takes up hemoglobin, double-membranous vesicles arise from the cytostome and are transferred to the FV, where the hemoglobin is degraded (Slomianny, 1990; Goldberg, 1993; Spielmann *et al.*, 2020). Hemoglobin degradation is very important for the parasite since this process provides amino acids for the *de novo* synthesis of proteins and amino acids are also important metabolites for many pathways (Goldberg, 2013; Krishnan & Soldati-Favre, 2021). During the proteolytic degradation of hemoglobin, toxic, heme byproducts are produced that must be neutralized by the parasite via oligomerization into the chemical unreactive hemozoin crystals (Pagola *et al.*, 2000; Banerjee, 2001; Egan *et al.*, 2002; Goldberg, 2005; Egan, 2008). To proteolytically process hemoglobin, several enzymes are necessary. The first steps are performed by aspartic proteases called Plasmepsins and the cysteine proteases falcipains, followed by the metalloprotease falcilysin and the dipeptidyl aminopeptidase 1 (*PfDPAP1*) (Goldberg *et al.*, 1990; Eggleston *et al.*, 1999; Klemba *et al.*, 2004). As not all amino acids can be produced by the parasite, the remaining amino acids that are either present in a limited amount (methionine, cysteine, glutamic acid and glutamine) or even absent (isoleucine) in hemoglobin must be taken up by the parasite from extracellular sources to fully cover the supply with amino acids (Divo *et al.*, 1985; Goldberg, 2005; Liu *et al.*, 2006). Besides the metabolic role of hemoglobin uptake and digestion, the parasite also uses endocytosis to gain space inside the host cell and prevent RBC lysis by regulating red blood cell homeostasis (Ginsburg, 1990; Lew *et al.*, 2003). To transfer the different nutrients across the FV membrane and to maintain the acidic environment inside the FV, different transporter proteins are present in the FV

membrane. This includes the multi-drug resistance protein 1 (*PfMDR1*) and the chloroquine resistance transporter (*PfCRT*), which are important for the import of soluble molecules, or the export of metabolites (Martin & Kirk, 2004; Rohrbach *et al.*, 2006; Shafik *et al.*, 2020). In both cases, variations of the transporters are associated with drug resistance (Fidock *et al.*, 2000; Reed *et al.*, 2000; Picot *et al.*, 2009). The ion homeostasis in the FV and inside the parasite is balanced by the V-type H<sup>+</sup>-ATPase and the V-type H<sup>+</sup>-PPase (*PfVPP1*) (McIntosh, 2001; Saliba *et al.*, 2003).

## 1.3 Malaria Prophylaxis and Treatment

### 1.3.1 Vector control and drug-based prevention of malaria

To combat malaria transmission and disease, vector control as well as chemical prevention measures are important tools of intervention. The currently most frequently used vector control measures has the aim to impede human – mosquito contact and comprise insecticide-treated nets (ITNs), untreated nets (UN), indoor residual spraying (IRS) (WHO, 2017c; Wangdi *et al.*, 2018). There are two different types of ITNs on the market: for the long-lasting insecticidal nets (LLINs) the insecticide is integrated in the fibers during the production process, which reduces the washing-off of the insecticide and prolongs protection. The second type of mosquito nets are the insecticide-treated nets, which need to be repeatedly impregnated with insecticide every six months to maintain their preventive character. For net impregnation pyrethroids are used, but unfortunately resistance against this type of insecticide is raising worldwide, including on the African continent (Chandre *et al.*, 1999; Hargreaves *et al.*, 2000; Hargreaves *et al.*, 2003; Stump *et al.*, 2004; Etang *et al.*, 2006; Glunt *et al.*, 2015). Nevertheless, pyrethroid impregnated ITNs currently still offer efficient protection against the mosquito vector (Curtis *et al.*, 2003; Curtis *et al.*, 2006; Wamae *et al.*, 2015; Wangdi *et al.*, 2016).

Beside the ITNs, IRS is also a highly effective method to prevent malaria transmission. For IRS, the house walls are sprayed periodically with insecticides to kill the *Anopheles* mosquito resting on the walls and this can also prevent the mosquitoes from entering the house (WHO, 2006; Hamusse *et al.*, 2012).

Another method to prevent malaria is the administration of chemoprophylactic drugs. Chemoprophylactic drugs are mainly given to non-immune, healthy persons, traveling from nonendemic to malaria endemic regions. The main administered prophylactic drugs used

today are sulphadoxine-pyrimethamine (SP), mefloquine (MQ), amodiaquine (AQ), dihydroartemisinin-piperaquine (DP) and artesunate (AS) (White, 2005; Greenwood, 2010). SP is the most widely administered drug, which resulted in an increase in resistance to this drug and treatment failures (Rønn *et al.*, 1996; Roper *et al.*, 2004; Mugittu *et al.*, 2005; Gosling *et al.*, 2009; Tan *et al.*, 2014). To counteract this trend, mefloquine and amodiaquine are more intensively used, either as a substitutional treatment or in combination with SP (Clerk *et al.*, 2008; Gosling *et al.*, 2009).

Overall, ITNs are still the most effective measure to reduce malaria transmission, since chemoprophylactic drug administration harbors certain uncertainties regarding i.e., administration policy, limitations in preventing *P. vivax* relapses, or severe side effects. Nevertheless, a combination of all prophylactic measures provides the highest protection and contribute to malaria elimination (Wangdi *et al.*, 2018).

### 1.3.2 Vaccines

Eliminating malaria is a challenging task that will likely only be achieved with the aid of a potent vaccine. Ideally, a vaccine would initiate an immune response against all life cycle stages of *Plasmodium*, inhibiting both transmission and clinical disease. In collaboration with the world's leading funders of malaria vaccine the WHO set up the Malaria Vaccine Technology Roadmap which is constantly evaluated and revised (PATH's Malaria Vaccine Initiative, 2015). The latest version of this roadmap has the aim to implement a global strategy to accelerate the development of an efficient malaria vaccine against *P. falciparum* and / or *P. vivax*. The overall goal is to design a next-generation vaccine with a protective efficiency of at least 75% and an immune response lasting for up to 2 years (Moorthy *et al.*, 2013).

#### 1.3.2.1 Pre-erythrocytic vaccines

The immune response triggered by a potential vaccine can target different developmental stages of the *Plasmodium* life cycle (Figure 7). Antigens of the invasive sporozoites or of liver stage parasites are targeted by the pre-erythrocytic vaccines (PEV), which are also called anti-infection vaccines. These vaccines activate the adaptive immune system via different surface antigens to produce antibodies or T cell responses to combat sporozoites present in the blood stream and skin or deplete infected hepatocytes. Pre-erythrocytic

vaccines can be subdivided into subunit vaccines or whole cell vaccines. Recent research mainly focused on subunit vaccine development based on the major sporozoite surface antigen termed circumsporozoite protein (CSP) (Dame *et al.*, 1984). The RTS,S/AS01E (Mosquirix™) vaccine incorporating a *P. falciparum* CSP fragment (Asn-Ala-Asn-Pro [NANP]) vaccine belongs to this group and represents the most developed malaria vaccine to date (Cohen, 1996; White *et al.*, 2015). The European Medicine Agency (EMA) approved RTS,S/AS01E to be the first malaria vaccine used in humans, which is currently tested in phase IV (WHO, 2017a). Earlier trials showed a protective efficacy of e.g. ~36% in young children treated with four vaccine doses in sub-Saharan Africa, but also decreasing efficacy was reported in the follow-up period, especially in the absence of a booster dose of the vaccine (RTS, 2014, 2015). A second promising vaccine candidate - R21/MM - was currently developed by the University of Oxford. This candidate is a derivative of RTS,S and is also based on the central NANP repeat of CSP coupled to a saponin-based adjuvant termed Matrix-M (R21/MM) (Dattoo *et al.*, 2021). In a randomized controlled trial conducted in Burkina Faso, children aged 5 – 17 months were treated with three doses R21/MM in a 4-week interval before the malaria season followed by a fourth vaccination one year later. Overall efficacy one year later was at 77% and participants had high antibody titers against the central NANP repeat of *Plasmodium*. Based on these findings this might represent a break-through in vaccine development to combat malaria.

Vaccines based on the full-length antigen of pre-erythrocytic stage parasites are the whole sporozoites vaccines (WSV) (Figure 7). Already in the 1970s attention was drawn to this type of vaccine since radiation-attenuated WSV to immunize humans resulted in a high protective efficacy. In these experiments, immune response against the invasive sporozoite stages, but not infection with blood-stage parasites, was demonstrated (Clyde *et al.*, 1973; Clyde, 1975). Three different approaches exist to attenuate sporozoites for WSV: The sporozoites can either be attenuated by radiation (PfSPZ Vaccine), or chemically attenuated by simultaneous administration of an antimalarial drug such as chloroquine (PfSPZ-CVac), or the parasites are genetically engineered to delete genes essential for liver stage development (Richie *et al.*, 2015; Duffy & Patrick Gorres, 2020; Metzger *et al.*, 2020).

### 1.3.2.2 Blood-stage vaccines

The second type of malaria vaccine, which is called blood-stage vaccines (BSV) (Figure 7), is designed to interrupt the asexual blood-stage replication, and ideally clear the infection. Immunization experiments performed in monkeys in the 1970s directed the interest of the

developers on the merozoite invasion process as a target for vaccine development (Siddiqui, 1977). The design of a merozoite-oriented vaccine faces a number of obstacles. Firstly, invasion into a new red blood cell lasts only a few seconds, such a vaccine therefore has only a very small part of the live cycle as the target. Secondly, merozoites display many surface antigens that are often variable between isolates (polymorphic) and the invasion process depends on different, redundant ligands, complicating the design of an effective vaccine. Thirdly, compared to other vaccine types, merozoite-based BSV need to target a large number of parasites at the same time.

From 2000 to 2015 antigens of MSP1 and AMA1 were the most prominent BSV vaccine targets, but also EBA-175 and MSP3 were tested as antigen candidates. Most of the completed trials registered at ClinicalTrials.gov showed now or only moderate efficiency (Duffy & Patrick Gorres, 2020). In an attempt to obtain merozoite vaccines with better protection levels, new antigen targets such as the lowly polymorphic *P. falciparum* reticulocyte binding protein homologue 5 (*PfRH5*) or the AMA1-RON2 complex are being developed (Srinivasan *et al.*, 2017).

### 1.3.2.3 Transmission-blocking vaccines

The third group of antimalarial vaccines are the transmission-blocking vaccines (TBV) (Figure 7). This type of vaccine is used to establish antibodies in the human host that target surface antigens of the sexual mosquito stages (gametes or zygotes). These antibodies are absorbed by the female *Anopheles* mosquito during the blood meal and aim to kill the parasites or prevent its development inside the mosquito to inhibit further transmission to a new host (Carter & Chen, 1976; Gwadz, 1976). The most promising targets for this type of vaccine are the *P. falciparum* gamete surface proteins Pfs230 and Pfs48/45, or the zygote surface proteins Pfs25 and Pfs28 (Carter & Kaushal, 1984; Grotendorst *et al.*, 1984; Duffy *et al.*, 1993). For TBVs to be efficient in blocking transmission, one obligatory demand is the generation of high and durable antibody titers in humans. This is mostly achievable via specific adjuvants. Another critical requirement for TBVs is the need for a remarkably high safety profile, as the vaccinated human does not benefit directly from the vaccine.

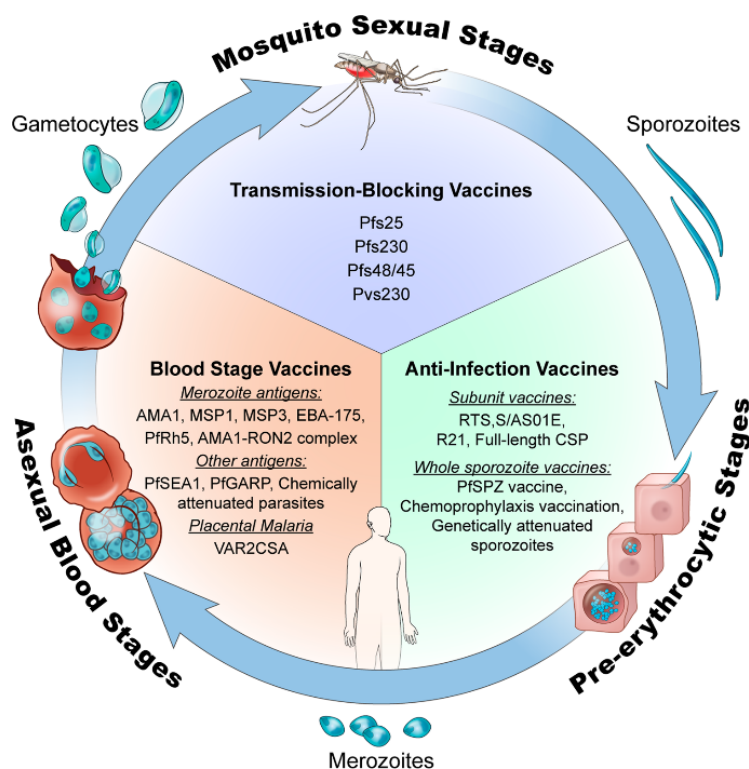


**Figure 7) Vaccine targets of *Plasmodium* stages.** Scheme describes different developmental stage of *Plasmodium* that can be targeted by vaccine candidates. (Duffy & Patrick Gorres, 2020)

### 1.3.3 Antimalarial drugs

Antimalarial drugs are a very important tool in the prevention (see section 1.3.1) and therapy of malaria disease. The WHO lists 14 drugs for malaria treatment and six agents for chemoprophylaxis, either applied as single or combination therapy in the WHO Model List of Essential Medicines (WHO, 2019b). Unfortunately, the success of antimalarial drugs is hampered by resistance of the parasite against all of the commercially used drugs. Development of new antimalarials, ranging from the modification of already existing drugs to the *de novo* synthesis of an efficient agent, is very laborious since they must be safe, highly effective, should be easy to apply and must be cheap (Burrows *et al.*, 2017). All these requirements are additionally complicated by the fact that the development of an antimalarial drug is relatively unprofitable for the pharmaceutical industry and hence there is very limited investment into the development of novel antimalarials. In 1999, the “Medicines for Malaria Venture” was founded in Switzerland, a non-profit product development partnership, which has the goal to reduce disease burden in malaria endemic countries (MMV Medicines for Malaria Venture, 2021). In collaboration with different

universities and pharmaceutical companies, this organization develops new antimalarial drugs for the treatment of malaria.

#### 1.3.3.1 Quinoline derivatives

Most of the commonly used drugs target the erythrocytic stages of *Plasmodium* parasites. Currently, there are four major drug classes on the market that target different specific processes of the parasite. The quinoline derivatives comprise a large group of agents (e.g. chloroquine, amodiaquine, quinine, mefloquine, piperazine, lumefantrine) that are either provided as single treatment or as combination therapy with other antimalarials, e.g. artemisinin derivatives. Quinolines and its derivatives target the hemoglobin digestion in the FV of the *Plasmodium* parasite by preventing the degradation byproduct heme from polymerizing into unreactive hemozoin crystals (Sullivan, 2002). This leads to the accumulation of toxic heme in the FV, causing parasite death. One of the most prominent representatives of this group is quinine, which was isolated from the cinchona tree in 1820 and was the first chemically purified agent used for the therapy of malaria. Another famous member is chloroquine, developed in 1934, which was widely used to treat all forms of malaria and was very well tolerated (F. Loeb *et al.*, 1946). Resistance to this drug was for the first time reported in the 1950s and was shown to be based on mutations in the *P. falciparum* chloroquine resistance transporter (*PfCRT*), resulting in an increased transport of chloroquine out of the FV (Payne, 1987; Fidock *et al.*, 2000; Wellems & Plowe, 2001).

#### 1.3.3.2 Antifolates

The second class of antimalarials are the antifolates. This group comprises the drugs sulfadoxine-pyrimethamine and atovaquone-proguanil, which target the essential folate metabolism of the parasite (Lumb *et al.*, 2011). Sulfadoxine-pyrimethamine is very inexpensive and thus substituted chloroquine as first-line treatment in various African countries. Unfortunately, widespread resistance results in total failure of the combination therapy (Curtis *et al.*, 1998; Christopher V. Plowe, 2001; Sibley *et al.*, 2001). However, in malaria-endemic African areas sulfadoxine-pyrimethamine is administered as intermittent preventive treatment during pregnancy (White, 2005; Zhao *et al.*, 2020).

### 1.3.3.3 Atovaquone

Atovaquone is another antimalarial that can be used in combination with the antifolate proguanil (Malarone™) either for prophylaxis or for treatment of malaria (Radloff *et al.*, 1996; Høgh *et al.*, 2000). This compound targets the cytochrome c oxidoreductase in mitochondria and results in the disruption of the mitochondrial membrane potential by inhibiting electron transport (Fry & Pudney, 1992; Vaidya & Mather, 2000).

### 1.3.3.4 Artemisinin and its derivatives

The most potent antimalarial drug at present is artemisinin and its derivatives (ART). Artemisinin is isolated from the plant *Artemisia annua*, a plant that has been used for long time in Chinese traditional medicine (Qinghaosu Antimalaria Coordinating Research Group, 1979). The Chinese researcher Youyou Tu was the first to extract artemisinin as the active ingredient from this herb in the 1970s and demonstrated its use as highly efficient antimalarial (Tu *et al.*, 1981; Tu, 2011). For her extraordinary work she was awarded with the Nobel Prize in Physiology and Medicine in 2015 (NobelPrize.org, 2015). To prevent resistance, artemisinin and its derivatives are provided in a combination therapy with a partner drug with a different mode of action compared to ART. The artemisinin combination therapy (ACT) consists of the short-acting artemisinin derivative (*in vivo* half-life ~ 1 hour in humans), resulting in a first major reduction of the parasite mass and a longer acting partner drug, clearing the remaining parasites circulating in the bloodstream (White, 2008b; Dondorp *et al.*, 2009; Enserink, 2010; White, 2013). The most common used combinations are artemether-lumefantrine, artesunate-amodiaquine and dihydroartemisinin-piperaquine. ACTs are recommended by the WHO as first-line treatment for uncomplicated *P. falciparum* malaria, but they are also used for the treatment of chloroquine-resistant *P. vivax* malaria (WHO, 2015). ACTs show a high efficacy in clearing the asexual blood stage parasites, but they are also active against gametocytes.

The most prominent artemisinin derivatives are artemether, artesunate and arteether, which are semi-synthetic plant prodrugs that are metabolized into the active metabolite dihydroartemisinin (DHA) (Eastman & Fidock, 2009). The antimalarial activity of artemisinin and its derivatives is dependent on an intramolecular endoperoxide bridge. Cleavage of this endoperoxide bridge is induced by hemoglobin degradation products (heme) in the FV which produces free radicals and reactive oxygen species that damage essential parasite proteins and lipids (Meshnick, 2002; Li & Zhou, 2010; Meunier & Robert, 2010; O'Neill *et*

*al.*, 2010; Klonis *et al.*, 2013; Wang *et al.*, 2015; Ismail *et al.*, 2016). This ART activation mechanism is further underlined by different studies, where hemoglobin degradation proteases (falcipains) were inhibited or inactivated, thus leading to a reduced hemoglobin digestion in the FV and subsequently less activated ART (Klonis *et al.*, 2011; Xie *et al.*, 2016). However, resistance to this drug also occurred (section 1.4) and the molecular basis has been elucidated (section 1.4.2).

## **1.4 Artemisinin resistance**

### **1.4.1 Definition of ART resistance and current situation worldwide**

Per definition by the WHO, parasites are resistant to ART when they are still detected by light microscopy on day three after combination therapy treatment or present an increased clearance half-life more than five hours after ACT treatment in the clinic (Flegg *et al.*, 2011; White, 2011b; World Health Organization, 2017). ART resistance is based on a reduced susceptibility of young ring stages to the drug, indicating that it is only a partial resistance (Witkowski & Khim *et al.*, 2013; Dogovski *et al.*, 2015).

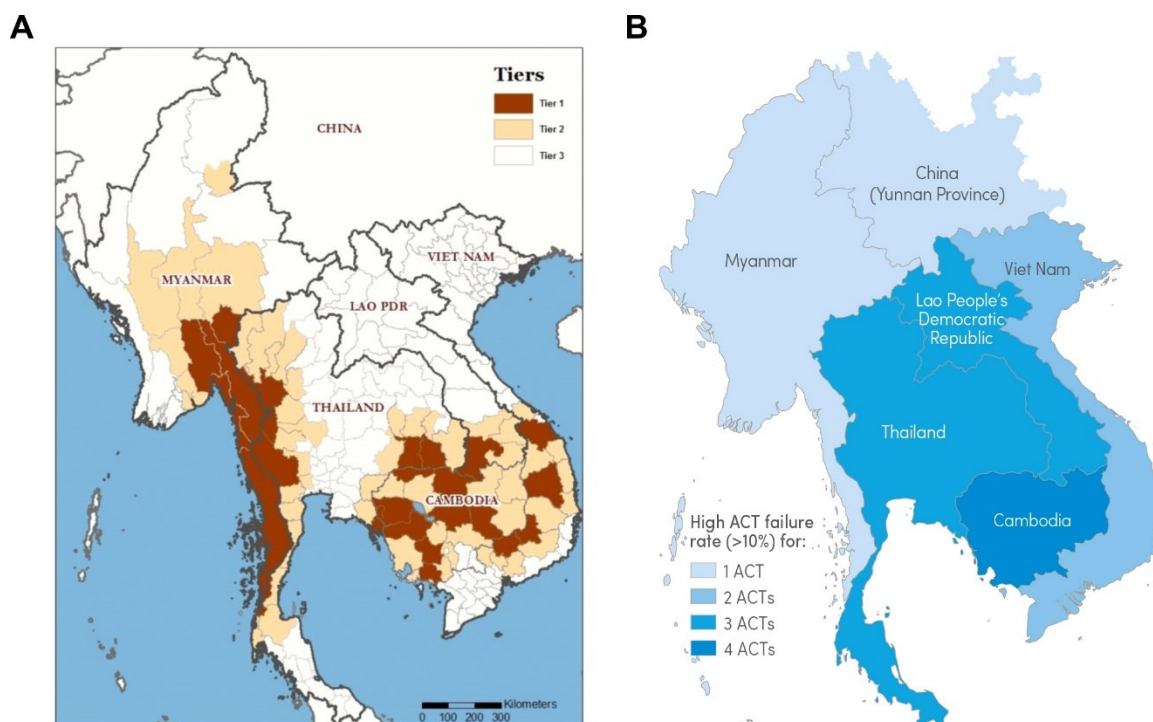


**Figure 8) Status of artemisinin resistance in 2014 and 2018.** (A) Status of ART resistance in 2014 where resistance was confirmed in five different countries of the Greater Mekong Subregion (GMS). (B) Number of ACTs failing to efficiently treat *P. falciparum* infection in the GMS in 2018 (failure rate > 10%). Currently five different ACTs are recommended by the WHO, and a sixth ACT is positively evaluated by the EMA in regions where all other combination therapies failed. Color code describes the number of failing ACTs in a distinct region. (modified from (WHO, 2014, 2018))

First evidence for ART resistance was found in Pailin, western Cambodia, in 2008 (Noedl *et al.*, 2008). Starting in western Cambodia, the resistance spread over the entire Greater Mekong Subregion (GMS) and by 2014 was also endemic in the Lao People's Democratic Republic, Myanmar, Thailand, and Viet Nam (Dondorp *et al.*, 2009; Amaratunga *et al.*, 2012; Hien *et al.*, 2012; Phyo *et al.*, 2012; Kyaw *et al.*, 2013; Ashley *et al.*, 2014) (Figure 8). Also at that time, a molecular marker of ART resistance was elucidated and confirmed to be causal for resistance in field isolates (see section 1.4.2) (Ariey *et al.*, 2014; Straimer *et al.*, 2015). To determine whether the decreased ART sensitivity developed independently at the different sites or originated from the same parasite strain in western Cambodia, the population structure was assessed based on genome sequencing and transcriptome data of different parasite isolates. These studies indicated that resistance in the GMS arose by both, clonal expansion, and *de novo* from a few founder populations (Miotto *et al.*, 2013; Miotto *et al.*, 2015; Imwong *et al.*, 2017; Zhu *et al.*, 2018). Besides the Southeast Asian subcontinent, ART resistance conferring mutations were also detected with low prevalence in South America and Oceania but at these sites there is little evidence for reduced parasite clearance after ACT treatment and treatment failures (Chenet *et al.*, 2016; WHO, 2019a).

Of major concern was the development of ART resistance in Africa and that resistance might spread from the Southeast Asian continent. For a long time, this seemed not to be the case and ART resistance conferring mutations were only sporadically detected in Africa and were without evidence for reduced parasite clearance or confirmed treatment failure (Mutabingwa *et al.*, 2005; Yeka *et al.*, 2005; Kanya *et al.*, 2007; Yeka *et al.*, 2008; WorldWide Antimalarial Resistance Network (WWARN) Lumefantrine PK/PD Study Group, 2015; Yeka *et al.*, 2016; Sagara *et al.*, 2018; Yeka *et al.*, 2019). One reasons for this may be that the partner drugs are still highly effective in African countries. Other reasons may be the overall high level of the population's immunity and the multiplicity of infection in malaria endemic African countries (Rosenthal, 2013). As it was shown that ART resistant strains display a reduced fitness level compared to sensitive parasites, resistance would mean a competitive disadvantage for parasites in the polyclonal African host environment (Rosenthal, 2013; Nair *et al.*, 2018). Unfortunately, current studies demonstrated the presence of ART resistance conferring mutations in Rwanda and found evidence for a link of this low prevalent genetic variation with reduced parasite clearance after ACT treatment in a therapeutic efficacy study (Uwimana *et al.*, 2020; Uwimana *et al.*, 2021). However, it was shown that this partial resistance established itself independently and did not spread from the Southeast Asian continent (Chenet *et al.*, 2016; Uwimana *et al.*, 2020).

## 1.4.2 Molecular markers of ART resistance

### 1.4.2.1 *Pf*Kelch13 as molecular marker of ART resistance

In 2014, a study performed by Arie *et al.* uncovered a molecular determinant of ART resistance. These authors selected an ART resistant parasite line by high doses of ART *in vitro* over several years and showed that the non-synonymous single nucleotide polymorphism (SNP) C580Y located in the propeller domain of the *P. falciparum* Kelch13 protein (*Pf*Kelch13; PF3D7\_1343700) is associated with delayed parasite clearance after ACT treatment as determined by a decreased ART sensitivity in the ring stage survival assay (RSA) (Arie *et al.*, 2014). Additionally, mutagenesis studies performed in ART-resistant field isolates underlined the fundamental role of *Pf*Kelch13 in the ART resistance pathway (Straimer *et al.*, 2015). The genomic information encoding the protein *Pf*Kelch13 is located on chromosome 13. The corresponding protein comprises 3 major functional domains (Figure 9): A N-terminal *Plasmodium*-specific sequence, followed by a BTB/POZ domain, a domain that in proteins of a similar domain structure was shown to be a regulator

of ubiquitin-directed degradation, and the C-terminal six blade Kelch propeller repeat that is predicted to serve as platform for protein-protein interactions (Ariey *et al.*, 2014). The C-terminal Kelch propeller region plays a key role in ART resistance. All so far known resistance conferring mutations are located in this repeat domain (WWARN K13 Genotype-Phenotype Study Group, 2019) (Figure 9).

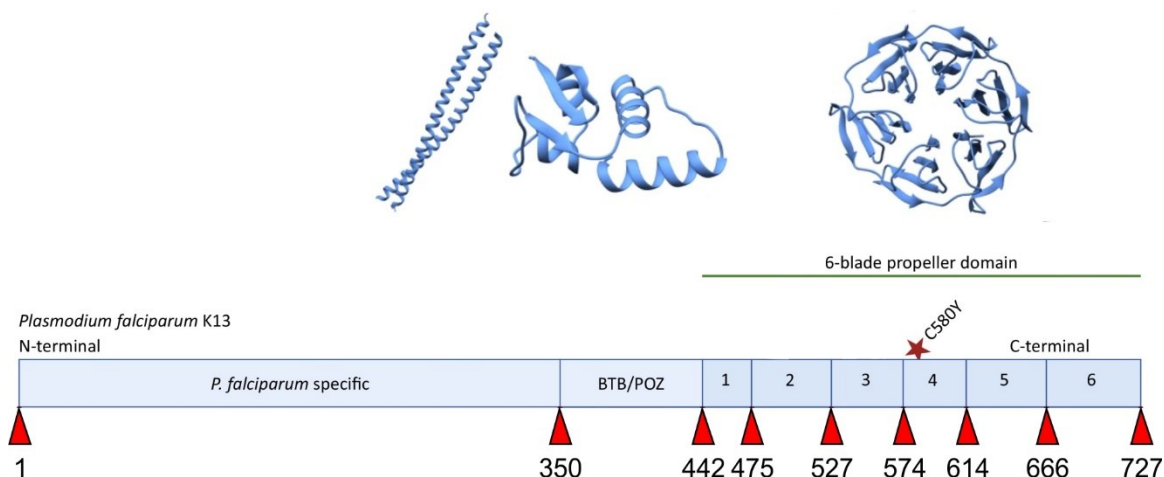


**Figure 9) Protein structure of *PfKelch13*.** (Top) Predicted 3D structure of different *PfKelch13* domains. (Bottom) Protein domains of *PfKelch13* consisting of an N-terminal parasite specific domain, a BTB/POZ domain and a C-terminal Kelch propeller domain. Red triangles indicate amino acid position. Position of ART resistance conferring mutation (C580Y) in the Kelch propeller domain is indicated. (modified from (Tilley *et al.*, 2016; Coppée *et al.*, 2019))

In order to measure ART resistance *in vitro*, the RSA is used to determine the *in vitro* survival rate of young ring stage parasites treated with a pharmacologically relevant ART pulse (dihydroartemisinin (DHA); 700 nM) for 6 hours (Figure 10). After removal of DHA and re-cultivation, the proportion of parasites that survived the drug exposure compared to the untreated control is determined by light microscopy of Giemsa-stained smears after 72 hours (Witkowski & Amaratunga *et al.*, 2013). The decreased *in vitro* drug sensitivity of young ring stages measured by RSA correlates with the observation of delayed parasite clearance in patients and a survival rate of 1% or higher is considered as clinically relevant resistance (Witkowski & Amaratunga *et al.*, 2013).

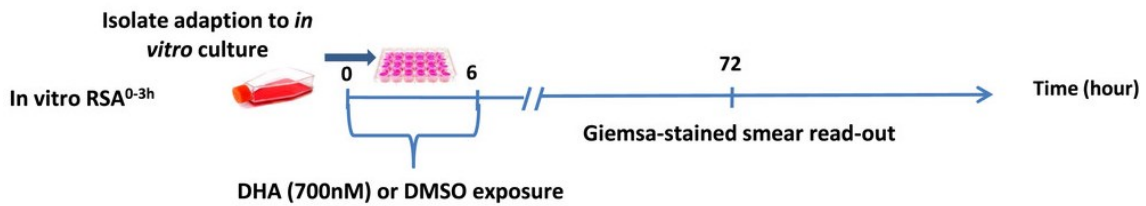


**Figure 10) Experimental procedure of standard *in vitro* RSA.** Young ring stage parasites are treated with 700 nM DHA for 6 hours. After DHA pulse, the drug is removed, and parasites are re-cultivated for another 66 hours. To assess the proportion of surviving parasites compared to the untreated culture, Giemsa smears are prepared 66 hours post DHA removal. (modified from (Niaré *et al.*, 2018)).

In general, a mutation is validated as molecular marker for ART resistance when this variation confers *in vitro* resistance in standard RSA and reduces the parasite clearance rate after treatment with an ACT in the patient (Witkowski & Amaratunga *et al.*, 2013; WHO, 2017b). The most dominant non-synonymous mutation present in Southeast Asia is the *PfKelch13* C580Y mutation (Ariey *et al.*, 2014). Interestingly, this mutation was also found in Guyana and Papua New Guinea, as well as in Africa where it was not associated with delayed parasite clearance after ACT treatment and displayed only a low prevalence level (< 5%) (Maiga *et al.*, 2012; Ouattara *et al.*, 2015; Chenet *et al.*, 2016; Miotto *et al.*, 2020). The most dominant *pfkelch13* variation in Africa is the SNP resulting in an A578S amino acid change that is present in at least 22 African countries and emerged independently in the different regions (Ménard *et al.*, 2016). This mutation was not associated with a reduced ART-sensitivity (WWARN K13 Genotype-Phenotype Study Group, 2019).

Over the years several different *pfkelch13* SNPs were detected worldwide, and a meta-analysis published in 2019 validated 20 mutations as potential molecular markers for ART resistance (WWARN K13 Genotype-Phenotype Study Group, 2019). Out of those, multiple *pfkelch13* polymorphisms from Southeast Asia were found to confer ART resistance. In contrast, most of the mutations detected in African field isolates do not change the sensitivity to ART and genetic analysis of the corresponding parasites showed only minor local selection of *pfkelch13* mutations (general prevalence lower than 5%) (Kamau *et al.*, 2015; Taylor *et al.*, 2015; MalariaGEN Plasmodium falciparum Community Project, 2016; Ménard *et al.*, 2016). Two recently published studies demonstrated the emergence of ART resistance in Rwanda, validating the *pfkelch13* mutation R561H as molecular marker associated with reduced *in vivo* parasite clearance (Uwimana *et al.*, 2020; Uwimana *et al.*, 2021).

#### 1.4.2.2 *PfKelch13* independent mutations contributing to ART resistance

Beside non-synonymous *pfkelch13* mutations, allelic variations in other candidate genes are suspected to play a role in ART resistance. Data from genotyping assays and Sanger sequencing of culture-adapted Cambodian clinical *P. falciparum* isolates indicated that parasites lacking *pfkelch13* mutations can also be less susceptible to ART as indicated by RSA (Mukherjee *et al.*, 2017).

In the murine parasite strain *P. chabaudi*, mutations in an orthologue of the *P. falciparum* ubiquitin-specific protease-1 (*pfubp1*) were shown to mediate ART resistance (Hunt *et al.*, 2007; Hunt *et al.*, 2010b). The *pfubp1* mutations, V2697F and V2728F, were also tested in *P. falciparum*, as well as *P. berghei*, and rendered parasites resistant to ART in both cases (Henrici *et al.*, 2019; Simwela *et al.*, 2020). Interestingly, one of the allelic variations (V2728F) also led to a reduced sensitivity against chloroquine, mefloquine and lumefantrine (Hunt *et al.*, 2007; Hunt *et al.*, 2010b; Borges *et al.*, 2011; Kinga Modrzynska *et al.*, 2012). Genome wide association studies (GWAS) performed in coastal Kenya also implicate *pfubp1* in ART resistance, as did an analysis of field isolates from Northwestern Thailand which resulted in the identification of different candidate mutations in *pfubp1* that may be involved in reduced ART susceptibility (Borrmann *et al.*, 2013; Cerqueira *et al.*, 2017). In another Kenyan study, *P. falciparum* field isolate samples were obtained from children suffering from malaria and displayed delayed parasite clearance after ACT treatment. These samples were genetically analyzed and also there *pfubp1* mutations were detected, further increasing the evidence for a potential involvement of this candidate gene in ART resistance (Henriques *et al.*, 2014).

In addition to mutations in *pfubp1*, variant alleles of the AP2 adaptor complex  $\mu$ -chain (*pfap2 $\mu$* ) were detected in the study conducted in Kenya (Henriques *et al.*, 2014). Initially, this candidate was suggested as a genetic marker for ART resistance in the *P. chabaudi* rodent malaria model (Henriques *et al.*, 2013). The SNP, resulting in the non-synonymous amino acid change I568T, in AP2 $\mu$  was found to be associated with delayed parasite clearance under laboratory conditions in *P. chabaudi* and this was also confirmed in *P. falciparum* but was not detected in parasites from infected individuals in the field (Henriques *et al.*, 2013; Henriques *et al.*, 2014; Henrici *et al.*, 2019). Another mutation in PfAP-2 $\mu$  (S160N/T) was identified in field isolates obtained from Kenyan children treated with ACTs and found to reduce sensitivity towards ART (Henriques *et al.*, 2014). This mutation was also shown to simultaneously reduce the susceptibility to quinine, chloroquine and lumefantrine (Henriques *et al.*, 2015).

In both cases, *pfubp1* and *pfap2μ*, parasite susceptibility to ART was reduced, while at the same time the sensitivity to potential partner drugs like mefloquine or lumefantrine was also changed.

A further gene implicated in ART resistance is the *Plasmodium* protein coronin. This protein is important for parasite motility by modulating the actin cytoskeleton (Olshina *et al.*, 2015; Bane *et al.*, 2016). In a long-term *in vitro* selection process with increasing concentrations of ART with a West African parasite strain, three *pfcoronin* mutations (G50E / R100K / E107V) were identified and validated by introducing them into the parental strain using CRISPR/Cas9. These variant alleles were then shown to reduce parasite susceptibility to ART by RSA (Demas *et al.*, 2018). In other studies, further mutations were identified *in vitro*, but none the coronin mutations have so far been found to be present in parasites from the field (Sharma *et al.*, 2019; Velavan *et al.*, 2019; Sharma *et al.*, 2020).

Other candidates that are potential markers for ART resistance are *pfeps15* (also annotated as *pfformin2*) and *pfmyosinF* (previously annotated as *pfmyosinC*). These candidates were identified by whole genome sequencing of patient samples collected in Northwestern Thailand. Analysis of long-term changes in allele frequencies revealed two mutations (*PfMyosinF*: N277S; *PfEps15*: K447R) that might be involved in ART resistance, but these mutations were so far not specifically tested *in vitro* for their ability to modulate ART sensitivity (Cerqueira *et al.*, 2017).

### 1.4.3 Mechanism of ART resistance

The molecular mechanism of ART resistance is widely debated. So far, it had been unclear how *PfKelch13* is involved in ART resistance (Dogovski *et al.*, 2015; Mbengue *et al.*, 2015; Mok *et al.*, 2015; Rocamora *et al.*, 2018).

One hypothesis suggests the upregulation of the unfolded protein response (UPR) as possible mechanism rendering parasites resistant to ART (Mok *et al.*, 2015). These authors analyzed the transcriptional profile of ART resistant isolates. Besides a delay of the intraerythrocytic development in young ring stages, parasites showed an upregulation of two major chaperon complexes that are involved in the UPR pathway (Mok *et al.*, 2015). Two other studies support the finding of an enhanced cellular stress response in ART resistance. Kinetic analysis and comparison of Cambodian wildtype and mutant *PfKelch13* isolates revealed and ART induced growth delay in these parasites and showed an increase of ubiquitinated proteins, suggesting and upregulation of the cellular stress response and

activation of the ubiquitin-mediated proteasomal degradation system in ART treated parasites (Dogovski *et al.*, 2015). A second study investigated the transcriptome of ART resistant isogenic 3D7 *P. falciparum* lineages obtained by long-term ART exposure (Rocamora *et al.*, 2018). These parasites did not contain *PfKelch13* mutations but were moderately resistant to ART and were proposed to achieve this through an increased capacity to handle oxidative stress during ART treatment. Such a function in resistance would be in line with the role of the closest homologues of *PfKelch13* in other systems, e.g. the human Kelch-like proteins (KLHLs) that function as adapters to E3 ubiquitin ligases (Adams *et al.*, 2000; Furukawa *et al.*, 2003; Zhang *et al.*, 2004; Arieu *et al.*, 2014). However, the variety of substrates of KLHLs and their function is very broad (Lee & Yuan *et al.*, 2010; Tseng & Bixby, 2011; Dhanoa *et al.*, 2013; Shi *et al.*, 2019). Hence, the potential substrate regulated by *PfKelch13* cannot be predicted based on the sequence similarity to KLHLs alone. This link to the cellular stress response based on sequence similarity of *PfKelch13* to KLHLs (Arieu *et al.*, 2014; Tilley *et al.*, 2016) is therefore rather tentative.

In the same year, as Mok *et al* and Dogovski *et al* postulated an upregulated unfolded protein response and enhanced cellular stress response as potential mechanisms of ART resistance, Mbengue *et al* provided data that indicated an increased level of phosphatidylinositol-3-phosphate (PI3P) to mediate ART resistance (Mbengue *et al.*, 2015). In this model, PI3P is generated by the phosphatidylinositol-3-kinase (PI3K) that was by this work indicated as a binding partner for wildtype *PfKelch13*. At the same time, PI3K is also target of the activated ART. *PfKelch13*-PI3K binding regulates the amount of PI3P and parasite growth. In contrast, mutant *PfKelch13* is unable to bind PI3K which leads to an increased PI3P level in the parasite. This higher PI3P level prepares the parasite to counteract the inhibition of PI3K through ART and survive the drug treatment.

In a recently published paper, *PfKelch13* was found to be important for the endocytosis of host cell hemoglobin by the parasite and this was investigated as a potential mechanism to regulate ART resistance (Birnbaum *et al.*, 2020). In a prior study, chemical inhibition of the hemoglobinases (falcipains) as well as genetic knockdown and knockout strategies indicated an importance of hemoglobin digestion for the resistance mechanism (Xie *et al.*, 2016). Another study, analyzing the proteomic, peptidomic and metabolic profiles of ART resistant field isolates revealed that in resistant strains the abundance of hemoglobin-derived peptides was reduced (Siddiqui *et al.*, 2017). Birnbaum *et al* defined a new intracellular compartment by identifying interacting partners of the *PfKelch13* protein (Birnbaum *et al.*, 2020). In a proximity biotinylation approach combined with quantitative mass spectrometry, several proteins were identified that were found to locate in foci in the cell together with Kelch13. This included homologues of proteins that in other organisms

are involved in endocytosis (e.g. *PfEps15*, *PfAP-2μ*), or had previously been suspected in ART resistance, e.g. *PfUBP1* (Tebar *et al.*, 1996; Hunt *et al.*, 2007; McMahon & Boucrot, 2011; Cerqueira *et al.*, 2017; Kadlecova *et al.*, 2017; Kaksonen & Roux, 2018). Besides these candidates, several other proteins were detected as potential interacting partners of *PfKelch13*, such as *PfMyosinF* and the *Plasmodium* metacaspase-2 (*PfMCA2*) (Birnbaum *et al.*, 2020). However, so far, it is not known if the latter two proteins indeed co-locate with *PfKelch13*, and the function of these proteins remains unclear. Initial work already showed that parasites with a disrupted *pfmca2* gene displayed a reduced sensitivity to ART (Birnbaum *et al.*, 2020).

## 1.5 Aims of the present thesis

Previous studies indicated that besides *PfKelch13*, other factors contribute to ART resistance (Hunt *et al.*, 2007; Borrmann *et al.*, 2013; Henriques *et al.*, 2013; Cerqueira *et al.*, 2017; Mukherjee *et al.*, 2017; Demas *et al.*, 2018). Using a novel version of BioID and quantitative mass spectrometry, a compartment containing various potential interaction partners of *PfKelch13* was identified (Birnbaum *et al.*, 2020). This analysis resulted in a list of high confidence hits which were mostly of unknown function and were named KICs (Kelch interacting candidates). Interestingly, this list also included proteins that had previously been suspected in ART resistance, such as *PfUBP1* or *PfEps15*, but also several proteins - e.g. *PfMCA2* and *PfMyosinF* - that had remained functionally uncharacterized in *P. falciparum* so far.

The aim of the thesis was to gain more insight in the newly defined Kelch13 compartment and its proteins and their role in resistance. In particular the aim was to analyze the potential *PfKelch13* interacting candidates *PfMCA2* and *PfMyosinF* in detail since they remain uncharacterized in *P. falciparum* to date. Moreover, a further goal was to assess whether different non-synonymous mutations in *PfKelch13* and in the potential *PfKelch13* compartment members mediate ART resistance in *P. falciparum*. Due to the prevalence of a few well defined *PfKelch13* mutations associated with resistance in Southeast Asia and the scarcity of such mutations in Africa, an additional focus of this thesis was non-synonymous SNPs that are mainly prevalent in Africa. The final aim was to investigate the resistance phenotype of ART resistant *PfKelch13* parasites and to assess the influence of specific mutations on parasite fitness.

## 2 Material

### 2.1 Antibodies

#### 2.1.1 Primary antibodies

Antigen	Dilution and application	Source
$\alpha$ -aldolase (rabbit)	1:2000 for WB	
$\alpha$ -GFP (mouse)	1:2000 for WB	Roche, Mannheim
$\alpha$ -HA (rabbit)	1:500 for IFA	
$\alpha$ -HA (rat)	1:500 for IFA 1:1000 for WB	Roche, Mannheim
$\alpha$ -RFP (rat)	1:500 for IFA	Chromotek, München

#### 2.1.2 Secondary antibodies

Antigen	Dilution and application	Source
$\alpha$ -rabbit HRP	1:2500 for WB	Molecular probes
$\alpha$ -rabbit 488	1:2000 for IFA	Molecular probes
$\alpha$ -mouse HRP	1:3000 for WB	Dianova
$\alpha$ -rat HRP	1:3000 for WB	Dianova
$\alpha$ -rat Alexa 594	1:2000 for IFA	Molecular probes

### 2.2 Bacteria and *Plasmodium* strains

*Escherichia coli* (XL-10 Gold)

Tet<sup>r</sup>  $\Delta(mcrA)$  183  $\Delta(mcrCB-hsdSMRmrr)$   
173 *endA1 supE44 thi-1 recA1 gyrA96*  
*relA1 lac Hte* [F' *proAB lacI<sup>q</sup> Z  $\Delta$ M15 Tn10*  
(Tet<sup>r</sup>) Amy Cam]

*Plasmodium falciparum* (3D7)

Clone of NF54 isolate (MRA-1000) from a malaria patient near Amsterdam airport (Walliker *et al.*, 1987)

## 2.3 Chemicals

Acrylamide solution (30%)	AppliChem GmbH, Darmstadt
Acetone	Roth, Karlsruhe
Agar LB (Lennox)	Roth, Karlsruhe
Agarose	Invitrogen, Karlsruhe
Albumax II	Gibco, Life Technologies, USA
Albumin bovine Fraction V (BSA)	Biomol, Hamburg
Ammonium persulfate (APS)	AppliChem GmbH, Darmstadt
Ampicillin	Roche, Mannheim
Bacto™ Pepton	Becton Dickinson, Heidelberg
Bacto™ yeast extract	Becton Dickinson, Heidelberg
β-Mercaptoethanol	Merck, Darmstadt
Blasticidin S	Invitrogen
Bromphenol blue	Roth, Karlsruhe
Concovalin A	Sigma Aldrich, Steinheim
Cytochalasin D	Calbiochem, Darmstadt
Desoxynucleotides (dNTPs)	Thermo Scientific, Lithuania
Developer solution G150 (Western Blot)	Agfa, Leverkusen
4',6-diamidino-2-phenylindole (DAPI)	Roche, Mannheim
Dihydroartemisinin (DHA)	AdipoGen Life Sciences
Dihydroethidium (DHE)	Cayman, Ann Arbor, USA
Dimethyl sulfoxide (DMSO)	Sigma-Aldrich, USA
Dipotassium phosphate	Roth, Karlsruhe
Disodium phosphate	Roth, Karlsruhe
1,4-dithiothreitol (DTT)	Roche, Mannheim
DSM1	BEI resources
Dulbecco's Phosphate Buffered Saline	PAN Biotech, Aidenbach
Ethanol	Roth, Karlsruhe
Ethidium bromide	Roth, Karlsruhe
Ethylenediaminetetraacetic acid (EDTA)	Biomol, Hamburg
Ethylene glycol tetraacetic acid (EGTA)	Biomol, Hamburg
Formaldehyde (10%)	Polyscience, Warrington PA, USA
G418 disulfate salt	Sigma Aldrich, Steinheim
Gentamycin	Ratiopharm, Ulm

Giemsa's azure, eosin, methylene blue solution	Merck, Darmstadt
D-Glucose	Merck, Darmstadt
Glutardialdehyd (25%)	Roth, Karlsruhe
Glycerol	Merck, Darmstadt
Glycine	Biomol, Hamburg
Hoechst33342	Cheomdex, Switzerland
(4-(2-Hydroxyethyl)-1-piperazineethanesulfonicacid) (HEPES)	Roche, Mannheim
Hydrochloric acid (HCl)	Merck, Darmstadt
Hypoxanthin	Biomol, Hamburg
Isopropanol	Roth, Karlsruhe
Magnesium chloride (MgCl <sub>2</sub> )	Merck, Darmstadt
Manganese (II) chloride (MnCl <sub>2</sub> )	Merck, Darmstadt
Methanol	Roth, Karlsruhe
Milk powder	Roth, Karlsruhe
3-(N-morpholino)propansulfonic acid (MOPS)	Sigma Aldrich, Steinheim
N, N, N, N-Tetramethylethylenediamin (TEMED)	Merck, Darmstadt
Percoll	GE Healthcare, Sweden
Phenylmethylsulfonylfluorid (PMSF)	Sigma Aldrich, Steinheim
Potassium chloride	Merck, Darmstadt
Protease inhibitor cocktail ("Complete Mini")	Roche, Mannheim
Rapalog (A/C Heterodimerizer AP21967)	Clontech, Mountain View, USA
Rubidium chloride	Sigma Aldrich, Steinheim
RPMI (Roswell Park Memorial Institute)-Medium	AppliChem, Darmstadt
Saponin	Sigma Aldrich, Steinheim
Sodium acetate	Merck, Darmstadt
Sodium chloride	Gerbu, Gaiberg
Sodium bicarbonate	Sigma Aldrich, Steinheim
Sodium dodecyl sulfate (SDS)	AppliChem, Darmstadt
Sodium dihydrogen phosphate	Roth, Karlsruhe
Sodium hydroxide	Merck, Darmstadt
Sorbitol	Sigma Aldrich, Steinheim
Tris base	Roth, Karlsruhe
Tris-EDTA (TE)	Invitrogen, Karlsruhe
Triton X-100	Biomol, Hamburg
Water for molecular biology (Ampuwa)	Fresenius Kabi, Bad Homburg

WR99210

Jacobus Pharmaceuticals,  
Washington, USA

## 2.4 DNA and protein ladders

GeneRuler™ 1000 bp ladder

Thermo Scientific, Schwerte

PageRuler™ Plus Prestained Protein Ladder  
(10 to 250 kDa)

Thermo Scientific, Schwerte

PageRuler™ Prestained Protein Ladder  
(10 to 180 kDa)

Thermo Scientific, Schwerte

## 2.5 Enzymes and polymerases

### 2.5.1 Restriction endonucleases

AvrII

New England Biolabs, Ipswich

BamHI-HF®

New England Biolabs, Ipswich

DpnI

New England Biolabs, Ipswich

KpnI- HF®

New England Biolabs, Ipswich

MluI- HF®

New England Biolabs, Ipswich

NotI- HF®

New England Biolabs, Ipswich

Sall- HF®

New England Biolabs, Ipswich

XhoI

New England Biolabs, Ipswich

### 2.5.2 Polymerases

FirePol DNA Polymerase [5 U/μl]

Solis Biodyne, Taipei

Phusion® High-Fidelity DNA Polymerase [2 U/μl]

New England Biolabs, Ipswich

### 2.5.3 Oligonucleotides

All oligonucleotides are listed in Appendix C

Sigma Aldrich, Steinheim

## 2.6 Kits

NucleoSpin. Extract II	Macherey-Nagel, Düren
NucleoSpin. Plasmid	Macherey-Nagel, Düren
QIAamp DNA Mini Kit	Qiagen, Hilden
QIAGEN Plasmid Midi Kit	Qiagen, Hilden
Western Blot ECL-Clarity Detection Kit	Bio-Rad, München
Western Blot ECL-SuperSignal West Pico	Thermo Scientific, Schwerte

## 2.7 Labware and disposables

Type	Specification	Distributor
Conical falcon tubes	15 ml, 50 ml	Sarstedt, Nümbrecht
Cryotubes	1.6 ml	Sarstedt, Nümbrecht
Culture bottles	50 ml	Sarstedt, Nümbrecht
Disposable pipette tips	1-10/20-200/100-1000 µl	Sarstedt, Nümbrecht
Filter tips	1-10/20-200/100-1000 µl	Sarstedt, Nümbrecht
Flow cytometry tubes	55.1579	Sarstedt, Nümbrecht
Glass cover slips	24x55 mm thickness 0.13-0.16 mm	R. Langenbrinck, Emmerdingen
Glass slides		Engelbrecht, Edermünde
Gloves, latex powder-free		Kimtech Science EcoShield
IFA glass slides	10 wells ER-208B-CE24; 6.7 mm	Thermo Scientific, USA
Leukosilk tape		BSN medical
Microscopy dishes, uncoated, hydrophobic		Ibidi, Martinsried
Multiply-µStrip Pro 8-Strip PCR reaction tubes		Sarstedt, Nümbrecht
Nitrocellulose blotting membrane Protean	Amersham 0.45 µm	GE Healthcare
One-way canulas		Braun, Melsungen
One-way syringe		Braun, Melsungen
Parafilm		Bemis, USA

Pasteur pipettes		Brand, Wertheim
Petri dishes	15x60 mm/14x90 mm	Sarstedt, Nümbrecht
Plastic pipettes	5/10/25 ml	Sarstedt, Nümbrecht
Reaction tubes	1.5/2 ml	Sarstedt, Nümbrecht Eppendorf, Hamburg
Scalpel		Braun, Melsungen
Sterile filter	0.22 µm	Sarstedt, Nümbrecht
Transfection cuvettes	0.2 cm	Bio-Rad, München
12-well cell culture plate		Sarstedt, Nümbrecht

## 2.8 Plasmids

Plasmid	Source
pSLI-3xHA (pARL1-3xHA-T2A-Neo <sup>R</sup> )	Mesen-Ramirez
pSLI-TGD (pARL1-GFP-T2A-Neo <sup>R</sup> )	Birnbaum Nat Comm 2017
pSLI-N-GFP-2xFKBP-loxP (DSM1 <sup>R</sup> )	Birnbaum Nat Comm 2017
<i>nmd3</i> 5'UTR_mCherry-Kelch13 (DSM1 <sup>R</sup> )	Birnbaum Nat Comm 2017
<i>nmd3</i> 5'UTR_chromobody (DSM1 <sup>R</sup> )	Sabitzki
<i>crt</i> 5'UTR_1xNLS-FRB-T2A-P40-mCherry (DSM1 <sup>R</sup> )	Flemming

## 2.9 Solutions, media, and buffer

### 2.9.1 Microbiological culture

10x LB stock solution	10% NaCl 5% peptone 10% yeast extract in dH <sub>2</sub> O, autoclaved
LB medium	1% (w/v) NaCl 0.5% (w/v) peptone 1% (w/v) yeast extract in dH <sub>2</sub> O in dH <sub>2</sub> O
LB Agar plate solution	1.5% Agar-Agar 1x LB medium
Ampicillin stock solution	100 mg/ml in 70% ethanol

Glycerol freezing solution	50% (v/v) glycerol in 1x LB medium
TFBI buffer	30 mM acetic acid 50 nM MnCl <sub>2</sub> 100 mM RbCl 10 mM CaCl <sub>2</sub> 15% (v/v) glycerol pH 5.8 (with 0.2 N acetic acid)
TFBII buffer	10 mM MOPS 75 mM CaCl <sub>2</sub> 10 mM RbCl 15% (v/v) glycerol pH 7.0 (with NaOH)

## 2.9.2 Molecular biological buffers and solutions

<u>DNA gel electrophoresis</u>	50x TAE	2 M Tris base 1 M Pure acetic acid 0.05 M EDTA pH 8.5
	6x Loading buffer	40% Glycerol (v/v) 2.5% (w/v) Xylene cyanol 2.5% (w/v) Bromophenol blue in dH <sub>2</sub> O
<u>DNA precipitation</u>	Sodium acetate	3 M NaAc, pH 5.2
	Tris-EDTA (TE) buffer	10 mM Tris-HCl pH 8.0 1 mM EDTA pH 8.0
<u>Gibson assembly buffers</u>	5x isothermal reaction buffer	3 ml 1 M Tris-HCl pH 7.5 150 µl 2 M MgCl <sub>2</sub> 60 µl each of 100 mM dGTP/dATP/dTTP/dCTP 300 µl 1 M DTT 1.5 g PEG-8000 300 µl 100 nM NAD ad 6 ml dH <sub>2</sub> O
	Assembly master mixture (1.2 ml)	320 µl 5x isothermal reaction buffer 0.64 µl 10 U/µl T5 exonuclease 20 µl 2 U/µl Phusion DNA polymerase 160 µl 40 U/µl Taq DNA ligase

ad 1.2 ml dH<sub>2</sub>O**2.9.3 Biochemical buffers and solutions**

10x Running buffer	29 g Tris base (24 mM) 144 g Glycine (192 mM) 10 g SDS (3.5 mM)
Separating gel buffer (buffer A)	1.5 M Tris 0.4% SDS pH 8.8
Stacking gel buffer (buffer B)	0.5 M Tris 0.4% SDS pH 6.8
Separating gel (10%) ( $\Sigma$ 10 ml; 2 gels)	4 ml dH <sub>2</sub> O 2.7 ml 1.5 M Tris pH 8.8 (buffer A) 3.3 ml 30% acrylamide 6 $\mu$ l TEMED 100 $\mu$ l 10% APS
Separating gel (8%) ( $\Sigma$ 10 ml; 2 gels)	4.8 ml dH <sub>2</sub> O 2.5 ml 1.5 M Tris pH 8.8 (buffer A) 2.7 ml 30% acrylamide 6 $\mu$ l TEMED 100 $\mu$ l 10% APS
Separating gel (6%) ( $\Sigma$ 10 ml; 2 gels)	5.3 ml dH <sub>2</sub> O 2.7 ml 1.5 M Tris pH 8.8 (buffer A) 2 ml 30% acrylamide 6 $\mu$ l TEMED 100 $\mu$ l 10% APS
Stacking gel ( $\Sigma$ 5 ml; 2 gels)	2.9 ml dH <sub>2</sub> O 1.25 ml 0.5 M Tris pH 6.8 (buffer B) 830 $\mu$ l 30% acrylamide 5 $\mu$ l TEMED 50 $\mu$ l 10% APS
Ammonium persulfate (APS)	10% (w/v) in dH <sub>2</sub> O
4x SDS sample buffer	3 ml 0.5 M Tris pH 6.8 2 ml dH <sub>2</sub> O 5 g sucrose 0.32 g SDS
10x Transfer Buffer	30.3 g Tris base 144.1 g glycine 3.7 g SDS

1x Transfer buffer + 20% methanol	1:10 dilution of 10x Transfer Buffer 20% methanol
-----------------------------------	--

#### 2.9.4 Cell biological buffers, media, and solutions (*P. falciparum* *in vitro* culture)

RPMI complete medium	1.587% (w/v) RPMI 1640 12 mM NaHCO <sub>3</sub> 6 mM D-Glucose 0.5% (v/v) Albumax II 0.2 mM Hypoxanthine 0.4 mM Gentamycin pH 7.2 in dH <sub>2</sub> O, sterile filtered
Synchronization solution	5% (w/v) D-Sorbitol in dH <sub>2</sub> O, sterile filtered
Parasite freezing solution	4.2% (w/v) D-Sorbitol 0.9% (w/v) NaCl 28% (v/v) Glycerol in dH <sub>2</sub> O, sterile filtered
Parasite thawing solution	3.5% (w/v) NaCl in dH <sub>2</sub> O, sterile filtered
Transfection buffer (Cytomix)	120 mM KCl 150 μM CaCl <sub>2</sub> 2 mM EGTA 5 mM MgCl <sub>2</sub> 10 mM K <sub>2</sub> HPO <sub>4</sub> /KH <sub>2</sub> PO <sub>4</sub> 25 mM HEPES pH 7.6 in dH <sub>2</sub> O, sterile filtered
Amaxa transfection buffer	90 mM NaPO <sub>4</sub> 5 mM KCl 0.15 mM CaCl <sub>2</sub> 50 mM HEPES pH 7.3 in dH <sub>2</sub> O, sterile filtered
WR99210 stock solution	20 mM WR99210 in DMSO
WR99210 working solution	1:1000 dilution of stock solution in RPMI complete medium sterile filtered
Blasticidin S (BSD) working solution	5 mg/ml BSD in RPMI complete medium sterile filtered

---

G418 working solution	50 mg/ml in RPMI complete medium sterile filtered
DSM1 stock solution (50x)	187.5 mM DSM1 in DMSO
DSM1 working solution	100 µl DSM1 stock solution ad 5 ml in 95% DMSO / 5% 1x PBS solution
Human red blood cells	Bloodgroup 0+, sterile concentrate, Blood bank Universitätsklinikum Eppendorf (UKE) Hamburg
Percoll stock solution	90% (v/v) Percoll 10% (v/v) 10x PBS
80% Percoll solution%	89% (v/v) Percoll stock solution 11% (v/v) RPMI complete medium 4% (w/v) sorbitol sterile filtered
60% Percoll solution	67% (v/v) Percoll stock solution 33% (v/v) RPMI complete medium 4% (w/v) sorbitol sterile filtered
40% Percoll solution	44% (v/v) Percoll stock solution 56% (v/v) RPMI complete medium 4% (w/v) sorbitol sterile filtered
Saponin solution for selective membrane permeabilization	0.03% Saponin in DPBS
Parasite lysis buffer	4% SDS 0.5% Triton 0.5x PBS in dH <sub>2</sub> O
Cytochalasin D working solution	10 µM Cytochalasin D in DMSO
E64 inhibitor working solution	33 µM in dH <sub>2</sub> O
DHA stock solution (250 µM)	1.1 mg DHA powder in 15 ml DMSO
DHA working solution (125 µM)	1:2 dilution of DHA stock solution in 1xPBS/DMSO (1:10)
DHE stock solution (10x)	5 mg DHE in 1 ml DMSO

DHE working solution (1x)	0.5 mg DHE in 1 ml DMSO
Hoechst33342 stock solution (10x)	4.5 mg Hoechst33342 in 1 ml DMSO
Hoechst33342 working solution (1x)	0.45 mg Hoechst33342 in 1 ml DMSO
FACS stop solution	0.5 µl Glutaraldehyde (25%) in 40 ml RPMI complete medium
Rapalog (AP21967) stock solution	500 mM Rapalog in ethanol
Rapalog working solution	1:20 dilution of stock solution in RPMI complete medium
Giemsa staining solution	1:10 dilution of stock solution in H <sub>2</sub> O
Fixing solution (formaldehyde/glutaraldehyde IFA)	2 ml formaldehyde 10% 1.5 µl glutaraldehyde 25% 500 µl 10x PBS ad dH <sub>2</sub> O to 5 ml total volume

## 2.10 Technical devices

Type	Specification	Distributor
Agarose gel chamber	Sub Cell GT basic	Bio-Rad, München
Analytical Balance	870	Kern
Blot device Gel holder cassettes Foam pads Electrode assembly Cooling unit	Mini Protean Tetra Cell System	Bio-Rad, München
Centrifuge	Megafuge 1.0R J2 HS Ultracentrifuge Rotor JA-12 Avanti J-26S XP Rotor JA-14	Hereaus, Hannover Beckmann Coulter, Krefeld
Table centrifuge	Eppendorf 5415 D	Eppendorf, Hamburg
Casting gel stuff Casting stand	Mini Protean	Bio-Rad, München

Casting plates		
Casting frames		
12-well combs		
Confocal microscope	Olympus FV1000	Olympus, Hamburg
Developer	ChemiDoc XRS+	Bio-Rad, München
Electrophoresis chamber	Mini Protean 67s	Bio-Rad, München
Electroporator	Gene Pulser X-Cell Nucleofector II AAD-1001N	Bio-Rad, München Amaza Biosystems, GER
Flow cytometer	LSR II	BD Instruments, USA
Ice machine	EF 156 easy fit	Scotsmann, Venon Hills, USA
Bacterial incubator	Thermo function line	Hereaus, Hannover
<i>P. falciparum</i> cell culture incubator	Heratherm IGS400	Thermo Scientific, Langenselbold
Shaking incubator	Max Q4000	Barnstead, Iowa, USA
Light microscope	Axio Lab A1	Zeiss, Jena
Fluorescence microscope	Axioscope M1/M2	Zeiss, Jena
Hamamatsu digital camera	Orca C4742-95	Hamamatsu Phototonics K.K., Japan
Microwave	Micro 750W	Whirlpool, China
Laboratory scale	Acculab Atilon-ATL	Sartorius, Göttingen
PCR mastercycler	epgradient	Eppendorf, Hamburg
pH meter	SevenEasy	Mettler-Toledo, Gießen
Photometer	NanoDrop	
Pipettes	1-10/200/1000 µl	Gilson, Middleton, USA
Pipettor	Pipetboy acu	IBS, USA
Power supply	EV31 Power Source 300V	Consort, Belgium VWR, Taiwan
Roller mixer	STR6	Stuart
Sterile bench	Steril Gard III Advance Safe 2020	Baker, Stanford, USA Thermo Scientific, Pinneberg
Thermoblock	Thermomixer compact	Eppendorf, Hamburg
Ultrapure water purification system	Milli-Q	Millipore, Bedford, USA
UV transilluminator	PHEROlum289	Biotec Fischer, Reiskirchen

Vacuum pump	BVC Control	Vacuubrand, Deutschland
Vortexer	VF2	Jank & Kunkel IKA Labortechnik
Waterbath	1083	GFL, Burgwedel

## 2.11 Bioinformatic tools and databases

Bioinformatic tool / database	Source
InterPro	<a href="https://www.ebi.ac.uk/interpro/">https://www.ebi.ac.uk/interpro/</a>
MalariaGEN	<a href="https://www.malariagen.net/">https://www.malariagen.net/</a>
MotifScan	<a href="http://myhits.isb-sib.ch/cgi-bin/motif_scan">http://myhits.isb-sib.ch/cgi-bin/motif_scan</a>
NCBI databases	<a href="https://www.ncbi.nlm.nih.gov/">https://www.ncbi.nlm.nih.gov/</a>
PlasmoDB	<a href="http://plasmodb.org/plasmo/">http://plasmodb.org/plasmo/</a>
PubMed	<a href="http://www.ncbi.nlm.nih.gov/pubmed">http://www.ncbi.nlm.nih.gov/pubmed</a>
WWARN	<a href="https://www.wwarn.org/">https://www.wwarn.org/</a>

## 2.12 Computer software

A plasmid Editor (ApE)	Open source ( <a href="https://jorgensen.biology.utah.edu/wayned/ape/">https://jorgensen.biology.utah.edu/wayned/ape/</a> )
Axio Vision 40 v4.7.0.0	Zeiss, Jena
Corel DRAW X8 (64-bit)	Corel Corporation, Ottawa
Corel PHOTO-PAINT X8 (64-bit)	Corel Corporation, Ottawa
FlowJo	Becton, Dickinson Company
GraphPad Prism 9	GraphPad Software, La Jolla, USA
ImageJ 1.53e	Wayne Rasband and contributors, NIH, USA
Image Lab v 5.2.1. build 11	Bio-Rad Laboratories, München
Imaris x64 7.8	Bitplane AG, Zürich, Switzerland
Microsoft Office 2020	Microsoft Corporations, Redmond, USA

### 3 Methods

#### 3.1 Molecular biological methods

##### 3.1.1 Polymerase chain reaction (PCR)

DNA product was amplified from 3D7 gDNA using two different DNA polymerases. The Phusion-high fidelity polymerase (NEB) has a proof-reading function and was mainly used to amplify DNA sequences with high need of accuracy, e.g. cloning of plasmids for parasite transfection. The second polymerase was the FIREPol polymerase (Solis Biodyne) which was used to amplify very long DNA sequences or was used to perform analytical PCRs like colony screens or integration checks, where no proof-reading function is needed. For each PCR amplification, the annealing or elongation time, as well as the respective temperature was adjusted. The basic settings for the PCR amplification and the PCR program are listed below. After PCR amplification, the PCR products were analyzed by gel electrophoresis to check the size of the amplified fragment.

Phusion PCR		FIREPol PCR	
5x Phusion buffer	10 µl	10x FIREPol buffer B	5 µl
dNTP`s	5 µl	dNTP`s	5 µl
Primer fw (1:10 dilution)	1 µl	MgCl <sub>2</sub>	4 µl
Primer rv (1:10 dilution)	1 µl	Primer fw (1:10 dilution)	2.5 µl
Phusion DNA polymerase	0.3 µl	Primer rv (1:10 dilution)	2.5 µl
Template	0.3 µl	FIREPol DNA polymerase	0.25 µl
dH <sub>2</sub> O	32.4 µl	Template	0.3 µl
		dH <sub>2</sub> O	30.75 µl

PCR program (Phusion)				PCR program (FIREPol)		
Denaturation	94°C	2 min	1 cycle	Denaturation	95°C	3 min
Denaturation	94°C	20 sec	30 cycles	Denaturation	95°C	40 sec
Annealing	43°C	30 sec		Annealing	43°C	45 sec
Elongation	63°C	*		Elongation	63°C	*
	72°C	4 min				

\* Time was adapted to the size of fragment.

### **3.1.2 Agarose gel electrophoresis (Garoff & Ansorge, 1981)**

To check the size of the DNA fragments either amplified by PCR or digested vector, a 1% agarose gel in 1xTAE buffer containing 1 µg/ml ethidium bromide was used. DNA fragments are separated in an electric field according to their length and negatively charged backbone. The agarose gel was prepared by dissolving the agarose (Invitrogen) in 1x TAE buffer to a final concentration of 1%. To melt the agarose, the solution was carefully heated in a microwave until the total amount of agarose was dissolved. The agarose solution was cooled, and ethidium bromide was added to a final concentration of 1 µg/ml. The agarose gel was poured into a gel tray, a 26-slot comb was added, and gel was cooled until it was completely polymerized. The solid agarose gel was then placed into the electrophoresis chamber, which was filled with 1x TAE buffer, covering the whole gel with liquid. DNA samples were diluted in 6x loading dye and were pipetted into the slots. Additionally, DNA ladder was added to check the size of the DNA fragment. Electrophoretic separation was performed for 25 – 30 min at 150 V. After separation, agarose gel was analyzed using the Chemidoc XRS+.

### **3.1.3 Clean-up of PCR product or digested plasmids**

Either the PCR product, or digested plasmid fragments were purified according to manufacturer protocol using the NucleoSpin Extract II Kit (Macherey-Nagel). The purified PCR product, or fragmented plasmid was eluted in 30 µl elution buffer (buffer AE) and stored at -20°C.

### **3.1.4 Enzymatic digestion of PCR products and plasmids**

Enzymatic digestion using different endonucleases was used for three different scenarios: For the cloning process, the vectors were digested with suitable restriction endonucleases to create sticky ends which enable ligation process. Moreover, to deplete residual methylated DNA, PCR products amplified from plasmid template (MINI or MIDI) were digested with the endonuclease DpnI for 1 hour at 37°C. In addition, restriction digest was

used to perform an analytical digest of MINI preparation product to exclude recombination events and check the correct size of the plasmid. Master mix for enzymatic digest is listed below. Both, the cloning vector, as well as the test digestion mix were incubated for 2.5 hours at 37°C.

Digestion for cloning		Test digestion	
10x CutSmart® Buffer (NEB)	5 µl	10x CutSmart® Buffer (NEB)	1 µl
Restriction enzyme	1 µl	Restriction enzyme	0.2 µl
Template (PCR product/vector)	10 µl	Template (MINI/vector)	2 µl
dH <sub>2</sub> O	ad 50 µl	dH <sub>2</sub> O	ad 10 µl

### 3.1.5 DNA ligation by Gibson assembly

DNA ligation via Gibson assembly is a one-step isothermal DNA assembly that enables the simultaneous ligation of 6 different inserts at a time (Gibson *et al.*, 2009). For an efficient ligation, no sticky ends but overlapping homologous regions at both ends of the insert of 15 – 35 bp are needed. When a PCR product was amplified from plasmid DNA, PCR product was digested with DpnI prior to ligation to deplete methylated DNA. The ligation mix is listed below, and Gibson mix was incubated at 50°C for 1 hour.

Gibson assembly	
Gibson mix	7.5 µl
pre-digested vector DNA	1 µl
PCR product	0.5 µl
dH <sub>2</sub> O	ad 10 µl

### 3.1.6 Colony-PCR to screen bacterial clones

After transformation (see 3.2.2), the bacterial clones were screened by PCR to detect single clones that carry the correct plasmid. For this, 10 µl FIREPoI PCR mix per tested clone were prepared, using an insert specific and a plasmid specific primer to detect the correct clones. The corresponding PCR mix is listed below. A single clone was picked using a pipette tip, plated onto a fresh pre-warmed LB ampicillin plate, and inoculated in 10 µl prepared PCR

mix. Per construct at least 10 single clones were screened. After PCR amplification, the size of the products controlled by agarose gel electrophoresis (see 3.1.2).

FIREPol PCR	
10x FIREPol buffer B	5 $\mu$ l
dNTP`s	5 $\mu$ l
MgCl <sub>2</sub>	4 $\mu$ l
Primer fw	2.5 $\mu$ l
Primer rv	2.5 $\mu$ l
FIREPol DNA polymerase	0.25 $\mu$ l
Template	0.3 $\mu$ l
dH <sub>2</sub> O	30.75 $\mu$ l

PCR program (FIREPol)			
1 cycle	Denaturation	95°C	3 min
25 cycles	Denaturation	95°C	40 sec
	Annealing	43°C	45 sec
	Elongation	63°C	*

\* Time was adapted to the size of fragment.

### 3.1.7 Sequencing of plasmids

To exclude recombination events or mutations, the plasmid isolated from a single bacterial clone was sent to Seqlab for sequencing. For this, ~40 ng/ $\mu$ l MINI preparation was mixed with 2  $\mu$ l premixed primer specific to the desired genomic sequence and adjusted with dH<sub>2</sub>O to a final volume of 15  $\mu$ l in an Eppendorf tube. The sequencing samples were then sent to Seqlab, Göttingen for sequence check.

### 3.1.8 DNA precipitation

After MIDI preparation, DNA was diluted in 200  $\mu$ l TE buffer and DNA concentration was determined by spectrometry. For transfection of *P. falciparum* either 50  $\mu$ g (merozoite

transfection) or 100 µg (ring transfection) DNA were needed. The respective MIDI volume containing 50 / 100 µg DNA was mixed with 1:10 volume sodium acetate 3 M, pH 5.0 and precipitated with three volumes of absolute ethanol. After this step, the precipitation mix was centrifuged at 16 000 g for 10 min and supernatant was carefully discarded. The pellet was washed once using 50 µl ethanol 70% and the mix was centrifuged again at 16 000 g for 5 min. After removal of the supernatant, the DNA pellet was air-dried under sterile conditions. For ring transfection, the air-dried DNA pellet was dissolved in 15 µl TE buffer and 385 µl cytomix. For schizont transfection, the DNA pellet was resuspended in 10 µl TE buffer and 90 µl Amaxa transfection buffer. The precipitated DNA was stored at -20°C until transfection.

### **3.1.9 Isolation of *P. falciparum* genomic DNA for integration check**

To check the correct integration of a plasmid into the endogenous locus of *P. falciparum*, genomic DNA (gDNA) was isolated from the parasite. For this, 5 -10 ml of *P. falciparum* cell culture were harvested containing a high trophozoite parasitemia. The parasite culture was pelleted at 1800 rpm for 5 min and supernatant was discarded. To store the parasite pellet and continue the gDNA isolation at a later time, the pellet was mixed with 20 µl proteinase K and frozen at -20°C. When the gDNA isolation was directly performed, the pelleted *Plasmodium* culture was processed according to manufacturer's protocol using the QIAamp DNA Mini Kit. After completion of the protocol, gDNA was dissolved in 200 µl TE buffer and stored at -20°C.

### **3.1.10 Integration check using PCR**

PCR amplification was used to check the correct integration of a construct into *Plasmodium* DNA. For this, genomic DNA was isolated from parasite cell culture (see 3.1.9) and PCR mix was prepared using FIREPol polymerase. For each approach 10 µl total master mix volume was prepared. The master mix and PCR program are listed below. To check the genetic integration, three different primer combinations were used. To confirm correct 5'UTR integration, a forward primer specific for the upstream region of the modified gene locus was combined with a reverse primer specific for the construct. The 3'UTR integration was tested using a forward primer, specific for the construct and a reverse primer, specific for a sequence downstream of the 3' end of the modified locus. To check depletion of original

locus in the modified parasites, the 5` forward primer, specific for the upstream region of the modified locus was combined with the 3`reverse primer, specific for a sequence downstream of the modified locus. After PCR amplification, the size of the DNA fragments was analyzed by agarose gel electrophoresis (see 3.1.2).

FIREPol PCR	
10x FIREPol buffer B	5 µl
dNTP`s	5 µl
MgCl <sub>2</sub>	4 µl
Primer fw	2.5 µl
Primer rv	2.5 µl
FIREPol DNA polymerase	0.25 µl
Template	0.3 µl
dH <sub>2</sub> O	30.75 µl

PCR program (FIREPol)			
1 cycle	Denaturation	95°C	3 min
25 cycles	Denaturation	95°C	40 sec
	Annealing	45°C	45 sec
	Elongation	61.5°C	*

\* Time was adapted to the size of fragment.

### 3.1.11 Sequencing of *P. falciparum* field isolates

During the Fever without source study, conducted at the Presbyterian Hospital of Agogo in Ghana between 2014 and 2015, *Plasmodium* gDNA from field isolates was purified from patient blood samples. To sequence the genome of these field isolates and to check for mutations in different loci, sequence specific primers were designed (see Appendix C). For this, the genomic sequences of the target genes were subdivided into sections of 3000 bp including the respective 5`UTR region and 3`UTR regions. For PCR amplification of the sections, primers for outer and nested PCR were designed. Additionally, primers for sequencing were designed. Here, the 3000 bp sections were subdivided again into fragments of ~300 bp. When PCR product was amplified, the DNA was cleaned up using the NucleoSpin Extract II Kit (Macherey-Nagel) and DNA fragments were sequenced either

in-house or PCR products were sent to SeqLab for sequencing (PCR amplification, in-house sequencing, and preparation of SeqLab performed by Birgit Förster). For SeqLab, ~15 ng/ $\mu$ l PCR product were mixed with 2  $\mu$ l of the specific sequencing primer and dH<sub>2</sub>O was added to a final volume of 15  $\mu$ l. The results of the sequencing were compared to the original genomic sequences to search for potential mutations.

## 3.2 Microbiological methods

### 3.2.1 Preparation of chemical competent *E. coli* bacteria (Hanahan, 1983)

To chemically prepare the *E. coli* bacteria for the transformation, the rubidium-chloride method was used, resulting in highly competent cells ready for plasmid uptake. A glycerol stock of XL-10 gold *E. coli* bacteria was inoculated in 20 ml LB medium, and bacteria were grown overnight in a 50 ml falcon. Here, the lid of the 50 ml falcon was not fully closed to supply the bacteria with a sufficient amount of fresh air. The next day, 8 ml of the overnight bacteria culture were given into 200 ml fresh, prewarmed LB medium and the culture was cultivated in a shaker at 750 rpm until the XL-10 gold *E. coli* reached an optical density (OD) of 0.5 to 0.6. When the correct optical density was achieved, the bacteria were cooled down rapidly on ice and centrifuged at 2400 g for 10 to 20 minutes (min) at 4°C. After this step, the bacteria pellet was resuspended in 60 ml TFB I buffer and incubated for 10 min on ice. The bacteria suspension was pelleted again (2400 g for 10 to 20 min at 4°C), supernatant was discarded, and the bacteria pellet was resolved in TFB II buffer. This *E. coli* suspension was then aliquoted in 100  $\mu$ l aliquots and stored at -80°C.

### 3.2.2 Transformation of chemical competent XL-10 gold *E. coli*

Before starting the transformation procedure, a fresh LB agar plate (containing ampicillin selection marker) was pre-warmed at 37°C in the incubator and an aliquot of XL-10 gold bacteria was thawed on ice for at least 15 min. For transformation, the total amount of prepared Gibson assembly mix (see 3.1.5) was added to the competent bacteria, mixed carefully, and put on ice for 10 min. In case of a re-transformation, 0.3  $\mu$ l of diluted plasmid (1:1000 in dH<sub>2</sub>O) was added to the XL-10 gold suspension and also incubated on ice for 10 min. The ice incubation period was followed by a heatshock at 42°C for 30 seconds (sec) after which, the transformation mix was incubated for another 10 min on ice. After the

second incubation, the bacteria were plated on the pre-warmed LB agar plate containing ampicillin. LB agar plates were incubated overnight at 37°C in the bacteria incubator. Next day, correct bacteria clones were detected via colony PCR screening (see 3.1.6) and a master plate of these clones was prepared and grown overnight at 37°C.

### **3.2.3 Overnight culture of transformed *E. coli* clone for plasmid purification**

A correct, single bacteria clone was detected by colony PCR screen and confirmed by sequencing (see 3.1.7), picked with a pipette tip from the LB agar master plate, and inoculated in fresh LB medium containing the antibiotic ampicillin. For a MINI precipitation, 2 ml LB ampicillin medium were prepared in an Eppendorf tube, while for MIDI precipitation 200 ml LB ampicillin medium were prepared in an Erlenmeyer flask. The MINI bacteria culture was incubated on a thermo shaker at 37°C, 750 rpm overnight and the MIDI bacteria culture was shaken at 37°C and 170 rpm overnight. Next day, the bacteria cultures, MINI or MIDI, were pelleted and either directly purified or stored at -20°C until the next precipitation was performed.

### **3.2.4 Freezing of *E. coli* culture**

For a plasmid-backup, a glycerol stock of the overnight culture containing a single *E. coli* clone was prepared. Here, 500 µl of the overnight culture were pelleted and the bacteria pellet was resuspended in 1 ml LB glycerol medium and stored immediately at -80°C.

### **3.2.5 Plasmid purification (MINI and MIDI preparation)**

To purify ~20 µg plasmid DNA via a MINI preparation, an overnight bacteria culture from a single clone was prepared, as described in section 3.2.3. The 2 ml MINI bacteria culture was pelleted by centrifugation at 11 000 g for 1 min, the supernatant was discarded, and bacteria pellet was processed according to the manufacturer protocol of using the NucleoSpin Plasmid Kit (Macherey-Nagel). After plasmid purification, DNA concentration was measured using the NanoDrop. The correctness of the plasmid was confirmed by a test digestion using the suitable restriction enzymes and the MINI plasmid DNA was sent for sequencing to SeqLab to exclude potential inserted mutations (see 3.1.7).

Higher amounts of plasmid DNA were isolated and prepared for parasite transfection using a MIDI preparation kit. For this, 200 ml overnight bacteria culture of a single, correct bacteria clone was prepared as described in section 3.2.3. The next day, the overnight culture was centrifuged at 6000 rpm, for 15 min at 4°C and the pellet was processed according to the manufacturer protocol using the Plasmid MIDI Kit (QIAGEN). After the plasmid purification, the DNA pellet was dissolved in 200 µl TE buffer and DNA concentration was determined by spectrometry.

### 3.3 Cell biological methods

#### 3.3.1 Cultivation of *P. falciparum* (Trager & Jensen, 1976)

Continuous cultivation of *P. falciparum* parasites was performed according to standard procedures (Trager & Jensen, 1976). Asexual blood stage parasites were grown at 37°C in 15 x 60 mm Petri dishes (5 ml RPMI complete medium) or 14 x 90 mm Petri dishes (10 ml RPMI complete medium) and atmosphere was adjusted to 1% O<sub>2</sub>, 5% CO<sub>2</sub>, 94% N<sub>2</sub>. Parasites were cultured in RPMI complete medium with 0.5% Albumax, human erythrocytes (blood group 0+) at a hematocrit of 5%. Every second day parasite cultures were smeared, diluted, or fed to keep parasitemia between 0.1% - 5%, and supplied with fresh blood and medium to avoid parasite starvation. In case of high parasitemia, RPMI medium was changed daily. Transgenic parasites were selected using 4 nM WR99210, 2 µg/ml blasticidin S or 0.9 µM DSM1.

#### 3.3.2 Preparation of blood smears and Giemsa staining of parasite cultures

To determine parasitemia during continuous *Plasmodium* culturing, blood smears were taken from the cultures and stained with Giemsa staining solution. Additionally, blood smears were used to determine the proportion of surviving parasites at 72 hours in a standard ring stage survival assay (RSA). For the blood smears, ~0.5 µl parasite culture were taken and dropped on a glass slide. A thin smear was prepared using a second glass slide, and thin blood smear was air-dried. The dry thin smears were fixed in methanol (100%) for 20 sec and stained in Giemsa solution (10% in H<sub>2</sub>O) for 15 min. After staining, the glass slides were rinsed with fresh tap water and air-dried. Parasitemia was assessed by light microscopy.

### 3.3.3 Freezing of *P. falciparum* culture for storage

For storage, parasite cell lines were frozen either at -80°C or in liquid nitrogen. Thus, only ring stage parasites will survive the freezing process, a parasite culture containing high ring parasitemia was prepared for freezing. For cryopreservation, 5 – 10 ml of cell culture were harvested and pelleted at 2000 rpm for 5 min. After centrifugation, the supernatant was removed, and the pellet was resuspended in 1 ml parasite freezing solution. The parasite solution was pipetted into a 2 ml cryotube, labelled and frozen either at -80°C or in liquid nitrogen for long-term storage.

### 3.3.4 Thawing of *P. falciparum* cryo-stabilates

To re-cultivate a parasite line after cryopreservation, the cryo-stabilates were thawed in a water bath at 37°C for 2 – 3 min. The thawed cell lines were transferred into a 2 ml Eppendorf tube and centrifuged at 3500 rpm for 1.5 min. The supernatant was discarded, and the pellet was carefully dissolved in parasite thawing solution. After another centrifugation step, the pellet was washed in fresh RPMI complete medium and centrifuged again. The parasite pellet was resuspended in 5 ml of fresh RPMI complete medium, placed in a Petri dish and fresh human blood was adjusted to a hematocrit of 5%. For transgenic parasites grown under drug pressure, selective drug was added on the second day after thawing.

### 3.3.5 Synchronization of asexual parasite culture

The synchronization of parasites is important for different experiments but is also necessary for the preparation of *P. falciparum* parasites for transfection. To synchronize an asexual parasite culture, two different approaches can be used.

Synchronization of parasites to 0 – 18 hours ring stages can be achieved by lysis of mature stages via 5% D-sorbitol (Lambros & Vanderberg, 1979). Here, the parasite culture was transferred to a 15 ml Falcon tube and pelleted at 2000 rpm for 5 min. The parasite pellet was resuspended in pre-warmed D-sorbitol solution (1 ml D-sorbitol for 5 ml culture and 2 ml D-sorbitol for 10 ml culture) and incubated in the water bath at 37°C for 7 min. After incubation, the cell culture was centrifuged at 2000 rpm for 5 min and pellet was washed

twice in fresh RPMI complete medium to remove leftover D-sorbitol. After washing, the parasite pellet was resuspended in fresh RPMI medium and recultivated in a Petri dish.

To synchronize an asexual parasite culture for schizonts, a Percoll gradient was used. Here the different parasite stages were separated due to their differences in permeability (Aley *et al.*, 1986). For this, 4 ml Percoll solution (60%) was pipetted into a 15 ml Falcon tube and 10 ml of asexual *Plasmodium* culture were carefully layered onto the Percoll solution without mixing parasite culture and Percoll. Layered parasite culture was centrifuged at 2000 rpm for 8 min. After centrifugation, a dark ring was visible between a medium layer and a Percoll layer containing schizont stage parasites. At the bottom of the Falcon tube a pellet containing the ring stage parasites was visible. The medium was carefully removed and the parasite layer including the Percoll layer was transferred into a fresh 15 ml Falcon. Parasites were washed in 10 ml fresh RPMI medium and after washing, the schizont pellet was pipetted into an Eppendorf tube containing 300  $\mu$ l fresh human blood and 500  $\mu$ l RPMI complete medium. The Eppendorf tube was placed on a thermo shaker and parasite culture was incubated for 30 min at 37°C, 600 rpm. After shaking, parasites were re-cultivated in a Petri dish and incubated at 37°C.

### 3.3.6 Transfection of *P. falciparum* parasites via electroporation

The correct plasmids were transfected in *P. falciparum* using electroporation. In general, two different methods were used to transfect the *Plasmodium* parasites. For the transfection of ring stage parasites (Fidock & Wellems, 1997), 100  $\mu$ g DNA were precipitated per transfection and resuspended in TE buffer and cytomix (see 3.1.8). The asexual parasite culture was grown to a high parasitemia between 5 – 10%, and the culture was synchronized via D-sorbitol to deplete later developmental stages. The synchronized culture was centrifuged at 2000 rpm for 5 min and supernatant was discarded. The pellet containing the ring stage parasites was resuspended in prepared DNA-cytomix solution, transferred into an electroporation cuvette (2 mm, Bio-Rad). For electroporation, the Gene Pulser Xcell (program: 310 V, 950  $\mu$ F,  $\infty$   $\Omega$ ) was used. After electroporation, the parasite culture was transferred into a fresh Petri dish and supplied with RPMI complete medium. The selection drug was added 24 hours after transfection of the parasites and medium was changed daily for the first week, and afterwards every second day.

For transfection of late schizont stages (Moon *et al.*, 2013), parasite culture was synchronized using 60% Percoll two days prior to the transfection (see 3.3.5). The DNA (50  $\mu$ g in TE buffer and Amaxa transfection buffer) was precipitated as described in 3.1.8. On

the day of transfection, the synchronous culture was synchronized again using 60% Percoll and the isolated schizont pellet was mixed with the prepared DNA mix, and transferred into an electroporation cuvette (2 mm, Bio-Rad). For the electroporation, the Amaxa system (Nucleofector II AAD-1001N, program: U-033) was used. After electroporation, the parasite mix was pipetted into a 1.5 ml Eppendorf tube containing 500  $\mu$ l fresh RPMI complete medium and 300  $\mu$ l fresh human blood. The Eppendorf tube was incubated on a thermo shaker for 30 min at 37°C and 600 rpm to support invasion of merozoites into new red blood cells. After shaking, the parasite culture was pipetted into a Petri dish and selection drug was added 24 hours later. For one week, medium was changed daily and afterwards every second day.

### 3.3.7 Selection of transgenic parasites via selection linked integration (SLI)

Transgenic parasites were selected by using SLI (Birnbaum *et al.*, 2017). For this, transgenic asexual *Plasmodium* cultures were selected with WR99210 for the presence of episomal construct and were grown to a parasitemia of 4 – 6%. The selection marker G418 was added to a final concentration of 400  $\mu$ g/ml. In case of yDHODH resistance, 0.9  $\mu$ M DSM1 were used for selection process. For the first seven days, RPMI complete medium containing the respective drug was changed daily and parasitemia was checked the latest on day three for surviving parasites. After the first week, medium was changed every second day and the culture was checked regularly every week for growing parasites until transgenic cultures came up again. In case of reappearing parasites, parasite culture was harvested, gDNA was isolated via the QIAamp DNA Mini Kit (see 3.1.9), and integration check was performed by PCR to confirm the correct integration of the construct in the genomic locus of the parasites (see 3.1.10). If residue of original locus were still traceable in the transgenic parasite culture, selective pressure, using either G418 or DSM1, was continued for another two weeks, after which the integration check was repeated. In general, the selection process was performed for up to three months and checked continuously for reemerging parasites. In case there were no reappearing parasites detected, cultures were discarded after this time.

### 3.3.8 Saponin lysis of *P. falciparum* infected erythrocytes

The detergent saponin is used to selectively permeabilize the membrane of the red blood cell, as well as the PVM. Due to its special lipid composition, the PPM around the parasite stays intact (Benting *et al.*, 1994; Ansorge *et al.*, 1996). Saponin lysis was performed to release the *Plasmodium* parasite from the RBC and deplete hemoglobin from parasite extract. For this, 10 ml parasite culture containing a high parasitemia of the desired developmental stage were harvested and centrifuged at 4000 g for 5 min. After this, the supernatant was removed and the pellet was washed once in 10 ml 1xPBS (room temperature, RT) and centrifuged again. The supernatant was discarded, and parasite pellet was resuspended in 5 ml ice-cold 0.03% saponin solution and incubated on ice for 10 min. Next, the parasite culture was pelleted at 4000 g for 15 min and the pellet was transferred to a 2 ml Eppendorf tube and centrifuged at maximum speed for 3 min. The pellet was washed with ice-cold 1xPBS until supernatant was clear and free of hemoglobin. Meanwhile, a master mix containing 450  $\mu$ l lysis buffer and 50  $\mu$ l PIC inhibitor was prepared. After washing the pellet, it was resuspended in the lysis buffer / PIC mix (volume dependent on the size of the pellet) and 1 – 2  $\mu$  PMSF was added and incubated on ice. The parasite suspension was centrifuged, and supernatant (in case of soluble proteins) was transferred into a fresh 1.5 ml Eppendorf tube. The supernatant was mixed with 30  $\mu$ l 4x SDS + 1 M DTT and samples were heated at 85°C for 5 min. In case of the *Pf*Kelch13 proteins, the saponin samples were not heated at 85°C for 5 min but treated with pre-warmed 4x SDS + 1 M DTT solution to avoid depletion of the protein. For SDS-PAGE, 10  $\mu$ l sample and 8  $\mu$ l marker were loaded onto the gel. In general, saponin samples could be stored at -20°C after heating to 85°C, but for *Pf*Kelch13 SDS-PAGE must be performed immediately after saponin pellet preparation to avoid depletion of the protein.

### 3.3.9 Inactivation of parasite proteins by knock sideways system

For inactivation of a target protein, the knock sideways system was used (Haruki *et al.*, 2008; Robinson *et al.*, 2010; Xu *et al.*, 2010). An asexual parasite culture was split into two parts, 2 ml culture were kept as control and 2 ml culture were treated with 250 nM rapalog (A/C heterodimerizer AP21967, Clontech). After 1, 2, 4, and 22 hours a Giemsa smear of the cultures was prepared (see 3.3.2) and assessed by light microscopy and additionally slides were prepared for fluorescence microscopy to estimate target mislocalization via live cell imaging.

### 3.3.10 Flow cytometry-based growth assay

To estimate the growth of a cell line after inactivation of a target protein, a flow cytometry-based growth assay was performed over a period of 5 days. To start the growth assay, the parasitemia of an asexual parasite culture was measured by flow cytometry (Malleret *et al.*, 2011). For this, the parasite cells (20  $\mu$ l) were stained for 20 min at room temperature with a master mix containing 80  $\mu$ l RPMI complete medium, 1  $\mu$ l Hoechst33342 (final concentration: 4.5  $\mu$ l/ml) working solution and 1  $\mu$ l DHE (0.5  $\mu$ g/ml) working solution. After 20 min, the staining was stopped by adding 400  $\mu$ l of 0.003% glutaraldehyde in RPMI complete medium. Measurement was performed using the LSR flow cytometer and the FACSDiva (BD). In total, 100 000 events were counted to estimate the parasitemia of the culture. After measuring the parasitemia, the parasite culture was adjusted to 0.1% parasitemia and split into two 2 ml Petri dishes. One dish was kept untreated as control, while to the other dish 250 nM rapalog (A/C heterodimerizer AP21967, Clontech) was added. Parasites were re-cultivated at 37°C and every 24 hours, parasitemia was measured by flow cytometry for 4 further days (5 days in total) to assess the impact of the mislocalization of a target protein on parasite growth. Medium and rapalog were changed daily, and additional Giemsa smears were taken each day.

### 3.3.11 *In vitro* ring-stage survival assay<sup>0-3h</sup> (RSA)

The standard ring-stage survival assay was performed to test whether parasites are resistant to ART. RSAs were performed as previously described (Witkowski & Amaratunga *et al.*, 2013). Percoll gradient (60%) was used to isolate mature schizonts from an asynchronous parasite culture containing 4 – 6% schizonts (see 3.3.5). The mature schizonts were allowed to invade fresh red blood cells (2 ml volume; 2.5% hematocrit per sample, meaning a hematocrit of 5% for control and DHA fraction in total) at 37°C for three hours in a 6 well plate and were then synchronized again in a 2 ml Eppendorf tube using 1 ml 5% D-sorbitol per tube to obtain ring stage parasites at the age of 0 – 3 hours (see 3.3.5). The rings were washed in a 2 ml Eppendorf tube twice with 1 ml fresh RPMI complete medium (3700 g; 1.5 min) and split in two fractions (2 ml volume per fraction in a 6 well plate; 2.5% hematocrit per sample). One part was treated with 700 nM DHA for 6 hours, whereas the other fraction was left untreated as control. For a standard RSA, after the 6 hours drug pulse, DHA was removed by washing the samples three times, each with 1 ml fresh RPMI complete in a 2 ml Eppendorf tube. After washing, the parasites were re-

cultivated for another 66 hours in a 6-well plate (2 ml volume) and Giemsa smears were prepared after 72 hours to determine the proportion of parasites that survived the DHA treatment (see 3.3.2). For control, at least 80 parasites and for DHA-treated fraction at least 150 panels were counted. To estimate parasite survival, parasitemia of the control was compared to the parasitemia of the DHA treated fraction. Parasites were defined as resistant, when mean survival rate exceeded the cut-off value of 1% (Witkowski & Amaratunga *et al.*, 2013).

To assess the effect of inactivation of a special target protein on the survival rate, the standard RSA was slightly modified. For this, parasites were cultured in the presence (inactivation via knock sideways system) or absence (control) of 250 nM rapalog (A/C heterodimerizer AP21967, Clontech). The start of knock sideways was induced depending on the respective target protein. For *Pf*UBP1 and *Pf*KIC7, inactivation was initiated 1 hour, for *Pf*AP-2 $\mu$  and *Pf*2102 7 hours, for 3D7, *Pf*Kelch13 and *Pf*MyosinF 12 hours, for *Pf*Eps15 18 hours, and additionally for *Pf*MyosinF 24 hours prior to Percoll purification of schizonts. The pre-incubation of 3D7 parasites served as a control to check for potential effects of rapalog alone. Rapalog exposure was maintained either until 1 hour after addition of DHA (*Pf*UBP1/*Pf*KIC7/*Pf*Eps15/*Pf*AP-2 $\mu$ /*Pf*2102), or up to the removal of DHA in the parasites for which no growth defect was expected (3D7/*Pf*Kelch13/*Pf*MyosinF). When rapalog was removed prior to DHA removal, parasite cultures were washed three times with 1 ml fresh RPMI complete medium (using a 2 ml Eppendorf tube) and 700 nM DHA were added again until 6 hours of drug exposure was completed. After the 6 h DHA pulse, DHA (and rapalog, where still present) was removed by washing the cultures for three times in 1 ml RPMI complete medium (using a 2 ml Eppendorf tube). Afterwards, the cultures were grown for another 66 hours in a 6-well plate (2 ml volume, 2.5% hematocrit) to complete the RSA. At the end (72 hours), Giemsa smears and parasite survival rate was calculated.

### 3.3.12 Consecutive *in vitro* ring-stage survival assay<sup>0-3h</sup> (RSA)

A consecutive RSA was performed to check whether already ART resistant parasites can become even more resistant by challenging them in series. For the consecutive RSA, a standard *in vitro* RSA was performed as described before (see 3.3.11) (Witkowski & Amaratunga *et al.*, 2013). In general, three technical and two biological replicates were performed regularly. At 72 hours, Giemsa smears were taken and the resistant parasites which survived the DHA treatment (DHA treated sample) were re-cultivated in a new Petri dish and grown at 37°C. After several days of recovery, these resistant parasites were

tested again in a new round of *in vitro* RSA. This procedure was continuously repeated for 30 weeks in a row, and parasite survival rate was determined by Giemsa smear.

### 3.3.13 Bloated food vacuole assay

The bloated food vacuole assay was used to check whether hemoglobin uptake is impaired by the inactivation of a specific target protein. Here, a bloated food vacuole phenotype appears when hemoglobin uptake is impaired. For this, an asynchronous parasite culture was synchronized twice using 5% D-sorbitol with 10 hours treatment apart to obtain ring stage parasites of 10 – 18 hours age. The rings were re-incubated at 37°C for another 8 hours to grow parasites into trophozoites of 18 – 26 hours. A sample was removed for imaging to estimate the size of the food vacuole at time point 0 and the parasite culture was split into two 1 ml cultures, and both were treated with 33 µM E64 protease inhibitor (Sigma Aldrich). To one culture rapalog was added to a final concentration of 250 nM, whereas the other cell culture was kept as control. The parasite cultures were incubated at 37°C for 8 hours and then microscopy samples were removed and stained at room temperature with 4.5 µg/ml dihydroethidium for 20 min. After staining, the samples were washed once with fresh RPMI complete medium and immediately imaged. The size of the bloated food vacuole was measured by DIC image using ImageJ (30 cells were imaged per approach) and number of vesicles was counted by DIC images. Before imaging, the operators were blinded to the conditions of the sample.

### 3.3.14 Cytochalasin D inhibitor treatment of *P. falciparum*

Cytochalasin D is an inhibitor that destabilizes actin filaments. To check whether inhibitor treatment influences parasite development, an asynchronous parasite culture was separated into two parts and cultivated for 1 hour either in the presence of 10 µM Cytochalasin D (Calbiochem), or absence of inhibitor (control) at 37°C. After treatment, cells were imaged immediately, and relative position of *Pf*MyosinF foci to *Pf*Kelch13 in trophozoite stages was assessed. For this, *Pf*MyosinF and *Pf*Kelch13 foci per cell were counted and classified into 3 conditions. Co-localization of *Pf*MyosinF and *Pf*Kelch13 was defined as total overlap, when yellow color was detected in the merge, partial co-localization was defined as 50% overlap, when yellow signal appeared in the merging region, and non-co-localization events as defined as touching foci that did not overlap or were further apart.

### 3.3.15 Parasite fitness assay

The fitness assay was used to compare the growth of different cell lines over several weeks (Tirrell *et al.*, 2019). For this, the cell lines were synchronized with 60% Percoll (see 3.3.5) and allowed to re-invade fresh RBCs for 6 hours at 37°C. After 6 hours, the parasites were synchronized again using 5% D-sorbitol to obtain a culture of 0 – 6 hours rings. Parasites were cultured at 37°C for another 20 – 24 hours and parasitemia was measured via flow cytometry (staining see 3.3.10) (Birnbaum *et al.*, 2017). For starting the fitness assay, the different cell lines were co-cultivated in a 5 ml Petri dish in a 1:1 ratio with 3D7 control based on the parasitemia measured by flow cytometry. The co-cultivated cell lines were grown either in RPMI complete or low amino acid medium. Cells were stained with Hoechst33342 (1:5000) for 10 min and the proportion of GFP-positive parasites was assessed by fluorescence microscopy every two days until one parasite line was overgrown by the other cell line of the co-culture (ratio of 95:5). Per condition (RPMI complete or Low AA), the non-linear regression curves were derived from the respective raw curves, expressing the proportional amount of GFP positive parasites per total parasitemia. The fitness cost per generation of the different strains were calculated based on the indicated functions (raw curves and calculations in Appendix H.1 – H.4). For this, in a first step the trendline factor from the indicated functions was duplicated (assumption that one generation corresponds to two days), and growth factor per generation was differentiated. Fitness cost per generation were calculated by subtracting the differentiated value from 1 (1 representing 100% fitness).

### 3.3.16 Measurement of protein amount by fluorescence intensity

Measurement of protein amount via fluorescence intensity was performed as described before (Birnbaum *et al.*, 2020). To determine the protein amount of different cell lines, parasites were synchronized twice using 5% D-sorbitol (see 3.3.5) in intervals of two days, to obtain 0-18 hours ring stage parasites. After the second sorbitol synchronization, the cell lines were cultivated at 37°C for another 2 hours, then the GFP signal of the ring-stage parasites was detected by fluorescence microscopy. Intensity of the GFP signal in comparison to intensity of the background signal was measured via ImageJ and correlated with the respective area of the GFP signal to obtain the total fluorescence. The mean fluorescence intensity was calculated via the average from three independent experiments.

## 3.4 Biochemical methods

### 3.4.1 Discontinuous SDS-polyacrylamide gel electrophoresis (SDS-PAGE)

The discontinuous sodium dodecyl sulphate polyacrylamide gel electrophoresis (SDS-PAGE) was used to separate proteins according to their molecular weight (Laemmli, 1970). To be able to separate the proteins based on their molecular weight, SDS was used to denature the proteins by unfolding them and providing a negative charge irrespective of their original charge. The SDS sample buffer was supplied with DTT to reduce the disulfide bonds of the protein and to promote denaturation. For the separation of the polypeptides, polyacrylamide gels of 6%, 8%, and 10% concentration were prepared (see 2.9.3). First, a casting gel stand (Bio-Rad) was assembled and tested on its impermeableness using dH<sub>2</sub>O. Next, the separation gels were cast between two glasses in the casting gel stand and polymerized for 30 min. To plane the gel border, isopropanol was carefully layered onto the gel during polymerization. When the gel was totally polymerized, isopropanol was removed and stacking gels were prepared (see 2.9.3) and carefully cast onto the polymerized separation gels. Directly after casting the stacking gel, a comb was put into the gel and the stacking gel was polymerized for another 30 min. When polymerization was completed, the gels were placed in an electrophoresis chamber (Bio-Rad) which was filled with 1x running buffer and gel combs were removed. The prepared saponin pellets diluted in 4x SDS buffer + 1 M DTT were loaded into the gel slots. In general, 8 µl pre-stained protein ladder (Thermo Fisher) and 10 µl protein samples were loaded into the slots. The SDS-PAGE was performed for the first 15 min at 100 V to carefully run the samples into the stacking gel, and then electrophoresis was continued at 150 V in the separation gel. SDS-PAGE was stopped when the dye front of the marker reached the bottom of the gel.

### 3.4.2 Western Blot analysis

Proteins were separated according to their molecular weight by SDS-PAGE (see 3.4.1). After the electrophoresis, proteins were transferred to a nitrocellulose membrane to identify them with specific antibodies detecting the immobilized proteins (Towbin *et al.*, 1979). For this, the blotting cassette was assembled. Prior to layering, all components were soaked in 1x transfer buffer, and the layering was started with the blotting foam, followed by three blotting papers. The SDS gel was carefully removed from the glass plate and layered on

the blotting paper. All air bubbles were removed, and blotting set up was constantly wetted to avoid destruction of the proteins. The gel was covered with a nitrocellulose membrane (PROTRAN), followed by three blotting papers and a second blotting foam. The blotting cassette was closed, placed in the blotting chamber, and filled up with ice-cold 1x transfer buffer. Icepacks were added to the chamber and blotting was performed at 299 mA, 390 V for 1.5 h at 4°C. When the blotting was completed, the blotting cassette was disassembled, and the nitrocellulose membrane containing the transferred proteins was blocked for 1 hour in 5% milk in 1x PBS at room temperature to prevent unspecific binding of antibodies.

### **3.4.3 Immunodetection of proteins**

To specifically detect the proteins blotted on the nitrocellulose membrane after blocking, the membrane was incubated with the primary antibody (see 2.1.1 in 2% milk in 1xPBS) overnight at 4°C. Next day, the primary antibody was removed by washing the membrane two times in 1x PBS-Tween for 15 min. After washing, the secondary antibody conjugated to horse radish peroxidase (HRP) (see 2.1.2 in 2% milk in 1x PBS) was added to the membrane and incubated for 1 hour at room temperature. After this incubation, the membrane was washed three times in 1x PBS-Tween, once in 1x PBS, and once in dH<sub>2</sub>O. For immunodetection, the membrane was placed on transparent film, and the ECL-Western blot detection Kit (Bio-Rad) was used to detect HRP by chemiluminescence. After 1 min incubation with the detection solutions, the signal intensities of the proteins were detected by ChemiDoc XRS+ imaging system (Bio-Rad). In total, the exposure time was 2 – 2400 sec wherein 35 pictures were taken. For loading control, the membrane was washed three times in 1x PBS after signal detection and blocked for 1 hour in 5% milk in 1x PBS. Antibody staining and imaging was performed as described before.

## **3.5 Microscopy**

### **3.5.1 Live cell imaging**

Live cell imaging was performed using the Zeiss AxioImager M1 equipped with a Hamamatsu Orca C4742-95 camera and the Zeiss Axiovision software (v 4.7). Here, a 100x / 1.4 – numerical aperture lens, and a 63x / 1.4 – numerical aperture lens was used. The microscopy images were processed via Corel PHOTO-PAINT X8 (64-bit) and CorelDRAW

X8 (64-bit). For staining of parasite nuclei, 500 µl parasite culture was stained either with DAPI (final concentration 1 µg/ml), or Hoechst33342 (1:5000) for 10 min at room temperature. After staining, parasite culture was washed once in fresh RPMI complete medium, centrifuged at 3700 rpm for 1 min and 4 µl parasite pellet was dropped onto a glass slide and covered with a coverslip.

### **3.5.2 Confocal imaging of parasites following DHA pulse in standard *in vitro* RSA**

To follow up the development of ART resistant parasites after a DHA pulse, RSA was combined with confocal imaging. For this, a standard *in vitro* RSA was performed with K13<sup>C580Y</sup> parasites as described in 3.3.11, and immediately after removal of DHA after 6 hours treatment parasites were prepared for imaging by confocal microscopy. The microscopy was performed using the Olympus FluoView 1000 confocal microscope. To detect the parasites, image stacks (30 Z-layers) were taken with the 488 nm laser line, using a 60x (1.35 numerical aperture) plan apochromate oil immersion lens and a 2.0-fold zoom via the FluoView software. Images were taken at 3 different time points: directly after DHA removal (0 h), 24 hours after DHA removal (24 h), and 39 hours after DHA removal (39 h). For image processing, the Imaris x64 7.8 (Bitplane) software and Corel Suite X8 were used. Snapshots from the DIC images were prepared and area of parasite cell was measured after 24 hours via ImageJ to assess the mean size of control and ART treated fraction. The 39 h time point was used to estimate the respective condition of the parasite and classify them into reinvading parasites, trophozoite or schizont stages or dead parasites.

### **3.5.3 Immunofluorescence assay (IFA) performed with acetone fixed cells**

To detect endogenously expressed parasite proteins, IFAs with acetone fixed cells were performed. For this, 500 µl of parasite culture containing ~5% parasitemia of all developmental stages were harvested and pelleted at 2000 rpm for 1 min. Parasite cells were washed twice with 1x PBS and were resuspended in a suitable volume of 1x PBS to obtain a hematocrit of ~ 3%. Of this parasite suspension, 50 µl were taken and transferred to a 10 well IFA slide aspirating the parasite suspension repeatedly per well to leave only a thin cell monolayer behind. The cells on the IFA slide were air-dried and fixed in fresh 100% acetone for 30 min. After fixation, IFA slides were air-dried and then rehydrated with 1x PBS. Each well was washed twice with 1x PBS and slide was placed in a humid chamber.

For epitope detection, antibody solution was prepared by diluting the primary antibody (see 2.1.1) in 3% BSA in 1x PBS supplied with 100 µg/ml ampicillin. The parasite cells were incubated with the primary antibody solution in the humid chamber for 1 hour at room temperature. After incubation, the IFA wells were washed five times with 1x PBS. The secondary antibody solution (see 2.1.2) was prepared by diluting the respective antibody in 3% BSA in 1x PBS. Parasite cells were incubated with the secondary antibody and 1 µg/ml DAPI staining solution for 1 hour at room temperature in a humid chamber. After incubation, IFA wells were washed five times with 1x PBS and slides were dried at 37°C in the incubator. Small drops of 1x PBS buffered glycerol were pipetted between the wells, a coverslip was placed onto the slide and sealed with nail polish. Acetone-fixed cells were imaged using the Zeiss Axioscope M1 as described before (see 3.5.1). For storage, the IFA slides were wrapped in aluminum foil and kept at 4°C.

#### **3.5.4 Immunofluorescence assay (IFA) performed with formaldehyde / glutaraldehyde-fixed cells**

For better preservation of cell morphology and detection of the endogenously expressed parasite proteins, a formaldehyde/glutaraldehyde-fixed immunofluorescence assay was performed. At the beginning, 1 ml of parasite culture was harvested from an asexual cell culture growing at a parasitemia of ~4%. The parasite culture was centrifuged at 1800 rpm for 5 min and pellet was washed twice in 1x PBS. After washing, the pellet was resuspended in 750 µl fixing solution (freshly prepared, see 2.9.4) and incubated at room temperature for 30 min. Next, the parasite suspension was centrifuged at maximum speed for two minutes and cell were permeabilized with 0.5% Triton X-100 in 1x PBS for 10 min at room temperature. Afterwards, the culture was pelleted and washed three times with 1x PBS. After washing, the cells were spun down at 16 000 rpm for 2 min and unspecific antigen binding sites were blocked for one hour at room temperature with 100 µl 3% BSA in 1xPBS with ampicillin (100 µg/ml). After blocking, cells were pelleted, washed once in 1x PBS, and incubated rolling with 100 µl of primary antibody solution (see 2.1.1 in 3% BSA in 1x PBS) for one hour at room temperature (alternatively at 4°C overnight). Next, the cells were pelleted again, washed three times in 1x PBS, and spun down at 3000 rpm for 2 minutes. The secondary antibody solution was prepared by diluting the respective antibody (see 2.1.2) in 3% BSA in 1x PBS with ampicillin (100 µg/ml), and additionally 1 µg/ml DAPI staining solution was added. The cells were resuspended in 100 µl secondary antibody solution, protected from light, and incubated rolling for one hour at room temperature.

Secondary antibody solution was removed by pelleting the cells and washing the parasites three times in 1x PBS. After washing, the parasite cells were spun down at 3000 rpm for 2 min and prepared for imaging. The cells were imaged using the Zeiss Axioscope M1 as described before (see 3.5.1). For storage, 100  $\mu$ l 1xPBS with 100  $\mu$ g/ml ampicillin were added to the pellet. To prevent bleaching, aluminum foil was wrapped around the tube and cells were kept at 4°C.

## 4 Results

### 4.1 Functional characterization of *PfMCA2* (PF3D7\_1438400)

#### 4.1.1 Localization of *PfMCA2* (PF3D7\_1438400)

Analysis of the Kelch13 compartment using DiQ-BioID and quantitative mass spectrometry revealed several candidates of *PfKelch13* interactors (Birnbaum *et al.*, 2020). One of the hits that so far was not validated to be present at the *PfKelch13*-defined compartment was the protein *PfMCA2* (PF3D7\_1438400). Since only little information about this protein exists, experiments were performed to first determine whether it indeed is a Kelch13 compartment protein and to further characterize it. Previously, several attempts employing SLI to C-terminally tag the protein with a sequence coding for FKBP domains and GFP failed (Birnbaum J., personal communication). Therefore, it was here attempted to tag *mca2* with the sequence encoding 3xHA by modification of the original genomic locus using SLI, resulting in the cell line *MCA2*<sup>wt</sup>-3xHA. Correct integration of the SLI construct was confirmed by PCR (Fig 11 A) and expression of the HA-tagged *PfMCA2* was verified by western blot analysis (Fig 11 B).

To investigate the localization of *PfMCA2* in the parasite, anti-HA IFAs were carried out with formaldehyde/glutaraldehyde-fixed cells. Fluorescence microscopy with these parasites showed that *PfMCA2* is expressed throughout the asexual cycle of *P. falciparum* (Fig 11 C). In ring stage parasites, one focus was visible whereas in trophozoite stage parasites two or more foci were detected. Interestingly, here one focus was often located close to the FV (yellow arrows Fig. 11 C) while the other focus was observed at structures visible in DIC that may represent vesicles at cell periphery (white arrows Fig. 11 C). In schizonts, detection of *PfMCA2* was more difficult since the signals was more diffuse at this stage but also in schizonts *PfMCA2* was seen in one focus localizing close to the FV.

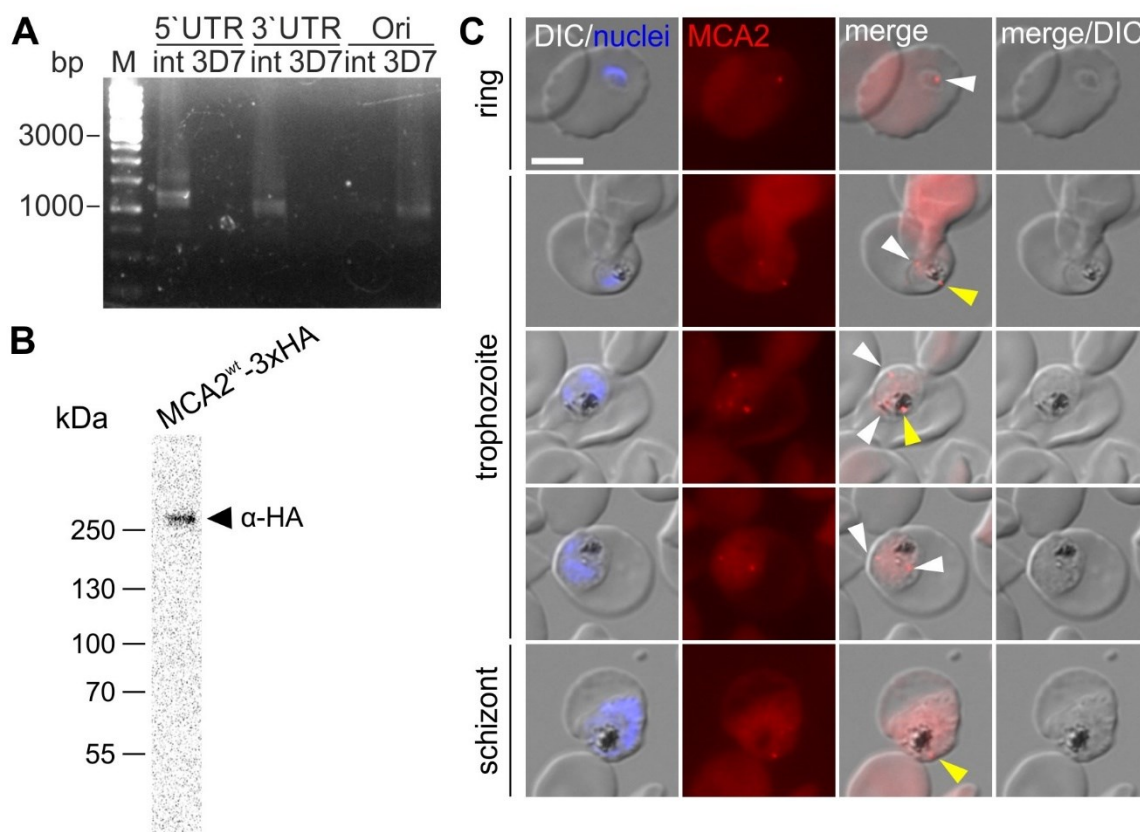


**Figure 11) *Pfmca2* (PF3D7\_1438400) localizes close to food vacuole and vesicles. A)** Agarose gel showing PCR products demonstrating correct integration of the SLI plasmid into 3D7 genome to obtain MCA2<sup>wt</sup>-3xHA parasites. Primers (see Appendix C) were used to confirm 5'-integration (5'UTR, 1273 bp) and 3'-integration (3'UTR, 1153 bp) and to demonstrate absence of original locus in the MCA2<sup>wt</sup>-3xHA parasites (Ori, 1100 bp). 3D7 gDNA was used as reference (ori 3D7 1100 bp). **B)** Western blot analysis with protein extracts of saponin-lysed parasites of MCA2<sup>wt</sup>-3xHA parasites. α-HA (from rat) was used to detect MCA2<sup>wt</sup>-3xHA (calculated molecular weight (MW) of 281 kDa). Molecular weight standard is indicated in kDa. Full blots are shown in Appendix F.2. **C)** IFA images of formaldehyde/glutaraldehyde-fixed MyoF<sup>wt</sup>-3xHA parasites. α-HA (from rat) was used to detect MCA2<sup>wt</sup>-3xHA. Nuclei were stained with DAPI. Yellow arrow, marks foci detected at the FV; white arrow, marks foci detected at vesicles at cell periphery; *bp*, base pairs; *M*, marker (GeneRuler™ 1 kb, Thermo Scientific); *int*, integrant; *ori*, original locus; *wt*, wildtype; *HA*, hemagglutinin; *DIC*, differential interference contrast. scale bar, 5 μm.

#### 4.1.2 *Pfmca2* is part of the Kelch13 compartment

For verification of the presence of *Pfmca2* at the Kelch13 compartment, the cell line MCA2<sup>wt</sup>-3xHA was transfected with an episomal plasmid containing a sequence coding for *PfKelch13* N-terminally tagged with mCherry, resulting in the cell line MCA2<sup>wt</sup>-3xHA+K13 (Fig 12 A).

To analyze the relative position of *PfMCA2* and *PfKelch13* in the parasite cell, *MCA2<sup>wt</sup>-3xHA+K13* parasites were acetone fixed and imaged using fluorescence microscopy (Fig 12 B). This showed similar to the formaldehyde/glutaraldehyde fixed parasites (see section 4.1.1), *PfMCA2* was detected throughout the asexual cycle of *P. falciparum* and one or more foci were found in close proximity to the FV. Episomal expressed *PfKelch13* was also found in all asexual stages and was detected close to *PfMCA2*. Quantification of the relative localization of *PfMCA2* and *PfKelch13* was performed (Fig 12 C). Here, *PfMCA2* and *PfKelch13* were defined as co-localizing when the foci totally overlapped (yellow color in merge). *PfMCA2* and *PfKelch13* were scored as partially co-localizing when around half of the foci size overlapped (yellow signal in the merging region), whereas both proteins were defined as non-colocalizing when they were closely located but the foci did not overlap. This revealed that 44% of *PfMCA2* foci co-localized with *PfKelch13*. Partial overlap was calculated for 24% of *PfMCA2* foci the cases, whereas 32% *PfMCA2* foci did not co-localize with *PfKelch13*. This data indicates that *PfMCA2* is part of the Kelch13 compartment but is also found at other foci.

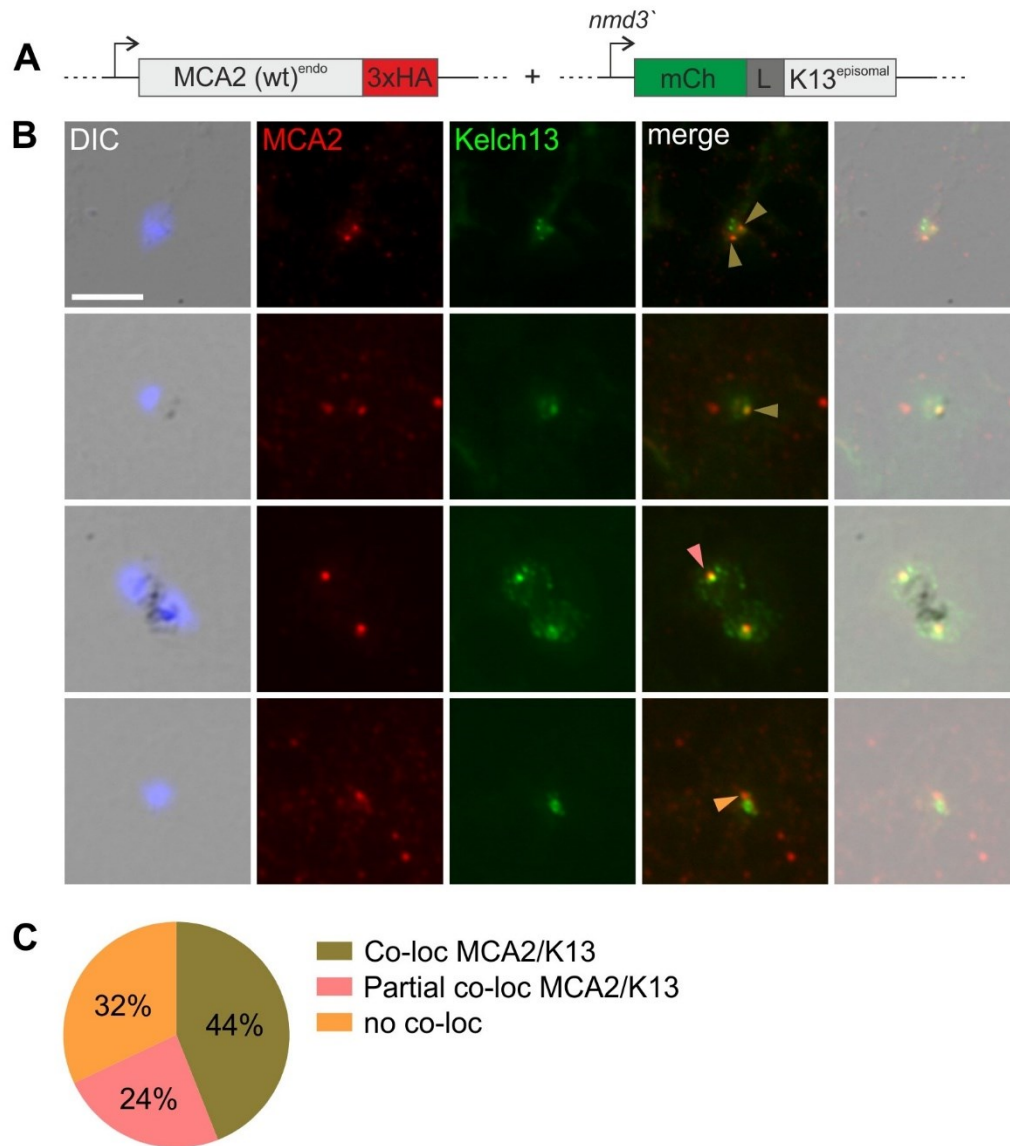


**Figure 12) Relative localization of *PfMCA2* to *PfKelch13*.** **A)** Schematic of modified endogenous locus of *MCA2*<sup>wt</sup>-3xHA parasites transfected with episomal mCherry-K13 plasmid. **B)** IFA images of acetone-fixed *MCA2*<sup>wt</sup>-3xHA+K13 parasites.  $\alpha$ -HA (from rabbit) was used to detect *MCA2*<sup>wt</sup>-3xHA.  $\alpha$ -RFP (from rat) was used to detect mCh-Kelch13. Nuclei were stained with DAPI. **C)** Quantification of spatial arrangement of *PfMCA2* and *PfKelch13* foci. Shown is percentage of *PfMCA2* foci that co-localize (full overlap when all of the *PfMCA2* focus resulted in a yellow signal in the merge), partially co-localize (partial overlap of foci resulting in a yellow signal in the merging region) or did not co-localize (foci closely located but no overlap). One acetone IFA was performed, and  $n = 30$  cells were scored. *wt*, wild type; *HA*, hemagglutinin; *mCh*, mCherry; *L*, linker; *DIC*, differential interference contrast; *green arrow* marks co-localizing foci, *pink arrow* marks partially co-localizing foci; *orange arrow* marks no co-localization between *PfMCA2* and *PfKelch13*; scale bar, 5 $\mu$ m.

#### 4.1.3 SNP found mainly in African field isolated leads to truncation of *PfMCA2* and renders parasite resistant to ART

By screening of the MalariaGEN *Plasmodium falciparum* Community Project (MalariaGEN *et al.*, 2021) a SNP at amino acid position 1344 of *PfMCA2* was found leading to a conversion of the corresponding codon into a stop (Fig 13 A). According to MalariaGEN, this SNP is found in Africa with a mean prevalence of 52% and in South Asia with 5% prevalence. Previous data showed that truncation of *PfMCA2* is possible for parasite growth and renders parasite resistant to ART (Birnbaum *et al.*, 2020). To investigate whether Y1344Stop also induces ART resistance, *PfMCA2* was disrupted at the respective position using SLI, leading to a cell line expressing a truncated version of *PfMCA2* (*MCA2*<sup>Y1344Stop</sup>-GFP). After selection of integrants, correct integration of the construct was confirmed via PCR (Fig 13 B) and correct expression of the truncated protein was verified by western blot analysis (Fig 13 C). Live cell imaging of *MCA2*<sup>Y1344Stop</sup>-GFP parasites revealed that the truncated version of *PfMCA2* is expressed throughout the asexual replication in the infected red blood cell similar to wild type *PfMCA2* (Fig. 13 D). In agreement with the findings with the *MCA2*<sup>wt</sup>-3xHA parasites (see Fig 11 C), ring stage parasites showed a single focus of *MCA2*<sup>Y1344Stop</sup>-GFP per cell, while in trophozoite stages two or more foci were detectable (Fig. 13 D). In most of the cells one focus was localized next to the FV, whereas the other foci are present in cell periphery often close to vesicular structures (Fig. 13 D, orange, and white arrows, respectively).

Performing standard RSA with the *MCA2*<sup>Y1344Stop</sup>-GFP cell line showed that truncation of the native *PfMCA2* locus at amino acid position 1344 rendered parasite resistant to ART with a mean parasite survival rate of 1,64% that is higher than the defined cut-off value of 1% (Witkowski & Amaratunga *et al.*, 2013) (Fig 13 E). This is in line with previous results demonstrating that disruption of *PfMCA2* at amino acid position 57 confers tolerance to ART (Birnbaum *et al.*, 2020).

In summary, the data indicates that disruption of *PfMCA2* at amino acid position 1344 is dispensable for parasite development and does not impair localization of *PfMCA2*. While this might indicate that this SNP found mainly in Africa may render parasite resistant to ART, the analysis of this sequence region from African parasite isolates revealed that it always seems to occur with a SNP at gene position 4030 which leads to an amino acid change from Y to K, rather than a stop (RNA sequencing data kindly provided by Anna Bachmann and Thorsten Thye). Hence, this SNP is likely not relevant for ART resistance in

the field, but the truncation analyzed here confirms the importance of *PfMCA2* for ART resistance.

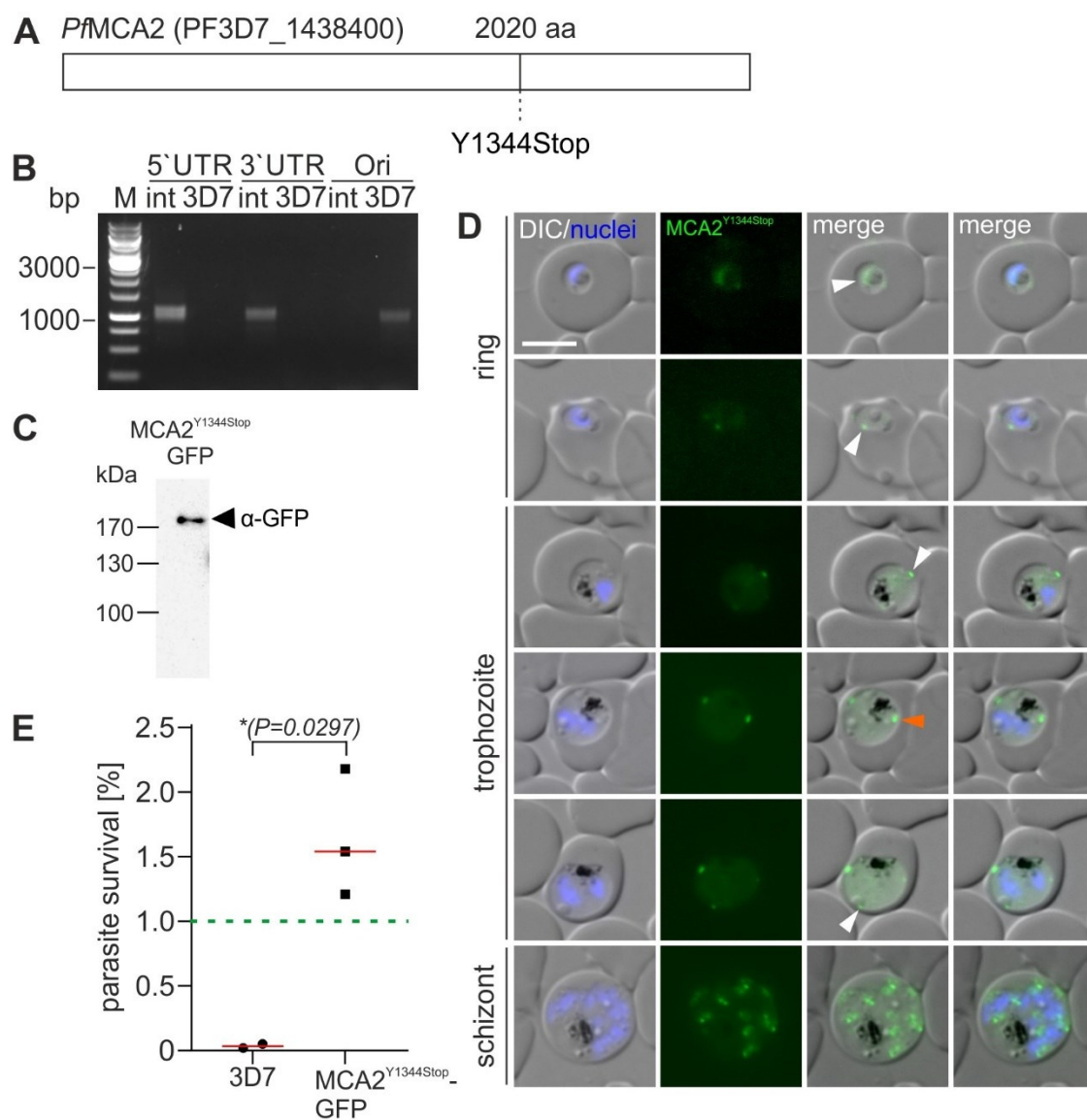


**Figure 13** SNP (Y1344Stop) found in field isolates that when introduced into 3D7 leads to truncation of *PfMCA2* and renders parasite resistant to ART. **A**) Scheme showing position of SNP in MCA2<sup>Y1344Stop</sup>-GFP cell line. **B**) Agarose gel showing PCR products demonstrating correct integration of the SLI plasmid into 3D7 genome to obtain MCA2<sup>Y1344Stop</sup>-GFP parasites. Primers (see Appendix C) were used to confirm 5'-integration (5'UTR, 1188 bp) and 3'-integration (3'UTR, 1120 bp) and to demonstrate absence of original locus in the MCA2<sup>Y1344Stop</sup>-GFP parasites (Ori, 1070 bp). 3D7 gDNA was used as reference (ori 3D7 1070 bp). **C**) Western blot analysis with protein extracts of saponin-lysed parasites of MCA2<sup>Y1344Stop</sup>-GFP parasites. α-GFP (from mouse) was used to detect MCA2<sup>Y1344</sup>-GFP (expected MW of 187 kDa). Molecular weight standard is indicated in kDa. Full blots are shown in Appendix F.2. **D**) Live cell images of different developmental stages of knock-in cell line MCA2<sup>Y1344Stop</sup>-GFP. **E**) Graph showing parasite survival rate (% survival compared to control without DHA) 72 hours after 6 h DHA treatment in standard RSA. Each point shows an independent experiment. Red vertical bar shows mean. Green dashed line shows 1% survival, above which parasites are considered resistant (Witkowski & Amaratunga *et al.*, 2013). aa, amino acid; M, marker (GeneRuler™ 1 kb, Thermo Scientific); bp, base pairs; int, integrant; ori, original locus; kDa,

kilodaltons; *DIC*, differential interference contrast; *GFP*, green fluorescent protein; *DAPI*, 4',6-Diamidin-2-phenylindol; *white arrow* marks localization at cell periphery and vesicles; *red arrow* marks localization of  $MCA2^{Y1344Stop}$  at FV. scale bar, 5  $\mu$ m.

#### 4.1.4 *PfMCA2*<sup>Y1344Stop</sup> co-localizes with *PfKelch13*

Next, co-localization of the truncated *PfMCA2* and *PfKelch13* was assessed to see whether the disruption influences the relative position of *PfMCA2* foci to *PfKelch13* foci. For this the  $MCA2^{Y1344Stop}$ -GFP cell line was transfected with the episomally maintained *PfKelch13*-mCherry plasmid, resulting in the parasite line  $MCA2^{Y1344Stop}$ -GFP+K13 (Fig 14 A). Live cell imaging was performed by fluorescence microscopy and relative localization of  $PfMCA2^{Y1344Stop}$  and *PfKelch13* foci was quantified (Fig 14 B). Quantification showed that 59% of the  $PfMCA2^{Y1344Stop}$  foci co-localized with *PfKelch13*, 20% of the foci showed partial co-localization and 21% of the  $PfMCA2^{Y1344Stop}$  foci did not co-localize to *PfKelch13* (Fig 14 B). *PfKelch13* foci move in the living cell and particularly ring stages also change their position in the host cell (Grüring *et al.*, 2011). To reduce incorrect quantification of relative localization of foci due to movement of the cell and foci during image acquisition, smears of  $MCA2^{Y1344Stop}$ -GFP+K13 parasites were made, air-dried, and imaged via fluorescence microscopy. Quantification of the signal in smeared parasites revealed that the number of co-localizing foci increased to up to 72%, whereas 28% of the  $PfMCA2^{Y1344Stop}$  foci did not co-localized with *PfKelch13* foci (Fig 14 C).

In summary the results indicate that truncation of *PfMCA2* neither influences the localization of this protein, nor the relative localization of *PfMCA2* to *PfKelch13*.

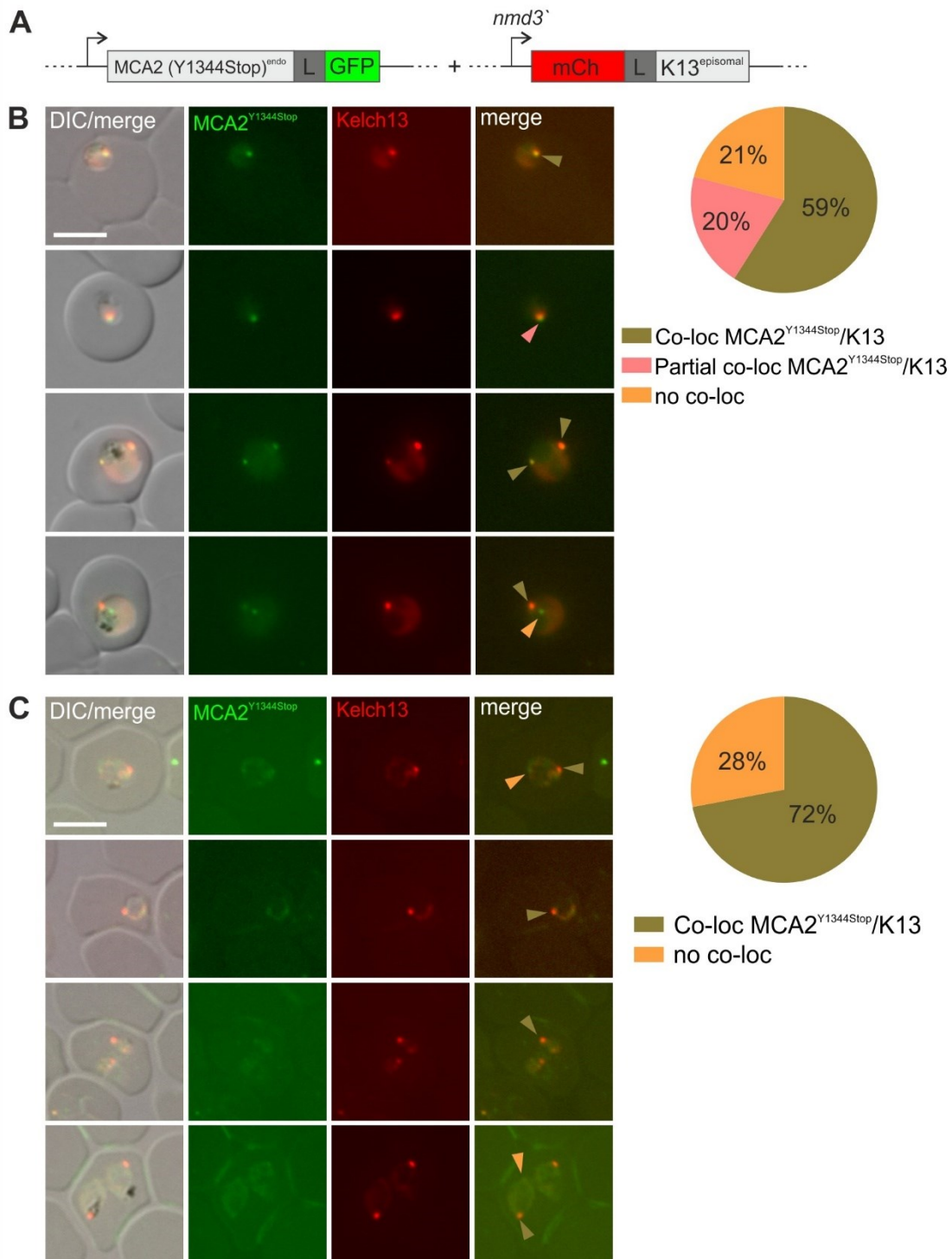


**Figure 14) Relative localization of *PfMCA2*<sup>Y1344Stop</sup>-GFP foci to *PfKelch13*.** **A)** Schematic of modified endogenous locus of *MCA2*<sup>Y1344Stop</sup>-GFP parasites transfected with episomal mCherry-K13 plasmid. **B)** Live cell images of *MCA2*<sup>Y1344Stop</sup>-GFP+K13 parasites and quantification of *PfMCA2*<sup>Y1344Stop</sup> and *PfKelch13* foci and calculation of percentage co-localization (total co-localization, yellow color in the merge), partial co-localization (half of the foci size overlaps) and non-co-localization (close foci but no overlap or foci were further apart) *PfMCA2* and *PfKelch13* foci. In total, three independent live cell imaging sessions were performed, and n = 46 cells were scored. **C)** Microscopy images of smeared, air-dried *MCA2*<sup>Y1344Stop</sup>-GFP+K13 parasites and quantification of *PfMCA2*<sup>Y1344Stop</sup> and *PfKelch13* foci and calculation of percentage co-localization, partial co-

localization, and non-co-localization foci (criteria same as in (B)). In total, two independent live cell imaging sessions were performed, and n = 20 cells were scored. *GFP*, green fluorescent protein; *mCh*, mCherry; *L*, linker; *DIC*, differential interference contrast; *green arrow* marks co-localizing foci, *pink arrow* marks partially co-localizing foci; *orange arrow* marks no co-localization between *PfMCA2<sup>Y1344Stop</sup>* and *PfKelch13*; scale bars, 5 $\mu$ m.

## 4.2 Functional characterization of *PfMyosinF* (PF3D7\_1329100, previously annotated as *PfMyosinC*)

### 4.2.1 *PfMyosinF* is found in close proximity to the Kelch13 compartment

DiQ-BioID and quantitative mass spectrometry revealed a series of potential interaction partners of *PfKelch13* of which more than 10 were previously validated to co-located with Kelch13 (Birnbaum *et al.*, 2020). One of the hits that had not previously been validated was *PfMyosinF* (previously annotated as *PfMyosinC*). Myosins are motor proteins working with actin (Cheney *et al.*, 1993; Sellers, 2000). *PfMyosinF* may therefore be a generator of force in the endocytosis process. Furthermore, mutations in *PfMyosinF* were previously associated with ART resistance in genome wide association studies (Cerqueira *et al.*, 2017). For these reasons this potential *PfKelch13* interactor was analyzed here.

To determine whether *PfMyosinF* is located at *PfKelch13* compartment and to assess its general cellular localization, native *PfMyosinF* was tagged with 3xHA through modification of the endogenous *PfmyosinF* gene using SLI (Fig 15 A) (Birnbaum *et al.*, 2017). Correct integration of the construct mediating the corresponding genomic modification was confirmed by PCR (Fig 15 B). In a next step, the cell line expressing the 3xHA tagged wild type *PfMyosinF* (MyoF<sup>wt</sup>-3xHA) was transfected with an episomal mCherry-Kelch13 plasmid (MyoF<sup>wt</sup>-3xHA+K13) (Fig 15 C). In order to assess the co-localization of both proteins, immune fluorescence assays were performed and the position of *PfMyosinF* relative to *PfKelch13* was determined in ring and trophozoite stage parasites. Here different fixation methods were applied, one that permits maximal antibody access but results in poor preservation of parasite morphology (acetone fixation) and one with less efficient antibody access but better cellular morphology (formaldehyde/glutaraldehyde fixation). For evaluation, the *PfMyosinF* foci were observed in view of their relative position to *PfKelch13* foci. Foci were defined as co-localizing when the totally overlapped, whereas partial co-localization was defined as foci which showed an overlap of 50%. Two foci were defined as close when they touched each other but showed no overlap or were not further apart than one focus size from each other. Foci were defined as non-colocalizing when they were further apart than one focus size.

In the parasites fixed with acetone, 80% of *PfMyosinF* signal was found in foci and accumulations near to the FV (in 8 out of 10 evaluated hemozoin containing cells; see Appendix B.1) (Fig. 15 D). When the relative position of *PfMyosinF* signal was compared to the *PfKelch13* signal, it was observed that 16% of the *PfMyosinF* foci co-localized with

*PfKelch13* (Fig 15 E). Herein, 2 co-localization events (18%) out of 11 *PfMyosinF* foci detected at the FV were counted (see Appendix B.1). 19% of *PfMyosinF* foci showed a partial co-localization of foci, 63% were found close (foci touching, or not further apart than one focus size) and 2% of the *PfMyosinF* foci were not proximal to *PfKelch13* foci (Fig 15 E). These results indicate that *PfMyosinF* rarely fully or partially co-localizes with *PfKelch13* but is found in a close spatial arrangement with the *PfKelch13* compartment.

To better preserve cellular morphology, parasites were also fixed in formaldehyde/glutaraldehyde and the position of *PfMyosinF* foci in relation to *PfKelch13* foci was evaluated again. Microscopy analysis of these cells showed that in 86% of cases (in 6 out of 7 hemozoin containing cells, see Appendix B.2) *PfMyosinF* foci were located near the parasite FV as evident by proximity to the hemozoin signal observed in DIC (Fig. 15 F). Similar to acetone fixation, only a small proportion of *PfMyosinF* foci fully or partially overlapped with *PfKelch13*, namely 17% and 10%. In contrast, 34% of *PfMyosinF* foci were closely located to *PfKelch13*, while 38% did not show any co-localization (Fig 15 G). Analysis of the overlapping foci showed, that in ring stage parasites, 20% of total *PfMyosinF* foci co-localized to *PfKelch13*, whereas in trophozoite stages, only 16% of all *PfMyosinF* foci showed co-localization to *PfKelch13* (see Appendix B.2). Since in ring stages it is not possible to analyze the relative position of foci to the FV, this was then investigated in trophozoite stages. Here, 30% of the co-localization events between *PfMyosinF* and *PfKelch13* (3 out of 10 *PfMyosinF* FV-foci) were detected at the FV (see Appendix B.2).

In summary, both immune fluorescence assays indicate that *PfMyosinF* foci show only limited overlap with the *PfKelch13* compartment but that most of the *PfMyosinF* foci are found in close proximity of the *PfKelch13* compartment.

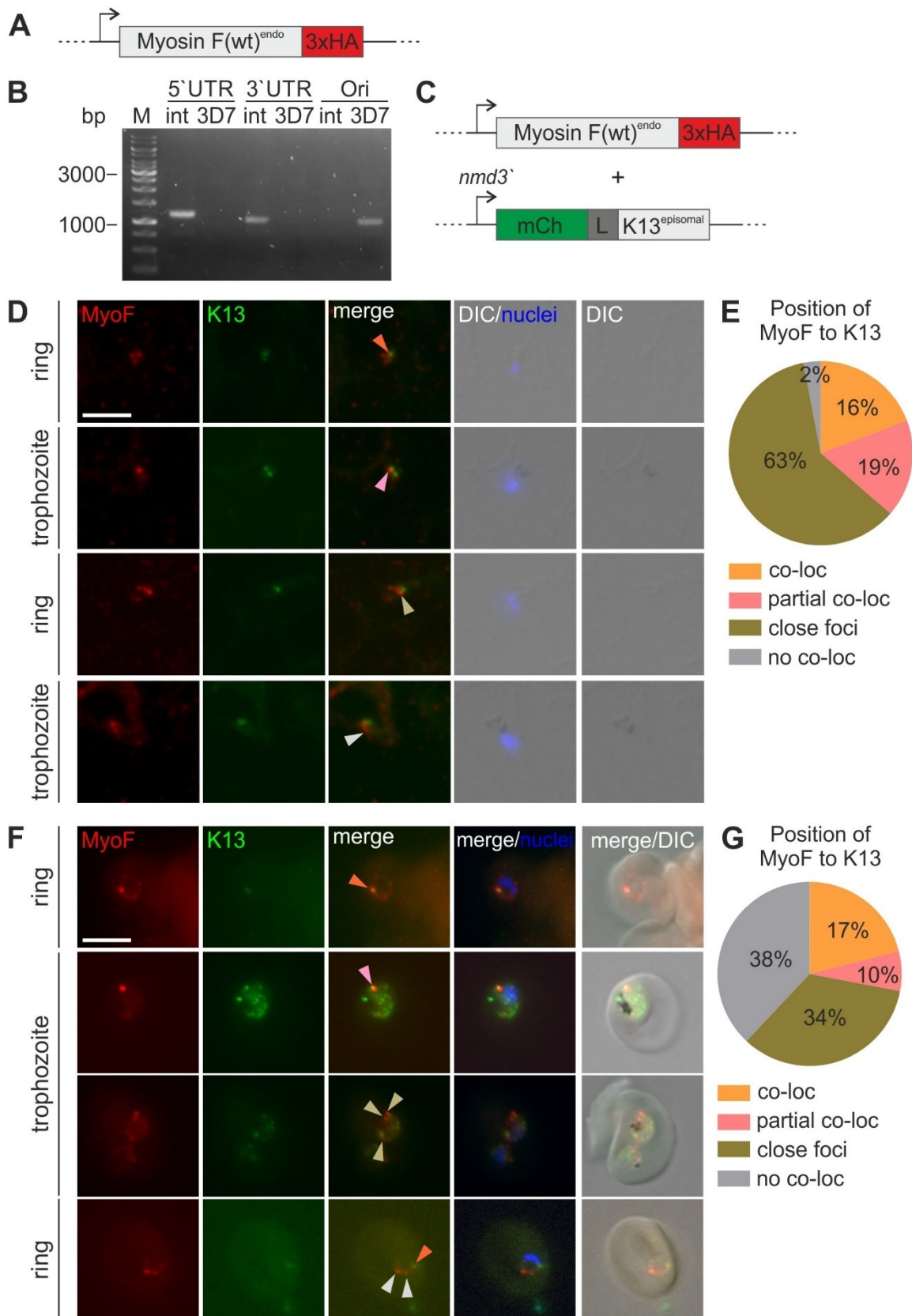


**Figure 15) Localization of *PfMyosinF* compared to *PfKelch13*.** **A)** Schematic of the modified endogenous *PfMyosinF* locus tagged with 3xHA. **B)** Agarose gel showing PCR products demonstrating correct integration of the SLI plasmid into 3D7 genome to obtain MyoF<sup>wt</sup>-3xHA

parasites. Primers (see Appendix C) were used to confirm 5'-integration (5'UTR, 1224 bp) and 3'-integration (3'UTR, 1093 bp) and to demonstrate absence of original locus in the MyoF<sup>wt</sup>-3xHA parasites (Ori, 1037 bp). 3D7 gDNA was used as reference (ori 3D7 1037 bp). **C**) Schematic of modified endogenous locus of MyoF<sup>wt</sup>-3xHA parasites transfected with episomal mCherry-K13 plasmid. **D**) Microscopy images of an IFA with acetone-fixed MyoF<sup>wt</sup>-3xHA+K13 parasites. *orange arrow* marks overlapping/co-localizing *Pf*MyosinF and *Pf*Kelch13 foci; *pink arrow* marks partially overlapping/co-localizing foci; *green arrow* marks foci localizing close to each other; *grey arrow* marks foci with no overlap/co-localization.  $\alpha$ -HA (from rabbit) was used to detect MyoF<sup>wt</sup>-3xHA.  $\alpha$ -RFP (from rat) was used to detect mCh-Kelch13 **E**) Quantification of spatial arrangement of *Pf*MyosinF and *Pf*Kelch13 foci. Shown is percentage of *Pf*MyosinF foci that co-localize (full overlap when all of the *Pf*MyosinF focus resulted in a yellow signal in the merge), partially co-localize (partial overlap of foci resulting in a yellow signal in the merging region), are closely located (foci touch or are not further apart than one focus size) or did not co-localize (foci further apart than one focus size). One acetone IFA was performed and n = 31 cells were scored. **F**) IFA images of formaldehyde/glutaraldehyde-fixed MyoF<sup>wt</sup>-3xHA+K13 parasites. Arrow legends see (D).  $\alpha$ -HA (from rabbit) was used to detect MyoF<sup>wt</sup>-3xHA.  $\alpha$ -RFP (from rat) was used to detect mCh-Kelch13. **G**) Quantification of *Pf*MyosinF and *Pf*Kelch13 foci (pie charts) as done in (E), n = 10 cells were scored from one IFA with this fixing method. *wt*, wild type; *endo*, endogenous; *HA*, hemagglutinin; *M*, marker (GeneRuler™ 1 kb, Thermo Scientific); *bp*, base pair; *mCh*, mCherry; *L*, linker; *DIC*, differential interference contrast; scale bars, 5 $\mu$ m.

To assess the localization of *Pf*MyosinF and its relative positioning to *Pf*Kelch13 in living parasites, a cell line expressing *Pf*MyosinF tagged with 2xFKBP-GFP-2xFKBP from the endogenous locus (MyoF<sup>wt</sup>-2x2) (kindly provided by Ernst Jonscher, cell line generated using SLI to modify *pfmyosinF* locus) was transfected with an episomal plasmid mediating expression of mCherry-Kelch13 (MyoF<sup>wt</sup>-2x2+K13) (Fig 16 A). Live cell imaging with MyoF<sup>wt</sup>-2x2+K13 parasites showed that in ring stages *Pf*MyosinF is only weakly expressed and was only detectable in older ring and trophozoite stage parasites (Fig 16 B). Quantification of co-localizing, partial co-localizing, close and non-co-localizing foci was performed as described for the IFAs before. This counting revealed that 8% of *Pf*MyosinF foci co-localized to *Pf*Kelch13, 12% showed a partial co-localization, 36% were closely located, while 44% of *Pf*MyosinF foci did not co-localized to *Pf*Kelch13 (Fig 16 C). Focusing especially on co-localization events of *Pf*MyosinF and *Pf*Kelch13 showed that 13% of the foci detected in late ring stages as well as in trophozoite stages co-localized at the FV confirming the results observed in acetone fixed MyoF<sup>wt</sup>-3xHA+K13 parasites (see Appendix B.3). Comparing live cell imaging and immune fluorescence assays of MyoF<sup>wt</sup>-3xHA+K13 revealed that formaldehyde/glutaraldehyde-fixed cells and live cell imaging achieved similar results with relatively high rates of non-co-localizing events, while acetone-fixed cells hardly detected non-co-localizing events.

In general, live cell imaging of the MyoF<sup>wt</sup>-2x2+K13 parasites confirmed that *Pf*MyosinF is present at the Kelch13 compartment with some more than half of the *Pf*MyosinF foci overlapping either fully or partial with *Pf*Kelch13 or being closely located to it.

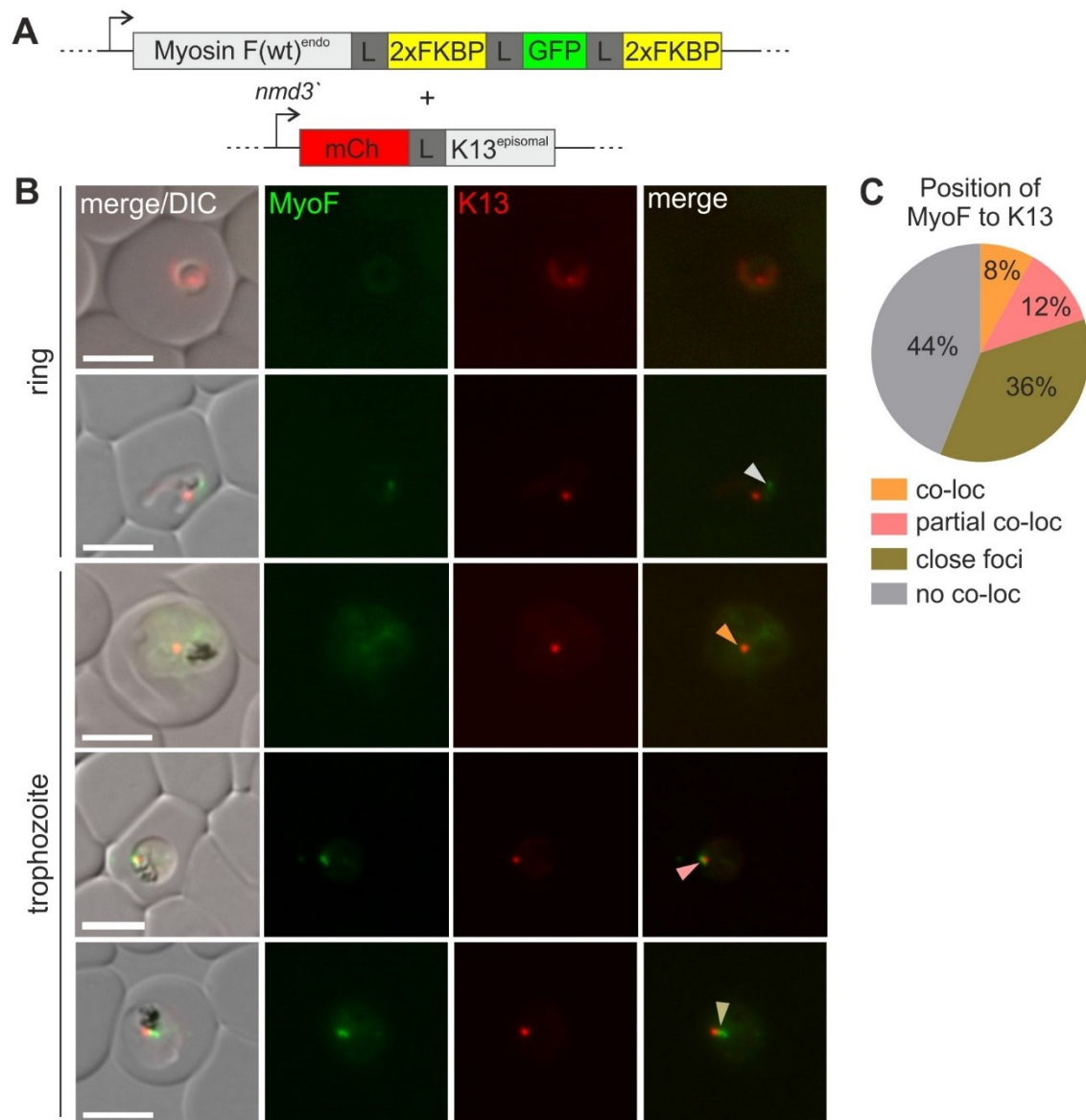


**Figure 16) Relative localization of *Pf*MyosinF to *Pf*Kelch13.** **A)** Schematic of modified endogenous locus of MyoF<sup>wt</sup>-2x2 parasites transfected with episomal mCherry-K13 plasmid. **B)** Live cell images of MyoF<sup>wt</sup>-2x2 + K13. *orange arrow* marks overlapping/co-localizing *Pf*MyosinF and *Pf*Kelch13 foci; *pink arrow* marks partially overlapping/co-localizing foci; *green arrow* marks foci localizing close to each other; *grey arrow* marks foci with no overlap/co-localization. **C)** Quantification of spatial arrangement of *Pf*MyosinF and *Pf*Kelch13 foci. Shown is percentage of *Pf*MyosinF foci that co-localize (full overlap when all of the *Pf*MyosinF focus resulted in a yellow signal in the merge), partially co-localize (partial overlap of foci resulting in a yellow signal in the merging region), are closely located (foci touch or are not further apart than one focus size) or did not co-localize (foci further apart than one focus size). Microscopy was performed on 3 independent days, n = 14 cells were scored. *wt*, wild type; *endo*, endogenous; *L*, linker; *FKBP*, FK506-binding protein; *GFP*, green fluorescent protein; *mCh*, mCherry; *DIC*, differential interference contrast; scale bars, 5µm.

#### 4.2.2 Cytochalasin D treatment causes dissociation of *PfMyosinF* and *PfKelch13* in trophozoites

The compound Cytochalasin D is a toxin derived from fungi that binds to actin and inhibits its filamentous association, leading to the disruption of actin filaments. The data in section 4.2.1 indicated that *PfMyosinF* is part of the *PfKelch13* compartment and localizes close to or overlaps with *PfKelch13*. Since myosin belongs to the actomyosin complex, it was here tested whether treatment with the actin inhibitor Cytochalasin D based disruption of actin filaments causes a dissociation of *PfMyosinF* and *PfKelch13* signals. For this, the cell line MyoF<sup>wt</sup>-2x2+K13 was treated with a final concentration of 10  $\mu$ M Cytochalasin D for one hour and parasites were imaged using fluorescence microscopy directly at the start of the experiment (when Cytochalasin D was added, 0 h) and one hour after Cytochalasin D addition (Fig 17 A). In this experiment co-localization (total co-localization / overlap, yellow signal in the merge), partial co-localization (50% overlap of focus size, yellow signal in merging region) and no co-localization (foci touched but did not overlap or were further apart) of *PfMyosinF* and *PfKelch13* was quantified using slightly changed criteria (Fig 17 B). The analysis showed that due to poor signal intensity of *PfMyosinF* foci in ring stage parasites of MyoF<sup>wt</sup>-2x2+K13 (see also section 4.2.1) this analysis was inconclusive at that stage and therefore quantification was performed in early and late trophozoite stages. In early trophozoites, directly at the start of the experiment (0 h) the control cell line showed co-localizing and overlapping foci of both proteins congruent with that observed in the control cell line one hour after Cytochalasin D addition (1 hour without Cytochalasin D). In contrast, the same parasites treated with 10  $\mu$ M Cytochalasin D for one hour showed no co-localization but partially overlapping foci, indicating the dissociation of *PfMyosinF* and *PfKelch13* foci in early trophozoites. In late trophozoite stages, a small proportion of co-localizing *PfMyosinF* and *PfKelch13* foci but no partial overlap was detected in the untreated control at the start of the experiment (0 h, time point when Cytochalasin D was added) and in the control one hour after Cytochalasin D addition (1 h without treatment). Here, in the parasites treated with 10  $\mu$ M Cytochalasin D a small proportion of foci dissociated after one hour treatment reducing the amount of co-localizing *PfMyosinF* and *PfKelch13* foci. This indicates that in later trophozoites also a dissociation of *PfMyosinF* and *PfKelch13* is detectable. Additionally, in these stages also a dispersion of *PfMyosinF* signal was seen (Fig 17 A, white asterisk).

In summary, these results indicate that the inhibition of actin polymerization using Cytochalasin D led to a reduction in the co-localization of *PfMyosinF* and *PfKelch13* foci in

early and late trophozoite stage parasites, and a dispersion of *Pf*MyosinF signal in late trophozoites indicating the dissociation of both proteins.

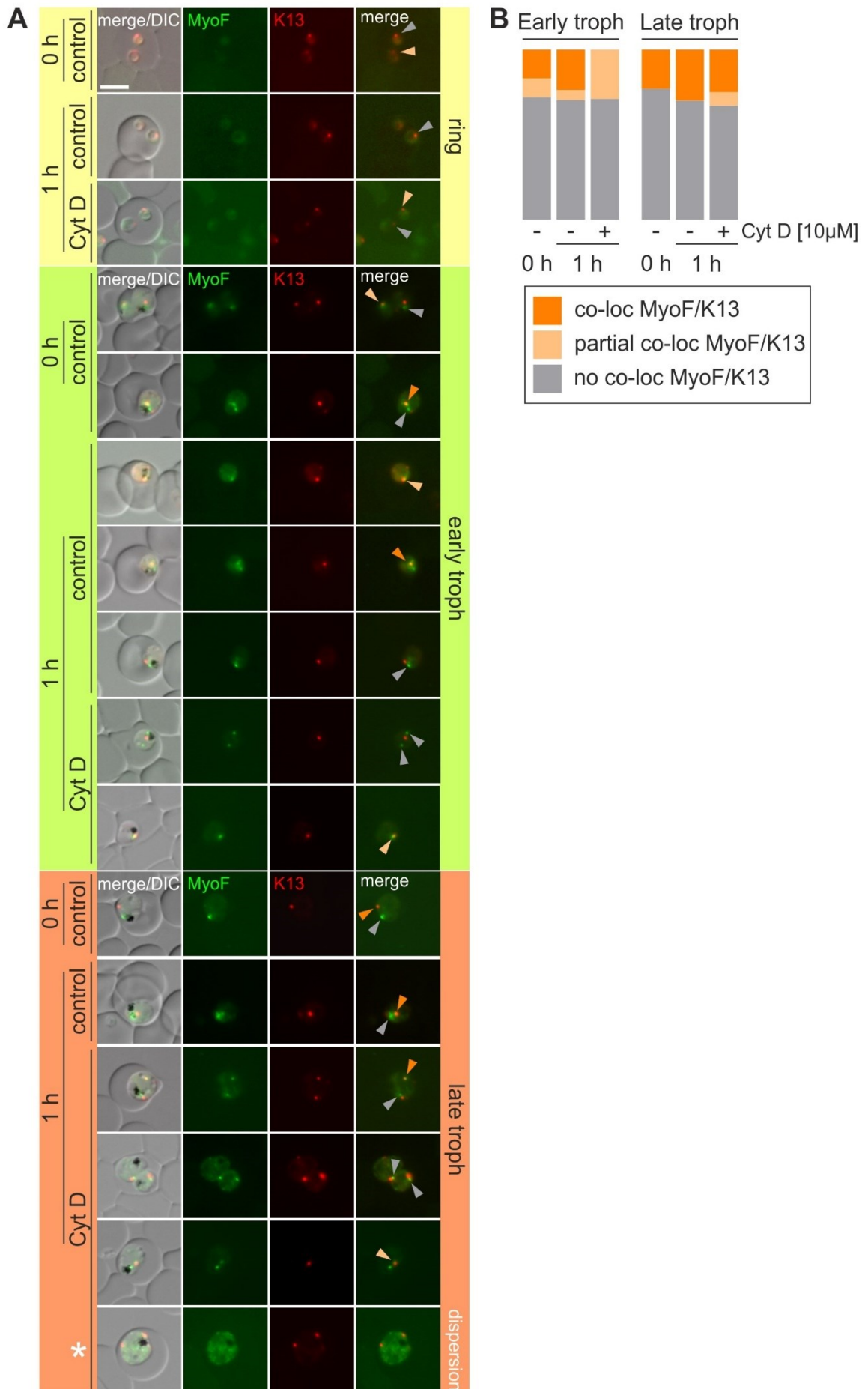


**Figure 17) Cytochalasin D treatment leads to dissociation of *PfMyosinF* and *PfKelch13* foci in early and late trophozoites.** **A)** Live cell images of MyoF<sup>wt</sup>-2x2+K13 parasites at different developmental stages. Images of control cell line and Cytochalasin D (10  $\mu$ M) treated parasites were taken at the start of experiment (0 h) and one hour after treatment (1 h). *dark orange arrow* marks co-localizing *PfMyosinF* and *PfKelch13* foci; *light orange arrow* marks partially co-localizing foci; *grey arrow* marks foci with no overlap/co-localization; *white asterisk* marks dispersion of *PfMyosinF* signal. **B)** Quantification of spatial arrangement of *PfMyosinF* and *PfKelch13* after Cytochalasin D treatment (calculations see Appendix B.5). Co-localization (total overlap, yellow color in merge), partial co-localization (50% overlap, yellow signal in merging region) and non-co-localization events (foci touch but do not overlap or are further apart). For start (0h), n = 17 cells, for the 1h control n = 13 and for Cytochalasin D-treated cells n = 20 cells were scored. *h*, hour; *DIC*, differential interference contrast; scale bar, 5 $\mu$ m.

### 4.3 *PfMyosinF* is important for parasite development

#### 4.3.1 Inactivation of *PfMyosinF* leads to a reduced parasite growth

To assess the essentiality of *PfMyosinF* for parasite development, a growth assay was performed after conditional inactivation of the protein using knock sideways. In a first step the mislocalization efficiency of the knock sideways was tested. For this, a previously generated cell line where the native *pfmyosinF* is endogenously tagged with *2xfkbp-gfp-2xfkbp* and episomally transfected with a 1xNLS mislocalizer was used (MyoF<sup>wt</sup>-2x2+1xNLS) (kindly provided by Ernst Jonscher). By adding rapalog, the inactivation of the target protein is induced via the mislocalization of the protein of interest into another cell compartment. Rapalog addition was continued for 22 hours in total and mislocalization was assessed at different timepoints via live cell imaging (Fig 18 A). Analysis of the data revealed that after one hour rapalog addition mislocalization of *PfMyosinF* started but was still incomplete, while after two hours accumulation of the target protein at one specific area (due to NLS signal *PfMyosinF* is targeted to the nucleus) increased although only partial mislocalization was observed and there was also *PfMyosinF* that remained at its site of action. Observation of *PfMyosinF* over 22 hours showed that the mislocalization was maintained but *PfMyosinF* foci close to the food vacuole were still observed, indicating only incomplete mislocalization.

To investigate the impact of *PfMyosinF* inactivation on parasite growth, a FACS-based growth assay was performed over 5 days (Fig 18 B). Asynchronous MyoF<sup>wt</sup>-2x2+1xNLS parasites were grown in the presence of rapalog for 5 days in total, and parasitemia was measured daily via flow cytometry. Simultaneously, a 3D7 control cell line was tested. This growth assay demonstrated that the partial inactivation of *PfMyosinF* slightly impaired parasite growth but did not lead to parasite death. In contrast, 3D7 parasites grown in the

presence of rapalog did not show an altered growth compared to the control without rapalog. Quantification of relative growth on the last day of the experiment showed, that MyoF<sup>wt</sup>-2x2+1xNLS cell line had a significant growth reduction of 25% compared to the same parasites grown without rapalog which was in contrast to the 3D7 control which showed no significant reduction in the culture grown with rapalog (Fig 18 C).

In summary, this data indicates that mislocalization of *Pf*MyosinF via knock sideways system is only partially successful but nevertheless significantly reduces parasite growth, indicating that this protein is important for parasite growth.

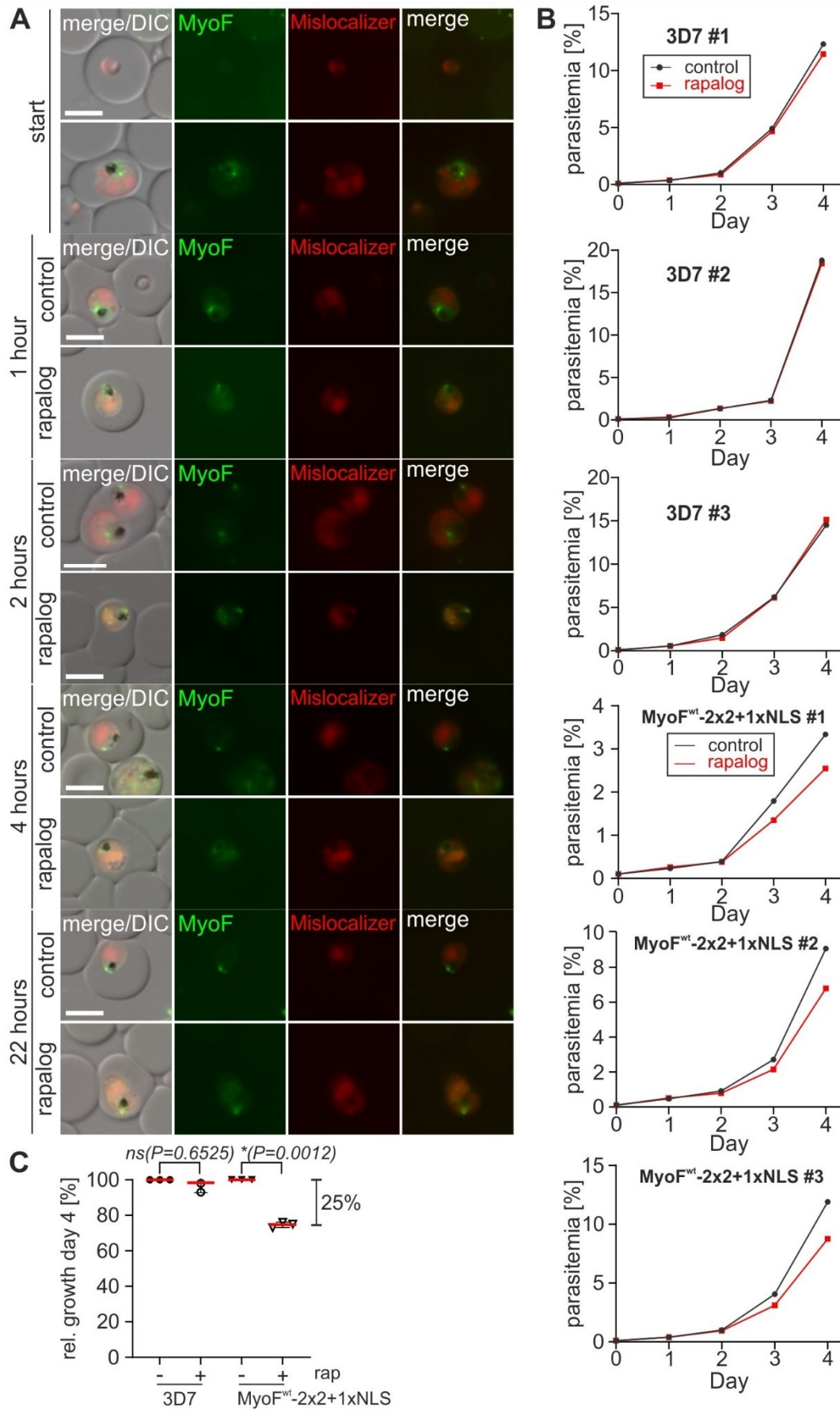


**Figure 18) *Pf*MyosinF is important for parasite development.** **A)** Live cell images of MyoF<sup>wt</sup>-2x2+1xNLS parasites. Control cell line and parasites cultured in the presence of rapalog (final concentration of 250nM) were imaged at different timepoints (indicated) after start of rapalog induction. **B)** Flow cytometry growth curves of asynchronous control and rapalog-treated 3D7 and MyoF<sup>wt</sup>-2x2+1xNLS parasites. Three independent experiments were conducted. **C)** Relative growth of rapalog treated 3D7 control and MyoF<sup>wt</sup>-2x2+1xNLS parasites at day 4 compared to respective untreated control. P value indicated, two-tailed, unpaired Welch's t test. *DIC*, differential interference contrast; *NLS*, nuclear localization signal; *rap*, rapalog; scale bars, 5µm.

#### 4.3.2 Inactivation of *Pf*MyosinF does not influence survival of ring stage parasites under ART treatment

The protein *Pf*MyosinF is part of the Kelch13 compartment and previous data showed that inactivation of *Pf*Kelch13 renders parasites resistant to ART. To test whether the inactivation of *Pf*MyosinF influences ART resistance, a standard RSA was carried out after the partial conditional inactivation of *Pf*MyosinF by knock sideways. Inactivation of *Pf*MyosinF was initiated either 12 hours or 24 hours prior to start of standard RSA and continued until one hour after the DHA pulse (Fig 19 A). Assessing the parasite survival rate 66 hours after DHA removal showed that inactivation of *Pf*MyosinF 12 hours prior to RSA start led to a survival rate of 0.27%, whereas a survival rate of 0.14% was reached when rapalog was added 24 hours prior to RSA start (Fig 19 B). The survival rate of the control (*Pf*MyosinF without rapalog) was even lower with 0.09% for rapalog addition 12 hours and 0.03% survival for rapalog addition 24 hours prior to the RSA. All survival rates were below the cut-off of 1% that defines resistance (Witkowski & Amaratunga *et al.*, 2013), indicating that inactivation of *Pf*MyosinF did not render parasite resistant to ART, although it should be noted that *Pf*MyosinF inactivation was only partial.

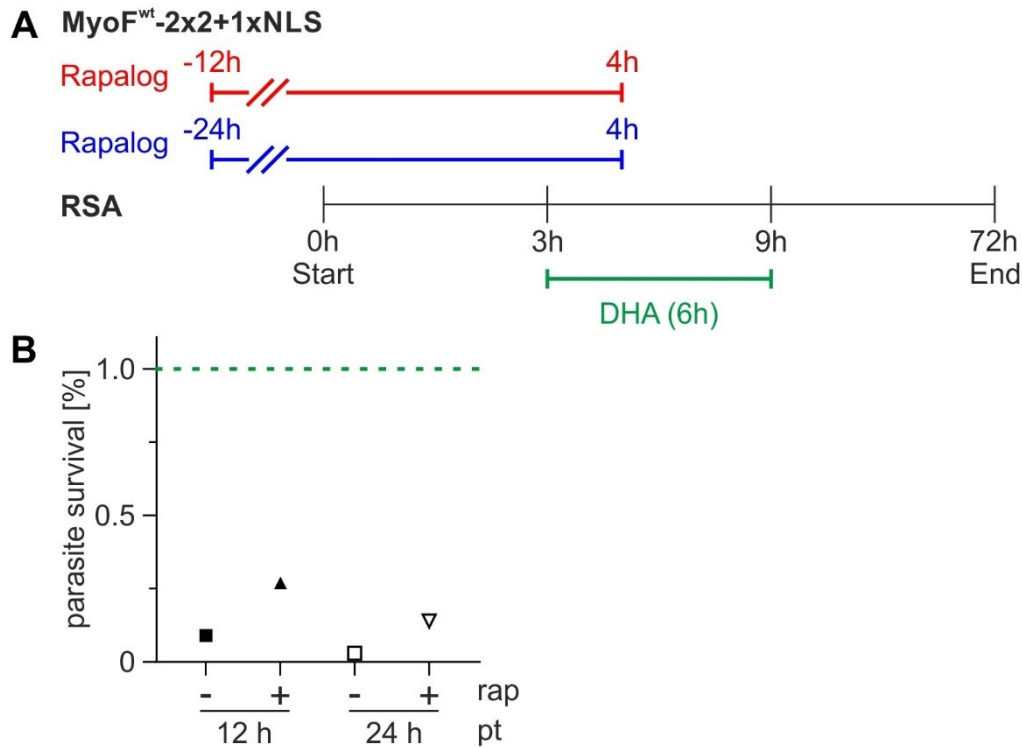


**Figure 19) RSA of MyosinF<sup>wt</sup>-2x2+1xNLS parasites after partial inactivation of *Pf*Myosin by knock sideways.** **A)** Scheme showing timing of inactivation (by addition of rapalog) (red) 12 hours and (blue) 24 hours prior to RSA start and of RSA with MyosinF<sup>wt</sup>-2x2+1xNLS parasites. **B)** Graph showing parasite survival rate in the RSA carried out as shown in (A). One experiment was performed per condition. *NLS*, nuclear localization signal; *h*, hour; *DHA*, dihydroartemisinin; *Rap*, rapalog; *red and blue line* indicates duration of rapalog treatment; *green line* indicates duration of DHA treatment; *green dotted line* marks cut-off value for resistance.

#### 4.3.3 *Pf*MyosinF is involved in hemoglobin uptake

Previous experiments showed that *Pf*Kelch13 influences endocytosis of hemoglobin and subsequently affects ART resistance since ART gets activated by the degradation products of hemoglobin. This raises the question whether *Pf*Kelch13 compartment members like *Pf*MyosinF are also involved in hemoglobin uptake. To test this hypothesis, a bloated food vacuole assay was performed using the MyoF<sup>wt</sup>-2x2+1xNLS cell line (kindly provided by Ernst Jonscher) to investigate if endocytosis was negatively affected when *Pf*MyosinF was inactivated. In this assay, the protease inhibitor E64 is used to block degradation of hemoglobin, leading to a bloated food vacuole phenotype when endocytosis is operational.

For this experiment, young trophozoites of 18 to 26 hours were treated with 33  $\mu$ M E64 and rapalog was simultaneously added to one culture to induce inactivation of *Pf*MyosinF,

whereas the other culture served as a control without rapalog. After eight hours, the cells were stained with dihydroethidium and the number of cells showing a bloated food vacuole phenotype was scored using live cell imaging. Inactivation of *PfMyosinF* under E64 treatment resulted in a reduction of the number of cells with a bloated food vacuole, while the control cells showed the typical bloated food vacuole phenotype (Fig 20 A). Quantification of the imaging data revealed that in two out of three experiments a significant reduction of bloated food vacuole phenotype was detected. On average, in all three experiments the untreated controls showed a mean proportion of 86% cells with bloated food vacuoles, whereas parasites grown in the presence of rapalog a mean proportion of 50% cells showed a significantly reduced bloated food vacuole phenotype (see Appendix B.4). Here, one representative experiment is depicted showing that 85% of control cells had bloated food vacuoles, while in rapalog cultivated parasites 32% of the cells developed a bloated food vacuole phenotype (Fig 20 B). Additionally, the number of vesicles was counted in the control and rapalog cell line resulting in a mean number of eight vesicles in the *MyoF<sup>wt</sup>-2x2+1xNLS* parasites cultivated in the presence of rapalog, and a mean number of five vesicles in untreated the control cell line (Fig 20 C). This indicates that *PfMyosinF* plays a role in endocytosis of hemoglobin.

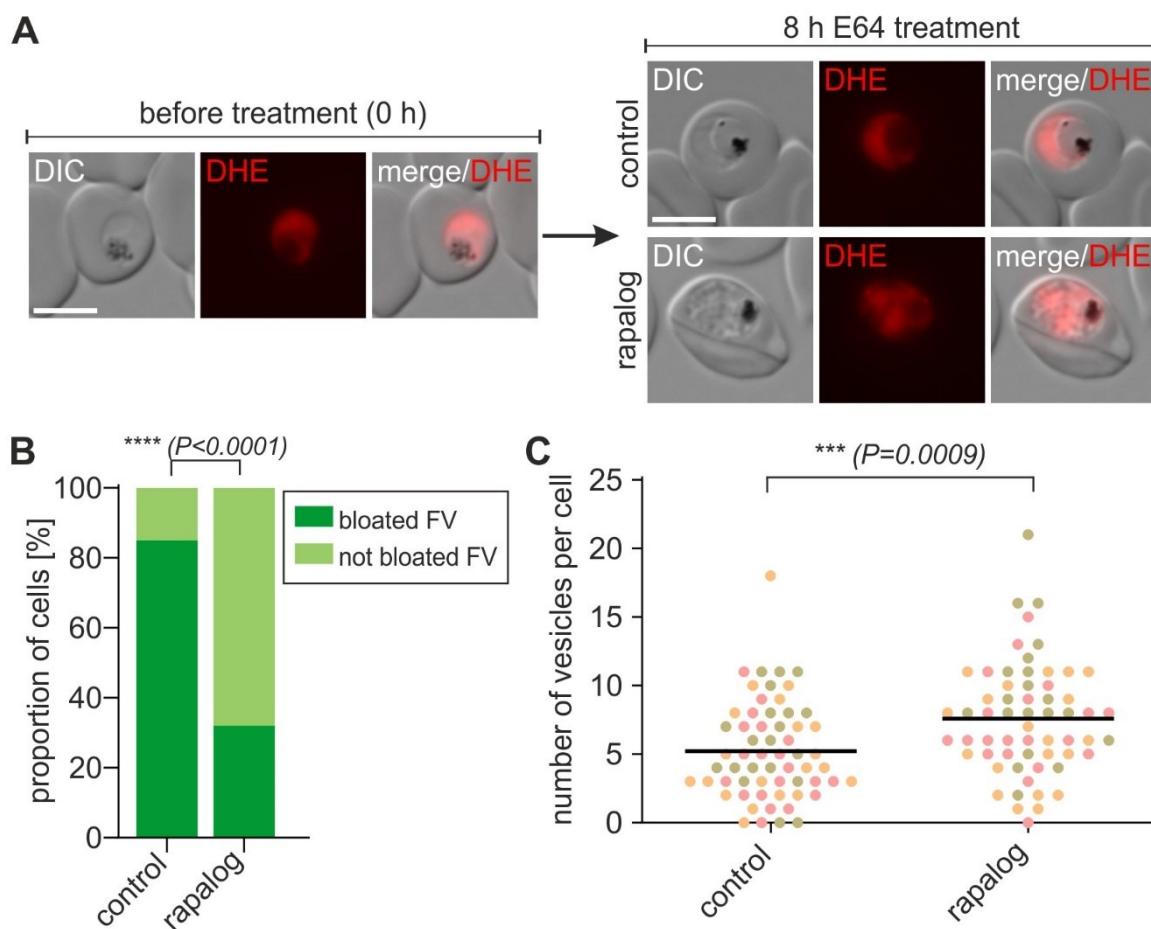


**Figure 20) Inactivation of *PfMyosinF* prevents hemoglobin uptake.** Bloated food vacuole assay performed with MyoF<sup>wt</sup>-2x2+1xNLS parasites eight hours after inactivation of *PfMyosinF*. **A)** Live cell images of MyoF<sup>wt</sup>-2x2+1xNLS parasites before addition of 33  $\mu$ M E64 and rapalog (final concentration of 250nM) (left) and eight hours after rapalog addition (right). Parasite cytoplasm was stained with dihydroethidium (DHE) for imaging. Samples were blinded before imaging. **B)** Quantification of number of cells with bloated food vacuoles from (A).  $n = 34$  cells were counted for each condition and Fisher's exact test was performed; one representative of three independent experiments is shown (see Appendix B.4). **C)** Number of vesicles per cell of DIC images generated for (A) was quantified.  $n = 20$  cells were evaluated in three independent experiments. P value is indicated, two-tailed, unpaired t test. *h*, hour; *DIC*, differential interference contrast; *DHE*, dihydroethidium; *FV*, food vacuole; scale bars, 5 $\mu$ m.

#### 4.3.4 Actin filaments accumulate close to *PfMyosinF*

The protein *PfMyosinF* is part of the actomyosin motor. To test the relative position of *PfMyosinF* to actin and monitor the assembly or disassembly of actin structures, the MyoF<sup>wt</sup>-2x2 cell line (kindly provided by Ernst Jonscher) was transfected with an episomal plasmid containing a sequence encoding the actin-chromobody (a kind gift of Markus Meissner, (Periz *et al.*, 2017) linked to mCherry (MyoF<sup>wt</sup>-2x2+chromobody) (Fig 21 A).

Live cell imaging was used to assess the location of *Pf*MyosinF and the actin-chromobody signal (Fig 21 B). Actin-chromobody was detected diffusely in the parasite cytosol probably referring to unbound chromobody since the marker is expressed in high levels by episomal plasmid (Periz *et al.*, 2017). Besides this diffuse pattern, actin-chromobody was also observed in filamentous structures at the cell periphery and in filaments shaping around vesicles. By evaluating the co-localization of *Pf*MyosinF and chromobody, the *Pf*MyosinF signal located next to the filamentous actin structures was scored, while the unbound cytosolic chromobody was not included. In ring stage parasites investigation of the relative position of *Pf*MyosinF to the chromobody was not possible since *Pf*MyosinF is very weakly expressed in this developmental stage (see also 4.2.1). In trophozoite stage parasites individual *Pf*MyosinF foci were detected that localized next to actin accumulations. Mostly, these closely localizing spots were observed close to the food vacuole but in some cases *Pf*MyosinF and actin accumulations were found at vesicles (as determined based on the DIC image) that were not proximal to the food vacuole. A total co-localization of the target protein with actin-marker was not detected.

In summary, this data indicates that *Pf*MyosinF is detected next to the food vacuole and vesicular structures and filamentous actin is accumulating close to *Pf*MyosinF foci.

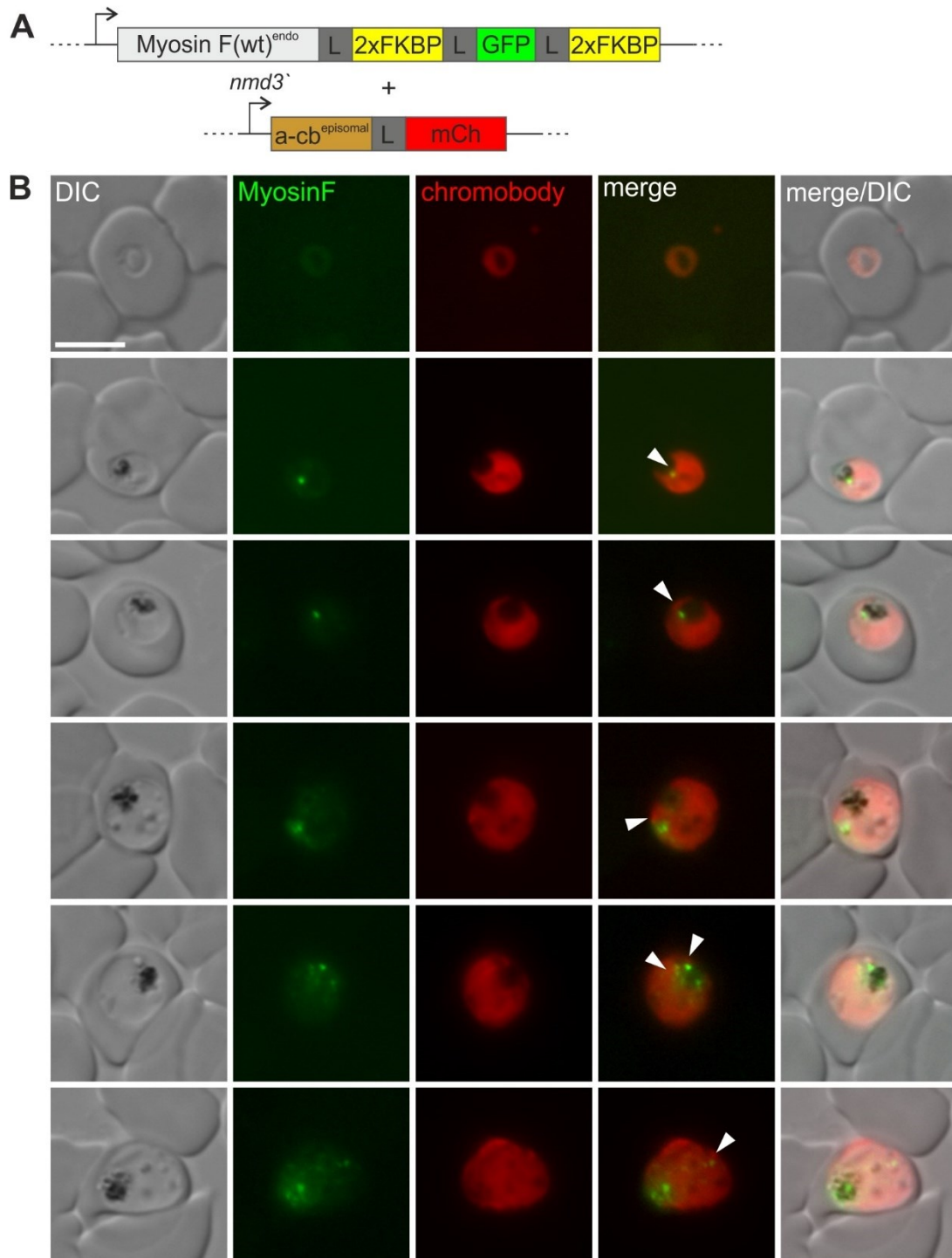


**Figure 21) Actin filaments accumulate next to *Pf*MyosinF.** **A)** Schematic of modified endogenous locus of MyoF<sup>wt</sup>-2x2 parasites transfected with episomal actin-chromobody fused to mCherry. **B)** Live cell images of MyoF<sup>wt</sup>-2x2+chromobody parasites. *wt*, wild type; *L*, linker; *FKBP*, FK506-binding protein; *GFP*, green fluorescent protein; *a-cb*, actin-chromobody; *mCh*, mCherry; *DIC*, differential interference contrast; *white arrow* marks accumulation of actin; scale bar, 5 $\mu$ m.

#### 4.3.5 Inactivation of *Pf*MyosinF increases co-localization with PI3P-positive structures at the food vacuole

Phosphatidylinositol 3-phosphate (PI3P) is a hallmark of early endosomes in eukaryotic cells and was previously detected at host cell cytosol filled vesicles when their transport to the food vacuole was prevented (Jonscher *et al.*, 2019). For these experiments, PI3P was detected using an mCherry tagged marker called P40PX, a widely used marker to detect this phosphoinositide (Balla, 2013). To investigate whether *Pf*MyosinF is important during endolysosomal pathway, and the knock sideways induced vesicles have endosomal character, the cell line MyoF<sup>wt</sup>-2x2 (kindly provided by Ernst Jonscher) was transfected with an episomal plasmid containing an expression cassette encoding 1xNLS-FRB-T2A-P40PX-mCherry, resulting in the parasite line MyoF<sup>wt</sup>-2x2+1xNLS-P40PX. If *Pf*MyosinF vesicles have endosomal character, the vesicles induced by knock sideways were expected to co-localize with P40PX signal, as this is a marker of endosomal vesicles.

The MyoF<sup>wt</sup>-2x2+1xNLS-P40PX cell line was grown in the presence of rapalog for 24 hours to induce inactivation of *Pf*MyosinF and live parasites were imaged at different time points (Fig 22 A). As expected (Tawk *et al.*, 2010; Boddey *et al.*, 2016), the P40PX marker predominantly labelled the food vacuole membrane or foci in proximity of the food vacuole and additionally, vesicular structures at cell periphery (Fig. 22 A). *Pf*MyosinF was mainly detected in foci close to the food vacuole and was also partially refractory to mislocalization up to 24 hours when rapalog was added. This is consistent with previous findings in section 4.3.1. The relative position of *Pf*MyosinF to the P40PX marker was scored (Fig. 22 B). Here, co-localization was defined as total overlapped of *Pf*MyosinF with P40PX foci or accumulations (yellow color in the merge), while *Pf*MyosinF was defined as closely located to P40PX when the foci touched but did not overlap or were not further apart than one focus size. No-colocalization was detected, when *Pf*MyosinF and P40PX were further apart than one focus size. Scoring was performed in trophozoite stage parasites since the *Pf*MyosinF signal is weakly expressed in ring stages (Fig 22 A; see also section 4.2.1). Quantification showed that at the start of the experiment when rapalog was added 70% of the *Pf*MyosinF foci were closely located to P40PX, and 30% of the foci co-localized to P40PX (see Appendix B.6). Similar results were seen in the control grown without rapalog after two hours. In contrast, in the MyoF<sup>wt</sup>-2x2+1xNLS-P40PX parasites cultivated in the presence of rapalog for two hours 91% of the *Pf*MyosinF foci co-localized to P40PX indicating an increase of co-localization events upon the inactivation of *Pf*MyosinF. Quantification of the samples taken after four hours, and 24 hours revealed similar results compared to the scoring after two hours confirming that inactivation of *Pf*MyosinF promotes the co-

localization with P40PX. These results were rather surprising, as due to the 1xNLS signal, *PfMyosinF* should be targeted to the nucleus and co-localization with P40PX should be mainly detected there. One option for the localization at the food vacuole could be, that the skip peptide between NLS-FRB and P40PX-mCherry is not fully skipped. This could result in the binding of the FKBP domains at *PfMyosinF* to the FRB on P40PX, recruiting the *PfMyosinF* to the P40PX structures.

In summary, the data indicates that *PfMyosinF* is closely located to PI3P positive structures represented by the P40PX marker. Upon addition of rapalog, which causes partial mislocalization of *PfMyosinF*, co-localization between P40PX and non-mislocalized *PfMyosinF* increased and was mainly detected at that food vacuole, since *PfMyosinF* localizes close to the food vacuole and was refractory to mislocalization. This preliminary experiment was performed to assess the relative position of *PfMyosinF* and P40PX. Because the mislocalization was only partial, and the skipping of the episomal construct is potentially insufficient, the data need to be confirmed by additional experiments.

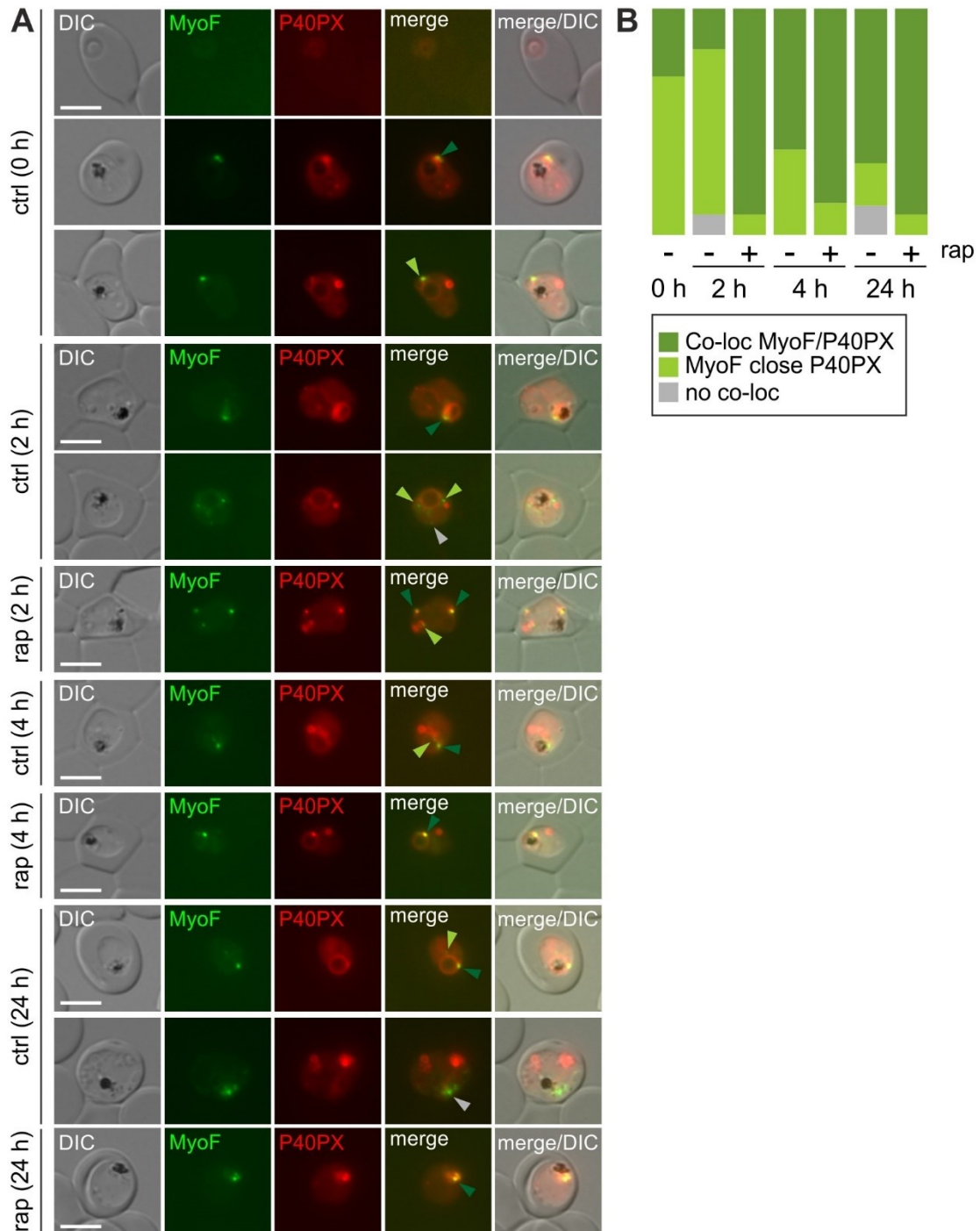


**Figure 22) Inactivation of *Pf*MyosinF leads to increased co-localization with PI3P-positive structures (P40PX marker) at the food vacuole. A)** Live cell images of MyoF<sup>wt</sup>-2x2+1xNLS-P40PX parasites at different time points after rapalogue induction. Images of control cell line and parasites grown in the presence of rapalogue (final concentration of 250nM) were taken at start of experiment and 2 h, 4 h and 24 hours after induction with rapalogue. *Dark green arrow*, marks co-localization of *Pf*MyosinF and P40PX; *light green arrow*, marks foci closely located, *grey arrow*, marks, no co-localization. **B)** Quantification of *Pf*MyosinF and PI3P-positive foci (P40PX) and calculation of co-localization of *Pf*MyosinF and PI3P-positive structures (total overlap of foci, yellow signal in the merge), close localization (foci are touching but not overlapping or foci are not further apart than one focus size) and non-co-localization events (foci are further apart than one focus size) (calculations see Appendix B.6). For start n = 8 cells, for 2 hours n = 7 (control) and n = 12 cells (rapalogue), for 4

hours n = 4 (control) and n = 11 cells (rapalog) and for 24 hours n = 10 (control) and n = 6 cells (rapalog) were scored. *Ctrl*, control (no rapalog induction); *rap*, rapalog (250nM final concentration); *h*, hour; *DIC*, differential interference contrast; *P40PX*, marker for PI3P-positive structures; scale bars, 5 $\mu$ m.

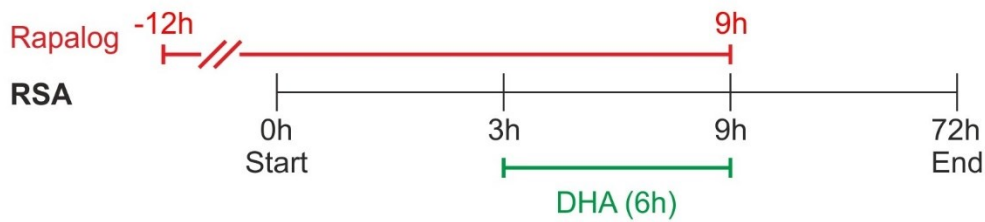
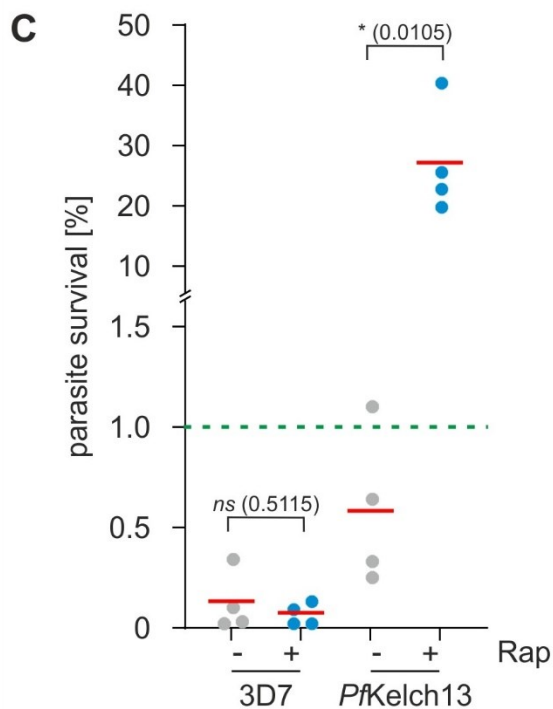
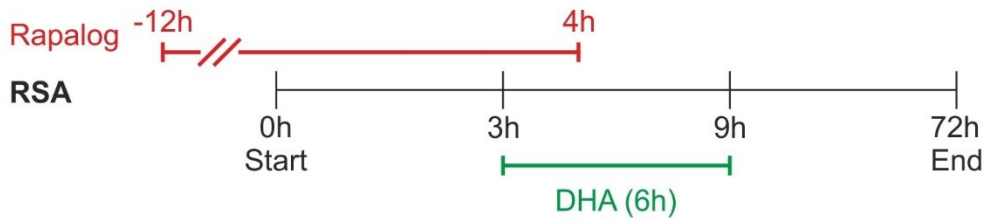
## 4.4 *Pf*Kelch13 compartment members are involved in ART resistance

As the *Pf*Kelch13 compartment contains other essential proteins involved in endocytosis (see section 4.3.3) it was here tested, if the inactivation of these proteins, namely *Pf*UBP1 (PF3D7\_0104300), *Pf*Eps15 (PF3D7\_1025000), *Pf*KIC7 (PF3D7\_0813000), and *Pf*AP-2 $\mu$  (PF3D7\_1218300), as well as inactivation of *Pf*Kelch13 (PF3D7\_1343700) itself lead to ART resistance.

For inactivation of the candidates, the knock sideways system was used (Birnbbaum *et al.*, 2017). The time of induction of inactivation prior to start of the RSA, as well as the duration of keeping rapalog during the test, was adjusted to the knock sideways efficiency and its effect on survival for each of the respective candidates. This was done to assure the successful inactivation of the protein, while at the same time avoiding a severe loss of viability of the parasites.

### 4.4.1 *Pf*Kelch13 mediated ART resistance

In a first step, we tested whether inactivation of *Pf*Kelch13 (PF3D7\_1343700) itself changes susceptibility to ART. For this, a standard *in vitro* RSA was performed with the 3xNLS *Pf*Kelch13 knock sideways parasites (Kelch13<sup>wt</sup>+3xNLS), a line that permits partial inactivation of *Pf*Kelch13 without loss of parasite viability (Birnbbaum *et al.*, 2017). Partial inactivation of *Pf*Kelch13 was initiated 12 hours prior to the start of the RSA through addition of rapalog and continued until ART was removed (Fig 23 A) and by this, parasites became resistant to ART as evident by a mean survival rate of 27.20%, (SD, +/- 8.05) (Figure 23 C). In contrast, the 3D7 control cell line, subjected to the same rapalog-addition regimen prior to the RSA, showed a mean survival rate of 0.08% (SD, +/- 0.05) (Fig 23 B, C).

**A** *PfKelch13* + 3xNLS**B** 3D7 control

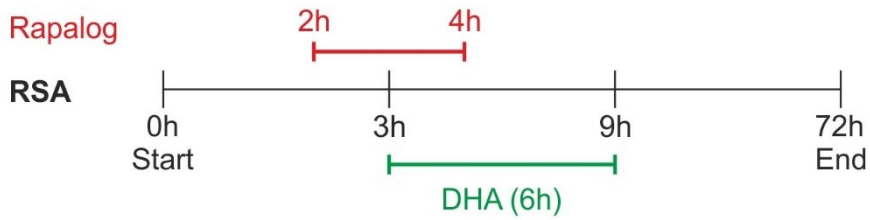
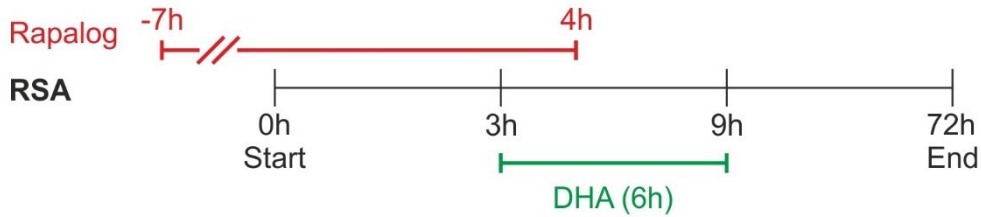
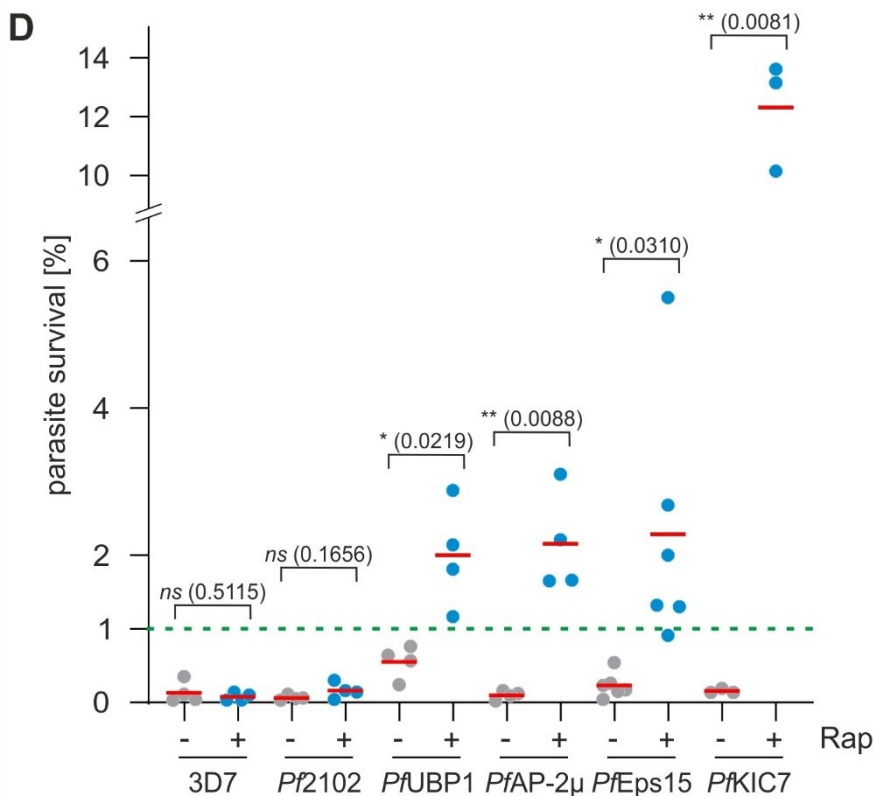
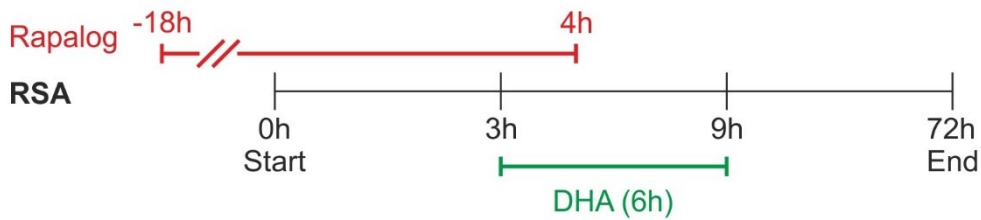
**Figure 23) RSA of *Kelch13*<sup>wt</sup>+3xNLS parasites after partial inactivation of *PfKelch13* by knock sideways. A, B** Scheme showing timing of inactivation (by addition of rapalog) and of RSA with *Kelch13*<sup>wt</sup>+3xNLS (A) and with 3D7 (B) control parasites. **C** Graph showing parasite survival rate 72 hours after start of the RSA carried out as shown in A) and B). Four independent experiments were performed. Each point shows an independent experiment. P value is indicated, two-tailed, unpaired Welch's t test. NLS, nuclear localization signal; h, hour; DHA, dihydroartemisinin; Rap, rapalog; red line indicates duration of rapalog treatment; green line indicated duration of DHA treatment; green dotted line marks 1% cut-off value for resistance (Witkowski & Amaratunga *et al.*, 2013).

#### 4.4.2 *PfKelch13*-independent ART resistance

Next, RSA were carried out after the essential *PfKelch13* compartment proteins were partially inactivated by knock sideways.

For *PfUBP1* (PF3D7\_0104300) rapalog, to induce the knock sideways and inactivate the protein, was added one hour prior to the ART pulse and was removed one hour after addition of ART (Fig 24 A). This partial inactivation resulted in a survival rate of 2.00% (SD, +/- 0.62), indicating that the parasites became resistant to ART to a moderate level (Fig 24 D). The next candidate, *PfAP-2 $\mu$*  (PF3D7\_1218300), was inactivated seven hours before the RSA start and rapalog treatment was continued until one hour after the addition of ART (Fig 24 B). Conditional removal of *PfAp-2 $\mu$*  using knock sideways rendered parasite resistant to ART with a mean survival rate of 2.16% (SD, +/- 0.59) (Fig 24 D), again resulting in moderate levels of survival. For *PfEps15* (PF3D7\_1025000), efficient inactivation required addition of rapalog 18 hours before starting the RSA and rapalog treatment was maintained until one hour after ART addition (Fig 24 C). This resulted in a mean survival rate of 2.29% (SD, +/- 1.55), comparable to the results obtained with *PfUBP1* and *PfAP-2 $\mu$*  (Fig 24 D). The highest resistance level was measured for *PfKIC7* (PF3D7\_0813000) that was inactivated the same way as *PfUBP1*, which resulted in a mean survival rate of 12.31% (SD, +/- 1.53). In contrast, addition of rapalog to 3D7 control cell line 12 hours prior to start of the RSA (Fig 23 B), as well as inactivation of *Pf2102* (PF3D7\_0210200) seven hours prior to start (Fig 24 B), an unrelated control protein that is not part of the *PfKelch13* compartment but is essential for parasite growth (Birnbaum *et al.*, 2017), did not result in detectable resistance as measured by RSA. The 3D7 control cell line achieved a mean survival rate of 0.08% (SD, +/- 0.05) (Fig. 24 D), while *Pf2102* showed a survival rate of 0.16% (SD, +/- 0.09) after inactivation of the target protein (Fig. 24 B, D).

In summary, these results show that partial inactivation of essential *PfKelch13* compartment proteins, all of which are involved in endocytosis, as well as inactivation of *PfKelch13* itself, reduces the responsiveness of *P. falciparum* parasites to ART. These finding indicate that these proteins are all part of the resistance pathway.

**A** *Pf*UBP1 +1xNLS / *Pf*KIC7 + 1xNLS**B** *Pf*AP-2 $\mu$  +1xNLS / *Pf*2102 + lyn**C** *Pf*Eps15 + 1xNLS

**Figure 24) RSA of essential *Pf*Kelch13-compartment members after partial inactivation of respective candidate by knock sideways. A, B, C) Scheme showing timing of inactivation (by addition of rapalog) and of RSA with *Pf*UBP1+1xNLS and *Pf*KIC7+1xNLS (A), with *Pf*AP-2 $\mu$ +1xNLS**

and *Pf2102+lyn* (B) and *PfEps15+1xNLS* (C). **D)** Graph showing parasite survival rate 72 hours after start of the RSA carried out as shown in (A), (B) and (C). Scheme of rapalog induction for 3D7 control parasites is depicted in Fig. 23 B. Each point shows an independent experiment. P value is indicated, two-tailed, unpaired Welch's t test. *NLS*, nuclear localization signal; *h*, hour; *DHA*, dihydroartemisinin; *Rap*, rapalog; *red line* indicates duration of rapalog treatment; *green line* indicated duration of DHA treatment; *green dotted line* marks 1% cut-off value for resistance (Witkowski & Amaratunga *et al.*, 2013).

## 4.5 Mutations in Africa and generation of mutation pools

### 4.5.1 Selection of SNPs for mutation pools

To test whether mutations in *PfKelch13* compartment members could be responsible for ART resistance in the field, different non-synonymous SNPs in *pfkic1* (PF3D7\_0606000), *pfkic2* (PF3D7\_1227700), *pfkic4* (PF3D7\_1246300), *pfkic5* (PF3D7\_1138700), *pfkic7* (PF3D7\_0813000), *pfkic9* (PF3D7\_1442400), *pfmyosinF* (PF3D7\_1329100), *pfubp1* (PF3D7\_0104300), identified in field samples were chosen and inserted into 3D7 parasites to test their relevance for ART resistance.

To search for new mutations, the following sources were used. First, from the MalariaGEN *Plasmodium falciparum* Community Project (MalariaGEN *et al.*, 2021), non-synonymous mutations were included for testing when they were mainly present in Africa with low to medium prevalence (0.1% to 40%). Furthermore, after personal communication with Oumou Maiga-Ascofaré, six mutations found in Southeast Asia were also added to the list. Overall, this resulted in 125 SNPs in 8 genes (Table 1).

In addition, mutations in these genes found in a sample obtained during the Fever without Source study in Ghana (Hogan *et al.*, 2018) and derived from a patient that was visiting the ward repeatedly, suffering from malaria were included. The person was treated several times with ART and sequencing confirmed that the patient was always infected with the same *Plasmodium* strain, indicating an infection with an ART resistant strain (Oumou Maiga-Ascofaré, personal communication). However, no mutation was present in *pfkelch13*, indicating *pfkelch13*-independent resistance. To investigate whether mutations in any of our genes of interest was the reason for this apparent resistance, genomic DNA was extracted from blood samples of this patient and our candidate genes were sequenced. This sequencing included *pfubp1*, *pfmyosin F*, *pfkic6*, *pfkic7*, *pfap-2 $\mu$* , *pfeps15* and parts of *pfap-2 $\alpha$*  and *pfmca2* (DNA extraction, PCR, sequencing, and preparation of samples for external sequencing at Microsynth SeqLab was kindly performed by Birgit Förster). This

revealed 18 non-synonymous mutations and 8 synonymous mutations (compared to 3D7 used as a reference), of which 7 non-synonymous and 6 synonymous mutations overlapped with SNPs also listed in MalariaGEN, and 11 non-synonymous and 2 synonymous mutations that had not been described before (Appendix D.1). Beside *pfkelch13*, no mutations were found for *PfKIC7* and *Pfap-2μ*. Overall, this resulted in 7 non-synonymous SNPs (including two mutations in *PfMyosinF* that had not been described before) in 3 genes that were selected for analysis together with the mutations selected from the database searches. The remaining 11 non-synonymous SNPs found in the sequencing were not tested in the pools since either the N-terminal location of the SNPs in very huge genes hindered their inclusion (i.e. for *PfUBP1*) or sequencing of the candidates was not finished until the pools were prepared and synthesized by GenScript (i.e. *PfMyosinF*).

To make possible to analyze this large number of mutations, the mutations were tested in pools (i.e. inserting all SNPs at the same time into the gene) in 3D7 using SLI to modify the corresponding genes (Table 1).

**Table 1) List of all SNPs collected for mutation pools of the candidate genes indicated.** Detailed description of the selected mutations is provided in the respective section of each candidate. Data on prevalence of the different candidates are listed in Appendix D.1. *Asterisk (\*)*, indicates SNP that were not tested in the pool since they were detected after SLI plasmids were prepared for transfection or were located in the N-terminal region of the gene which would have complicated their inclusion due to the large size of this gene; *asterisk (\*\*)*, mark synonymous mutations that were not included in the testing.

Candidate	Mutation	Reference
<i>PKIC1</i> (PF3D7_0606000)	D483H	MalariaGen
	D535G	MalariaGen
	D862V	MalariaGen
	I873M	MalariaGen
	K231E	MalariaGen
	K676N	MalariaGen
	K883T	MalariaGen
	N179K	MalariaGen
	N633Y	MalariaGen
	N634Y	MalariaGen
	N688Y	MalariaGen
	N971S	MalariaGen
	Q1042K	MalariaGen
	S394N	MalariaGen
	S429P	MalariaGen
	T679A	MalariaGen
	V543F	MalariaGen





<i>Pf</i> UBP1 (PF3D7_0104300)	D2704E	MalariaGen
	D2925N	MalariaGen
	G2810C	MalariaGen
	K3013Q	MalariaGen
	M2618V	MalariaGen
	N2165I	MalariaGen
	N2669S	MalariaGen
	Q2355E	MalariaGen
	Y2530H	MalariaGen
	N1710S*	Sequencing Ghana
	K1914N*	Sequencing Ghana
	E1915K*	Sequencing Ghana
	1283F**	Sequencing Ghana

#### 4.5.2 *Pf*KIC1 (PF3D7\_0606000)

The candidate *Pf*KIC1 (PF3D7\_0606000) is a protein encoded by a gene located on chromosome 6 with a predicted protein comprising 1063 amino acids (aa). Functional analysis of the protein sequence using InterPro 84.0 yielded no domain prediction for this candidate. Seventeen different non-synonymous mutations were all simultaneously introduced into the genomic *pfkic1* using the SLI-system, resulting in the following amino acid changes of the encoded protein compared to 3D7 sequence: N179K / K231E / S394N / S429P / D483H / D535G / V543T / N633Y / N634Y / K676N / T679A / N688Y / D862V / I873M / K883T / N971S / Q1042K (Fig. 25 A). A sequence encoding GFP was also added, to permit detection of the mutated protein and to facilitate detection of integration of the construct. PCR confirmed correct integration of the construct, resulting in a parasite line expressing the modified *Pf*KIC1 with the 17 mutations (*KIC1*<sup>mutpool</sup>) from the endogenous locus (Fig 25 B). To exclude the possibility that the GFP-tag interfered with the result, a parasite line wherein the wild type *pfkic1* gene was fused to the sequence encoding 2xFKBP-GFP-2xFKBP (*KIC1*<sup>wt</sup>) (kindly provided by Jakob Birnbaum) was used as a control. *KIC1*<sup>mutpool</sup> showed a location in foci of which one was always at the parasite's digestive vacuole, which is typical for *Pf*Kelch13 and the Kelch13 compartment members (Fig 25 C) resembling the location of *KIC1*<sup>wt</sup> in previous work (Birnbaum, 2017). Per definition 1% marks the cut-off value for parasite resistance to artemisinin by RSA (Witkowski & Amaratunga *et al.*, 2013). Since *KIC1*<sup>mutpool</sup> parasites reached a mean survival rate of only 0.12%, comparable to the *KIC1*<sup>wt</sup> control, it can be assumed that none of the mutations changed the susceptibility of the parasites to ART (Fig 25 D).

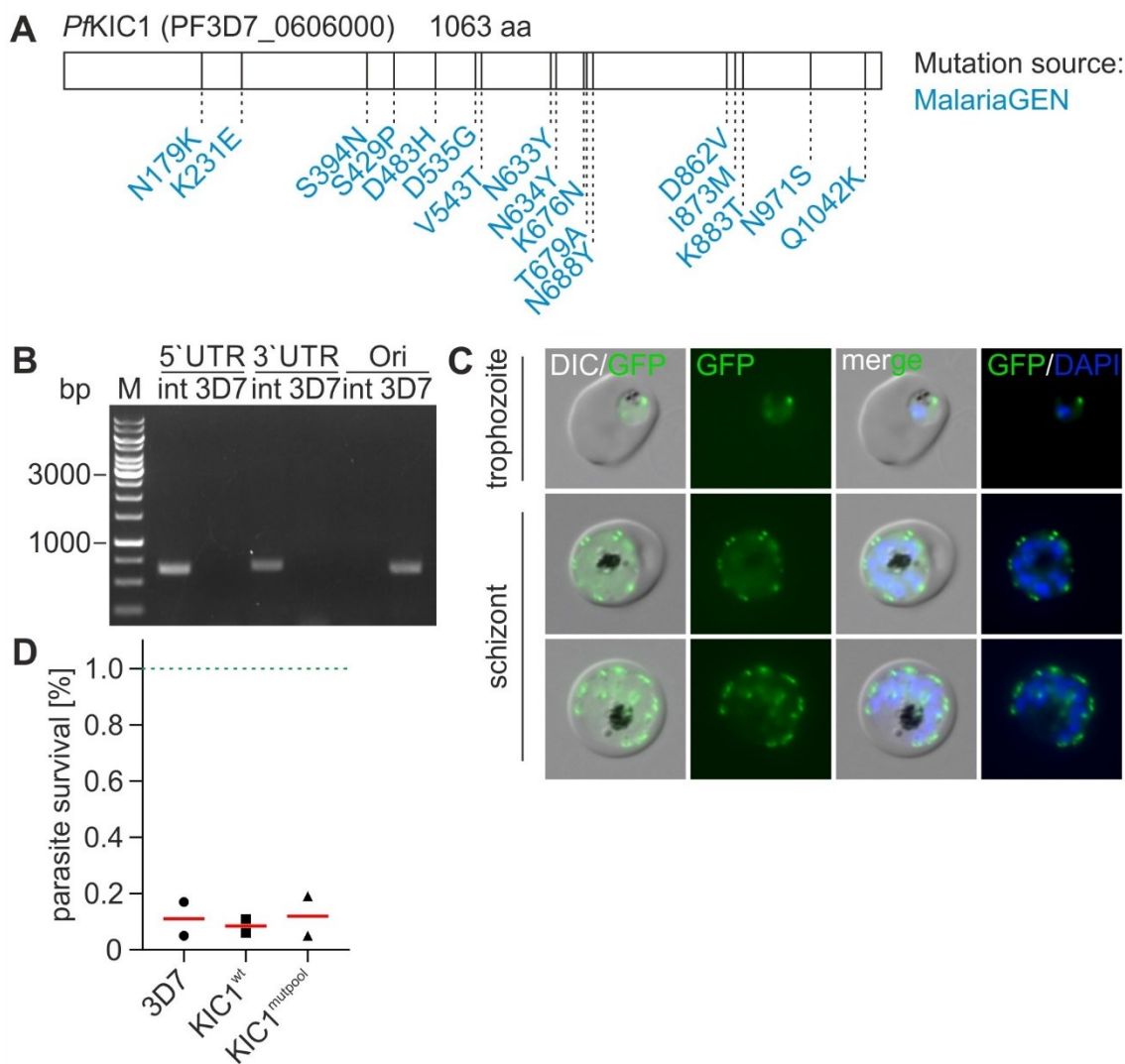


**Figure 25) Analysis of mutant *PfKIC1* (PF3D7\_0606000)** **A**) Scheme showing mutations included in *KIC1*<sup>mutpool</sup>. **B**) Agarose gel showing PCR products demonstrating correct integration of the SLI plasmid into 3D7 genome to obtain *KIC1*<sup>mutpool</sup> parasites. Primers (see Appendix C) were used to confirm 5'-integration (5'UTR, 632 bp) and 3'-integration (3'UTR, 678 bp) and to demonstrate absence of original locus in the *KIC1*<sup>mutpool</sup> parasites (Ori, 638 bp). 3D7 gDNA was used as reference (ori 3D7 638 bp). **C**) Live cell images of different developmental stages of knock-in cell line *KIC1*<sup>mutpool</sup>. **D**) Graph showing parasite survival rate (% survival compared to control without DHA) 72 hours after 6 h DHA treatment in standard RSA. Each point shows an independent experiment. Red vertical bar shows mean. Green dashed line shows 1% survival, above which parasites are considered resistant (Witkowski & Amaratunga *et al.*, 2013). aa, amino acid; DIC, differential interference contrast; GFP, green fluorescent protein; DAPI, 4',6-Diamidin-2-phenylindol; M, marker (GeneRuler™ 1 kb, Thermo Scientific); bp, base pairs; int, integrant; ori, original locus; wt, wildtype; mut, mutant.

### 4.5.3 *PfKIC2* (PF3D7\_1227700)

The candidate *PfKIC2* (PF3D7\_1227700) is located on chromosome 12 and encodes a protein of 771 aa. InterPro 84.0 predicted no domain for *PfKIC2*. The SLI-system was used to simultaneously incorporate seven non-synonymous SNPs chosen from MalariaGEN into the genomic *pfkic2* locus, resulting in the amino acid changes G167D / E207Q / K321N / E343K / N449T / Y472F / K651M compared to 3D7 sequence (Fig 26 A). In addition, the sequence encoding GFP was C-terminally added to the mutated *PfKIC2*. Correct integration of the gene modification construct was confirmed by PCR (Fig. 26 B). The resulting *KIC2<sup>mutpool</sup>* showed a comparable localization in a pattern typical of *PfKelch13* and its compartment members by fluorescence microscopy (Fig. 26 C) compared to a previously generated endogenously FKBP and GFP-tagged unmodified *PfKIC2* (*KIC2<sup>wt</sup>*) (kindly provided by Jakob Birnbaum). *In vitro* DHA resistance of *KIC2<sup>mutpool</sup>* parasites was tested in a standard RSA. The *KIC2<sup>mutpool</sup>* parasites showed a mean survival rate of 0.05% and showed no significant change in sensitivity to DHA compared to the *KIC2<sup>wt</sup>* cell line that reached a mean survival rate of 0.08% (Fig 26 D). Since the survival rates of the *KIC2<sup>mutpool</sup>* parasites was below the 1% cut-off value (Witkowski & Amaratunga *et al.*, 2013), this indicated that none of the seven mutations confers resistance to ART.

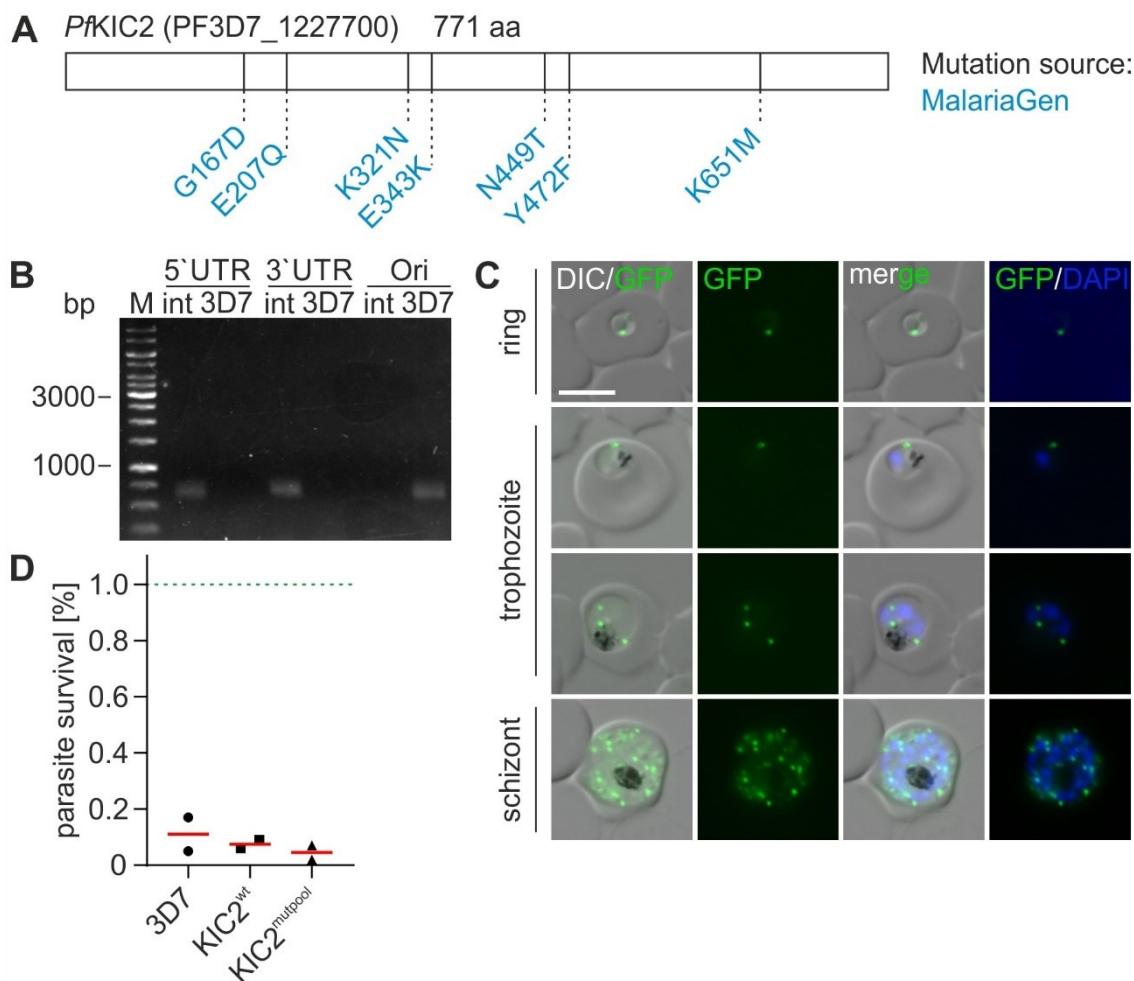


**Figure 26) Analysis of mutant *PfKIC2* (PF3D7\_1227700)** **A**) Scheme showing mutations included in KIC2<sup>mutpool</sup>. **B**) Agarose gel showing PCR products demonstrating correct integration of the SLI plasmid into 3D7 genome to obtain KIC2<sup>mutpool</sup> parasites. Primers (see Appendix C) were used to confirm 5'-integration (5'UTR, 627 bp) and 3'-integration (3'UTR, 652 bp) and to demonstrate absence of original locus in the KIC2<sup>mutpool</sup> parasites (Ori, 613 bp). 3D7 gDNA was used as reference (ori 3D7 613 bp). **C**) Live cell images of different developmental stages of knock-in cell line KIC2<sup>mutpool</sup>. **D**) Graph showing parasite survival rate (% survival compared to control without DHA) 72 hours after 6 h DHA treatment in standard RSA. Each point shows an independent experiment. Red vertical bar shows mean. Green dashed line shows 1% survival, above which parasites are considered resistant (Witkowski & Amaratunga *et al.*, 2013). aa, amino acid; DIC, differential interference contrast; GFP, green fluorescent protein; DAPI, 4',6-Diamidin-2-phenylindol; M, marker (GeneRuler™ 1 kb, Thermo Scientific); bp, base pairs; int, integrant; ori; original locus; wt, wildtype; mut, mutant.

#### 4.5.4 *PfKIC4* (PF3D7\_1246300)

Kelch13 interacting candidate 4 (PF3D7\_1246300) is a protein of 888 aa and the encoding gene is located on chromosome 12. According to InterPro 84.0, the C-terminal part of this protein contains a clathrin adaptor domain. In total, 12 non-synonymous SNPs were chosen

to be included in the mutation pool, leading to the following amino acid changes in *PfKIC4* compared to 3D7 sequence: D120N / I121V / N123S / P170S / Y179C / M375V / N405S / V619A / P621A / N624I / N661H / T888A (Fig. 27 A). The SLI system was used to integrate the construct harboring the 12 mutations into the 3D7 genome resulting in a parasite line expressing the modified *PfKIC4* (*KIC4<sup>mutpool</sup>*) fused to GFP from the endogenous locus and correct integrations was confirmed by PCR (Fig 27 B). *KIC4<sup>mutpool</sup>* was expressed in all asexual developmental stages and localized in foci, similar to wild type *PfKIC4* fused to FKBP and GFP (*KIC4<sup>wt</sup>*) in a pattern typical for *PfKelch13* and its compartment proteins (Birnbaum, 2017) (Fig 27 C). The resistance of *KIC4<sup>mutpool</sup>* parasites to artemisinin was determined by standard RSA and showed no change of responsiveness to the drug compared to 3D7 or the *KIC4<sup>wt</sup>* control parasites (Fig. 27 D). The mean survival rate of *KIC4<sup>mutpool</sup>* was 0.08%, whereas the mean survival rate of *KIC4<sup>wt</sup>* was 0.65%, both clearly below the cut-off value of 1% (Witkowski & Amaratunga *et al.*, 2013). Hence, none of the SNPs inserted into *PfKIC4* influences the responsiveness of the parasite to ART.

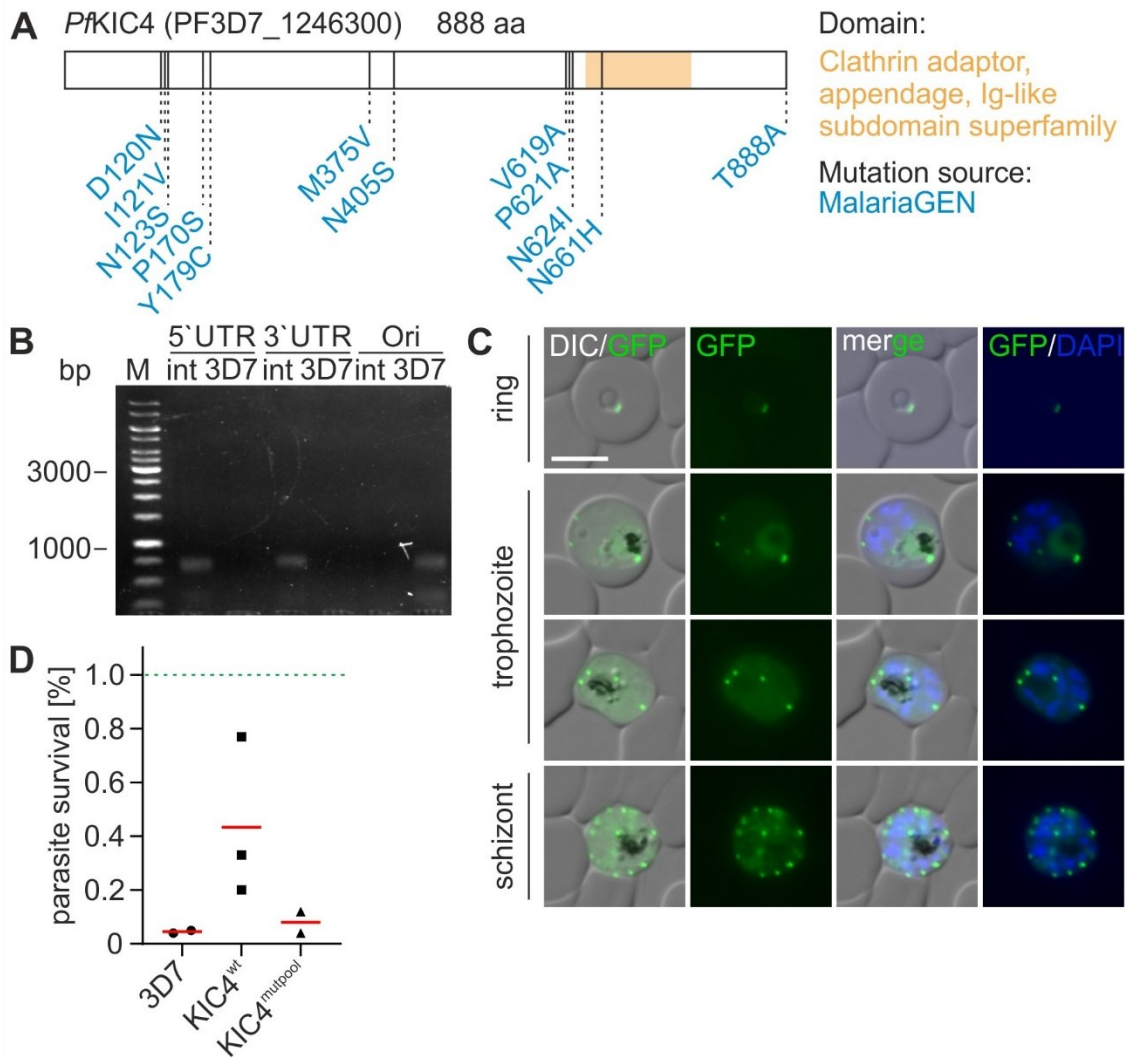


**Figure 27) Analysis of mutant *PfKIC4* (PF3D7\_1246300)** **A)** Scheme showing mutations included in *KIC4*<sup>mutpool</sup>. **B)** Agarose gel showing PCR products demonstrating correct integration of the SLI plasmid into 3D7 genome to obtain *KIC4*<sup>mutpool</sup> parasites. Primers (see Appendix C) were used to confirm 5'-integration (5'UTR, 628 bp) and 3'-integration (3'UTR, 671 bp) and to demonstrate absence of original locus in the *KIC4*<sup>mutpool</sup> parasites (Ori, 627 bp). 3D7 gDNA was used as reference (ori 3D7 627 bp). **C)** Live cell images of different developmental stages of knock-in cell line *KIC4*<sup>mutpool</sup>. **D)** Graph showing parasite survival rate (% survival compared to control without DHA) 72 hours after 6 h DHA treatment in standard RSA. Each point shows an independent experiment. Red vertical bar shows mean. Green dashed line shows 1% survival, above which parasites are considered resistant (Witkowski & Amaratunga *et al.*, 2013). aa, amino acid; DIC, differential interference contrast; GFP, green fluorescent protein; DAPI, 4',6-Diamidin-2-phenylindol; M, marker (GeneRuler™ 1 kb, Thermo Scientific); bp, base pairs; int, integrant; ori; original locus; wt, wildtype; mut, mutant.

#### 4.5.5 *PfKIC5* (PF3D7\_1138700)

Kelch13 interaction candidate 5 (PF3D7\_1138700) is encoded on chromosome 11 and is a protein of 1870 aa. The C-terminal part of this protein from position 1849 to 1866 contains a hydrophobic region predicted to be a transmembrane domain according to InterPro 84.0, but not TMHMM which is typically used to predict such domains in *P. falciparum* proteins (VEuPathDB, 2021). Overall, 33 non-synonymous SNPs were included in the mutation pool resulting in the following amino acid changes compared to 3D7 sequence: V72I / H138Y / D169N / M324V / E497Q / P516S / N525S / F570L / G727E / K751Q / V836I / M975I / K985N / R1040K / E1055G / Q1127K / H1198Y / N1268H / T1381A / Q1421K / E1646G / S1721A / Q110E / K258R / G264D / V348I / K384I / A471T / S1044R / L1066P / E1354D / K1411R / G1417D (Fig 28 A). A C-terminal GFP tag was also added. After successful selection of the cell line expressing the modified *PfKIC5* from the endogenous *pfkic5* locus (*KIC5*<sup>mutpool</sup>), correct integration was confirmed by PCR (Fig. 28 B). The localization of *KIC5*<sup>mutpool</sup> was assessed by live cell imaging (Fig 28 C). *KIC5*<sup>mutpool</sup> was expressed throughout the asexual cycle and the localization was typical for a *PfKelch13* compartment protein and was similar to the localization of the unmodified *PfKIC5* fused to 2xFKBP-GFP-2xFKBP (*KIC5*<sup>wt</sup>) that had previously been generated (kindly provided by Jakob Birnbaum) and was used here as a control for the RSA. The *KIC5*<sup>mutpool</sup> parasites reached a mean survival rate of 0.15% in a standard RSA, while the *KIC5*<sup>wt</sup> parasites showed a mean survival rate of 0.3% (Fig 28 D). Since both values were comparable and below the cut-off value of 1% (Witkowski & Amaratunga *et al.*, 2013), it can be concluded that the 33 mutations introduced into *PfKIC5* in the *KIC5*<sup>mutpool</sup> parasites did not render them resistant to ART.

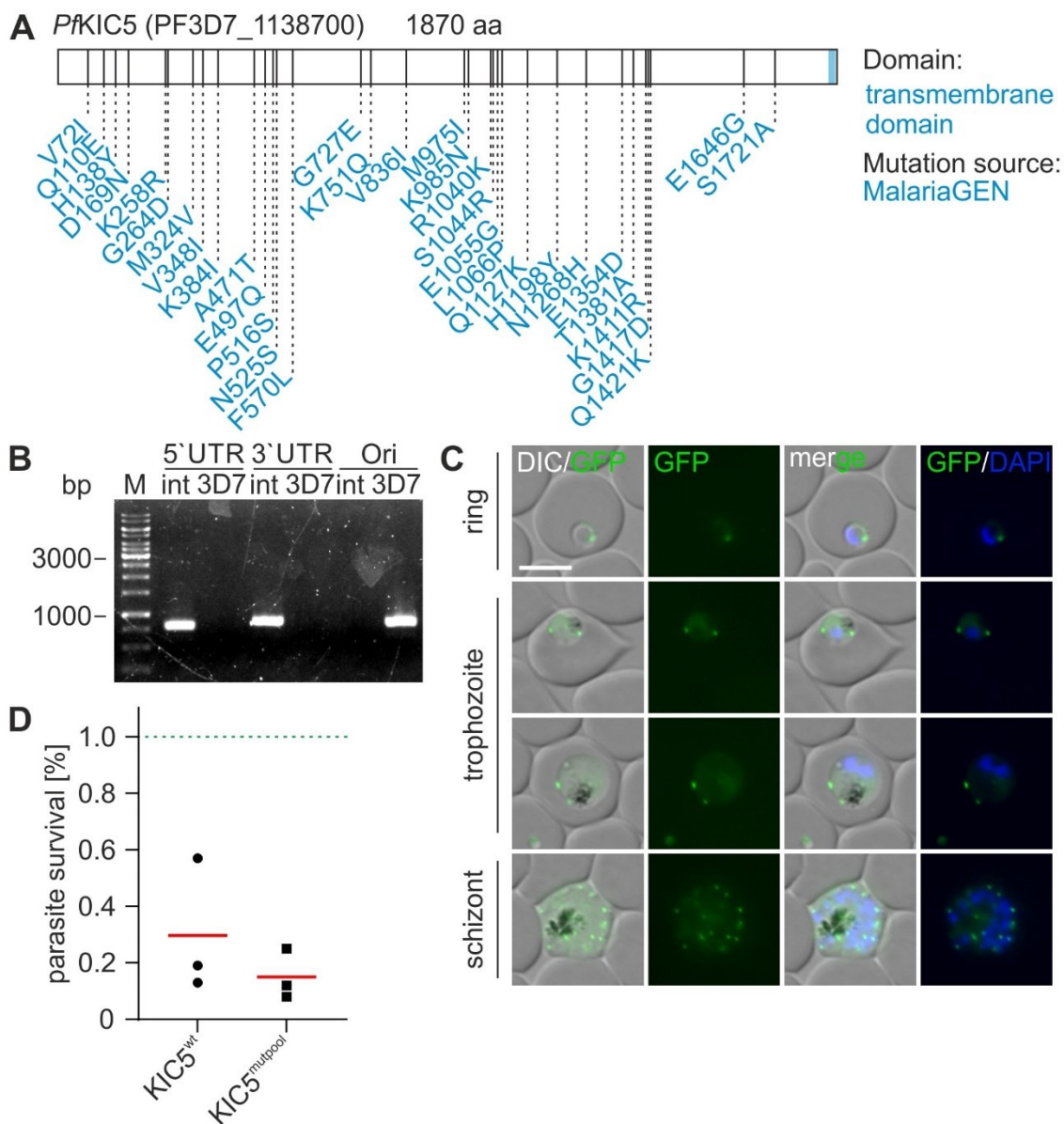


**Figure 28) Analysis of mutant *PfKIC5* (PF3D7\_1138700)** **A)** Scheme showing mutations included in *KIC5*<sup>mutpool</sup>. **B)** Agarose gel showing PCR products demonstrating correct integration of the SLI plasmid into 3D7 genome to obtain *KIC5*<sup>mutpool</sup> parasites. Primers (see Appendix C) were used to confirm 5'-integration (5'UTR, 779 bp) and 3'-integration (3'UTR, 848 bp) and to demonstrate absence of original locus in the *KIC5*<sup>mutpool</sup> parasites (Ori, 817 bp). 3D7 gDNA was used as reference (ori 3D7 817 bp). **C)** Live cell images of different developmental stages of knock-in cell line *KIC5*<sup>mutpool</sup>. **D)** Graph showing parasite survival rate (% survival compared to control without DHA) 72 hours after 6 h DHA treatment in standard RSA. Each point shows an independent experiment. Red vertical bar shows mean. Green dashed line shows 1% survival, above which parasites are considered resistant (Witkowski & Amaratunga *et al.*, 2013). aa, amino acid; DIC, differential interference contrast; GFP, green fluorescent protein; DAPI, 4',6-Diamidin-2-phenylindol; M, marker (GeneRuler™ 1 kb, Thermo Scientific); bp, base pairs; int, integrant; ori; original locus; wt, wildtype; mut, mutant.

#### 4.5.6 *PfKIC7* (PF3D7\_0813000)

The gene of the Kelch13 interacting candidate *PfKIC7* (PF3D7\_0813000) is located on chromosome 8 and encodes a protein of 599 aa. Search on InterPro 84.0 predicted no protein domains for this candidate. Using the SLI-system, five different non-synonymous mutations were simultaneously introduced into the genomic *pfkic7*, leading to the following amino acid changes compared to 3D7 sequence: I130V / P318S / N434S / S576N / N596K (Fig 29 A). Correct integration of the construct was confirmed by PCR (Fig. 29 B). The resulting parasite line expressing a modified *PfKIC7* (*KIC7<sup>mutpool</sup>*) from the endogenous locus showed that *KIC7<sup>mutpool</sup>* was expressed throughout the asexual life cycle in foci showing the typical pattern of *PfKelch13* compartment proteins and similar to the wild type *PfKIC7* fused to GFP and FKBP (*KIC7<sup>wt</sup>*) (Birnbaum, 2017) (Fig 29 C). Parasite survival rate of the *KIC7<sup>mutpool</sup>* parasites was tested by standard RSA and compared to the survival of *KIC7<sup>wt</sup>*. The mean survival rate of *KIC7<sup>mutpool</sup>* was 0.13%, whereas the *KIC7<sup>wt</sup>* parasites showed a survival rate of 0.26% (Fig 29 D). Since both parasite lines showed comparable survival rates and were clearly below the cut-off value of 1% (Witkowski & Amaratunga *et al.*, 2013), it can be assumed that none of the selected non-synonymous mutations rendered the parasites resistant to ART.

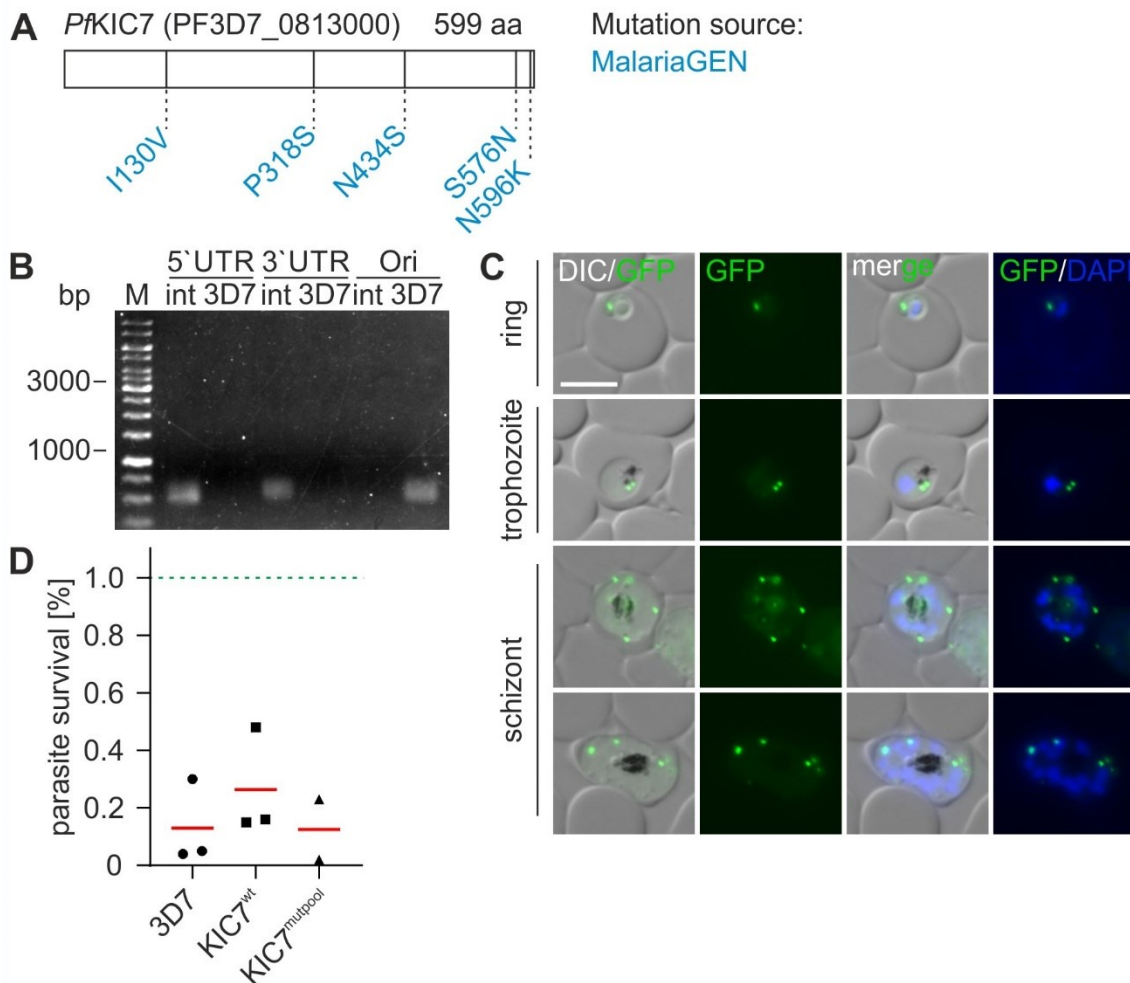


**Figure 29) Analysis of mutant *PfKIC7* (PF3D7\_0813000)** **A)** Scheme showing mutations included in *KIC7*<sup>mutpool</sup>. **B)** Agarose gel showing PCR products demonstrating correct integration of the SLI plasmid into 3D7 genome to obtain *KIC7*<sup>mutpool</sup> parasites. Primers (see Appendix C) were used to confirm 5'-integration (5'UTR, 485 bp) and 3'-integration (3'UTR, 522 bp) and to demonstrate absence of original locus in the *KIC7*<sup>mutpool</sup> parasites (Ori, 483 bp). 3D7 gDNA was used as reference (ori 3D7 483 bp). **C)** Live cell images of different developmental stages of knock-in cell line *KIC7*<sup>mutpool</sup>. **D)** Graph showing parasite survival rate (% survival compared to control without DHA) 72 hours after 6 h DHA treatment in standard RSA. Each point shows an independent experiment. Red vertical bar shows mean. Green dashed line shows 1% survival, above which parasites are considered resistant (Witkowski & Amaratunga *et al.*, 2013). aa, amino acid; DIC, differential interference contrast; GFP, green fluorescent protein; DAPI, 4',6-Diamidin-2-phenylindol; M, marker (GeneRuler™ 1 kb, Thermo Scientific); bp, base pairs; int, integrant; ori; original locus; wt, wildtype; mut, mutant.

#### 4.5.7 *PfKIC9* (PF3D7\_1442400)

The candidate *PfKIC9* (PF3D7\_1442400) is a protein encoded by a gene located on chromosome 14 encoding a protein of 2113 aa. According to InterPro, no protein domain is predicted for this candidate. Overall, 34 non-synonymous mutations were introduced into

the genomic *pfkic9* locus using the SLI-system resulting in the following amino acid changes compared to 3D7 sequence: L279I / N286H / S341N / I429S / M618T / G674V / K837I / N927H / I960V / T990R / K1039N / Q1045E / I1280L / D1345N / M1507I / V1586I / K1626N / I1688V / H1710R / E1861K / D1879V / P249Q / S282N / Y293N / D388E / K589R / D734Y / S753T / G984R / T996I / N1402K / S1549N / D2018E / V2072M (Fig. 30 A). After successful transfection of the plasmid and selection of the integrants, correct integration was confirmed by PCR (Fig. 30 B), resulting in a cell line expressing a modified version of *PfKIC9* (*KIC9<sup>mutpool</sup>*). Fluorescence microscopy showed that the localization of *KIC9<sup>mutpool</sup>* was typical for a Kelch13 compartment protein (Fig. 30 C) and comparable to the control cell line expressing the wild type *PfKIC9* fused to GFP and FKBP (*KIC9<sup>wt</sup>*) (kindly provided by Jakob Birnbaum). *KIC9<sup>mutpool</sup>* was expressed over the entire asexual developmental cycle with a very faint signal in ring stages and the typical foci pattern in later stages (Fig 30 C). In the standard RSA, *KIC9<sup>mutpool</sup>* parasites had a mean survival rate of 0.16%, whereas *KIC9<sup>wt</sup>* showed a mean survival rate of 0.09% (Fig 30 D). These survival rates were comparable to that of 3D7 (mean survival rate of 0.21%) and lower than the cut-off value of 1% (Witkowski & Amaratunga *et al.*, 2013). This indicates that none of the SNPs introduced into *Pfkic9* rendered the parasites ART resistant.

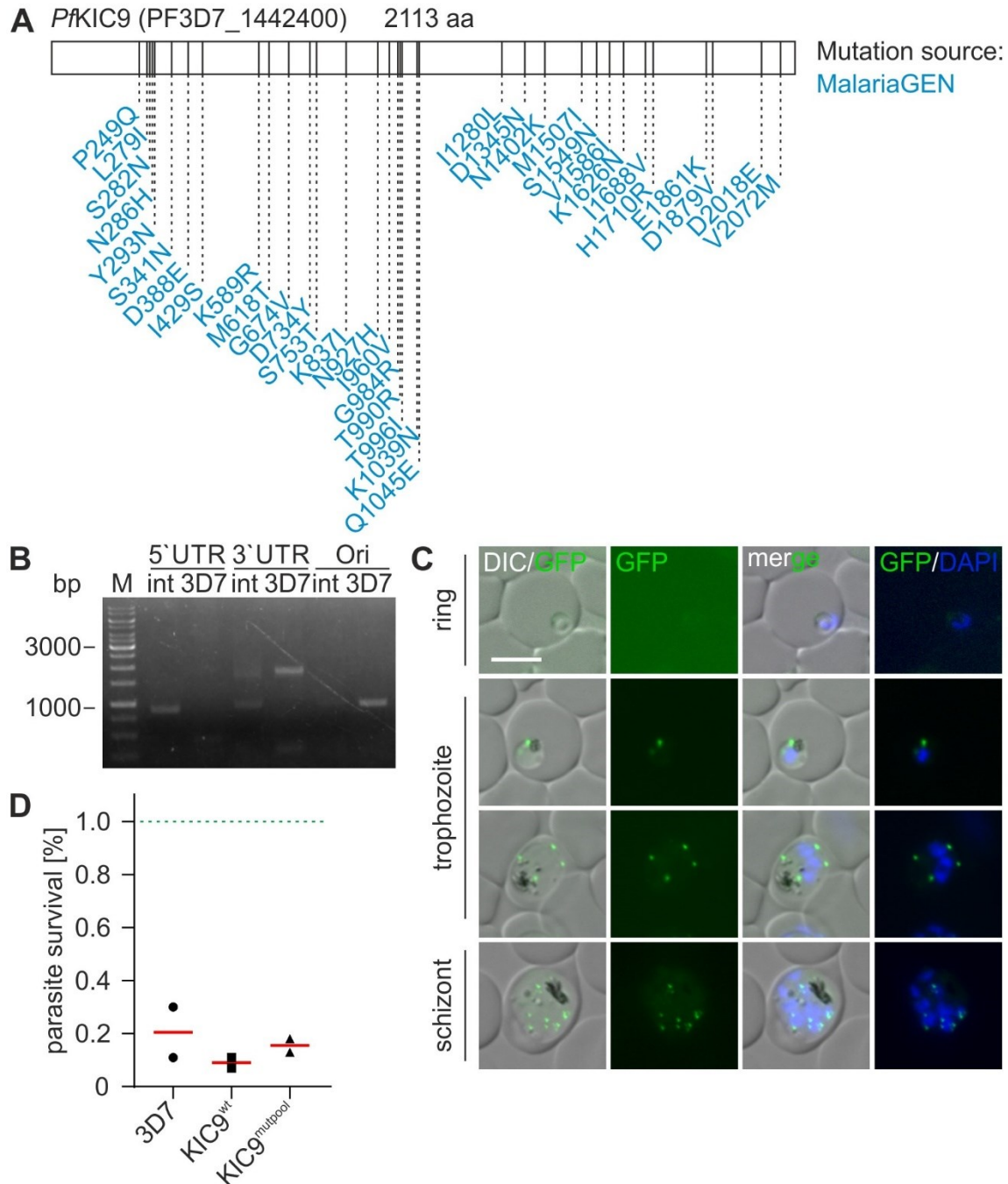


**Figure 30** Analysis of mutant *PfKIC9* (PF3D7\_1442400) **A**) Scheme showing mutations included in KIC9<sup>mutpool</sup>. **B**) Agarose gel showing PCR products demonstrating correct integration of the SLI plasmid into 3D7 genome to obtain KIC9<sup>mutpool</sup> parasites. Primers (see Appendix C) were used to confirm 5'-integration (5'UTR, 871 bp) and 3'-integration (3'UTR, 921 bp) and to demonstrate absence of original locus in the KIC9<sup>mutpool</sup> parasites (Ori, 914 bp). 3D7 gDNA was used as reference (ori 3D7 914 bp). **C**) Live cell images of different developmental stages of knock-in cell line KIC9<sup>mutpool</sup>. **D**) Graph showing parasite survival rate (% survival compared to control without DHA) 72 hours after 6 h DHA treatment in standard RSA. Each point shows an independent experiment. Red vertical bar shows mean. Green dashed line shows 1% survival, above which parasites are considered resistant (Witkowski & Amaratunga *et al.*, 2013). aa, amino acid; DIC, differential interference contrast; GFP, green fluorescent protein; DAPI, 4',6-Diamidin-2-phenylindol; M, marker (GeneRuler™ 1 kb, Thermo Scientific); bp, base pairs; int, integrant; ori, original locus; wt, wildtype; mut, mutant.

#### 4.5.8 *Pf*MyosinF (PF3D7\_1329100)

*Pf*MyosinF (PF3D7\_1329100) is a protein of 2160 aa encoded by a gene located on chromosome 13. InterPro 84.0 detected a myosin head domain in the N-terminal part in position 67 to 831. This domain is followed by two P-loop containing nucleoside triphosphate hydrolases and an IQ motif EF-hand binding site at position 1008 to 1060. In the C-terminal part, several WD40 repeats are located (Fig. 31 A). In total, eight non-synonymous mutations were included in the mutation pool, causing the following amino acid changes compared to 3D7 sequence: G873D / V1193E / C1196S / M1872L / L1165V / I2068T / H1587R / N1615K (Fig 31 A). Via the SLI system, the eight non-synonymous mutations were introduced into the endogenous *pfmyosinF* locus resulting in a cell line with the modified *Pf*MyosinF (MyosinF<sup>mutpool</sup>) as verified by PCR (Fig. 31 B). Localization of MyosinF<sup>mutpool</sup> was assessed by live cell imaging. The protein was found to be mainly expressed in trophozoite to schizont stages but also a very faint signal was visible in ring stages (see section 4.2.1) (Fig 31 C). When MyosinF<sup>mutpool</sup> parasites were tested in standard RSA, a mean survival rate of 0.11% was observed, which was below the 1% cut-off value (Witkowski & Amaratunga *et al.*, 2013), indicating that the selected mutations did not render parasites resistant to ART (Fig 31 D).

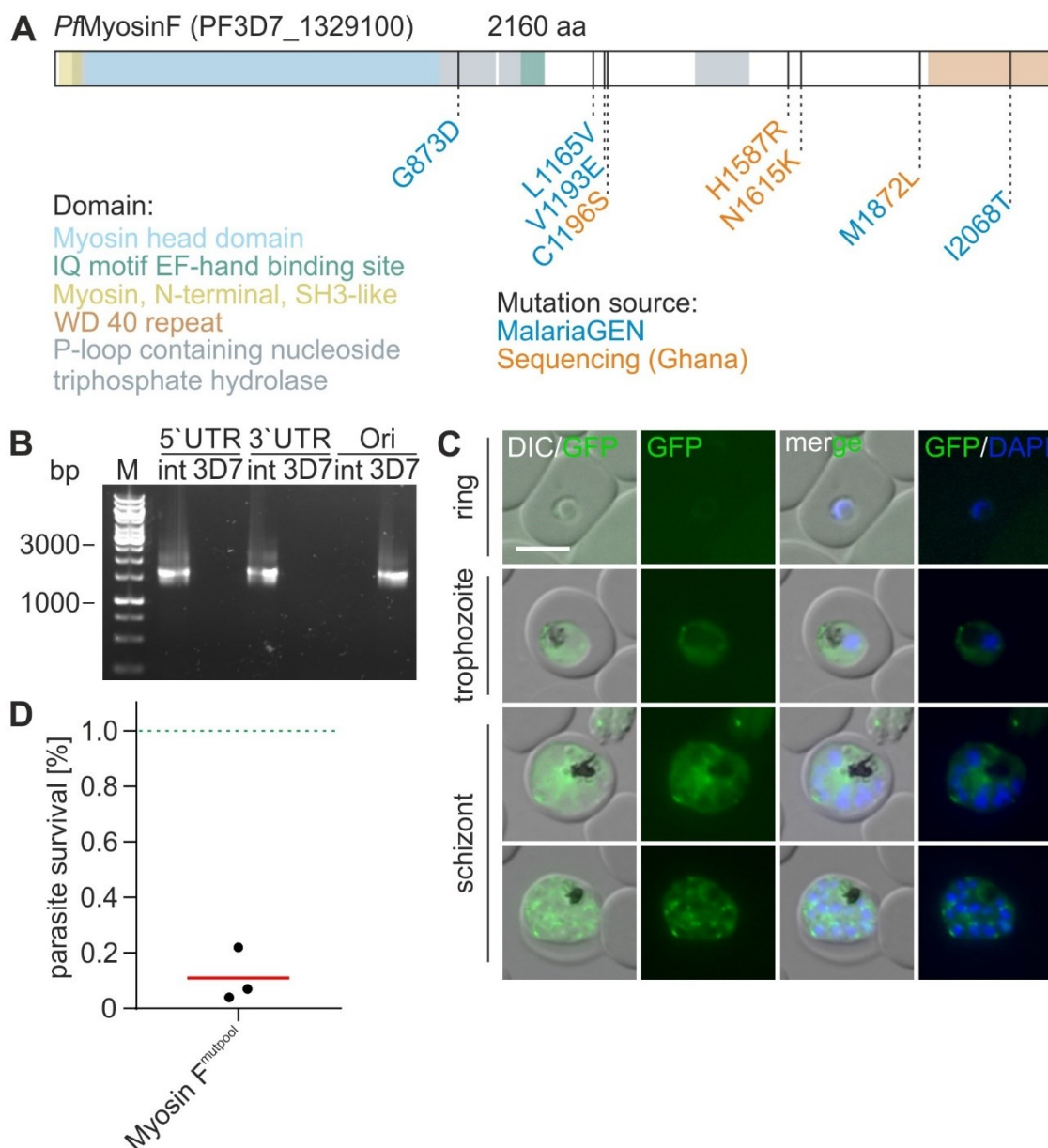


**Figure 31) Analysis of mutant *Pf*MyosinF (PF3D7\_1329100)** **A**) Scheme showing mutations included in MyosinF<sub>mutpool</sub>. **B**) Agarose gel showing PCR products demonstrating correct integration of the SLI plasmid into 3D7 genome to obtain MyosinF<sub>mutpool</sub> parasites. Primers (see Appendix C) were used to confirm 5'-integration (5'UTR, 1639 bp) and 3'-integration (3'UTR, 1676 bp) and to demonstrate absence of original locus in the MyosinF<sub>mutpool</sub> parasites (Ori, 1630 bp). 3D7 gDNA was used as reference (ori 3D7 1630 bp). **C**) Live cell images of different developmental stages of knock-in cell line MyosinF<sub>mutpool</sub>. **D**) Graph showing parasite survival rate (% survival compared to control without DHA) 72 hours after 6 h DHA treatment in standard RSA. Each point shows an independent experiment. *Red vertical bar* shows mean. *Green dashed line* shows 1% survival, above which parasites are considered resistant (Witkowski & Amaratunga *et al.*, 2013). aa, amino acid; DIC, differential interference contrast; GFP, green fluorescent protein; DAPI, 4',6-Diamidin-2-phenylindol; M, marker (GeneRuler™ 1 kb, Thermo Scientific); bp, base pairs; int, integrant; ori; original locus; wt, wildtype; mut, mutant.

#### 4.5.9 *Pf*UBP1 (PF3D7\_0104300)

A further member of the Kelch13 compartment is the ubiquitin carboxyl-terminal hydrolase, *Pf*UBP1 (PF3D7\_0104300) that is encoded by a gene located on chromosome 1 that encodes a protein of 3499 aa. Domain prediction via InterPro 84.0 revealed a ubiquitin specific protease domain from position 3170 to 3489. Using the SLI-system, nine mutations were simultaneously incorporated into the endogenous *pfubp1* locus that resulted in the following amino acid changes compared to 3D7 sequence: N2165I / Q2355E / Y2530H / M2618V / N2669S / D2704E / G2810C / D2925N / K3031Q (Fig 32 A). PCR verified correct integration of the construct, resulting in a cell line expressing a mutated *Pf*UBP1 (UBP1<sup>mutpool</sup>) from endogenous locus (Fig 32 B). The protein carrying the nine mutations showed a similar localization to *Pf*UBP1 2xFKBP-GFP of the wild type parasite line (UBP1<sup>wt</sup>) (Birnbaum, 2017) (Fig 32 C). In the standard RSA, the 1% cut-off value (Witkowski & Amaratunga *et al.*, 2013) was not exceeded, neither by UBP1<sup>mutpool</sup> (mean survival rate 0.15%), nor by UBP1<sup>wt</sup> (mean survival rate 0.13%), suggesting that none of the introduced mutations change the responsiveness of the parasites to ART (Fig 32 D).

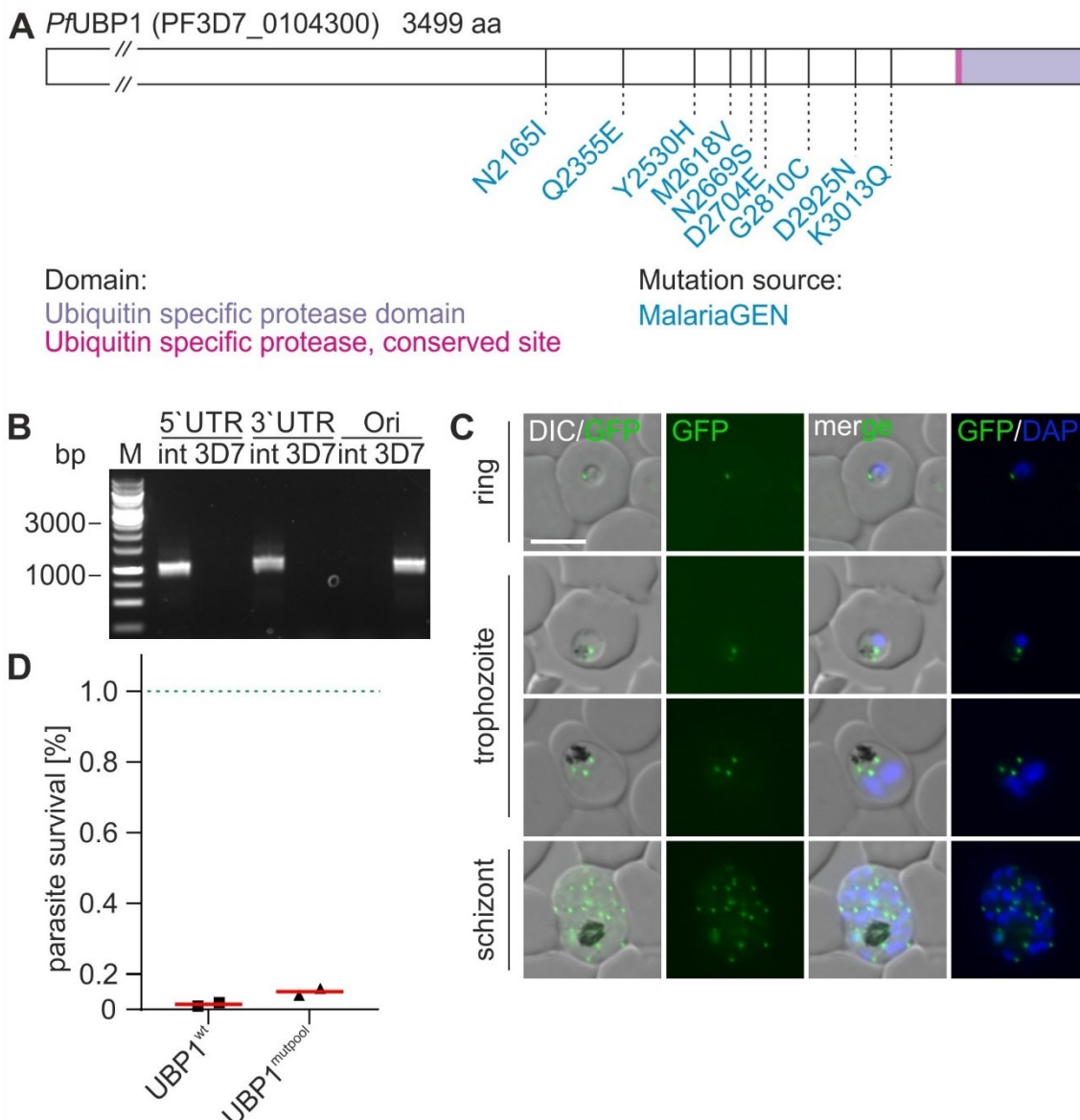


**Figure 32) Analysis of mutant *Pf*UBP1 (PF3D7\_0104300)** **A)** Scheme showing mutations included in UBP1<sup>mutpool</sup>. **B)** Agarose gel showing PCR products demonstrating correct integration of the SLI plasmid into 3D7 genome to obtain UBP1<sup>mutpool</sup> parasites. Primers (see Appendix C) were used to confirm 5'-integration (5'UTR, 1092 bp) and 3'-integration (3'UTR, 1179 bp) and to demonstrate absence of original locus in the UBP1<sup>mutpool</sup> parasites (Ori, 1129 bp). 3D7 gDNA was used as reference (ori 3D7 1129 bp). **C)** Live cell images of different developmental stages of knock-in cell line UBP1<sup>mutpool</sup>. **D)** Graph showing parasite survival rate (% survival compared to control without DHA) 72 hours after 6 h DHA treatment in standard RSA. Each point shows an independent experiment. Red vertical bar shows mean. Green dashed line shows 1% survival, above which parasites are considered resistant (Witkowski & Amaratunga *et al.*, 2013). aa, amino acid; DIC, differential interference contrast; GFP, green fluorescent protein; DAPI, 4',6-Diamidin-2-phenylindol; M, marker (GeneRuler™ 1 kb, Thermo Scientific); bp, base pairs; int, integrant; ori, original locus; wt, wildtype; mut, mutant.

## 4.6 Non-synonymous SNPs tested individually on their contribution to ART resistance

### 4.6.1 Non-synonymous SNPs in *PfMyosinF* (PF3D7\_1329100) do not influence ART resistance

*PfMyosinF* is part of the Kelch13 compartment and partially co-localizes with *PfKelch13* (see section 4.2.1). Besides testing various non-synonymous SNPs in the multi-pooled screening (section 4.5.8), five different non-synonymous SNPs were tested individually for their capability to induce ART resistance. The first reason for not including these SNPs into the pool was because four of the five SNPs are located in the N-terminal region of *pfmyosinF* which would have complicated their inclusion due to the large size of this gene. Secondly, some of these SNPs were selected for testing after the plasmid for the multipool analysis was already prepared for transfection. In total, five SLI plasmids were generated, each intended to result in one of the following amino acid changes in *PfMyosinF* compared to 3D7: N277S / D500G / Q635H / S969P / S1457L (Fig 33 A). Integration into the endogenous *pfmyosinF* locus was successful for all but the plasmid generating the amino acid change N277S, which failed to correctly integrate in 12 independent integration attempts. Correct integration of the remaining constructs was confirmed by PCR (see Appendix F.1), resulting in the four different parasite lines MyoF<sup>D500G</sup>, MyoF<sup>Q635H</sup>, MyoF<sup>S969P</sup> and MyoF<sup>S1457L</sup>. Standard RSA was performed with each of the cell lines and showed a mean parasite survival rate of 0.08% for MyoF<sup>D500G</sup>, 0.03% for MyoF<sup>Q635H</sup>, 0.07% for MyoF<sup>S969P</sup> and 0.05% for MyoF<sup>S1457L</sup> (Fig 33 B). All survival rates were therefore below the cut-off value of 1% that defines resistance (Witkowski & Amaratunga *et al.*, 2013), indicating that none of the tested non-synonymous SNPs rendered parasites resistant to ART.

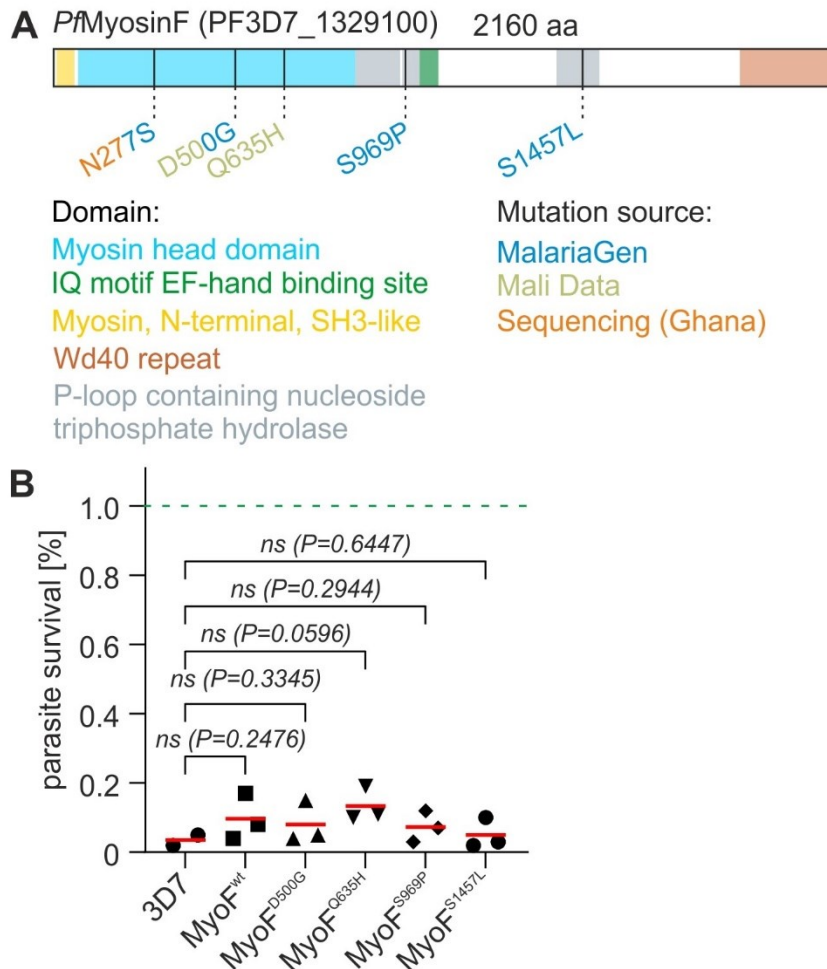


**Figure 33) Individually tested SNPs of *pfmyosinF*.** **A)** Scheme showing non-synonymous SNPs of *Pf*MyosinF chosen for separate testing in standard RSA. SNPs shown in more than one color were found in multiple sources. **B)** Graph showing parasite survival rate (% survival compared to control without DHA) 72 hours after 6 h DHA treatment in standard RSA. Each point shows an independent experiment. P value is indicated, two-tailed, unpaired Welch's t test. *Red vertical bar* shows mean. *Green dashed line* shows 1% survival, above which parasites are considered resistant (Witkowski & Amaratunga *et al.*, 2013). aa, amino acid; wt, wild type.

#### 4.6.2 Parasites with a SNP in *Pf*AP-2 $\alpha$ (PF3D7\_0617100) show a very mild reduction in susceptibility to ART compared to 3D7

The protein *Pf*AP-2  $\alpha$  comprises 1236 aa and is encoded by a gene located on chromosome 6. This candidate is interesting in the context of ART resistance since it is part of the AP-2 adaptor complex that is enrolled in endocytosis and it was shown before that other components of the AP-2 adaptor complex co-localize to *Pf*Kelch13 and influence ART resistance (see section 4.4.2). In 2018, *Rocamora et al.* reported that 3D7 parasites

artificially selected for ART contained a non-synonymous SNP leading to an H817P change in *PfAP-2α* (Rocamora *et al.*, 2018) (Fig 34 A). To test whether this non-synonymous SNP renders parasites resistant to ART, the SLI-system was used to incorporate the SNP into the endogenous *pfap-2α* locus of 3D7 parasites (*AP-2α*<sup>H817P</sup> cell line, kindly provided by Jakob Birnbaum), and a standard RSA was performed. In the standard RSA, the mean survival rate of the *AP-2α*<sup>H817P</sup> parasites was 0.68% which is under the cut-off value of 1% (Witkowski & Amaratunga *et al.*, 2013) (Fig 34 B). While this indicated that this SNP did not render the parasites resistant to ART according to the current 1% cut off, there was nevertheless a significant difference to the mean survival rate of the 3D7 control (mean survival rate 0.15%), indicating that this codon change resulted in a very mild increase in ART resistance.

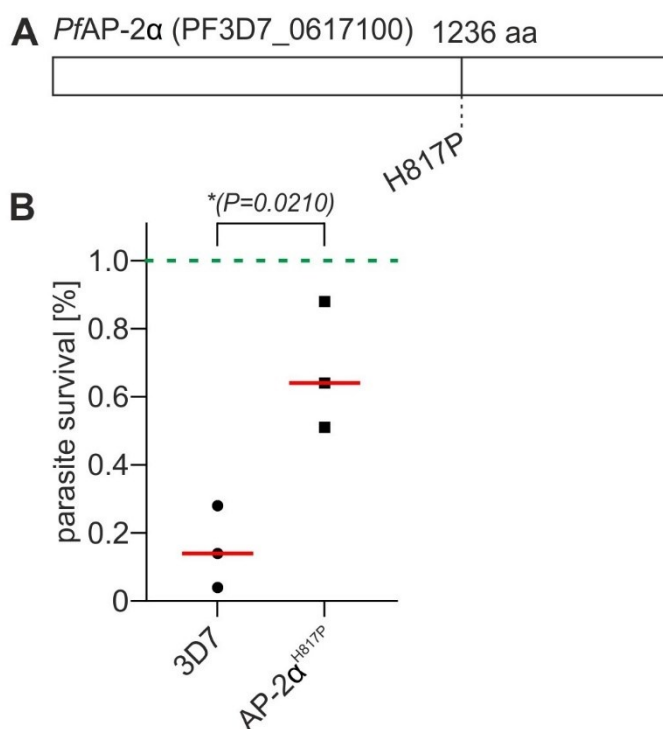


**Figure 34) Individual tested SNP of *pfap-2α*.** **A)** Scheme showing non-synonymous SNP of *PfAP-2α* chosen for separate testing in standard RSA. **B)** Graph showing parasite survival rate (% survival compared to control without DHA) 72 hours after 6 h DHA treatment in standard RSA. Each point shows an independent experiment. P value is indicated, two-tailed, unpaired Welch's t test. *Red vertical bar* shows mean. *Green dashed line* shows 1% survival, above which parasites are considered resistant (Witkowski & Amaratunga *et al.*, 2013). aa, amino acid.

#### 4.6.3 Asian non-synonymous SNP identified in *PfEps15* (PF3D7\_1025000) does not influence ART resistance

A genomic surveillance study including whole-genome sequencing data of *P. falciparum* isolates collected in Thailand from 2001 and 2014 reported a series of SNPs associated with ART resistance which included a non-synonymous SNP leading to the amino acid change K447R in *PfEps15* (Cerqueira *et al.*, 2017) (Fig 35 A). As *PfEps15* is part of the Kelch13 compartment and its inactivation renders parasites resistant to ART (see section 4.4.2), it was here tested if the K447R change in this protein decreases the sensitivity of the parasite to ART. In order to test this, the SLI-system was used to introduce the corresponding mutation into the *pfeps15* locus. At the same time, the sequence encoding *gfp* was added resulting in the cell line Eps15<sup>K447R</sup> (kindly provided by Jakob Birnbaum). When a standard RSA was performed with the Eps15<sup>K447R</sup> cell line, parasites reached a mean survival rate of 0.17% which is under the cut-off value of 1% (Witkowski & Amaratunga *et al.*, 2013), indicating that the parasites with the modified *pfeps15* locus did not become resistant to ART (Fig 35 B).

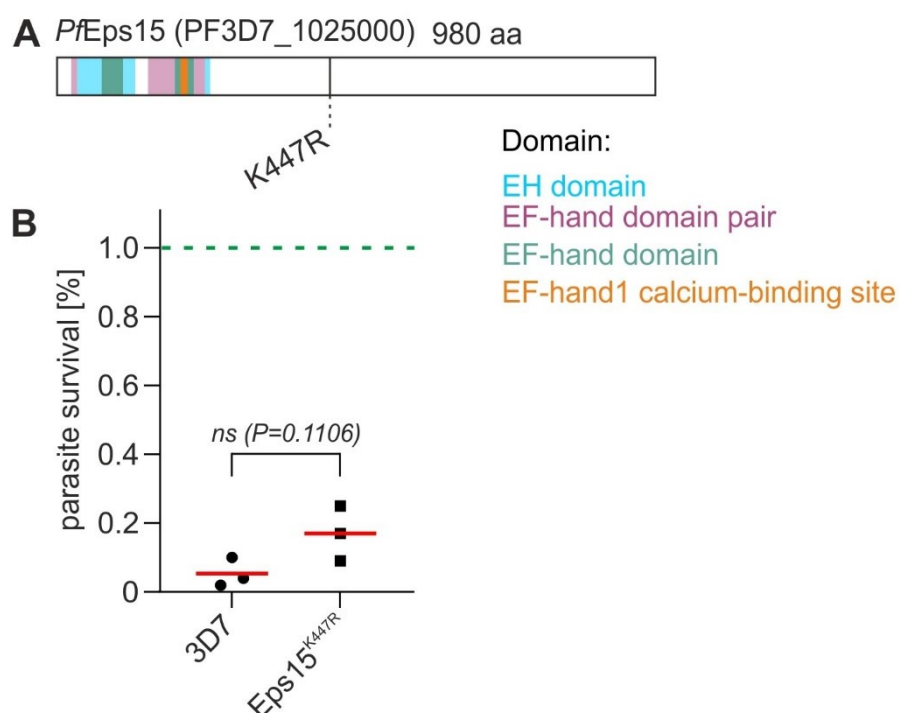


**Figure 35) Individual tested SNP of *pfeps15*.** **A)** Scheme showing non-synonymous SNP of *PfEps15* chosen for separate testing in standard RSA. **B)** Graph showing parasite survival rate (% survival compared to control without DHA) 72 hours after 6 h DHA treatment in standard RSA. Each point shows an independent experiment. P value is indicated, two-tailed, unpaired Welch's t test. Red vertical bar shows mean. Green dashed line shows 1% survival, above which parasites are considered resistant (Witkowski & Amaratunga *et al.*, 2013). aa, amino acid.

#### 4.6.4 *Pf*UBP1 (PF3D7\_0104300) SNP detected in Asia confers tolerance to ART

The candidate *Pf*UBP1 belongs to the Kelch13 compartment (Birnbaum *et al.*, 2020) and influences sensitivity of the parasite to ART when the protein is inactivated (see section 4.4.2). Genome surveillance data of field isolates collected in Thailand indicated that a non-synonymous SNP at codon 3138 of *pfubp1*, resulting in the amino acid change R3138H, was associated with ART resistance ((Cerqueira *et al.*, 2017) Fig 36 A). To test whether this mutation indeed leads to ART resistant parasites, the SLI system was used to incorporate this SNP into the endogenous *pfubp1* locus. In addition, the mutated protein was tagged with a sequence encoding a 3xHA tag. Correct integration of the construct was confirmed by PCR (Fig 36 B), resulting in the cell line UBP1<sup>R3138H</sup> and expression of the modified protein was verified using western blot analysis (expected molecular weight 420 kDa) (Fig 36 C). In the western blot a second band at ~460 kDa was identified which corresponds with the size of the unskipped protein. Fluorescence microscopy was performed with formaldehyde/glutaraldehyde-fixed UBP1<sup>R3138H</sup> parasites which showed an expression of the protein throughout the asexual replication in the RBC (Fig 36 D). In trophozoite and schizont stages, always one focus was located next to the food vacuole, similar to the other members of the Kelch13 compartment. The UBP1<sup>R3138H</sup> cell line was tested in a standard RSA. These experiments showed a mean survival rate of 1.51% with the UBP1<sup>R3138H</sup> parasites which was significantly different from 3D7 parasites (mean survival rate 0.23%) and the control cell line, a similarly 3xHA-tagged UBP1<sup>wt</sup> (mean survival rate 0.13%) (Fig 36 E). Since the survival of the UBP1<sup>R3138H</sup> parasites was higher than that resistance defining cut-off value of 1% (Witkowski & Amaratunga *et al.*, 2013), it can be concluded that the R3138H mutation renders the parasite resistant to ART.

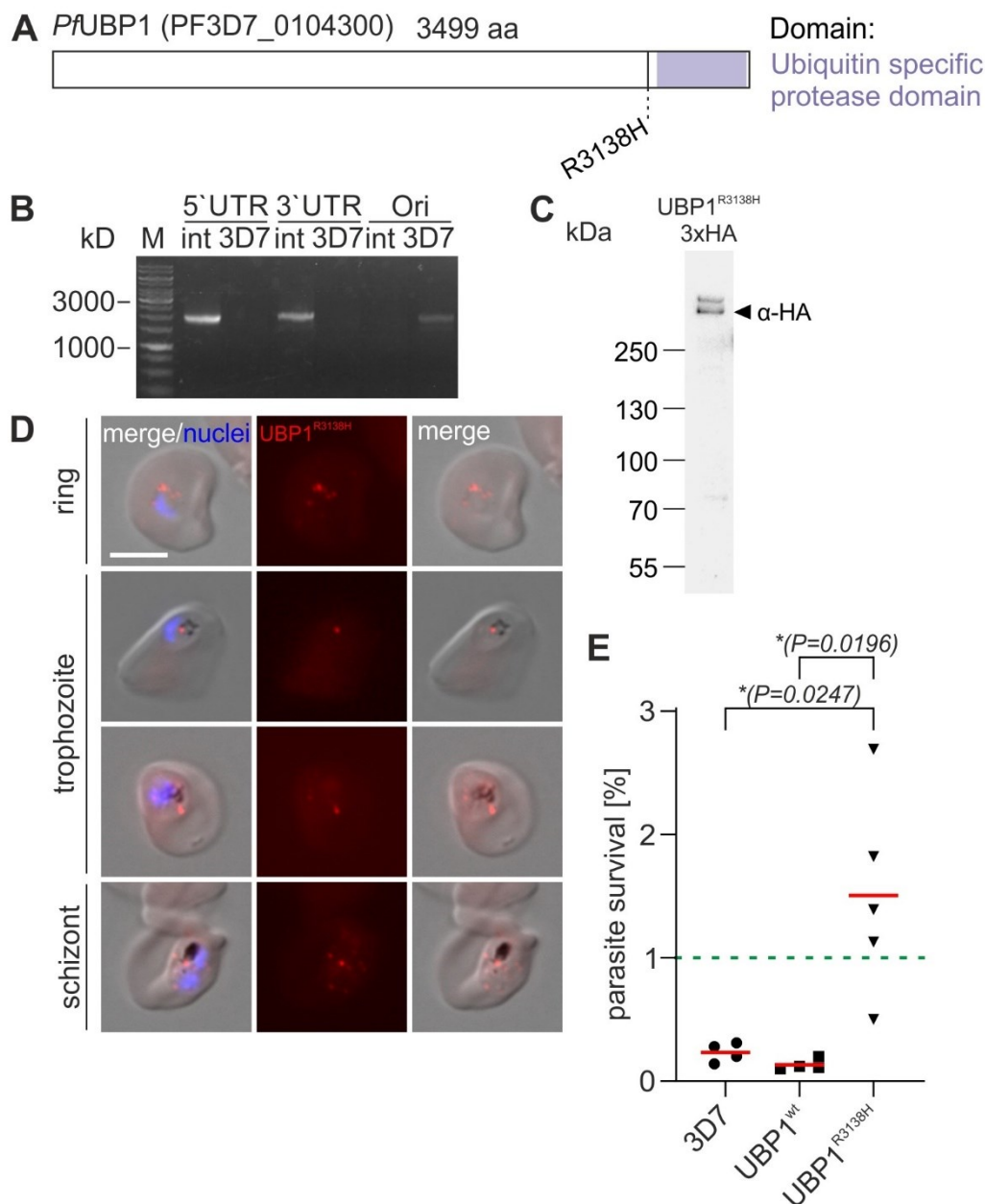


**Figure 36) UBP1<sup>R3138H</sup> renders parasite resistant to ART.** **A)** Scheme showing non-synonymous SNP of *Pf*UBP1 chosen for separate testing in standard RSA. **B)** Agarose gel showing PCR products demonstrating correct integration of the SLI plasmid into 3D7 genome to obtain UBP1<sup>R3138H</sup> parasites. Primers (see Appendix C) were used to confirm 5'-integration (5'UTR, 2103 bp) and 3'-integration (3'UTR, 2150 bp) and to demonstrate absence of original locus in the UBP1<sup>R3138H</sup> parasites (Ori, 2120 bp). 3D7 gDNA was used as reference (ori 3D7 2120 bp). **C)** Western blot analysis with protein extracts of saponin-lysed parasites of UBP1<sup>R3138H</sup> parasites. α-HA (from rat) was used to detect UBP1<sup>R3138H</sup> (expected MW of 420 kDa). Molecular weight standard is indicated in kDa. Full blots are shown in Appendix F.2. **D)** IFA images of formaldehyde/glutaraldehyde-fixed UBP1<sup>R3138H</sup> parasites. Nuclei were stained with DAPI. **E)** Graph showing parasite survival rate (% survival compared to control without DHA) 72 hours after 6 h DHA treatment in standard RSA. Each point shows an independent experiment. P value is indicated, two-tailed, unpaired Welch's t test. Red vertical bar shows mean. Green dashed line shows 1% survival, above which parasites are considered resistant (Witkowski & Amaratunga *et al.*, 2013). aa, amino acid; kD, kilodalton; M, marker (GeneRuler™ 1 kb, Thermo Scientific); int, integrant; ori; original locus; HA, hemagglutinin; wt, wildtype; size bar, 5µm.

#### 4.6.5 Two non-synonymous SNPs detected in *PfKelch13* (PF3D7\_1343700) reduce ART susceptibility in *P. falciparum*

The gene encoding *PfKelch13* is located on chromosome 13 and is translated into a protein of 726 aa. The protein consists of different domains, the N-terminal *Plasmodium* specific region, followed by the BTB/POZ domain in the middle and a C-terminal 6-blade Kelch propeller domain. In 2014, *Ariey et al.* showed that single point mutations in *PfKelch13* are associated with ART resistance (*Ariey et al.*, 2014), and since then various studies were performed to identify non-synonymous SNPs in *kelch13* that cause resistance to ART. Here, four non-synonymous SNPs were tested for their capability to render parasite resistant, resulting in the following amino acid changes in comparison to the 3D7 reference sequence: V520A / V520I / V589I / E612K (Fig 37 A). The SNP V520A was found 2006 in Africa during a molecular epidemiologic study and showed the highest prevalence of 4% in the Democratic Republic of Congo (*Taylor et al.*, 2015). Another SNP also located at the same codon results in the amino acid change V520I compared to 3D7 reference sequence: This SNP was identified 2014 in Asia and had a prevalence of 0.57% (*Ménard et al.*, 2016). In 2011, the codon change V589I was found in Mali with a prevalence of 1.15% (*Ouattara et al.*, 2015). The final non-synonymous SNP that was included here was E612K which was found in 2016 in Cameroon with a prevalence of 0.83% (*Eboumbou Moukoko et al.*, 2019).

Four SLI plasmids were generated to insert each of the four codon changes into the 3D7 genome and the mutated *PfKelch13* gene was additionally tagged with a sequence encoding GFP and 2xFKBP. After selection of integrants, correct integration of the different constructs was confirmed by PCR (Fig 37 B, representative images of two cell lines are shown) and expression of the mutated and tagged *PfKelch13* protein was confirmed by western blot analysis (Fig 37 C, representative images of two cell lines are shown), resulting in the four cell lines K13<sup>V520A</sup>, K13<sup>V520I</sup>, K13<sup>V589I</sup>, K13<sup>E612K</sup>. The localization of the modified *PfKelch13* was assessed by live cell imaging and compared to a previously established wild type *PfKelch13* cell line where the native protein is tagged with GFP and 2xFKBP (K13<sup>wt</sup>, kindly provided by Jakob Birnbaum). Comparison of the cell lines K13<sup>V520A</sup>, K13<sup>V520I</sup>, K13<sup>V589I</sup>, K13<sup>E612K</sup> to K13<sup>wt</sup> revealed no apparent difference in the localization of the mutated *PfKelch13* which were found in foci in a pattern typical for K13<sup>wt</sup> (Fig 37 D, representative images of two cell lines are shown). When the four parasite lines were tested in standard RSA, the K13<sup>E612K</sup> parasite line showed a mean survival rate of 0.60%, and the K13<sup>V520I</sup> line a mean survival rate of 0.54% (Fig 37 E). Both values were below the resistance defining cut-off value of 1% (*Witkowski & Amaratunga et al.*, 2013) and not significantly different than the survival of the K13<sup>wt</sup> parasites, indicating that the two SNPs did not render the

parasite resistant to ART. In contrast, RSA with the K13<sup>V520A</sup> cell line resulted in a mean parasite survival rate of 1.10%, and the K13<sup>V589I</sup> parasites showed a mean survival rate of 1.92%. As these values were above the 1% cut-off for resistance although there was no significant difference compared to K13<sup>wt</sup> control, it can be concluded that these two non-synonymous SNPs decrease the susceptibility of the parasites to ART at a low level.

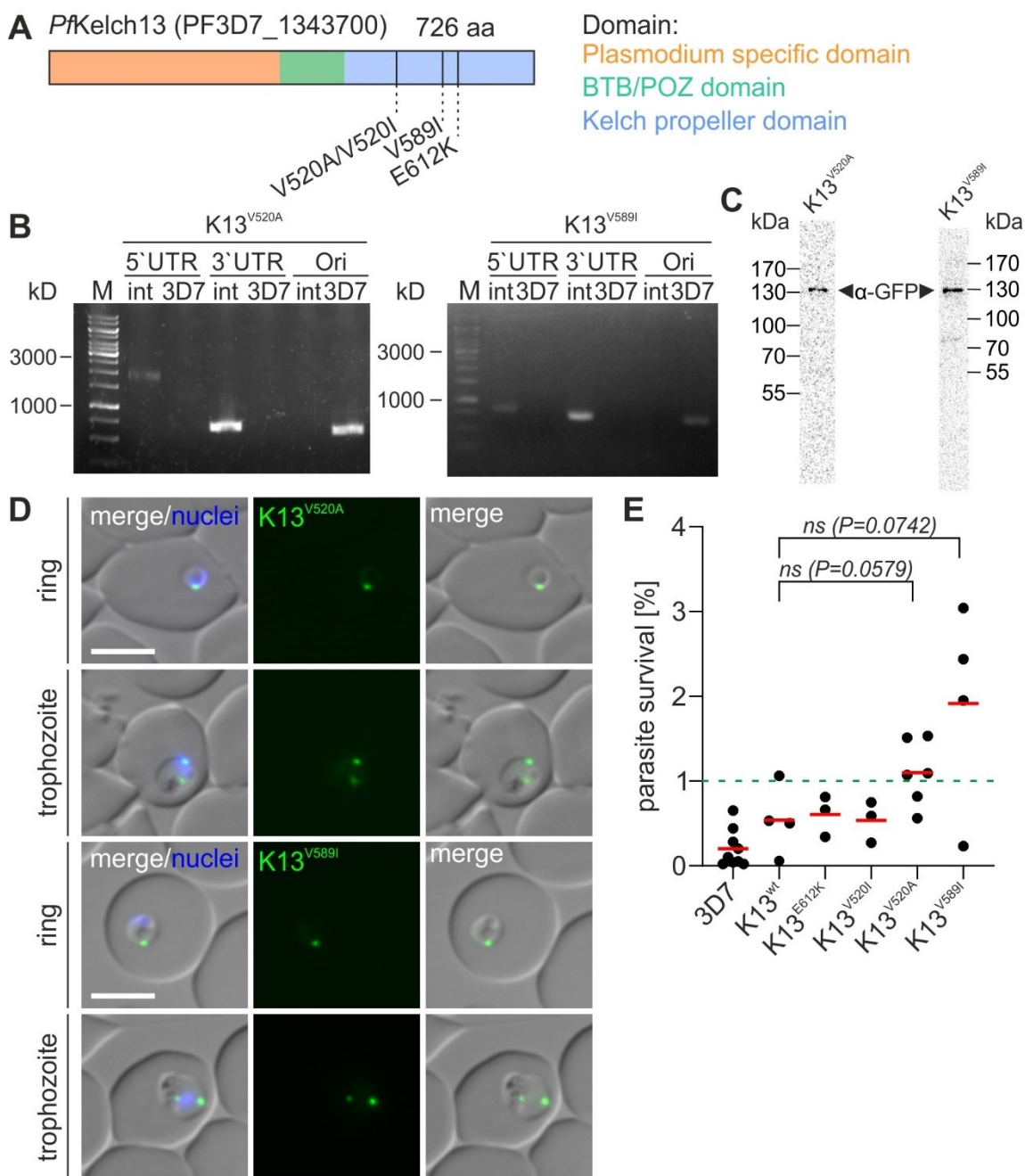


**Figure 37) K13<sup>V520A</sup> and K13<sup>V589I</sup> render parasites resistant to ART. A)** Scheme showing non-synonymous SNPs of *PfKelch13* chosen for separate testing in standard RSA. **B)** Representative agarose gels showing PCR products demonstrating correct integration of the SLI plasmids into 3D7 genome to obtain K13<sup>V520A</sup> and K13<sup>V589I</sup> parasites. Primers (see Appendix C) were used to confirm

5'-integration (5'UTR, 1850 bp (K13<sup>V520A</sup>) and 805 bp (K13<sup>V589I</sup>)) and 3'-integration (3'UTR, 671 bp (K13<sup>V520A</sup> and K13<sup>V589I</sup>)) and to demonstrate absence of original locus in the K13<sup>V520A</sup> and K13<sup>V589I</sup> parasites (Ori, 604 bp (K13<sup>V520A</sup> and K13<sup>V589I</sup>)). 3D7 gDNA was used as reference (ori 3D7 604 bp (K13<sup>V520A</sup> and K13<sup>V589I</sup>)). Agarose gels of K13<sup>E612K</sup> and K13<sup>V520I</sup> are shown in the Appendix F.1. **C**) Western blot analysis with protein extracts of saponin-lysed parasites of K13<sup>V520A</sup> and K13<sup>V589I</sup> parasites.  $\alpha$ -GFP (from mouse) was used to detect K13<sup>V520A</sup> and K13<sup>V589I</sup> (expected MW of 138 kDa). Molecular weight standard is indicated in kDa. Full blots are shown in Appendix F.2. **D**) Representative live cell images of K13<sup>V520A</sup> and K13<sup>V589I</sup> parasites. Nuclei were stained with DAPI. **E**) Graph showing parasite survival rate (% survival compared to control without DHA) 72 hours after 6 h DHA treatment in standard RSA. Each point shows an independent experiment. P value is indicated, two-tailed, unpaired Welch's t test. *Red vertical bar* shows mean. *Green dashed line* shows 1% survival, above which parasites are considered resistant (Witkowski & Amaratunga *et al.*, 2013). *aa*, amino acid; *kD*, kilodalton; *M*, marker (GeneRuler™ 1 kb, Thermo Scientific); *int*, integrant; *ori*; original locus; *GFP*, green fluorescent protein; *wt*, wildtype; size bars, 5 $\mu$ m.

## 4.7 K13<sup>C580Y</sup> parasites become more resistant to DHA after consecutively performed standard RSAs

### 4.7.1 ART resistant K13<sup>C580Y</sup> parasites show reinvasion of fresh RBCs and less far development after DHA pulse

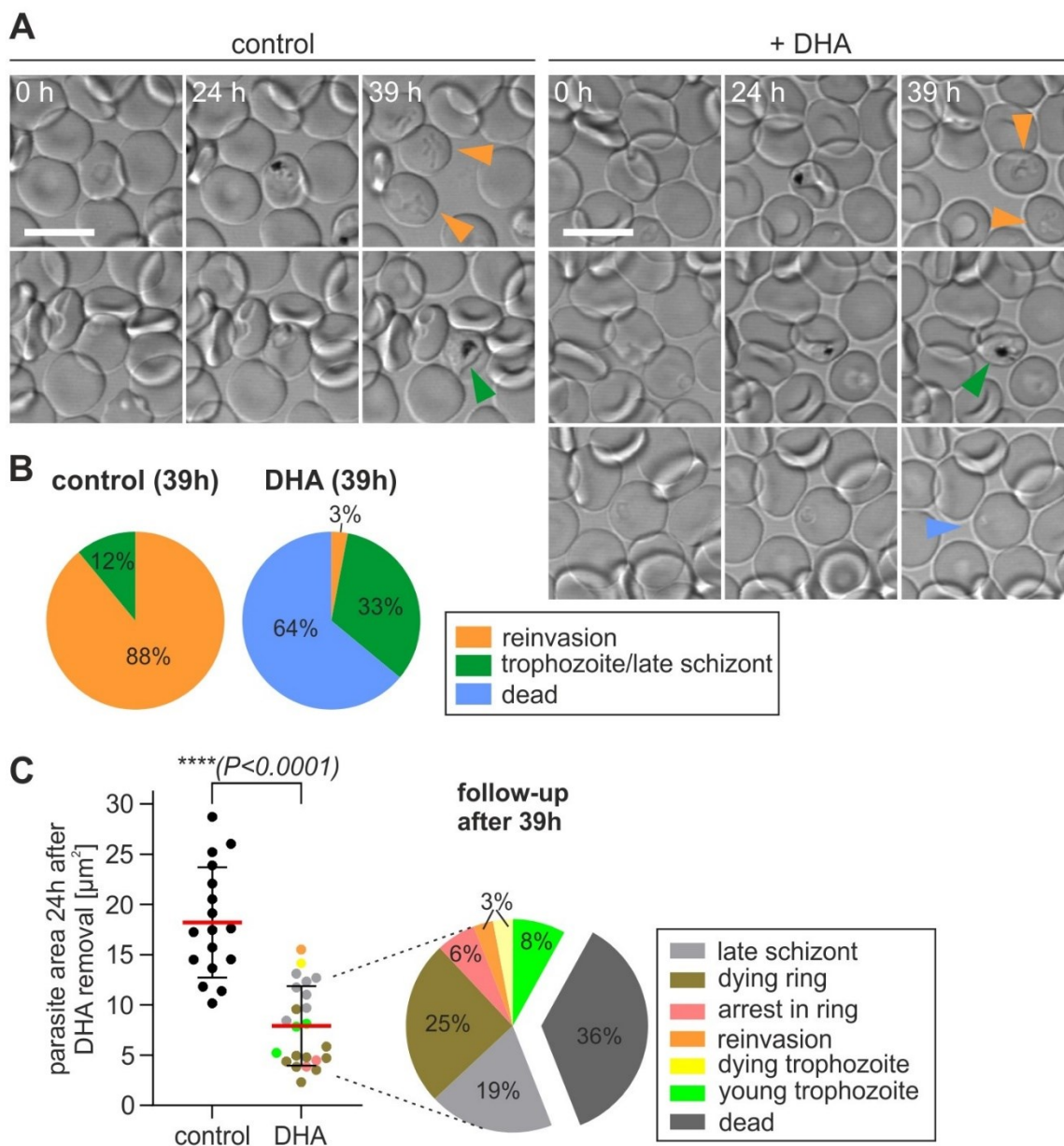
Different hypotheses about the behavior of ART resistant parasites after treatment with the drug exist (Kyle, 1996; Hoshen *et al.*, 2000; Teuscher *et al.*, 2010; Codd *et al.*, 2011), but so far individual surviving parasites were never visualized over time during an RSA before. To do so, a standard RSA (Witkowski & Amaratunga *et al.*, 2013) was performed with ART resistant K13<sup>C580Y</sup> parasites (Birnbaum *et al.*, 2017) and after removal of DHA parasites were analyzed using long term confocal imaging (Grüring *et al.*, 2011) alongside an untreated control. Images of the same areas were taken at three different timepoints, the start after DHA removal (expected stage: rings), at 24 h (expected stage: trophozoites) and 39 hours (expected stage: schizonts or rings of next cycle) (Fig 38 A). In the untreated K13<sup>C580Y</sup> control 88% of the parasites reinvaded fresh RBCs at the 39 hours' time point, whereas 12% of the parasites were late schizont stages (Fig 38 B). In contrast, the 39 hours' time point in the DHA-treated K13<sup>C580Y</sup> parasites, indicated that 64% of the cells had died after the DHA pulse, whereas 33% showed further development to the late trophozoite stage and schizont stage although only one (3%) of the DHA-treated K13<sup>C580Y</sup> parasites completed the cycle and produced new rings (Fig. 38 B). While it is unclear if the other parasites would have given rise to new rings at a later time point or had suffered damage from the DHA pulse or the imaging that prevented completion of the cycle, it can overall be

---

concluded that the DHA-treated parasites were less far developed, consistent with a growth delay of the survivors.

To better analyze this, it was assessed whether there is a developmental difference between the untreated control and the DHA-treated K13<sup>C580Y</sup> parasites, by measuring the parasite size 24 hours after DHA removal (Fig 38 C). At this time point, the parasites that developed further (36%) the average size was 8 $\mu\text{m}^2$ , which was still significantly lower than the average size of 18  $\mu\text{m}^2$  of the untreated parasites that developed, indicating that the DHA treated parasites were delayed in growth in the first part of the cycle, possible during the DHA pulse or possibly because only more slowly developing parasites survive DHA. Further tracking of the parasites measured in Fig 38 C on their development at 39 hours showed that 3% survived DHA pulse and reinvaded new RBCs, whereas 6% arrested in ring stage phase, 8% developed into young trophozoites and 19% into late schizonts. Additionally, 25% of the quantified parasites in Fig 38 C died as ring stage and 3% as trophozoite stage parasites, whereas 36% were dead after 24 hours.

In summary, the survival of a DHA resistant K13<sup>C580Y</sup> parasite was imaged for the first time and the data indicates that DHA treatment of resistant parasites delays development after the drug pulse or only the subset of more slowly growing parasites survives.



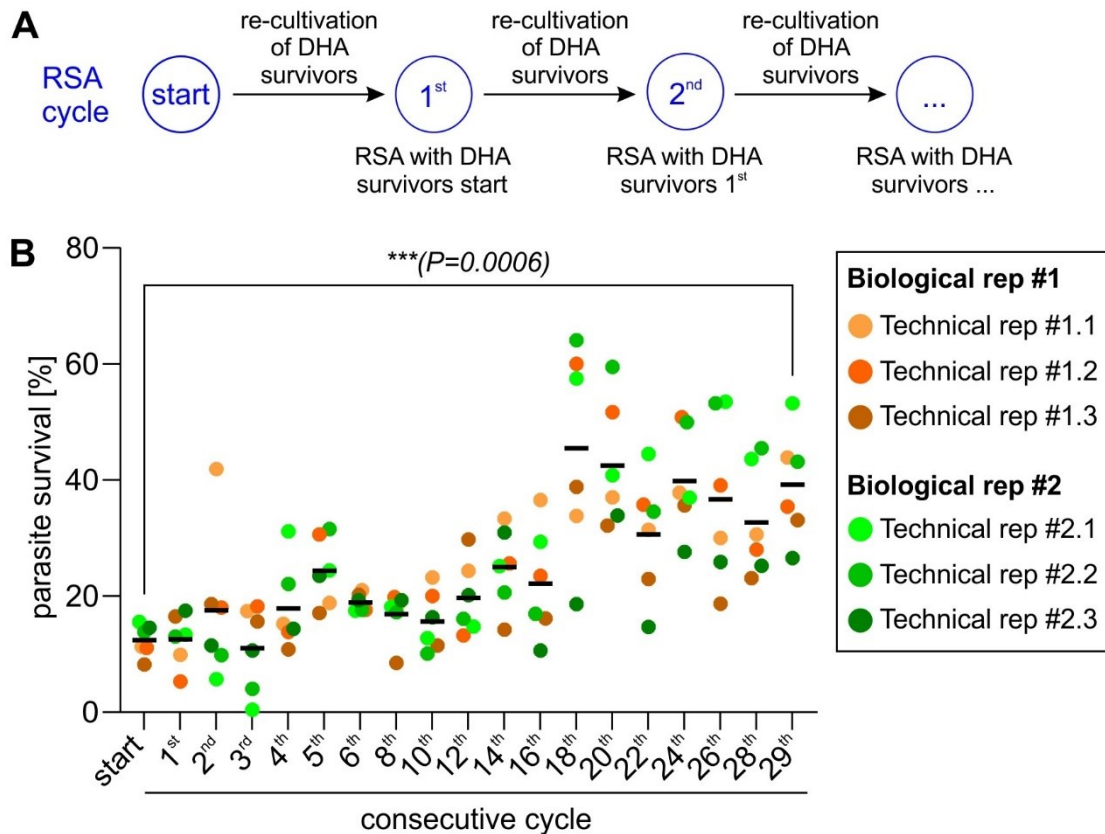
**Figure 38) K13<sup>C580Y</sup> parasites develop less far after DHA pulse. A)** Confocal microscopy images (single z-plane of an image stack is shown) of the same K13<sup>C580Y</sup> parasites tracked over time after removal of DHA in a standard RSA. Images of untreated control and DHA treated K13<sup>C580Y</sup> parasites were taken at three different timepoint, directly after removal of DHA (0 h), 24 hours and 39 hours after DHA removal. **B)** Quantification of number of K13<sup>C580Y</sup> parasites of the indicated phenotype (reinvansion: defined by disappearance of schizont and appearance of new rings in the vicinity; trophozoites/late schizont: parasites that did not complete the cycle; dead: pyknotic or dying parasites) 39 hours after DHA removal. One experiment was performed, and all parasites detected in the experiment were analyzed, for control  $n = 17$  cells and for the DHA-treated fraction  $n = 36$  cells were analyzed. All confocal images are shown in Appendix G.1. *Orange arrows* indicate reinvaded parasites, *green arrows* mark parasites developing into late schizonts, *blue arrows* mark dead parasites. **C)** Parasite area measurement of K13<sup>C580Y</sup> parasites 24 hours after removal of DHA. Only the parasites that were still alive at 39 h were included in the size measurement. Parasite measured at 24 hours were followed-up at 39 hours and their fate classified into dying parasites (defined as pyknotic or vanishing parasites), arresting in the ring stage, or developing into young trophozoites / late schizonts, or reinvading parasites (indicated as percent of all parasites and depicted in a pie-

chart). All calculations are shown in Appendix G.2. Control n = 17 cells, DHA-treated parasites n = 36 cells. P value is indicated, two-tailed unpaired t test. Scale bar, 10µm.

#### 4.7.2 Consecutive cycles of standard RSA render K13<sup>C580Y</sup> parasites even more resistant to ART

Kelch13-based ART resistance is not a complete resistance and even in resistant cell lines only a proportion of parasites survive (Witkowski & Amaratunga *et al.*, 2013; Amaratunga *et al.*, 2014; Ariey *et al.*, 2014; Straimer *et al.*, 2015). It is unclear if the survivors harbor particular properties and if they can be selected to obtain more resistant parasites. To test whether the ART resistant K13<sup>C580Y</sup> parasites (Birnbaum *et al.*, 2017) can become more resistant, a special experimental setup of consecutive cycles of standard RSAs (Witkowski & Amaratunga *et al.*, 2013) was employed to avoid the loss of resistance characteristics between RSAs, for instance if parasites with a heightened resistance display reduced growth (Fig 39 A). For this experiment, K13<sup>C580Y</sup> parasites were used that derived from a cryo-stabilates of correct freshly integrated parasites, that were in culture for not longer than four to five weeks after thawing. To start the long-term-experiment, K13<sup>C580Y</sup> parasites were subjected to a standard RSA. After completion of the initial RSA (Fig. 39 A, start), Giemsa smears of control (untreated K13<sup>C580Y</sup> parasites) and DHA-treated K13<sup>C580Y</sup> parasites were prepared at the time this is done in the RSA (72 hours post RSA initiation) to assess the proportion of surviving parasites. The DHA-treated K13<sup>C580Y</sup> culture was recultivated in fresh blood and medium to continue growth of the parasites that survived the DHA pulse and when they started the next replication cycle cryo-stabilates of ring stage parasites were prepared. The parasites were grown until they reached at least 2-3 % parasitemia (typically 4 – 5 days of culture) and then tested in a subsequent RSA cycle (1<sup>st</sup>). In total, this long-term experiment was performed over 30 weeks, with one conducted RSA per week and continuous recultivation of DHA surviving K13<sup>C580Y</sup> parasites after each RSA cycle.

At the beginning of the experiment, the starting K13<sup>C580Y</sup> had a mean parasite survival of 12.43%. After 29 further consecutive cycles of standard RSAs each time with the DHA-survivors of the prior RSA cycle, the mean parasite survival rate had increased significantly to 39.23% (Fig 39 B). Altogether, the data indicates that ART resistant K13<sup>C580Y</sup> can become even more resistant to ART after consecutive cycles of standard RSAs.



**Figure 39) Consecutive cycles of standard RSA with DHA survivors render  $K13^{C580Y}$  parasites more resistant over time. A)** Scheme of experimental procedure of consecutive standard RSA cycles performed with DHA survivors of the respective prior cycle. **B)** Graph showing parasite survival rate of  $K13^{C580Y}$  (% survival compared to control without DHA) 72 hours after 6 h DHA treatment in standard RSA (Witkowski & Amaratunga *et al.*, 2013). Six experiments per cycle were performed consisting of two biological and three technical replicates (see color code). P value is indicated, two-tailed, Welch's t test. Red bars show mean.

## 4.8 Non-synonymous SNPs of *pfkelch13* influence protein amount and parasite fitness

### 4.8.1 Non-synonymous SNPs causing ART resistance influence *PfKelch13* protein amount

Previous studies showed, that the C580Y mutation influences the abundance of the *PfKelch13* protein present in the cell, thus determining the endocytosis rate and consequently regulating ART resistance (Birnbbaum *et al.*, 2020). This data raised the question whether, and to which extent, other non-synonymous SNPs modulate the

*PfKelch13* protein amount. To test this, the *PfKelch13* amount in the cell lines with mutations here found to confer moderate resistance, K13<sup>V520A</sup>, K13<sup>C580Y</sup> (section 4.6.5) and the highly resistant K13<sup>C580Y\_29th</sup> of the consecutive RSA experiment (section 4.7.2) was measured and compared to K13<sup>wt</sup> and non RSA-selected K13<sup>C580Y</sup> parasites. Here again, K13<sup>C580Y</sup> as well as K13<sup>V520A</sup> parasites were used that derived from cryo-stabilates of correct freshly integrated parasites that were in culture for not longer than four to five weeks after thawing (see section 3.3.4). To start the experiment, all parasite lines were synchronized twice, using sorbitol, and *PfKelch13* protein amount was assessed by recording the GFP fluorescence intensity of *PfKelch13* foci in ring stage parasites using ImageJ with microscopy images (acquired using identical settings) of live cells (Fig 40 A).

In comparison to *PfKelch13* foci in the K13<sup>wt</sup> parasites (mean fluorescence intensity 0.038, calculated average from three independent experiments where total fluorescence of GFP signal was measured), the total fluorescence of the foci in K13<sup>V520A</sup> parasites was reduced by 16% (mean fluorescence intensity 0.032). The *PfKelch13* foci in K13<sup>C580Y</sup> parasites showed 56% less total fluorescence (mean fluorescence intensity 0.017) compared to K13<sup>wt</sup> control, whereas the highly resistant K13<sup>C580Y\_29th</sup> cell line showed the highest reduction of 70% (mean fluorescence intensity 0.011). When the highly resistant K13<sup>C580Y\_29th</sup> cell line was compared to its original K13<sup>C580Y</sup> parasite line, the *PfKelch13* protein amount was reduced by 31%.

The resistance level of the different *PfKelch13* cell lines negatively correlated with the *PfKelch13* protein amount present (Fig 40 B). The higher the parasite survival of the respective parasites in standard RSA (Witkowski & Amaratunga *et al.*, 2013) was, the lower the amount of *PfKelch13* protein in the cell (Fig 40 B). The K13<sup>C580Y\_29th</sup> cell lines which had a survival rate of 39.23% showed the lowest protein amount, while the sensitive K13<sup>wt</sup> parasites (mean survival rate of 0.54% in RSA) showed the highest *PfKelch13* levels. The K13<sup>V520A</sup> parasite line which had a mean survival rate of 1.10% in standard RSA, showed protein levels between K13<sup>wt</sup> and K13<sup>C580Y</sup>.

In summary, these data show that different non-synonymous SNPs influence the *PfKelch13* protein amount per focus in rings (and hence per cell) and that parasite susceptibility to ART inversely correlates with protein amount present in the cell.

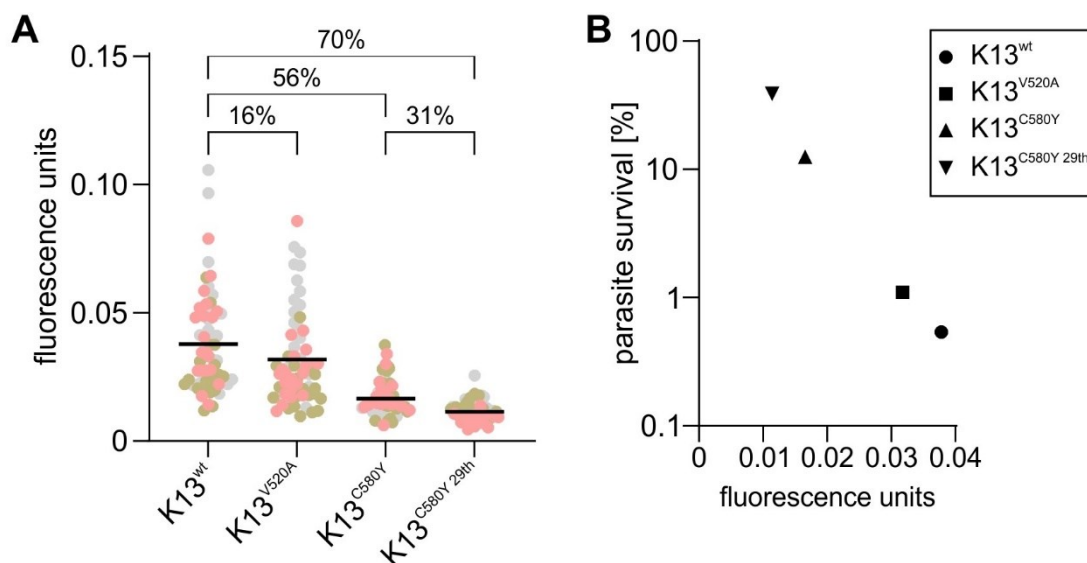


**Figure 40) Resistance-causing non-synonymous SNPs reduce *PfKelch13* protein amount. A)** Quantification of *PfKelch13* protein amount expressed by the different mutant measured by GFP-fluorescence intensity. Total fluorescence intensity of individual *PfKelch13* foci of young ring stage parasites was measured by subtracting background signal (cytosolic fluorescence) from detected fluorescence signal, multiplied with the focus area. Three independent experiments were performed represented by the colors, and per experiment  $n = 20$  cells were recorded. Numbers indicate the *PfKelch13* protein reduction between  $K13^{wt}$  control and the different mutants. *Black bars* indicate mean. **B)** Mean parasite survival rate in standard RSAs (Witkowski & Amaratunga *et al.*, 2013) plotted against *PfKelch13* protein amount measured by GFP-fluorescence intensity (log scale). For this comparison, the RSA data from section 4.6.5 and 4.7.2 were used where the mean parasite survival rate was calculated from at least three independent experiments per cell line. *wt*, wild type.

#### 4.8.2 Parasite fitness is influenced by different non-synonymous SNPs and negatively correlates with ART resistance

Previously, it was shown that ART resistant  $K13^{C580Y}$  parasites have a reduced fitness (Rosenthal, 2013; Hott *et al.*, 2015; Nair *et al.*, 2018; Stokes *et al.*, 2021). In order to test if the parasites carrying with the non-synonymous SNP that results in only moderate ART resistance have a higher fitness than the more resistant  $K13^{C580Y}$  parasites. It was therefore here tested how the fitness level of the  $K13^{V520A}$  cell line compares to that of the  $K13^{C580Y}$  and the  $K13^{wt}$  parasites.

To assess the fitness cost of  $K13^{wt}$ ,  $K13^{V520A}$  and  $K13^{C580Y}$  parasites, a GFP fluorescence-based fitness assay was performed where the different cell lines were co-cultivated in a 1:1 ration with 3D7 parasites. This took advantage of the fact that 3D7 parasites do not contain GFP and are therefore easily discerned from the transgenic parasites. The co-cultures were

grown until one of the different cultures overgrew the other co-culture (cut-off of less than 5 % of all parasites). In regular intervals, the proportions of 3D7 to K13<sup>wt</sup>, K13<sup>V520A</sup> and K13<sup>C580Y</sup> parasites was measured by live cell imaging and the percentage of GFP positive cells in the respective culture was recorded (Raw curves of individual experiments shown in Appendix H.1 and H.3). To estimate the relative growth based on the individual fitness, a non-linear regression was performed, resulting in a formula that was used to estimate the fitness cost per generation (Fig 41 A). Additionally, the fitness assay was conducted in a growth medium containing a limiting amount of amino acids (Low AA medium) to test for the additional influence of low nutrients.

In comparison to K13<sup>wt</sup>, which had a mean fitness cost per generation of 0.015 in RPMI complete medium and 0.017 in low AA medium, the K13<sup>V520A</sup> parasites had an increased fitness cost of 0.21 in RPMI complete medium and 0.14 in a medium with a limiting amount of amino acids. The K13<sup>C580Y</sup> parasites had the highest fitness cost per generation compared to the K13<sup>wt</sup> control with 0.30 in RPMI complete and 0.39 in low AA medium (Fig 41 B). It should be noted that there was some variation in the individual experiments for the K13<sup>V520A</sup> parasites that either leaned more closely to the fitness of the K13<sup>wt</sup> control or that of the K13<sup>C580Y</sup> parasites (Appendix H.1 and H.3). Nevertheless, its placement between the two parasite lines in terms of fitness was consistent.

When the fitness cost of the different *PfKelch13* cell lines were compared to the respective parasite survival rates of the standard RSA (Witkowski & Amaratunga *et al.*, 2013), a positive correlation was observed (Fig 41 C), and hence also inversely correlating with the *PfKelch13* protein amount per cell. K13<sup>C580Y</sup>, which had the highest RSA survival rate of the tested cell lines had the highest fitness costs, while the K13<sup>V520A</sup> cell line displayed a moderate ART resistance level and a lower fitness cost.

Altogether, the fitness experiments showed that the non-synonymous SNPs C580Y and V520A of *PfKelch13* reduce the fitness of the parasite. It was also shown that the fitness deficiency is higher in the highly resistant K13<sup>C580Y</sup> than in the moderately resistant K13<sup>V520A</sup> parasites. These data suggest that non-synonymous SNPs present in Africa cause lower levels of ART resistance but may be advantageous for the parasite since their fitness is less impaired which might be a benefit in endemicity settings with frequent multiple infections and lower rate of ART treatment due to semi-immunity.

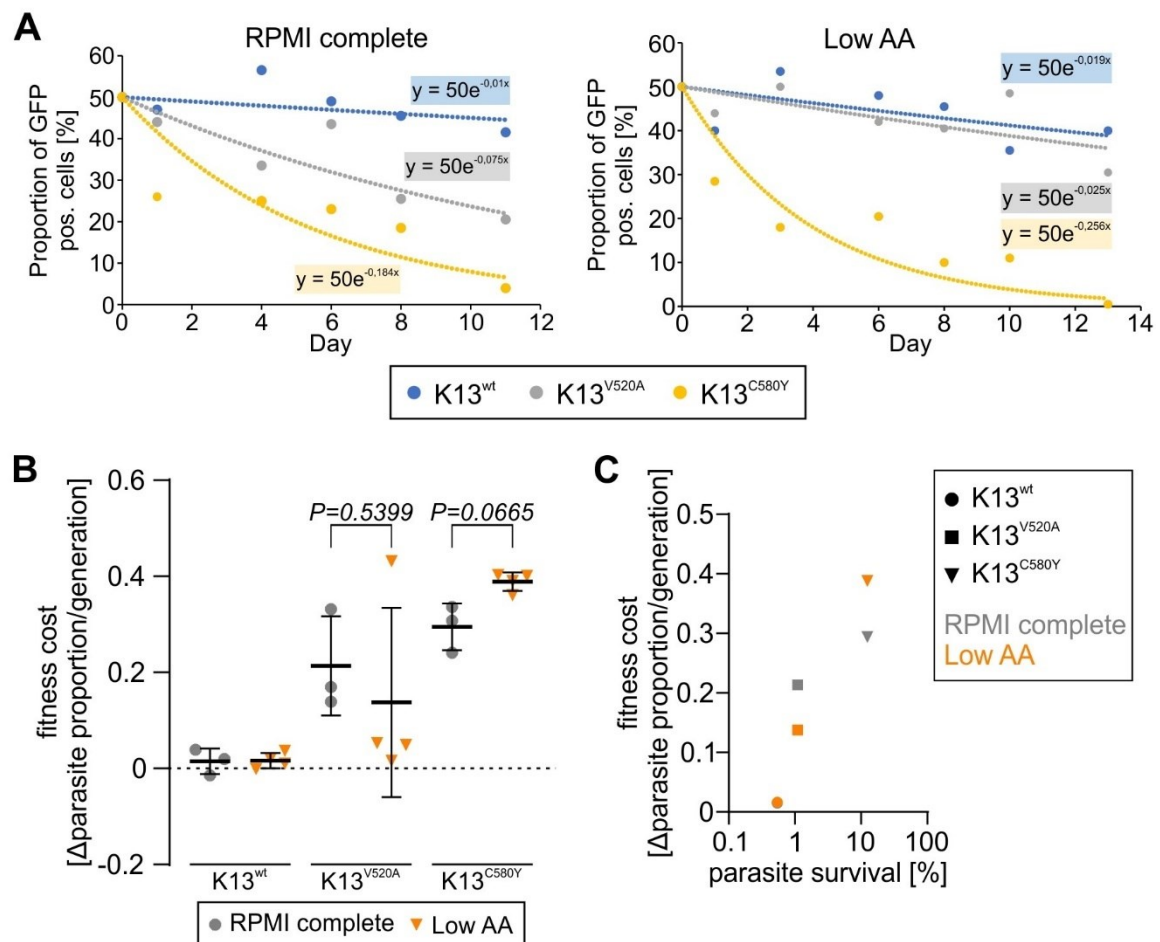


**Figure 41) Higher ART resistance level results in higher fitness cost. A)** Competitive GFP-based fitness assay performed in RPMI complete medium and a medium with limited amount of amino acids (low AA). Proportional growth of K13<sup>wt</sup>, K13<sup>V520A</sup> and K13<sup>C580Y</sup> parasites compared to 3D7 wild type parasites grown in the same culture. One representative non-linear regression curve per condition (RPMI complete or Low AA) is depicted deriving from respective raw curves expressing the proportional amount of GFP positive parasites per total parasitemia. Fitness cost per generation of the different strains were calculated based on the indicated functions (raw curves in Appendix H.1 and H.3). **B)** Fitness cost per generation of the different *PfKelch13* strains in RPMI complete and low AA medium (calculations see Appendix H.2 and H.4). For this, in a first step the trendline factor from the functions indicated in (A) was duplicated (assumption that one generation corresponds to two days), and growth factor per generation was differentiated. Fitness cost per generation were calculated by subtracting the differentiated value from 1 (1 representing 100% fitness). Black bars indicate mean fitness cost per generation. Three independent experiments with two technical replicates were performed in RPMI complete medium and 4 independent experiments with two technical replicates in low AA medium. P values are indicated, two-tailed Welch's t test. **C)** Fitness cost per generation of K13<sup>wt</sup>, K13<sup>V520A</sup> and K13<sup>C580Y</sup> parasites in RPMI complete and low aa medium as assessed in (A) and plotted against mean parasite survival (log scale) in RSA (Witkowski & Amaratunga *et al.*, 2013). For this comparison, the RSA data from section 4.6.5 and 4.7.2 were used where the mean parasite survival rate was calculated from at least three independent experiments per cell line. *wt*, wild type.

## 5 Discussion

### 5.1 *Pf*Kelch13-independent ART resistance

Previous work demonstrated that ART resistance is mediated either in a *Pf*Kelch13-dependent manner or can also be caused by a *Pf*Kelch13-independent mechanism (Mukherjee *et al.*, 2017). To identify interacting partners of *Pf*Kelch13, a modulated version of the proximity dependent biotin identification (BioID) was used, called dimerization-induced quantitative BioID (DiQ-BioID) (Birnbaum *et al.*, 2020). This newly developed BioID technique, in combination with quantitative mass spectrometry, helped define a novel Kelch13 compartment in the parasite. This analysis resulted in a list of high confident hits that were mostly of unknown function and were named KICs. Interestingly, the list also included proteins which had been suspected in ART resistance before or were detected by genome-wide association studies as potential resistance markers, such as *Pf*UBP1, *Pf*Eps15, *Pf*KIC6 and *Pf*MyosinF (Hunt *et al.*, 2007; Hunt *et al.*, 2010a; Borrmann *et al.*, 2013; Henriques *et al.*, 2014; Cerqueira *et al.*, 2017). These findings indicated that the identified hits define a pathway together with *Pf*Kelch13 that is relevant for ART resistance. More than 10 members of the Kelch13 compartment were validated as true interactors of *Pf*Kelch13 whereas two candidates, *Pf*MCA2 (PF3D7\_1438400) and *Pf*MyosinF (PF3D7\_1329100; previously annotated as *Pf*MyosinC), had not previously been validated to co-localize with *Pf*Kelch13. One aim of the thesis was to functionally characterize these two candidates as well as confirm their co-localization with *Pf*Kelch13 to validate them as true members of the Kelch13 compartment.

#### 5.1.1 *Pf*MCA2 belongs to the Kelch13 compartment and truncated versions of the protein mediate ART resistance *in vitro*

Only little information exists about the functional role of *Pf*MCA2 in *Plasmodium* parasites despite the fact that metacaspases represent an interesting antimalarial target since metacaspases are not present in humans. Metacaspases are cysteine-dependent proteases that are distantly related to metazoan caspases, having a Cys-His catalytic dyad but different substrate specificity (Uren, 2000; Tsiatsiani *et al.*, 2011). They are classified into three different types based on structural features (Tsiatsiani *et al.*, 2011). Type I metacaspases are found in protozoans and fungi, while plants express both, type I and II

metacaspases. In plants, type I metacaspases represent the dominating class. Type I metacaspases contain an N-terminal pro-domain comprising a proline-rich repeat motif and a zinc finger motif (Vercammen *et al.*, 2004; Tsiatsiani *et al.*, 2011). The currently identified type III metacaspases are exclusively found in algae which have undergone secondary endosymbiosis (Klemenčič & Funk, 2018b). Irregular distribution of homologues across different phyla hinders the functional specification of metacaspases. In the plant *Arabidopsis thaliana*, a total of nine different metacaspases were identified (Cox, 2011). Looking at the protozoan *Leishmania*, a single metacaspase is encoded in all species, except for *L. donovani* and *L. infantum* subtypes which express two different metacaspases (Meslin & Zalila *et al.*, 2011). In contrast, *Trypanosoma brucei* encodes five different redundant metacaspases (*TbMCA1* – 5). The *Trypanosoma* metacaspases were shown to likely be involved in the regulation of the programmed cell death (Szallies *et al.*, 2002) which is similar to *Leishmania* metacaspases (Casanova *et al.*, 2015) and is a central role of metazoan caspases. Additionally, *Trypanosoma* metacaspases are enrolled in cytokinesis (Helms *et al.*, 2006), and cell proliferation (Meslin & Zalila *et al.*, 2011). For *Plasmodium* parasites, three different metacaspases were reported in *P. falciparum* (*PfMCA1* (PF3D7\_1354800); *PfMCA2* (PF3D7\_1438400) and *PfMCA3* (PF3D7\_1416200)), *P. vivax* (*PvMCA1-3*) and the murine species *P. berghei* (*PbMCA1-3*). Earlier studies suggested a role for *Plasmodium* metacaspases in stress response-related programmed cell death, and in the regulation of growth and development (Picot *et al.*, 1997; Meslin *et al.*, 2007; Ch'ng *et al.*, 2010; Rathore *et al.*, 2015). Nevertheless, the specific roles of these metacaspases are unknown and it is difficult to make predictions about function based on the similarity to metacaspases in other organisms (Shrestha & Megeney, 2012; Vandana *et al.*, 2019). Hence, there is little that can be drawn from metacaspases in other organisms to define the function of *PfMCA2* and its potential role in the Kelch13 compartment in more detail. *PfMCA2* also possesses a Cys-His catalytic dyad which shows its structural similarity to metazoan caspases (Tsiatsiani *et al.*, 2011). This metacaspase belongs to the C14 family of clan CD proteases, comprising two catalytic domains, a large p20 subunit and a small p10 subunit (Klemenčič & Funk, 2018a). In a recent publication, Vandana *et al.* performed experiments to elucidate the enzymatic activity and substrate specificity of *PfMCA2* (Vandana *et al.*, 2018). This work showed that *PfMCA2* has an arginine/lysine substrate specificity and cleaves *PfTSN*, which is an essential functional component of the spliceosome Sm core complex (Rathore *et al.*, 2015). Additionally, it was suggested that *PfMCA2* plays a potential role in stress response related cell death (Vandana *et al.*, 2018; Vandana *et al.*, 2020).

Prior attempts to tag the full-length *PfMCA2* C-terminally with a sequence coding for GFP and 2xFKBP-GFP failed (personal communication, Jakob Birnbaum). In this work, using the

SLI system (Birnbaum *et al.*, 2017), a sequence encoding a 3xHA was fused successfully to the C-terminus of the full-length *pfmca2* endogenous locus for the first time (section 4.1.1). This allowed the localization of full length *PfMCA2* in blood stage parasites, demonstrating that it is expressed throughout the entire asexual cycle. In ring stage parasites, *PfMCA2* was found in one focus, while in trophozoite stage parasites one or more foci were detected. These foci were either located close to the parasite food vacuole or to vesicles in the cell periphery. In schizont stages, *PfMCA2* was more difficult to detect as the signal was more diffuse but nevertheless these parasites usually had one focus close to the food vacuole (section 4.1.1). Besides, the *MCA2<sup>wt</sup>-3xHA* cell line, a GFP-tagged *MCA2* cell line was generated, where *pfmca2* was disrupted at amino acid position 1344 (*MCA2<sup>Y1344Stop</sup>*). The underlying nucleotide change represents a SNP that is listed in MalariaGEN to be present in Africa and SEA. Live cell imaging revealed a similar localization of *MCA2<sup>Y1344Stop</sup>* as wild type *PfMCA2* in the 3xHA tagged cell line (section 4.1.3). A localization of *PfMCA2* in the parasite cytoplasm is supported by the findings of Vandana *et al.* who showed that *PfMCA2* requires a neutral pH, indicating that it is likely functional in the cytoplasm or in organelles with neutral pH (Vandana *et al.*, 2018). Analysis of mRNA transcript level in *P. falciparum* revealed that *PfMCA2* is mainly expressed in schizonts and gametocytes, while ring and trophozoite stage parasites show a lower abundance of *PfMCA2* mRNA transcripts (Young *et al.*, 2005; Bártfai *et al.*, 2010; Toenhake *et al.*, 2018; Vandana *et al.*, 2018). However, the work in this thesis clearly shows that *PfMCA2* is expressed in rings and trophozoites. The expression and localization of *PfMCA2-3xHA* in schizont and gametocyte stages needs to be analyzed in more detail, and in a next step the signal intensity could be compared between ring, trophozoite, schizont and gametocyte stage parasites via fluorescence microscopy or western blot analysis to determine the stage-specific protein levels which often deviate from that of the transcripts (Foth *et al.*, 2011).

DiQ-BioID data indicated that *PfMCA2* is present at the Kelch13 compartment. To clarify this finding, co-localization experiments with the *MCA2<sup>wt</sup>-3xHA* cell line transfected with an episomal Kelch13 construct were performed and demonstrated that both *PfMCA2* and *PfKelch13* co-localize (section 4.1.2). The data was additionally confirmed by live cell imaging of the *MCA2<sup>Y1344Stop</sup>* cell line transfected with an episomal Kelch13 construct (section 4.1.4). These experiments also showed that the truncation did not alter the localization of *PfMCA2* or interfered with the relative positioning of *PfMCA2* to *PfKelch13*. To verify that the co-localization between both proteins also means that they interact would require co-immunoprecipitation experiments.

It was previously shown that it is possible to disrupt the original genomic locus of the protein at amino acid position 57 via SLI-TGD and express a truncated version of the *PfMCA2*

(Birnbbaum *et al.*, 2020). Determination of essentiality of *PfMCA2* for parasite growth via SLI-TGD and flow cytometry-based growth rate analysis demonstrated, that *PfMCA2* is dispensable for parasite development during the asexual replication, although some reduction in growth was apparent when compared to wild type 3D7 (Birnbbaum *et al.*, 2020). However, this truncation rendered parasites less susceptible to ART, indicating that *PfMCA2* has a role in the pathway involved in ART resistance and that other changes in this gene could be important for Kelch13-independent resistance in the field. In correlation to these results, *in vitro* deletion of *PfMCA2* in 3D7 parasites by a non-synonymous mutation, listed in MalariaGEN at position 1344, leading to the amino acid change Y1344Stop compared to 3D7 sequence, was successful (section 4.1.3). The corresponding SNP, T to A at position 4032 of the coding DNA, is found in African field isolates with a mean prevalence of 52%, and in SEA with 5% mean prevalence. *In vitro* deletion of *PfMCA2* in 3D7 parasites at position 1344 was successful and when tested in RSA, the *MCA2*<sup>Y1344Stop</sup> displayed a reduced susceptibility to ART, indicating that although this protein was still correctly localized, it had been inactivated sufficiently to mimic the result with the truncation at amino acid position 57 (see (Birnbbaum *et al.*, 2020); section 4.1.3). Performing a motif scan, using the ExPasy Swiss Bioinformatics Resource Portal, to predict the different domains of *PfMCA2* revealed that the putative catalytic caspase domains are located at amino acid positions 1546 – 1626 (E-value 6.1e<sup>-05</sup>) and 1546 – 1777 (E-value 0.0012) (Sigrist *et al.*, 2010). This means that by both truncations, either by targeted gene disruption using SLI or deleting the original *pfmca2* locus through the Y1344Stop mutation, resulted in the loss of the catalytical caspase domain. Interestingly, the truncation at amino acid position 57 achieved a higher parasite survival rate (mean survival rate ~5%), while the truncation at amino acid position 1344 resulted in a moderate survival rate (mean survival rate 1.64%) (section 4.1.3). This suggests that the truncation at amino acid position 1344 does potentially less inactivate *PfMCA2*, resulting in a lower ART resistance level.

To test whether the non-synonymous SNP is relevant in the field, RNA sequence data from African field isolates were analyzed. In 13 analyzed samples, the mutation was found (position 4032 of coding DNA sequence; data kindly provided by Anna Bachmann). Interestingly, by analyzing the RNA seq data a second mutation was found two base pairs upstream, in the same codon, at position 4030 of the coding DNA sequence, resulting in the codon change Y1344K compared to 3D7 reference sequence. This second detected mutation (position 4030) was simultaneously present together with the SNP in position 4032 in all 13 samples, resulting in an amino acid change and maintenance of the reading frame, not a truncation, indicating that the Y1344Stop change likely does not occur in the field and likely is not relevant for resistance *in vivo*.

Functional data about the specific role of *PfMCA2* in the Kelch13 compartment and its involvement in ART resistance are still missing. Experiments conducted in yeast models showed that the metacaspase YCA1 is responsible for the regulation of the cellular stress response and maintenance of protein homeostasis in *S. cerevisiae* (Lee & Brunette *et al.*, 2010; Meslin & Zalila *et al.*, 2011). In *P. falciparum* it was demonstrated that the redundant metacaspase *PfMCA1* is a main regulator of oxidative stress response, causing apoptosis-like cell death, organelle dysfunction and disruption of cellular homeostasis (Picot *et al.*, 1997; Meslin & Beavogui *et al.*, 2011; Rathore *et al.*, 2015). In 2018, Vandana *et al.* showed that *PfMCA2* is potentially involved in programmed cell death and functional studies indicated an increased oxidative stress after treatment with an effector caspase inhibitor in *P. falciparum* due to a downregulation of *PfMCA2* (Vandana *et al.*, 2018). This work further tested whether *PfMCA2* is involved in the cleavage of hemoglobin, similar to other cysteine proteases such as falcipains or plasmepsins, but found no interaction between hemoglobin and the metacaspase, suggesting a lack of suitable binding sites (Vandana *et al.*, 2018). Besides this data, a study performed in *Aspergillus fumigatus* showed that fungal metacaspases are involved in ER-related stress response and regulate the UPR pathways in fungi (Richie *et al.*, 2007). Altogether the findings suggest that *PfMCA2* is potentially involved in the regulation of oxidative stress response and the UPR pathway. Since an increased cellular stress response as well as an upregulated UPR pathway was detected in ART resistant parasites, this would provide a link between *PfMCA2*, *PfKelch13*, and ART resistance (Dogovski *et al.*, 2015; Mok *et al.*, 2015). To further investigate this in *P. falciparum*, the level of reactive oxygen species in *MCA2<sup>wt</sup>-3xHA* and *MCA2<sup>Y1344Stop</sup>* parasites could be analyzed and compared. This could be achieved by analyzing the genomic expression pattern of wildtype *PfMCA2* and comparing it to the *PfMCA2* transcription level of the different truncated versions in the presence or absence of oxidative stress. This could provide insight into stress response mechanisms, as analysis of altered genetic expression in yeast, mammals, and *Drosophila* helped to define such processes in more detail in these organisms (Nadal *et al.*, 2011). Additionally, N-terminal tagging of *PfMCA2* might permit to obtain a full length GFP and FKBP tagged version which could be used to conditionally inactivate it. This could be used to obtain direct functional insights into the role of *PfMCA2* in *P. falciparum*. Similar to *PfKelch13*, DiQ-BioID experiments combined with quantitative mass spectrometry would help to unravel the interactome of *PfMCA2* and further confirm the co-localization with *PfKelch13* and the Kelch13 compartment. Such experiments could provide a link of the stress response pathways metacaspases are suspected to be involved with endocytosis and resistance to ART.

### 5.1.2 *PfMyosinF* is an actin-associated protein that is part of the Kelch13 compartment and contributes to hemoglobin uptake in *P. falciparum* parasites

*PfMyosinF* was indicated by the DiQ-BioID data as potential interaction partner of *PfKelch13* (Birnbaum *et al.*, 2020). As neither the presence of *PfMyosinF* in the Kelch13 compartment nor a true interaction to *PfKelch13* was so far verified and only little information exists about its functional role in *P. falciparum*, *PfMyosinF* was investigated in this work.

To assess the co-localization of *PfMyosinF* with *PfKelch13*, a cell line where the native *PfMyosinF* locus was modified to tag this protein with 2xFKBP-GFP-2xFKBP (MyoF<sup>wt</sup>-2x2 cell line, kindly provided by Ernst Jonscher), was transfected with an episomally expressed mCherry-*PfKelch13* construct (section 4.2.1). Live cell images of the original MyoF<sup>wt</sup>-2x2 cell line showed that these parasites spontaneously developed vesicles in trophozoite and schizont stages that were not (or less frequently) present in the 3D7 parent. Thus, a second integrant cell line was newly established as control where the full-length *PfMyosinF* protein was tagged with a sequence coding for 3xHA (MyoF<sup>wt</sup>-3xHA parasites). Imaging revealed that this cell line did not develop spontaneous vesicles in trophozoite and schizont stages. These parasites were transfected with an episomally expressed mCherry-*PfKelch13* construct. Immunofluorescence assays using the MyoF<sup>wt</sup>-3xHA+K13 cell line and live cell imaging of the MyoF<sup>wt</sup>-2x2+K13 parasites showed only limited co-localization of *PfMyosinF* with *PfKelch13* but revealed that *PfMyosinF* was mostly found in close proximity to the Kelch13 compartment (section 4.2.1). This was observed in both, Formaldehyde/glutaraldehyde-fixed MyoF<sup>wt</sup>-3xHA+K13 parasites and MyoF<sup>wt</sup>-2x2+K13 parasites, indicating that the vesicular phenotype in trophozoite and schizont stages did not influence the relative localization of both proteins. Performing an IFA with acetone-fixed MyoF<sup>wt</sup>-3xHA+K13 parasites resulted in the detection of more partially co-localizing and closely localizing *PfMyosinF* and *PfKelch13* foci (see section 4.2.1). This indicated that either the fixation method influenced the accessibility of antigen epitopes by the detecting antibodies, resulting in the loss of some closely localizing foci in formaldehyde/glutaraldehyde-fixed parasites. Alternatively, the fixing method may have affected the spatial arrangement of closely apposed compartments or may have led to a partial loss of integrity of the compartments which may have resulted in the observed differences. Nevertheless, the co-localization of *PfMyosinF* and *PfKelch13*, or rather the close association, were clearly apparent with both methods. Overall, the failure of the two proteins to fully overlap in most instances were unexpected since *PfMyosinF* was found in the DiQ-BioID hit list, although with lower enrichment and probability than the hits that were so far validated to belong to the Kelch13 compartment.

To functionally characterize the *Pf*MyosinF protein, knock sideways experiments using the MyoF<sup>wt</sup>-2x2 cell line transfected with an episomal nuclear mislocalizer (MyoF<sup>wt</sup>-2x2+1xNLS, kindly provided by Ernst Jonscher) were performed to assess the essentiality of the protein for asexual replication. Flow cytometry-based growth assays, as well as live cell imaging revealed that inactivation via mislocalization of *Pf*MyosinF into another cell compartment was only partially achieved but nevertheless significantly reduced parasite growth (section 4.3.1). Fluorescence microscopy showed that *Pf*MyosinF is only weakly expressed in ring stages, while in later developmental stages one *Pf*MyosinF foci was always localized close to the food vacuole and two, or sometimes more foci, were detected close to vesicles (based on appearance in DIC) in the cell periphery (section 4.3.1). These findings suggest that *Pf*MyosinF may be involved in endocytic processes and potentially supports the *Pf*Kelch13-mediated hemoglobin uptake (Birnbaum *et al.*, 2020).

In general, myosins represent molecular motor proteins which are dependent on actin. Most eukaryotic organisms are reliant on this actomyosin motor for various cellular functions such as organellar or vesicle transport, cell movement, and mitotic processes (Raposo *et al.*, 1999; Hasson, 2003; Salas-Cortes *et al.*, 2005; Arden *et al.*, 2007; Woolner *et al.*, 2008; Rump *et al.*, 2011; Hartman & Spudich, 2012; Carmeille *et al.*, 2021). To assess the relative position of *Pf*MyosinF to actin filaments, the MyoF<sup>wt</sup>-2x2 cell line was transfected with an episomal construct expressing an actin-chromobody (a kind gift of Markus Meissner; (Periz *et al.*, 2017)). Live cell imaging revealed that filamentous actin accumulated close to the *Pf*MyosinF foci which were present at the FV or the vesicular structures at the cellular periphery (section 4.3.4). This finding indicates that *Pf*MyosinF is part of the actomyosin motor in *P. falciparum* and that *Pf*MyosinF together with actin contribute to endocytic vesicular trafficking. Further experiments need to be performed to clarify the association of *Pf*MyosinF and actin. A next step would be to observe the relative position of *Pf*MyosinF and actin upon the inactivation of *Pf*MyosinF via the knock sideways system.

Myosins consist of three main domains. The N-terminal head domain, which is conserved across different phyla, is responsible for ATPase activity and for the generation of moving forces mediated via the binding of the myosin heavy chain to actin filaments. The head domain is used to classify myosins into different classes. The second domain is the short neck which interacts with the myosin light chain. The third domain, the C-terminal tail domain, regulates the binding to different cargoes or other proteins defining the specificity of the myosin protein (Foth *et al.*, 2006). *Pf*MyosinF belongs to the class XXII myosins. In the C-terminal tail region this protein contains five WD40 repeats that are known to mediate the binding to other proteins, resulting in the formation of multiprotein complexes (Stirnemann *et al.*, 2010). Since the data presented here in this work may indicate an

interaction of *Pf*MyosinF and *Pf*Kelch13 (section 4.2.1), this characteristic domain feature would suggest the hypothesis that *Pf*MyosinF is interacting with *Pf*Kelch13 and its compartment members via the WD40 repeats-containing tail region, thereby regulating the Kelch13 compartment controlled endocytic processes. In this work, it was seen that C-terminally tagging of *Pf*MyosinF resulted in a partial phenotype, leading to the accumulation of vesicles in later developmental stages (section 4.3.4). This suggests that the C-terminus, might be important for vesicular trafficking to the food vacuole, which is impaired when the C-terminus is altered by tagging. Additionally, it was seen in live cell images of the MyoF<sup>wt</sup>-2x2+K13 cell line that ~44% of the *Pf*MyosinF foci did not co-localize to *Pf*Kelch13, suggesting that C-terminal tagging here potentially affected the interaction between both proteins (section 4.2.1). To further investigate this theory, binding assays would need to be performed to define the potential binding of *Pf*Kelch13 and its compartment members to the different *Pf*MyosinF domains. Additionally, the interaction with other proteins needs to be clarified, e.g. using the DiQ-BioID approach to see whether *Pf*MyosinF interacts with further members of the Kelch13 compartment. Alternatively, it is also possible that the influence of *Pf*MyosinF on the endocytosis process is less direct and involves transport of Kelch13 compartment-derived endocytic structures to the FV rather than a direct interaction to *Pf*Kelch13. In that case the contact to *Pf*Kelch13 and its compartment proteins may be more spurious or short-lived.

In a further step it was analyzed whether the spatial arrangement of *Pf*MyosinF and *Pf*Kelch13 foci depends on actin. To test this, an inhibitor of actin polymerization, Cytochalasin D, was used to see whether the inhibition influences the relative position of *Pf*MyosinF and *Pf*Kelch13 foci (section 4.2.2). Treatment of the MyoF<sup>wt</sup>-2x2+K13 parasites for one hour with Cytochalasin D resulted in the dissociation of *Pf*MyosinF and *Pf*Kelch13 foci in trophozoite stages and the dispersion of the *Pf*MyosinF signal in late trophozoites. This data indicates that upon Cytochalasin D treatment the actomyosin motor is impaired, leading to a disruption of the spatial arrangement of the Kelch13 compartment and *Pf*MyosinF. To further verify these findings, the experiment needs to be repeated with more cells. Furthermore, a synchronous culture could be used to better assess the effect since this preliminary experiment was performed with an asynchronous culture.

Recent data demonstrated that inactivation of *Pf*Kelch13 and its compartment members results in ART resistance due to reduced hemoglobin uptake and thus reduced ART activation (Birnbaum *et al.*, 2020). The data obtained here indicates that *Pf*MyosinF is found close to *Pf*Kelch13 in the parasite cell and that its function as motor protein may be involvement in endocytosis. To test whether *Pf*MyosinF is involved in hemoglobin uptake, a bloated food vacuole assay was performed (section 4.3.3). In this assay, a bloated food

vacuole phenotype is detectable when hemoglobin uptake is operational. The experiment revealed that upon inactivation of *Pf*MyosinF by knock sideways, endocytic uptake of hemoglobin was reduced (section 4.3.3). This finding suggests that *Pf*MyosinF is important for the transport of hemoglobin containing vesicles to the food vacuole, which is impaired when *Pf*MyosinF is partially inactivated. Comparison of the vesicle number between control parasites and rapalog-cultured parasites showed, that the control of the MyoF<sup>wt</sup>-2x2+1xNLS cell line already had ~ 5 vesicles per cell (average number of three independent experiment), whereas the parasites where rapalog was added had ~ 8 vesicles per cell (average number of three independent experiments). Prior experiments in a parasite line where *Pf*VPS45 (a protein known to be involved in host cell cytosol uptake) can be conditionally inactivated the control parasites had ~ 2 vesicles per cell, while the parasites with rapalog (*Pf*VPS45 inactivation) displayed ~ 10 vesicles per cell (Jonscher *et al.*, 2019). This indicated that already the tagging of *Pf*MyosinF resulted in a partial phenotype as these parasites had an increased number of vesicles compared to the baseline of the VPS45 cell line. To further clarify whether this is an artificial effect caused by the C-terminal tagging of the full-length *Pf*MyosinF with 2xFKBP-GFP-2xFKBP, the experiments need to be repeated using 3D7 parasites as a control in parallel. Additionally, the MyoF<sup>wt</sup>-3xHA cell line could be used as another control since this cell line did not appear to display an increased number of vesicles during normal culturing.

Another hint to the involvement of *Pf*MyosinF in endocytosis or vesicular trafficking is based on its C-terminal WD40 repeat domains. Prior data obtained in mammalian cells indicated that WD40 domains can bind to phosphoinositides (Jeffries *et al.*, 2004; Proikas-Cezanne *et al.*, 2007). To investigate whether *Pf*MyosinF is associated to PI3P positive structures, the PI3P-marker P40PX was used to assess the relative localization of *Pf*MyosinF and PI3P positive structures (section 4.3.5). Since PI3P is a hallmark of early endosomes in eukaryotic cells (Balla, 2013) and was detected earlier at vesicles involved in host cell cytosol uptake (Jonscher *et al.*, 2019), this would give further support for a function of *Pf*MyosinF in the endolysosomal pathway. Additionally, it was shown in *Toxoplasma* that *Tg*MyosinF is involved in the organization of vesicle transport and of the endomembrane system (Carneille *et al.*, 2021). Inactivation of *Pf*MyosinF in this thesis via knock sideways demonstrated that the mislocalization of the protein into another compartment increased the localization of PI3P-positive structures (represented by the P40PX-marker) at the FV in trophozoites (section 4.3.5). It is important to mention that only one experiment in an asynchronous culture was performed to assess this association, and further that *Pf*MyosinF is refractory to complete mislocalization and thus some of this protein remained at the FV. Nevertheless, this experiment, as well as the bloated food vacuole assay, suggest that

*PfMyosinF* has a function in hemoglobin endocytosis. For more definite results, these experiments need to be repeated with more parasites, and additionally in a further step, synchronized cultures could be used to better isolate the detected effect.

As the data presented here showed that *PfMyosinF* is located close to *PfKelch13* foci and is additionally involved in hemoglobin uptake, this suggests that *PfMyosinF* could possibly influence ART resistance. For this, RSAs were performed with parasites wherein *PfMyosinF* was inactivated prior to the initiation of the RSA (section 4.3.2). This experiment showed that inactivation of *PfMyosinF* via the knock sideways system did not render parasites resistant to ART, indicating that *PfMyosinF* is not involved in endocytic processes in ring stages. Two possibilities exist that could explain this result. One option would be that due to the incomplete mislocalization of *PfMyosinF* an insufficient amount of *PfMyosinF* is inactivated to assess the effect of ART treatment on the ring stage parasites. A second explanation would be that *PfMyosinF* is only weakly expressed in early ring stages, the stage which is most important for ART resistance and thus inactivation of the protein in this stage has no effect on ART resistance (section 4.2.1). However, this would also mean that in rings *PfMyosinF* is not needed for endocytosis, possibly because in this stage endocytic vesicular transport is not actomyosin dependent. This could be tested by measuring endocytosis after inactivation of *PfMyosinF* in rings using fluorescent tracers loaded into RBC, as done before to show the function of *PfKelch13* in endocytosis in that stage (Birnbaum *et al.*, 2020). To further investigate ART response upon inactivation of *PfMyosinF*, a trophozoite-stage survival assay (TSA) could be performed, the developmental stage this protein is more strongly expressed.

The knowledge about *Plasmodium* myosins is limited. Six genes encoding myosins have been discovered in the genome of malaria parasites (Wall *et al.*, 2019). Several homologous genes are known in *Toxoplasma* which encode 11 myosin genes in their genome. Initially, the different myosins were named in order of their discovery which was often done independently for each species (Heintzelman & Schwartzman, 1997; Hettmann *et al.*, 2000; Heintzelman & Schwartzman, 2001; Matuschewski *et al.*, 2001; Lew *et al.*, 2002; Heintzelman, 2004; Chaparro-Olaya *et al.*, 2005). Consequently, the problem arose, that non-homologous genes of *Plasmodium* and *Toxoplasma* carried the same name (Chaparro-Olaya *et al.*, 2005). To avoid confusion, a new systematic designation was proposed, leading to similar naming of homologous myosin genes across taxa. This is why *PfMyosinF* (PF3D7\_1329100), which was previously annotated as *PfMyosinC*, was renamed. The homologue of *PfMyosinF* in *Toxoplasma* is *TgMyosinF*. In 2013, Jacot *et al.* showed that *TgMyoF* is an actin-dependent motor protein that is involved in the correct positioning of the centromeres at the beginning of parasite division and is important for the inheritance of the

apicoplast in *Toxoplasma* (Jacot *et al.*, 2013). The data obtained in this thesis for *P. falciparum* indicated that *PfMyosinF* in some cases localized close to DAPI-stained nuclei in trophozoites and was seen in schizont stage parasites also close to the nuclei. This might indicate a function of *PfMyosinF* for cell division, but this needs to be further confirmed by other experiments. To assess whether functions in cell division and apicoplast inheritance of *PfMyosinF* may also be possible in *Plasmodium* parasites, co-localization experiments with an apicoplast marker and centrosome-marker need to be performed.

### 5.1.3 Other proteins besides *PfKelch13* influence ART resistance

Several proteins of the newly defined Kelch13 compartment were suspected in ART resistance in previous work (Hunt *et al.*, 2007; Hunt *et al.*, 2010a; Borrmann *et al.*, 2013; Henriques *et al.*, 2014; Cerqueira *et al.*, 2017) and were shown to be essential for parasite development in the host red blood cell (Birnbaum *et al.*, 2020). Partial inactivation of *PfAP-2 $\mu$* , *PfEps15*, *PfUBP1*, *PfKIC7* rendered parasites resistant to ART, indicating that they are part of the resistance pathway (section 4.4.2). Since it was shown before that non-synonymous SNPs in other genes than *PfKelch13* are able to reduce susceptibility of *P. falciparum* parasites to ART, mutations of different Kelch13 compartment members were tested in the present work for their capacity to cause ART resistance. A special focus was set on non-synonymous mutations that display a low to medium prevalence in Africa, and SNPs were either tested simultaneously in a mutation pool or individually. Creating mutation pools had the advantage to accelerate the screening process since none of the introduced mutations should be harmful for parasite development, as they were found *in vivo*. While a detrimental effect due to combining all mutations cannot be predicted, the fact that most of the pools were successfully integrated (8 of 9), indicates that this was mostly not the case. The only multipool candidate that failed to integrate was *PfEps15*, suggesting that the introduced mutations impaired parasite growth. To continue the analysis of several of the *PfEps15* mutations at a time, one possibility would be to subdivide the multipool construct of *PfEps15* into smaller parts for integration and test e.g. N-terminal, mid part, or C-terminal mutation pools separately, leaving the other regions unchanged.

A potentially limiting factor of the mutation pools is the time-consuming cloning process due to the large size of some of the candidate genes. Furthermore, gene synthesis of the mutated recodonized gene sequence is very cost intensive. However, individual testing of each mutation would have been much more labor intensive and in many instances would

also have required the cloning of large fragments. Hence, overall this approach is a viable option to test many mutations with a single cell line.

Testing the different mutation pools in standard RSA revealed that none of the introduced mutations rendered parasites resistant to ART (section 4.5). The mutation pools included data from the MalariaGEN *Plasmodium falciparum* Community Project (MalariaGEN *et al.*, 2021). One future approach for mutation screening could be that the inclusion criteria are adapted in such a way that mutations with medium to higher prevalence are included. Although this may again not reveal African mutations in resistance since non-synonymous SNPs with higher population frequencies would mean that clinical resistance should already have been detected if such mutations would cause ART resistance. Another option would be to test different combinations of mutated genes, based on the hypothesis that different genetic combinations are important for the development of resistance. However, without prior indication for the combination of genes, this is difficult to achieve in a targeted approach due to the large number of possibilities. Overall, taking into consideration that clinical failures with ACTs in Africa seem to be absent or rare, it is at present unclear if any of the Kelch13 compartment proteins can mediate a reduced susceptibility to ART in the field apart from the *Pf*UBP1 mutation already detected (R3138H) that however derives from SEA (Cerqueira *et al.*, 2017).

A further approach to detect SNPs causing ART resistance in this work was attempted by sequencing of field isolate DNA deriving from a Ghanaian patient suffering repeatedly from malaria even after ART treatment. This resulted in several non-synonymous SNPs found in different Kelch13 compartment members which were tested either in the mutation pools or individually. Since no mutation was detected in *Pf*Kelch13, a *Pf*Kelch13-independent cause was suspected to mediate ART resistance in this patient. However, none of the here tested mutations rendered parasites resistant to ART. To finally find the reason for the suspected ART resistance of the parasites from this patient, sequencing of the DNA samples must be continued, including further genes of the Kelch13 compartment. One option would be to sequence the entire genome of these parasites, but without further indicators, the large number of SNPs that can be expected to result from this are unlikely to easily reveal the cause of resistance. Another possibility would be that ART resistance is driven by an altered expression level of a particular candidate. Thus, the respective promotor regions of each candidate could be analyzed for mutations that potentially alter the expression level of the corresponding gene. It should also be noted that resistance of these parasites was not tested *in vitro* as only DNA is available, and it should also be considered that these parasites might have re-surfaced in this patient due to other reason than ART resistance.

Besides the data from different databases and patient sample sequencing, also mutations mentioned in the literature were experimentally tested in this thesis. With this approach two mutations, found in *PfAP-2 $\alpha$*  and *PfUBP1*, reduced the sensitivity of the parasite to ART (section 4.6). The H817P mutation of *PfAP-2 $\alpha$*  rendered parasites only mildly resistant to ART. This suggests that this protein, which is part of the heterotetrameric adaptor protein complex that co-localizes with the Kelch13 compartment (Birnbaum *et al.*, 2020), may be involved in endocytosis but that the H817P mutation does only minimally affect this process. This would be in line with the only mild resistance phenotype in the parasites this gene was found mutated in and it should also be noted that other changes in these parasites might be involved in the lowered susceptibility to ART (Rocamora *et al.*, 2018). Previous data showed that mutations in the Mu subunit of the AP-2 complex (*PfAP-2 $\mu$* ) increased the tolerance of the parasites to ART (Henriques *et al.*, 2015; Henrici *et al.*, 2019) and partial inactivation of this protein also caused resistance as shown in this thesis. To further test the role of the *PfAP-2* complex in ART resistance, more mutations in the different *PfAP-2* subunits could be tested.

In contrast to the *PfAP-2 $\alpha$*  mutation, introducing the R3138H mutation (Cerqueira *et al.*, 2017) in the *PfUBP1* genomic locus resulted in significant resistance of the parasites to ART (section 4.6.4). This goes in line with prior data obtained in murine parasite models where *PfUBP1* was associated with ART resistance (Borrmann *et al.*, 2013; Henriques *et al.*, 2014; Henrici *et al.*, 2019).

## 5.2 *PfKelch13*-dependent ART resistance

### 5.2.1 Further mutations detected in the Kelch13 propeller domain of *PfKelch13* that mediate ART resistance

Molecular markers provide a powerful tool for the molecular surveillance of ART resistance worldwide. This was already shown for earlier resistance monitoring for chloroquine and for sulfadoxine-pyrimethamine resistance, where tracking of the causative genetic markers, *pfcr1* (for CQ), *pfdhfr* and *pfdhps* (for sulfadoxine-pyrimethamine) was performed to adapt treatment policy and prevent treatment failure (Dieckmann & Jung, 1986; Cowman *et al.*, 1988; Fidock *et al.*, 2000; Djimdé *et al.*, 2001; WHO, 2020a). Currently, 11 mutations of *PfKelch13* (F446I, N458Y, M476I, Y493H, R539T, I543T, P553L, R561H, P574L, C580Y and A675V) have been validated as resistance conferring mutations, resulting in delayed

parasite clearance (WWARN K13 Genotype-Phenotype Study Group, 2019). The first confirmed marker for ART resistance was C580Y together with Y493H, R539T, and I543T which was firstly detected in SEA along the Thai-Myanmar and Thai-Cambodian borders (Noedl *et al.*, 2008; Dondorp *et al.*, 2009). Molecular surveillance data indicated that resistance emerged independently and spread over the entire SEA subcontinent (Miotto *et al.*, 2015). Outside the GMS, parasites with C580Y mutations were detected and emerged independently in Papua New Guinea and Guyana (Miotto *et al.*, 2020; Mathieu *et al.*, 2020). Various studies assessing the prevalence of African *pfkelch13* mutations have been published and so far, six validated resistance-conferring *pfkelch13* mutations (M476I, P553L, R561H, P574L, C580Y and A675V) have been reported in four different African countries (Kamau *et al.*, 2015; Kayiba *et al.*, 2021; Ndwiga *et al.*, 2021). Recently published work performed with Rwandan samples detected the non-synonymous mutations R561H in *pfkelch13* and validated this mutation as a marker for ART resistance by *in vitro* experiments using CRISPR-Cas9 genome editing and provided evidence for *in vivo* resistance by molecular surveillance (Uwimana *et al.*, 2020; Uwimana *et al.*, 2021). This mutation was already detected in SEA and was listed as validated ART resistance marker (WWARN K13 Genotype-Phenotype Study Group, 2019). Besides Rwanda, the R561H mutation was reported locally in Uganda and Tanzania at low frequency levels (Bwire *et al.*, 2020; Asua *et al.*, 2021; Moser *et al.*, 2021). Interestingly, all *pfkelch13* mutations identified in Africa are present at low frequency but display a high allelic variation (MalariaGEN Plasmodium falciparum Community Project, 2016; Ocan *et al.*, 2019), which may be based on the infrequent use of ART in African countries due to high semi-immunity. In contrast to SEA, where ART was already used in the 1970s for malaria treatment, in Africa ART was implemented between the years 2000 and 2005. Thus, there was less time for the parasite to establish resistance conferring mutations with a high prevalence (Li *et al.*, 1994). Another option for the low frequency of resistance-conferring mutations in Africa may be a genetic background in African *Plasmodium* parasites that is less suitable for ART resistance and *PfKelch13* mutations than the parasites in SEA (Borrmann *et al.*, 2013; Mita *et al.*, 2016; Cerqueira *et al.*, 2017; Demas *et al.*, 2018; Henrici & Sutherland, 2018; Velavan *et al.*, 2019). Besides this, the partner drugs are still very effective in Africa compared to SEA which means that *pfkelch13* mutations cannot establish themselves as the parasites are eliminated by the partner drug.

The non-synonymous *pfkelch13* mutations (V520A, V520I, V589I, and E612K) tested in the present work were present in Africa (V520A, V589I, E612K) and Asia (V520I) with a low prevalence level. While the V520I and the E612K mutation did not render parasites resistant to ART *in vitro*, V520A and V589I conferred moderate resistance to ART (section 4.6.5).

Both mutations are located in the C-terminal Kelch propeller domain (amino acids 443-726). Structural analysis of the *Pf*Kelch13 protein revealed that most allelic variations are located in this propeller domain (Ariey *et al.*, 2014; Ashley *et al.*, 2014; Anderson *et al.*, 2017). The Kelch domain consists of six repeated kelch blades, each blade arranged in a  $\beta$ -sheet secondary structure (Adams *et al.*, 2000; Ariey *et al.*, 2014). Additionally, the *Plasmodium* Kelch13 protein comprises an *Apicomplexa*-specific N-terminal region and two highly conserved domains, the coiled-coil domain (amino acids 212-341) and the BTB domain (aa 350-437). To date, only two crystal structure analyses (PDB IDs: 4YY8 and 4ZGC) of *Pf*Kelch13 exist which show the conformational arrangement of the BTB and the Kelch propellers (Jiang *et al.*, 2015). Comparative structural and evolutionary analyses published by Coppée *et al.* in 2019 revealed potential functional sites of *Pf*Kelch13 and provided insight in structural alteration caused by the *pfkelch13* mutations C580Y and R539T (Coppée *et al.*, 2019). The bottom side of the *Pf*Kelch13 hexamer contains a shallow pocket which is highly conserved and may provide a binding site for interaction partners (Coppée *et al.*, 2019). These authors noted that resistance conferring mutations are distributed largely across the Kelch domain but are all located outside this shallow pocket. Additionally, they showed that these mutations may lead to a structural destabilization of the Kelch domain. As it is now known that reduced *Pf*Kelch13 levels explain ART resistance (Siddiqui *et al.*, 2017; Yang *et al.*, 2019; Birnbaum *et al.*, 2020), such alterations might mediate ART resistance by regulating protein abundance, stability, or folding. This agrees with data from other studies, demonstrating that binding of the Kelch domain is regulated by the shallow pocket in structurally related Kelch proteins (Canning *et al.*, 2013; Schumacher *et al.*, 2014; Canning *et al.*, 2015). Transferring these findings to the data presented in this thesis suggests that non-synonymous mutations altering the same amino acid position can result in different outcomes due to differential affection on Kelch domain stability. Even though the V520A and the V520I mutation are located at the same position, and both turn valine into an amino acid with hydrophobic properties, only the amino acid change from valine to alanine rendered parasites resistant to ART whereas the change from valine to isoleucine did not (section 4.6.5). This gives a hint that the additional methyl groups present in the V520I mutation may potentially stabilize the shallow pocket or the entire domain and thus protein interactions, while V520A mutation led to a destabilization resulting in resistance. A recently published study by Goel *et al.* also performed a structural analysis of the *Pf*Kelch13 using Small-Angle X-ray Scattering (SAXS), including the N-terminal Apicomplexan-specific domain and the coiled-coil domain, parts that were ignored in prior crystal structure studies (Goel *et al.*, 2021). These authors suggest that the Kelch domain assembles into a hexameric structure, forming a cauldron-like architecture. According to their data, conformational changes due to mutations in the Kelch propeller hexamer cause alterations

affecting the specific associations between the N-terminal ends of the different hexamer stabilizing chains. Consequently, the substrate-specificity of PfKelch13 might be negatively influenced or protein complex formation may be interfered with, either of which might lead to ART resistance (Goel *et al.*, 2021). However, it should also be noted that no difference in the interaction profile of wild type and PfKelch13 C580Y was observed, indicating that general stability rather than interaction to a specific substrate is the cause of resistance (Birnbaum *et al.*, 2020).

Altogether, a standardized, prospective surveillance monitoring (which is still lacking in African countries) in combination with molecular modelling of candidate markers would provide information about resistance trends in Africa and could support tailored adaptation of treatment policies (Kayiba *et al.*, 2021; Ndwiga *et al.*, 2021).

### 5.2.2 Does dormancy provide an explanation for ART resistance?

Artemisinin and its derivatives are very short-acting with only a short serum half-life (White, 2008b; Dondorp *et al.*, 2009). It was suggested that this may be the reason for the recrudescence of parasites in patients which occurs with frequency of up to 50% when a three-day ART monotherapy regimen is applied (Bunnag *et al.*, 1991; Looareesuwan *et al.*, 1992; Meshnick *et al.*, 1996; White, 1997; Kyle *et al.*, 1998; Phan *et al.*, 2002). Nevertheless, prolonging ART treatment duration for more than three days did not change the re-emergence of parasites, which indicates that this treatment failure is not based on drug potency or ART pharmacokinetics alone (Nguyen *et al.*, 1993; McIntosh & Olliaro, 2000; Giao *et al.*, 2001; Cheng *et al.*, 2012). Recrudescence after drug treatment has been observed in various organisms such as bacteria, parasitic protozoans, yeast, fungi, and mammalian cells (LaFleur *et al.*, 2006; Sánchez-valdéz *et al.*, 2018; Vallette *et al.*, 2019). For malaria parasites, *in vitro* studies and mathematical modelling led to the proposal of a new hypothesis which suggests that a phenomenon called dormancy is responsible for parasite recrudescence (Kyle, 1996; Hoshen *et al.*, 2000). According to this, a subpopulation of parasites, either resistant to ART or not, enter a dormant status by arrest in the ring phase to evade elimination. This dormant or persistent status was reported in *in vitro* experiments, while *in vivo* data of *P. falciparum* dormancy did not exist to date (Teuscher *et al.*, 2010). However, it was shown in the rodent *P. vinckei* malaria model that ring stage parasites were less susceptible to artesunate treatment than later developmental stages and that the day of treatment more impacts recrudescence than the total artesunate dose that is administered (LaCrue *et al.*, 2011). Thus, they suggest that the rings present

following 24 h artesunate treatment, displaying a condensed nucleus and pyknotic phenotype, are potential dormant *P. vinckei* stages, showing a similar morphology compared to the *in vitro* phenotype (pyknotic parasites) detected in *P. falciparum* after ART treatment (LaCrue *et al.*, 2011). Altogether, the data raised the question whether the phenomenon of dormancy provides a mechanism for ART resistance in *P. falciparum*.

To get more insight into this process (what are the properties of ART surviving parasites on a morphological level?), an ART resistant parasite line carrying the C580Y mutation in the *pfkelch13* locus was imaged by confocal microscopy directly after ART removal during an RSA and additionally 24 h and 39 h post ART removal (section 4.7.1). The confocal imaging revealed that after 39 hours only a small proportion of ART resistant parasites survived the ART pulse, and that the drug treated parasites were less far developed than the control fraction (section 4.7.1). To better define this finding, the average size of the parasites was measured 24 hours after ART removal, demonstrating that the control parasites were significantly larger than the drug treated parasites. Interestingly, the parasites that had the largest average size in the ART treated population were the same size as the smallest parasites measured in the untreated control. Additionally, the “large” parasites belonged to those that were still alive at 39 hours and continued growing. In summary, the data indicates that either ART treatment delays development of resistant parasites in the first part of the asexual cycle, potentially already during drug pulse, or that resistance is based on a subpopulation of parasites that display a generally slower growth. This goes in line with the finding that parasites where *PfKelch13* is inactivated via the knock sideways system have a prolonged ring stage phase and show a reduced level of hemoglobin endocytosis which results in less ART activation (Birnbaum *et al.*, 2020).

These experiments indicated a lower average age of the parasites surviving the ART pulse compared to the untreated control. From this finding two hypotheses are possible that could explain the delayed growth of parasites upon ART treatment: either a reduced growth is induced directly by ART, conferring tolerance to the parasites, or the survivors represent a subpopulation of parasites that would have grown less irrespective of ART treatment but survived due to their lower growth rate. In both cases, the parasites surviving did not take up the morphology associated with dormancy, suggesting that this is not the usual mechanism to overcome ART treatment. A similar conclusion was recently reached in a controlled human infection model (Watts *et al.*, 2020). Recrudescence of *P. falciparum* in parasites with *PfKelch13* mutations is therefore likely not a process akin to what was defined as dormancy (Breglio *et al.*, 2018; Welles *et al.*, 2020). In line with this, dormancy is not a process that is unique to treatment with ART since it was also reported for parasites

recovering from treatment with mefloquine or pyrimethamine, suggesting it is a more general effect (Nakazawa *et al.*, 2002).

### 5.2.3 Fitness and *PfKelch13* protein levels vary in parasites with different *pfkelch13* mutations

In this work it was shown that different *pfkelch13* mutations cause different levels of ART resistance (section 4.6.5). Additionally, it was demonstrated that an already resistant cell line became even more resistant by re-growing survivors in consecutive RSAs (section 4.7.2). In 2018, it was published by Nair *et al.* that C580Y and R561H *pfkelch13* mutants differ in their respective fitness level (Nair *et al.*, 2018). This raised the question whether there are differences in fitness level of the C580Y and V520A mutants compared to wild type *PfKelch13* parasites, particularly as the latter mutation resulted in a much lower level of ART resistance. Competitive growth assays revealed that in co-cultivation with 3D7 parasites, the C580Y mutant cell line displayed the highest fitness cost, while the V520A mutation resulted in an intermediate fitness phenotype compared to wild type *pfkelch13* parasites (section 4.8.2). Interestingly, this inversely correlated with the respective parasite survival rate upon ART treatment, showing that highly resistant C580Y parasites had the highest fitness cost whereas the moderately resistant V520A mutants had similar fitness costs than the wild type parasites (section 4.8.2). The data obtained for the C580Y mutants agrees with the data presented by Nair *et al.*, which showed that these mutant parasites have higher fitness costs compared to another *pfkelch13* mutation (R561H) (Nair *et al.*, 2018). These findings also match with observations in bacteria and viruses where it was seen that drug resistant strains displayed reduced fitness compared to sensitive strains (Andersson & Hughes, 2010; Götte, 2012; Wargo & Kurath, 2012). Despite of this, it is quite intriguing that the C580Y mutation is very successful in the field, as it is the most prevalent ART resistance mutation in SEA (e.g. ~ 88% in Cambodia, WWARN). In contrast, the V520A mutation is present in African countries at rather low frequencies (e.g. ~1.3% in Ghana and ~4% in DRC, WWARN) and is absent in SEA. Since this mutation only caused a very mild fitness reduction (section 4.8.2), this could be beneficial in African settings where infections with multiple *P. falciparum* parasite strains is common in high-transmission areas (Arnot, 1998; Juliano *et al.*, 2010). This multiplicity of infection causes intra-host competition between different strains, resulting in an increased negative selection of the parasite strain suffering the largest fitness cost (Roode *et al.*, 2003; Roode *et al.*, 2004). Thus, it may be advantageous for parasites in African settings to display only mild ART resistance, resulting

in lower fitness cost, to be able to survive in a polyclonal host environment. Additionally, in malaria endemic areas with a high parasite transmission rate, an overall stable anti-disease immunity exists against *P. falciparum* infections, resulting in less frequent drug treatment (Bull & Marsh, 2002; Rosenthal, 2013; Fowkes *et al.*, 2016). In contrast, mutations rendering parasites resistant to ART at a high level - such as C580Y - may have an advantage to survive among other parasites strains if treatment is frequent.

Another factor that may influence the fitness of ART resistant parasites are additional genomic adaptations to compensate growth disadvantages in the absence of selection pressure, which are due to the resistance mechanism (Walliker *et al.*, 2005). For this, the parasite needs to establish compensatory genetic modifications to be able to persist besides the wild type parasites, which is energetically cost-intensive and consequently results in a lowered fitness level. The importance of the genetic background was highlighted by work showing that the introduction of C580Y in different field isolates deriving either from SEA, or Africa, resulted in different fitness cost but also different levels of resistance (Straimer *et al.*, 2017; Nair *et al.*, 2018; Stokes *et al.*, 2021). For future experiments, it would be interesting to introduce the V520A mutations into field isolates deriving from Africa to assess the difference in fitness and resistance in different genetic backgrounds. Further research is also needed to define the impact of secondary genetic factors on parasite fitness that mediate ART resistance in a *PfKelch13*-independent manner (e.g *PfUBP1*, *Pfcoronin*, *PfAP-2 $\mu$* ) (Henriques *et al.*, 2014; Cerqueira *et al.*, 2017; Demas *et al.*, 2018; Henrici *et al.*, 2019). Mutations in *pfkelch13* often render parasites resistant to ART to a higher extent than mutations in *pfubp1* or *pfap-2 $\mu$* . As *PfKelch13* function is only relevant in ring stages but *PfUBP1* or *PfAP-2 $\mu$*  are important in all asexual developmental stages, the latter mutations might result in a higher fitness cost. To investigate this idea, competition assays could be performed with parasites carrying a mutation in *pfkelch13* versus parasites carrying for instance a *pfubp1* mutation.

Besides looking at the fitness phenotype of different resistance conferring mutations, one can also speculate about the mechanisms behind the differences in fitness cost. Birnbaum and Scharf *et al.* demonstrated that ART resistance is based on a reduced hemoglobin endocytosis which results in less activated ART (Birnbaum *et al.*, 2020). Additionally, it was shown that ART resistant parasites showed lower abundance of *PfKelch13*, indicating that *PfKelch13* protein levels and levels of endocytosis correlate with resistance. Based on this finding, the *PfKelch13* protein levels of different *PfKelch13* mutants were measured in this work. Fluorescence intensity measurements revealed, that the C580Y and the highly resistant C580Y mutant obtained by consecutive RSAs (K13<sup>C580Y-29th</sup>) had the lowest *PfKelch13* protein level compared to *PfKelch13* wild type parasite, while the V520A mutant

showed an intermediate *PfKelch13* protein level (section 4.8.1). This data, in combination with the data published by *Birnbaum and Scharf et al.*, indicates that due to lower *PfKelch13* protein amount the C580Y mutants show a reduced hemoglobin endocytosis, reducing the fitness level of these mutants. In contrast, the V520A mutants have lower fitness costs due to a more moderate reduction in *PfKelch13* protein levels but likely also more moderate downregulation of hemoglobin uptake and, as demonstrated here, more moderate resistance. To gain further insight into this correlation, hemoglobin uptake assays need to be performed with the different *pfkelch13* mutants.

## 6 References

- Abu Bakar, N., Klonis, N., Hanssen, E., Chan, C. & Tilley, L. (2010) Digestive-vacuole genesis and endocytic processes in the early intraerythrocytic stages of *Plasmodium falciparum*. *Journal of Cell Science*, 123(Pt 3), 441–450. Available from: <https://doi.org/10.1242/jcs.061499>.
- Adams, J., Kelso, R. & Cooley, L. (2000) The kelch repeat superfamily of proteins: propellers of cell function. *Trends in cell biology*, 10(1), 17–24. Available from: [https://doi.org/10.1016/s0962-8924\(99\)01673-6](https://doi.org/10.1016/s0962-8924(99)01673-6).
- Adl, S.M., Simpson, A.G.B., Farmer, M.A., Andersen, R.A., Anderson, O.R. & Barta, J.R. et al. (2005) The new higher level classification of eukaryotes with emphasis on the taxonomy of protists. *The Journal of Eukaryotic Microbiology*, 52(5), 399–451. Available from: <https://doi.org/10.1111/j.1550-7408.2005.00053.x>.
- Aguilar, R., Magallon-Tejada, A., Achtman, A.H., Moraleda, C., Joice, R. & Cisteró, P. et al. (2014) Molecular evidence for the localization of *Plasmodium falciparum* immature gametocytes in bone marrow. *Blood*, 123(7), 959–966. Available from: <https://doi.org/10.1182/blood-2013-08-520767>.
- Aikawa, M. (1966) The fine structure of the erythrocytic stages of three avian malarial parasites, *Plasmodium fallax*, *P. lophurae*, and *P. cathemerium*. *The American Journal of Tropical Medicine and Hygiene*, 15(4), 449–471. Available from: <https://doi.org/10.4269/ajtmh.1966.15.449>.
- Aikawa, M. (1971) *Plasmodium*: The fine structure of malarial parasites. *Experimental parasitology*, 30(2), 284–320. Available from: [https://doi.org/10.1016/0014-4894\(71\)90094-4](https://doi.org/10.1016/0014-4894(71)90094-4).
- Aikawa, M., Carter, R., Ito, Y. & Nijhout, M.M. (1984) New observations on gametogenesis, fertilization, and zygote transformation in *Plasmodium gallinaceum*. *The Journal of Protozoology*, 31(3), 403–413. Available from: <https://doi.org/10.1111/j.1550-7408.1984.tb02987.x>.
- Aikawa, M., Hepler, P.K., Huff, C.G. & Sprinz, H. (1966) The feeding mechanism of avian malarial parasites. *The Journal of Cell Biology*, 28(2), 355–373. Available from: <https://doi.org/10.1083/jcb.28.2.355>.
- Aikawa, M., Miller, L.H., Johnson, J. & Rabbege, J. (1978) Erythrocyte entry by malarial parasites. A moving junction between erythrocyte and parasite. *The Journal of Cell Biology*, 77(1), 72–82. Available from: <https://doi.org/10.1083/jcb.77.1.72>.
- Aikawa, M., Torii, M., Sjölander, A., Berzins, K., Perlmann, P. & Miller, L.H. (1990) Pf155/RESA antigen is localized in dense granules of *Plasmodium falciparum* merozoites. *Experimental parasitology*, 71(3), 326–329. Available from: [https://doi.org/10.1016/0014-4894\(90\)90037-d](https://doi.org/10.1016/0014-4894(90)90037-d).
- Alexander, D.L., Mital, J., Ward, G.E., Bradley, P. & Boothroyd, J.C. (2005) Identification of the moving junction complex of *Toxoplasma gondii*: a collaboration between distinct secretory organelles. *PLoS Pathogens*, 1(2), e17. Available from: <https://doi.org/10.1371/journal.ppat.0010017>.
- Aley, S.B., Sherwood, J.A., Marsh, K., Eidelman, O. & Howard, R.J. (1986) Identification of isolate-specific proteins on sorbitol-enriched *Plasmodium falciparum* infected erythrocytes from Gambian patients. *Parasitology*, 92 (Pt 3)(3), 511–525. Available from: <https://doi.org/10.1017/S0031182000065410>.
- Alphonse Charles Laveran (1881) *Un nouveau parasite trouvé dans le sang des malades atteints de fièvre palustre: origine parasitaire des accidents de l'impaludisme*.
- Ally, A.S.I., Vaughan, A.M. & Kappe, S.H.I. (2009) Malaria parasite development in the mosquito and infection of the mammalian host. *Annual Review of Microbiology*, 63, 195–221. Available from: <https://doi.org/10.1146/annurev.micro.091208.073403>.
- Amaratunga, C., Sreng, S., Suon, S., Phelps, E.S., Stepniewska, K. & Lim, P. et al. (2012) Artemisinin-resistant *Plasmodium falciparum* in Pursat province, western Cambodia: a parasite clearance rate study.

- The Lancet Infectious Diseases*, 12(11), 851–858. Available from: [https://doi.org/10.1016/S1473-3099\(12\)70181-0](https://doi.org/10.1016/S1473-3099(12)70181-0).
- Amaratunga, C., Witkowski, B., Dek, D., Try, V., Khim, N. & Miotto, O. et al. (2014) Plasmodium falciparum founder populations in western Cambodia have reduced artemisinin sensitivity in vitro. *Antimicrobial Agents and Chemotherapy*, 58(8), 4935–4937. Available from: <https://doi.org/10.1128/AAC.03055-14>.
- Anderson, R.M. & May, R.M. (1992) *Infectious Diseases of Humans: Dynamics and Control*. OUP Oxford.
- Anderson, T.J.C., Nair, S., McDew-White, M., Cheeseman, I.H., Nkhoma, S. & Bilgic, F. et al. (2017) Population Parameters Underlying an Ongoing Soft Sweep in Southeast Asian Malaria Parasites. *Molecular Biology and Evolution*, 34(1), 131–144. Available from: <https://doi.org/10.1093/molbev/msw228>.
- Andersson, D.I. & Hughes, D. (2010) Antibiotic resistance and its cost: is it possible to reverse resistance? *Nature Reviews Microbiology*, 8(4), 260–271. Available from: <https://doi.org/10.1038/nrmicro2319>.
- Ansorge, I., Benting, J., Bhakdi, S. & Lingelbach, K. (1996) Protein sorting in Plasmodium falciparum-infected red blood cells permeabilized with the pore-forming protein streptolysin O. *Biochemical Journal*, 315 (Pt 1)(Pt 1), 307–314. Available from: <https://doi.org/10.1042/bj3150307>.
- Arden, S.D., Puri, C., Au, J.S.-Y., Kendrick-Jones, J. & Buss, F. (2007) Myosin VI is required for targeted membrane transport during cytokinesis. *Molecular Biology of the Cell*, 18(12), 4750–4761. Available from: <https://doi.org/10.1091/mbc.e07-02-0127>.
- Ariey, F., Witkowski, B., Amaratunga, C., Beghain, J., Langlois, A.-C. & Khim, N. et al. (2014) A molecular marker of artemisinin-resistant Plasmodium falciparum malaria. *Nature*, 505(7481), 50–55. Available from: <https://doi.org/10.1038/nature12876>.
- Annot, D. (1998) Clone multiplicity of Plasmodium falciparum infections in individuals exposed to variable levels of disease transmission. *Transactions of the Royal Society of Tropical Medicine and Hygiene*, 92(6), 580–585. Available from: [https://doi.org/10.1016/s0035-9203\(98\)90773-8](https://doi.org/10.1016/s0035-9203(98)90773-8).
- Ashley, E.A., Dhorda, M., Fairhurst, R.M., Amaratunga, C., Lim, P. & Suon, S. et al. (2014) Spread of artemisinin resistance in Plasmodium falciparum malaria. *The New England Journal of Medicine*, 371(5), 411–423. Available from: <https://doi.org/10.1056/NEJMoa1314981>.
- Ashley, E.A., Pyae Phyo, A. & Woodrow, C.J. (2018) Malaria. *The Lancet*, 391(10130), 1608–1621. Available from: [https://doi.org/10.1016/S0140-6736\(18\)30324-6](https://doi.org/10.1016/S0140-6736(18)30324-6).
- Asua, V., Conrad, M.D., Aydemir, O., Duval Saint, M., Legac, J. & Duarte, E. et al. (2021) Changing Prevalence of Potential Mediators of Aminoquinoline, Antifolate, and Artemisinin Resistance Across Uganda. *The Journal of Infectious Diseases*, 223(6), 985–994. Available from: <https://doi.org/10.1093/infdis/jiaa687>.
- Balla, T. (2013) Phosphoinositides: tiny lipids with giant impact on cell regulation. *Physiological Reviews*, 93(3), 1019–1137. Available from: <https://doi.org/10.1152/physrev.00028.2012>.
- Bane, K.S., Lepper, S., Kehrer, J., Sattler, J.M., Singer, M. & Reinig, M. et al. (2016) The Actin Filament-Binding Protein Coronin Regulates Motility in Plasmodium Sporozoites. *PLoS Pathogens*, 12(7), e1005710. Available from: <https://doi.org/10.1371/journal.ppat.1005710>.
- Banerjee (2001) *DE Goldberg in The Antimalarial Chemotherapy: Mechanisms of Action, Resistance and New Directions in Drug Discovery*”.
- Bannister, L., Hopkins, J., Fowler, R., Krishna, S. & Mitchell, G. (2000) A Brief Illustrated Guide to the Ultrastructure of Plasmodium falciparum Asexual Blood Stages. *Parasitology today (Personal ed.)*, 16(10), 427–433. Available from: [https://doi.org/10.1016/s0169-4758\(00\)01755-5](https://doi.org/10.1016/s0169-4758(00)01755-5).
- Bannister, L.H., Butcher, G.A., Dennis, E.D. & Mitchell, G.H. (1975) Structure and invasive behaviour of Plasmodium knowlesi merozoites in vitro. *Parasitology*, 71(3), 483–491. Available from: <https://doi.org/10.1017/s0031182000047247>.

- Bannister, L.H., Hopkins, J.M., Margos, G., Dluzewski, A.R. & Mitchell, G.H. (2004) Three-dimensional ultrastructure of the ring stage of *Plasmodium falciparum*: evidence for export pathways. *Microscopy and Microanalysis : the Official Journal of Microscopy Society of America, Microbeam Analysis Society, Microscopical Society of Canada*, 10(5), 551–562. Available from: <https://doi.org/10.1017/S1431927604040917>.
- Bannister, L.H. & Mitchell, G.H. (1989) The fine structure of secretion by *Plasmodium knowlesi* merozoites during red cell invasion. *The Journal of Protozoology*, 36(4), 362–367. Available from: <https://doi.org/10.1111/j.1550-7408.1989.tb05527.x>.
- Bannister, L.H., Mitchell, G.H., Butcher, G.A. & Dennis, E.D. (1986) Lamellar membranes associated with rhoptries in erythrocytic merozoites of *Plasmodium knowlesi*: a clue to the mechanism of invasion. *Parasitology*, 92 (Pt 2), 291–303. Available from: <https://doi.org/10.1017/s0031182000064064>.
- Barat, L.M., Palmer, N., Basu, S., Worrall, E., Hanson, K. & Mills, A. (2004) Do malaria control interventions reach the poor? A view through the equity lens. *The American Journal of Tropical Medicine and Hygiene*, 71(2 Suppl), 174–178. Available from: <https://pubmed.ncbi.nlm.nih.gov/15331835/>.
- Bártfai, R., Hoeijmakers, W.A.M., Salcedo-Amaya, A.M., Smits, A.H., Janssen-Megens, E. & Kaan, A. et al. (2010) H2A.Z demarcates intergenic regions of the *Plasmodium falciparum* epigenome that are dynamically marked by H3K9ac and H3K4me3. *PLoS Pathogens*, 6(12), e1001223. Available from: <https://doi.org/10.1371/journal.ppat.1001223>.
- Bartoloni, A. & Zammarchi, L. (2012) Clinical aspects of uncomplicated and severe malaria. *Mediterranean Journal of Hematology and Infectious Diseases*, 4(1), e2012026. Available from: <https://doi.org/10.4084/MJHID.2012.026>.
- Baruch, D.I., Pasloske, B.L., Singh, H.B., Bi, X., Ma, X.C. & Feldman, M. et al. (1995) Cloning the *P. falciparum* gene encoding PfEMP1, a malarial variant antigen and adherence receptor on the surface of parasitized human erythrocytes. *Cell*, 82(1), 77–87. Available from: [https://doi.org/10.1016/0092-8674\(95\)90054-3](https://doi.org/10.1016/0092-8674(95)90054-3).
- Baum, J., Richard, D., Healer, J., Rug, M., Krnajska, Z. & Gilberger, T.-W. et al. (2006) A conserved molecular motor drives cell invasion and gliding motility across malaria life cycle stages and other apicomplexan parasites. *The Journal of Biological Chemistry*, 281(8), 5197–5208. Available from: <https://doi.org/10.1074/jbc.M509807200>.
- Beck, J.R., Muralidharan, V., Oksman, A. & Goldberg, D.E. (2014) PTEX component HSP101 mediates export of diverse malaria effectors into host erythrocytes. *Nature*, 511(7511), 592–595. Available from: <https://doi.org/10.1038/nature13574>.
- Beckers, C.J., Dubremetz, J.F., Mercereau-Puijalon, O. & Joiner, K.A. (1994) The *Toxoplasma gondii* rhoptry protein ROP 2 is inserted into the parasitophorous vacuole membrane, surrounding the intracellular parasite, and is exposed to the host cell cytoplasm. *Journal of Cell Biology*, 127(4), 947–961. Available from: <https://doi.org/10.1083/jcb.127.4.947>.
- Beeson, J.G. & Brown, G.V. (2002) Pathogenesis of *Plasmodium falciparum* malaria: the roles of parasite adhesion and antigenic variation. *Cellular and Molecular Life Sciences : CMLS*, 59(2), 258–271. Available from: <https://doi.org/10.1007/s00018-002-8421-y>.
- Behari, R. & Haldar, K. (1994) *Plasmodium falciparum*: protein localization along a novel, lipid-rich tubovesicular membrane network in infected erythrocytes. *Experimental Parasitology*, 79(3), 250–259. Available from: <https://doi.org/10.1006/expr.1994.1088>.
- Benting, J., Mattei, D. & Lingelbach, K. (1994) Brefeldin A inhibits transport of the glycoprotein-binding protein from *Plasmodium falciparum* into the host erythrocyte. *Biochemical Journal*, 300 (Pt 3)(Pt 3), 821–826. Available from: <https://doi.org/10.1042/bj3000821>.

- Besteiro, S., Dubremetz, J.-F. & Lebrun, M. (2011) The moving junction of apicomplexan parasites: a key structure for invasion. *Cellular Microbiology*, 13(6), 797–805. Available from: <https://doi.org/10.1111/j.1462-5822.2011.01597.x>.
- Bhattacharjee, S., van Ooij, C., Balu, B., Adams, J.H. & Haldar, K. (2008) Maurer's clefts of *Plasmodium falciparum* are secretory organelles that concentrate virulence protein reporters for delivery to the host erythrocyte. *Blood*, 111(4), 2418–2426. Available from: <https://doi.org/10.1182/blood-2007-09-115279>.
- Billker, O., Dechamps, S., Tewari, R., Wenig, G., Franke-Fayard, B. & Brinkmann, V. (2004) Calcium and a Calcium-Dependent Protein Kinase Regulate Gamete Formation and Mosquito Transmission in a Malaria Parasite. *Cell*, 117(4), 503–514. Available from: [https://doi.org/10.1016/s0092-8674\(04\)00449-0](https://doi.org/10.1016/s0092-8674(04)00449-0).
- Billker, O., Lindo, V., Panico, M., Etienne, A.E., Paxton, T. & Dell, A. et al. (1998) Identification of xanthurenic acid as the putative inducer of malaria development in the mosquito. *Nature*, 392(6673), 289–292. Available from: <https://doi.org/10.1038/32667>.
- Billker, O., Miller, A.J. & Sinden, R.E. (2000) Determination of mosquito bloodmeal pH in situ by ion-selective microelectrode measurement: implications for the regulation of malarial gametogenesis. *Parasitology*, 120 (Pt 6), 547–551. Available from: <https://doi.org/10.1017/s0031182099005946>.
- Birnbaum, J. (2017) *A novel genetic system for the functional analysis of essential proteins of the human malaria parasite Plasmodium falciparum*.
- Birnbaum, J., Flemming, S., Reichard, N., Soares, A.B., Mesén-Ramírez, P. & Jonscher, E. et al. (2017) A genetic system to study *Plasmodium falciparum* protein function. *Nature Methods*, 14(4), 450–456. Available from: <https://doi.org/10.1038/nmeth.4223>.
- Birnbaum, J., Scharf, S., Schmidt, S., Jonscher, E., Hoesijmakers, W.A.M. & Flemming, S. et al. (2020) A Kelch13-defined endocytosis pathway mediates artemisinin resistance in malaria parasites. *Science (New York, N.Y.)*, 367(6473), 51–59. Available from: <https://doi.org/10.1126/science.aax4735>.
- Blackman, M.J. & Bannister, L.H. (2001) Apical organelles of Apicomplexa: biology and isolation by subcellular fractionation. *Molecular and Biochemical Parasitology*, 117(1), 11–25. Available from: [https://doi.org/10.1016/S0166-6851\(01\)00328-0](https://doi.org/10.1016/S0166-6851(01)00328-0).
- Blackman, M.J. & Carruthers, V.B. (2013) Recent insights into apicomplexan parasite egress provide new views to a kill. *Current Opinion in Microbiology*, 16(4), 459–464. Available from: <https://doi.org/10.1016/j.mib.2013.04.008>.
- Blackman, M.J., Fujioka, H., Stafford, W.H., Sajid, M., Clough, B. & Fleck, S.L. et al. (1998) A subtilisin-like protein in secretory organelles of *Plasmodium falciparum* merozoites. *The Journal of Biological Chemistry*, 273(36), 23398–23409. Available from: <https://doi.org/10.1074/jbc.273.36.23398>.
- Blisnick, T., Morales Betoulle, M.E., Barale, J.-C., Uzureau, P., Berry, L. & Desroses, S. et al. (2000) Pfsbp1, a Maurer's cleft *Plasmodium falciparum* protein, is associated with the erythrocyte skeleton. *Molecular and Biochemical Parasitology*, 111(1), 107–121. Available from: [https://doi.org/10.1016/s0166-6851\(00\)00301-7](https://doi.org/10.1016/s0166-6851(00)00301-7).
- Boddey, J.A. & Cowman, A.F. (2013) *Plasmodium* nesting: remaking the erythrocyte from the inside out. *Annual Review of Microbiology*, 67, 243–269. Available from: <https://doi.org/10.1146/annurev-micro-092412-155730>.
- Boddey, J.A., O'Neill, M.T., Lopaticki, S., Carvalho, T.G., Hodder, A.N. & Nebl, T. et al. (2016) Export of malaria proteins requires co-translational processing of the PEXEL motif independent of phosphatidylinositol-3-phosphate binding. *Nature Communications*, 7(1), 10470. Available from: <https://doi.org/10.1038/ncomms10470>.
- Borges, S., Cravo, P., Creasey, A., Fawcett, R., Modrzynska, K. & Rodrigues, L. et al. (2011) Genomewide scan reveals amplification of *mdr1* as a common denominator of resistance to mefloquine, lumefantrine,

- and artemisinin in *Plasmodium chabaudi* malaria parasites. *Antimicrobial Agents and Chemotherapy*, 55(10), 4858–4865. Available from: <https://doi.org/10.1128/AAC.01748-10>.
- Borrmann, S., Straimer, J., Mwai, L., Abdi, A., Rippert, A. & Okombo, J. et al. (2013) Genome-wide screen identifies new candidate genes associated with artemisinin susceptibility in *Plasmodium falciparum* in Kenya. *Scientific Reports*, 3(1), 3318. Available from: <https://doi.org/10.1038/srep03318>.
- Brancucci, N.M.B., Bertschi, N.L., Zhu, L., Niederwieser, I., Chin, W.H. & Wampfler, R. et al. (2014) Heterochromatin protein 1 secures survival and transmission of malaria parasites. *Cell Host & Microbe*, 16(2), 165–176. Available from: <https://doi.org/10.1016/j.chom.2014.07.004>.
- Brancucci, N.M.B., Gerdt, J.P., Wang, C., Niz, M. de, Philip, N. & Adapa, S.R. et al. (2017) Lysophosphatidylcholine Regulates Sexual Stage Differentiation in the Human Malaria Parasite *Plasmodium falciparum*. *Cell*, 171(7), 1532-1544.e15. Available from: <https://doi.org/10.1016/j.cell.2017.10.020>.
- Breglio, K.F., Rahman, R.S., Sá, J.M., Hott, A., Roberts, D.J. & Wellems, T.E. (2018) Kelch Mutations in *Plasmodium falciparum* Protein K13 Do Not Modulate Dormancy after Artemisinin Exposure and Sorbitol Selection In Vitro. *Antimicrobial Agents and Chemotherapy*, 62(5). Available from: <https://doi.org/10.1128/AAC.02256-17>.
- Breman, J.G., Egan, A. & Keusch, G.T. (2001) The intolerable burden of malaria: a new look at the numbers. *The American Journal of Tropical Medicine and Hygiene*, 64(1-2 Suppl), iv–vii. Available from: <https://doi.org/10.4269/ajtmh.2001.64.iv>.
- Bull, P.C. & Marsh, K. (2002) The role of antibodies to *Plasmodium falciparum*-infected-erythrocyte surface antigens in naturally acquired immunity to malaria. *Trends in microbiology*, 10(2), 55–58. Available from: [https://doi.org/10.1016/s0966-842x\(01\)02278-8](https://doi.org/10.1016/s0966-842x(01)02278-8).
- Bunnag, D., Viravan, C., Looareesuwan, S., Karbwang, J. & Harinasuta, T. (1991) Double blind randomised clinical trial of two different regimens of oral artesunate in falciparum malaria. *Southeast Asian J Trop Med Public Health*. Available from: <https://pesquisa.bvsalud.org/portal/resource/pt/sea-34340>.
- Burrows, J.N., Duparc, S., Gutteridge, W.E., van Hooft Huijsduijnen, R., Kaszubska, W. & Macintyre, F. et al. (2017) New developments in anti-malarial target candidate and product profiles. *Malaria Journal*, 16(1), 26. Available from: <https://doi.org/10.1186/s12936-016-1675-x>.
- Bwire, G.M., Ngasala, B., Mikomangwa, W.P., Kilonzi, M. & Kamuhabwa, A.A.R. (2020) Detection of mutations associated with artemisinin resistance at k13-propeller gene and a near complete return of chloroquine susceptible falciparum malaria in Southeast of Tanzania. *Scientific Reports*, 10(1), 3500. Available from: <https://doi.org/10.1038/s41598-020-60549-7>.
- Canning, P., Cooper, C.D.O., Krojer, T., Murray, J.W., Pike, A.C.W. & Chaikuad, A. et al. (2013) Structural basis for Cul3 protein assembly with the BTB-Kelch family of E3 ubiquitin ligases. *Journal of Biological Chemistry*, 288(11), 7803–7814. Available from: <https://doi.org/10.1074/jbc.M112.437996>.
- Canning, P., Sorrell, F.J. & Bullock, A.N. (2015) Structural basis of Keap1 interactions with Nrf2. *Free Radical Biology & Medicine*, 88(Pt B), 101–107. Available from: <https://doi.org/10.1016/j.freeradbiomed.2015.05.034>.
- Carneille, R., Schiano Lomoriello, P., Devarakonda, P.M., Kellermeier, J.A. & Heaslip, A.T. (2021) Actin and an unconventional myosin motor, TgMyoF, control the organization and dynamics of the endomembrane network in *Toxoplasma gondii*. *PLoS Pathogens*, 17(2), e1008787. Available from: <https://doi.org/10.1371/journal.ppat.1008787>.
- Carter, R. & Chen, D.H. (1976) Malaria transmission blocked by immunisation with gametes of the malaria parasite. *Nature*, 263(5572), 57–60. Available from: <https://doi.org/10.1038/263057a0>.

- Carter, R. & Kaushal, D.C. (1984) Characterization of antigens on mosquito midgut stages of *Plasmodium gallinaceum*. III. Changes in zygote surface proteins during transformation to mature ookinete. *Molecular and Biochemical Parasitology*, 13(2), 235–241. Available from: [https://doi.org/10.1016/0166-6851\(84\)90116-6](https://doi.org/10.1016/0166-6851(84)90116-6).
- Casanova, M., Gonzalez, I.J., Sprissler, C., Zalila, H., Dacher, M. & Basmaciyan, L. et al. (2015) Implication of different domains of the *Leishmania major* metacaspase in cell death and autophagy. *Cell Death & Disease*, 6(10), e1933. Available from: <https://doi.org/10.1038/cddis.2015.288>.
- Cerqueira, G.C., Cheeseman, I.H., Schaffner, S.F., Nair, S., McDew-White, M. & Phyto, A.P. et al. (2017) Longitudinal genomic surveillance of *Plasmodium falciparum* malaria parasites reveals complex genomic architecture of emerging artemisinin resistance. *Genome Biology*, 18(1), 78. Available from: <https://doi.org/10.1186/s13059-017-1204-4>.
- Chandre, F., Darrier, F., Manga, L., Akogbeto, M., Faye, O. & Mouchet, J. et al. (1999) Status of pyrethroid resistance in *Anopheles gambiae sensu lato*. *Bulletin of the World Health Organization*, 77(3), 230–234. Available from: <https://pubmed.ncbi.nlm.nih.gov/10212513/>.
- Chang, H.H., Falick, A.M., Carlton, P.M., Sedat, J.W., DeRisi, J.L. & Marletta, M.A. (2008) N-terminal processing of proteins exported by malaria parasites. *Molecular and Biochemical Parasitology*, 160(2), 107–115. Available from: <https://doi.org/10.1016/j.molbiopara.2008.04.011>.
- Chaparro-Olaya, J., Margos, G., Coles, D.J., Dluzewski, A.R., Mitchell, G.H. & Wasserman, M.M. et al. (2005) *Plasmodium falciparum* myosins: transcription and translation during asexual parasite development. *Cell Motility and the Cytoskeleton*, 60(4), 200–213. Available from: <https://doi.org/10.1002/cm.20055>.
- Chenet, S.M., Akinyi Okoth, S., Huber, C.S., Chandrabose, J., Lucchi, N.W. & Talundzic, E. et al. (2016) Independent Emergence of the *Plasmodium falciparum* Kelch Propeller Domain Mutant Allele C580Y in Guyana. *The Journal of Infectious Diseases*, 213(9), 1472–1475. Available from: <https://doi.org/10.1093/infdis/jiv752>.
- Cheney, R.E., O'Shea, M.K., Heuser, J.E., Coelho, M.V., Wolenski, J.S. & Espreafico, E.M. et al. (1993) Brain myosin-V is a two-headed unconventional myosin with motor activity. *Cell*, 75(1), 13–23. Available from: <https://pubmed.ncbi.nlm.nih.gov/8402892/>.
- Cheng, Q., Kyle, D.E. & Gatton, M.L. (2012) Artemisinin resistance in *Plasmodium falciparum*: A process linked to dormancy? *International Journal for Parasitology. Drugs and Drug Resistance*, 2, 249–255. Available from: <https://doi.org/10.1016/j.ijpddr.2012.01.001>.
- Ch'ng, J.-H., Kotturi, S.R., Chong, A.G.-L., Lear, M.J. & Tan, K.S.-W. (2010) A programmed cell death pathway in the malaria parasite *Plasmodium falciparum* has general features of mammalian apoptosis but is mediated by clan CA cysteine proteases. *Cell Death & Disease*, 1(2), e26. Available from: <https://doi.org/10.1038/cddis.2010.2>.
- Christopher V. Plowe (2001) Folate Antagonists and Mechanisms of Resistance. In: *Antimalarial Chemotherapy*. Humana Press, Totowa, NJ, pp. 173–190.
- Clerk, C.A., Bruce, J., Affipunguh, P.K., Mensah, N., Hodgson, A. & Greenwood, B. et al. (2008) A randomized, controlled trial of intermittent preventive treatment with sulfadoxine-pyrimethamine, amodiaquine, or the combination in pregnant women in Ghana. *The Journal of Infectious Diseases*, 198(8), 1202–1211. Available from: <https://doi.org/10.1086/591944>.
- Clyde, D.F. (1975) Immunization of man against *falciparum* and *vivax* malaria by use of attenuated sporozoites. *The American Journal of Tropical Medicine and Hygiene*, 24(3), 397–401. Available from: <https://doi.org/10.4269/ajtmh.1975.24.397>.

- Clyde, D.F., Most, H., McCarthy, V.C. & Vanderberg, J.P. (1973) Immunization of man against sporozite-induced falciparum malaria. *The American Journal of the Medical Sciences*, 266(3), 169–177. Available from: <https://doi.org/10.1097/0000441-197309000-00002>.
- Codd, A., Teuscher, F., Kyle, D.E., Cheng, Q. & Gatton, M.L. (2011) Artemisinin-induced parasite dormancy: a plausible mechanism for treatment failure. *Malaria Journal*, 10, 56. Available from: <https://doi.org/10.1186/1475-2875-10-56>.
- Cogswell, F.B. (1992) The hypnozoite and relapse in primate malaria. *Clinical Microbiology Reviews*, 5(1), 26–35. Available from: <https://doi.org/10.1128/CMR.5.1.26>.
- Cohen, J. (1996) Patent WO1998005355A1.
- Coleman, B.I., Skillman, K.M., Jiang, R.H.Y., Childs, L.M., Altenhofen, L.M. & Ganter, M. et al. (2014) A Plasmodium falciparum histone deacetylase regulates antigenic variation and gametocyte conversion. *Cell Host & Microbe*, 16(2), 177–186. Available from: <https://doi.org/10.1016/j.chom.2014.06.014>.
- Collins, W.E. (2012) Plasmodium knowlesi: a malaria parasite of monkeys and humans. *Annual Review of Entomology*, 57, 107–121. Available from: <https://doi.org/10.1146/annurev-ento-121510-133540>.
- Collins, W.E. & Jeffery, G.M. (2005) Plasmodium ovale: parasite and disease. *Clinical Microbiology Reviews*, 18(3), 570–581. Available from: <https://doi.org/10.1128/CMR.18.3.570-581.2005>.
- Collins, W.E. & Jeffery, G.M. (2007) Plasmodium malariae: parasite and disease. *Clinical Microbiology Reviews*, 20(4), 579–592. Available from: <https://doi.org/10.1128/CMR.00027-07>.
- Colluzzi (1999) *The clay feet of the malaria giant and its African roots: hypotheses and inferences about origin, spread and control of Plasmodium falciparum*.
- Coppée, R., Jeffares, D.C., Miteva, M.A., Sabbagh, A. & Clain, J. (2019) Comparative structural and evolutionary analyses predict functional sites in the artemisinin resistance malaria protein K13. *Scientific Reports*, 9(1), 10675. Available from: <https://doi.org/10.1038/s41598-019-47034-6>.
- Cowman, A.F. & Crabb, B.S. (2002) The Plasmodium falciparum genome—a blueprint for erythrocyte invasion. *Science (New York, N.Y.)*, 298(5591), 126–128. Available from: <https://doi.org/10.1126/science.1078169>.
- Cowman, A.F. & Crabb, B.S. (2006) Invasion of red blood cells by malaria parasites. *Cell*, 124(4), 755–766. Available from: <https://doi.org/10.1016/j.cell.2006.02.006>.
- Cowman, A.F., Healer, J., Marapana, D. & Marsh, K. (2016) Malaria: Biology and Disease. *Cell*, 167(3), 610–624. Available from: <https://doi.org/10.1016/j.cell.2016.07.055>.
- Cowman, A.F., Morry, M.J., Biggs, B.A., Cross, G.A. & Foote, S.J. (1988) Amino acid changes linked to pyrimethamine resistance in the dihydrofolate reductase-thymidylate synthase gene of Plasmodium falciparum. *Proceedings of the National Academy of Sciences of the United States of America*, 85(23), 9109–9113. Available from: <https://doi.org/10.1073/pnas.85.23.9109>.
- Cox, P.N. (2011) *Characterisation of the metacaspase gene family in Arabidopsis thaliana*.
- Craik, R. (1920) A NOTE ON THE ERYTHROCYTES IN MALARIA. *The Lancet*, 195(5047), 1110. Available from: [https://doi.org/10.1016/s0140-6736\(00\)92210-4](https://doi.org/10.1016/s0140-6736(00)92210-4).
- Culvenor, J.G., Day, K.P. & Anders, R.F. (1991) Plasmodium falciparum ring-infected erythrocyte surface antigen is released from merozoite dense granules after erythrocyte invasion. *Infection and Immunity*, 59(3), 1183–1187. Available from: <https://doi.org/10.1128/iai.59.3.1183-1187.1991>.
- Curtis, C.F., Jana-Kara, B. & Maxwell, C.A. (2003) Insecticide treated nets: impact on vector populations and relevance of initial intensity of transmission and pyrethroid resistance. *Journal of Vector Borne Diseases*, 40(1-2), 1–8. Available from: <https://pubmed.ncbi.nlm.nih.gov/15119065/>.
- Curtis, C.F., Maxwell, C.A., Magesa, S.M., Rwegoshora, R.T. & Wilkes, T.J. (2006) Insecticide-Treated Bed-Nets for Malaria Mosquito Control. *Journal of the American Mosquito Control Association*, 22(3), 501–506. Available from: [https://doi.org/10.2987/8756-971X\(2006\)22\[501:IBFMMC\]2.0.CO;2](https://doi.org/10.2987/8756-971X(2006)22[501:IBFMMC]2.0.CO;2).

- Curtis, J., Duraisingh, M.T. & Warhurst, D.C. (1998) In vivo selection for a specific genotype of dihydropteroate synthetase of *Plasmodium falciparum* by pyrimethamine-sulfadoxine but not chlorproguanil-dapsone treatment. *The Journal of Infectious Diseases*, 177(5), 1429–1433. Available from: <https://doi.org/10.1086/517831>.
- Cyrklaff, M., Sanchez, C.P., Kilian, N., Bisseye, C., Simporé, J. & Frischknecht, F. et al. (2011) Hemoglobins S and C interfere with actin remodeling in *Plasmodium falciparum*-infected erythrocytes. *Science (New York, N.Y.)*, 334(6060), 1283–1286. Available from: <https://doi.org/10.1126/science.1213775>.
- Dame, J.B., Williams, J.L., McCutchan, T.F., Weber, J.L., Wirtz, R.A. & Hockmeyer, W.T. et al. (1984) Structure of the gene encoding the immunodominant surface antigen on the sporozoite of the human malaria parasite *Plasmodium falciparum*. *Science (New York, N.Y.)*, 225(4662), 593–599. Available from: <https://doi.org/10.1126/science.6204383>.
- Danilewsky (1885) *Zur parasitologie des blutes*.
- Dattoo, M.S., Natama, M.H., Somé, A., Traoré, O., Rouamba, T. & Bellamy, D. et al. (2021) Efficacy of a low-dose candidate malaria vaccine, R21 in adjuvant Matrix-M, with seasonal administration to children in Burkina Faso: a randomised controlled trial. *The Lancet*, 397(10287), 1809–1818. Available from: [https://doi.org/10.1016/S0140-6736\(21\)00943-0](https://doi.org/10.1016/S0140-6736(21)00943-0).
- Demas, A.R., Sharma, A.I., Wong, W., Early, A.M., Redmond, S. & Bopp, S. et al. (2018) Mutations in *Plasmodium falciparum* actin-binding protein coronin confer reduced artemisinin susceptibility. *Proceedings of the National Academy of Sciences of the United States of America*, 115(50), 12799–12804. Available from: <https://doi.org/10.1073/pnas.1812317115>.
- Dembélé, L., Franetich, J.-F., Lorthois, A., Gego, A., Zeeman, A.-M. & Kocken, C.H.M. et al. (2014) Persistence and activation of malaria hypnozoites in long-term primary hepatocyte cultures. *Nature Medicine*, 20(3), 307–312. Available from: <https://doi.org/10.1038/nm.3461>.
- Dhanoa, B.S., Cogliati, T., Satish, A.G., Bruford, E.A. & Friedman, J.S. (2013) Update on the Kelch-like (KLHL) gene family. *Human Genomics*, 7(1), 13. Available from: <https://doi.org/10.1186/1479-7364-7-13>.
- Dieckmann, A. & Jung, A. (1986) Mechanisms of sulfadoxine resistance in *Plasmodium falciparum*. *Molecular and Biochemical Parasitology*, 19(2), 143–147. Available from: [https://doi.org/10.1016/0166-6851\(86\)90119-2](https://doi.org/10.1016/0166-6851(86)90119-2).
- Divo, A.A., Geary, T.G., Jensen, J.B. & Ginsburg, H. (1985) The mitochondrion of *Plasmodium falciparum* visualized by rhodamine 123 fluorescence. *The Journal of Protozoology*, 32(3), 442–446. Available from: <https://doi.org/10.1111/j.1550-7408.1985.tb04041.x>.
- Djimé, A., Doumbo, O.K., Cortese, J.F., Kayentao, K., Doumbo, S. & Diourté, Y. et al. (2001) A molecular marker for chloroquine-resistant *falciparum* malaria. *The New England Journal of Medicine*, 344(4), 257–263. Available from: <https://doi.org/10.1056/NEJM200101253440403>.
- Dogovski, C., Xie, S.C., Burgio, G., Bridgford, J., Mok, S. & McCaw, J.M. et al. (2015) Targeting the cell stress response of *Plasmodium falciparum* to overcome artemisinin resistance. *PLoS Biology*, 13(4), e1002132. Available from: <https://doi.org/10.1371/journal.pbio.1002132>.
- Dondorp, A.M., Lee, S.J., Faiz, M.A., Mishra, S., Price, R. & Tjitra, E. et al. (2008) The relationship between age and the manifestations of and mortality associated with severe malaria. *Clinical Infectious Diseases : an Official Publication of the Infectious Diseases Society of America*, 47(2), 151–157. Available from: <https://doi.org/10.1086/589287>.
- Dondorp, A.M., Nosten, F., Yi, P., Das, D., Phyto, A.P. & Tarning, J. et al. (2009) Artemisinin resistance in *Plasmodium falciparum* malaria. *The New England Journal of Medicine*, 361(5), 455–467. Available from: <https://doi.org/10.1056/NEJMoa0808859>.

- Duffy, P.E. & Patrick Gorres, J. (2020) Malaria vaccines since 2000: progress, priorities, products. *Npj Vaccines*, 5(1), 1–9. Available from: <https://doi.org/10.1038/s41541-020-0196-3>.
- Duffy, P.E., Pimenta, P. & Kaslow, D.C. (1993) Pgs28 belongs to a family of epidermal growth factor-like antigens that are targets of malaria transmission-blocking antibodies. *Journal of Experimental Medicine*, 177(2), 505–510. Available from: <https://doi.org/10.1084/jem.177.2.505>.
- Eastman, R.T. & Fidock, D.A. (2009) Artemisinin-based combination therapies: a vital tool in efforts to eliminate malaria. *Nature Reviews Microbiology*, 7(12), 864–874. Available from: <https://doi.org/10.1038/nrmicro2239>.
- Eboumbou Moukoko, C.E., Huang, F., Nsango, S.E., Kojom Foko, L.P., Ebong, S.B. & Epee Eboumbou, P. et al. (2019) K-13 propeller gene polymorphisms isolated between 2014 and 2017 from Cameroonian Plasmodium falciparum malaria patients. *PLoS One*, 14(9), e0221895. Available from: <https://doi.org/10.1371/journal.pone.0221895>.
- Egan, T.J. (2008) Haemozoin formation. *Molecular and Biochemical Parasitology*, 157(2), 127–136. Available from: <https://doi.org/10.1016/j.molbiopara.2007.11.005>.
- Egan, T.J., Combrinck, J.M., Egan, J., Hearne, G.R., Marques, H.M. & Ntenti, S. et al. (2002) Fate of haem iron in the malaria parasite Plasmodium falciparum. *The Biochemical Journal*, 365(Pt 2), 343–347. Available from: <https://doi.org/10.1042/BJ20020793>.
- Eggleston, K.K., Duffin, K.L. & Goldberg, D.E. (1999) Identification and characterization of falcilysin, a metallopeptidase involved in hemoglobin catabolism within the malaria parasite Plasmodium falciparum. *The Journal of Biological Chemistry*, 274(45), 32411–32417. Available from: <https://doi.org/10.1074/jbc.274.45.32411>.
- Eichner, M., Diebner, H.H., Molineaux, L., Collins, W.E., Jeffery, G.M. & Dietz, K. (2001) Genesis, sequestration and survival of Plasmodium falciparum gametocytes: parameter estimates from fitting a model to malariatherapy data. *Transactions of the Royal Society of Tropical Medicine and Hygiene*, 95(5), 497–501. Available from: [https://doi.org/10.1016/s0035-9203\(01\)90016-1](https://doi.org/10.1016/s0035-9203(01)90016-1).
- Eksi, S., Morahan, B.J., Haile, Y., Furuya, T., Jiang, H. & Ali, O. et al. (2012) Plasmodium falciparum gametocyte development 1 (Pfgdv1) and gametocytogenesis early gene identification and commitment to sexual development. *PLoS Pathogens*, 8(10), e1002964. Available from: <https://doi.org/10.1371/journal.ppat.1002964>.
- Elford, B.C., Cowan, G.M. & Ferguson, D.J. (1995) Parasite-regulated membrane transport processes and metabolic control in malaria-infected erythrocytes. *The Biochemical Journal*, 308 (Pt 2)(Pt 2), 361–374. Available from: <https://doi.org/10.1042/bj3080361>.
- Elford, B.C., Cowan, G.M. & Ferguson, D.J. (1997) Transport and trafficking in malaria-infected erythrocytes. *Trends in microbiology*, 5(12), 463–465. Available from: [https://doi.org/10.1016/S0966-842X\(97\)01169-4](https://doi.org/10.1016/S0966-842X(97)01169-4).
- Elsworth, B., Matthews, K., Nie, C.Q., Kalanon, M., Charnaud, S.C. & Sanders, P.R. et al. (2014) PTEX is an essential nexus for protein export in malaria parasites. *Nature*, 511(7511), 587–591. Available from: <https://doi.org/10.1038/nature13555>.
- Enserink, M. (2010) Malaria's drug miracle in danger. *Science*, 328(5980), 844–846. Available from: <https://doi.org/10.1126/science.328.5980.844>.
- Etang, J., Fondjo, E., Chandre, F., Morlais, I., Brengues, C. & Nwane, P. et al. (2006) First report of knockdown mutations in the malaria vector Anopheles gambiae from Cameroon. *The American Journal of Tropical Medicine and Hygiene*, 74(5), 795–797. Available from: <https://pubmed.ncbi.nlm.nih.gov/16687682/>.

- F. Loeb, W. M. Clark, G. R. Coatney, L. T. Coggeshall, F. R. Dieuaide & A. R. Dochez et al. (1946) ACTIVITY of a new antimalarial agent, chloroquine (SN 7618). *Journal of the American Medical Association*, 130(16), 1069. Available from: <https://doi.org/10.1001/jama.1946.02870160015006>.
- Farfour, E., Charlotte, F., Settegrana, C., Miyara, M. & Buffet, P. (2012) The extravascular compartment of the bone marrow: a niche for Plasmodium falciparum gametocyte maturation? *Malaria Journal*, 11(1), 285. Available from: <https://doi.org/10.1186/1475-2875-11-285>.
- Fidock, D.A., Nomura, T., Talley, A.K., Cooper, R.A., Dzekunov, S.M. & Ferdig, M.T. et al. (2000) Mutations in the P. falciparum Digestive Vacuole Transmembrane Protein PfCRT and Evidence for Their Role in Chloroquine Resistance. *Molecular cell*, 6(4), 861–871. Available from: [https://doi.org/10.1016/s1097-2765\(05\)00077-8](https://doi.org/10.1016/s1097-2765(05)00077-8).
- Fidock, D.A. & Wellems, T.E. (1997) Transformation with human dihydrofolate reductase renders malaria parasites insensitive to WR99210 but does not affect the intrinsic activity of proguanil. *Proceedings of the National Academy of Sciences of the United States of America*, 94(20), 10931–10936. Available from: <https://doi.org/10.1073/pnas.94.20.10931>.
- Filarsky, M., Fraschka, S.A., Niederwieser, I., Brancucci, N.M.B., Carrington, E. & Carrió, E. et al. (2018) GDV1 induces sexual commitment of malaria parasites by antagonizing HP1-dependent gene silencing. *Science (New York, N.Y.)*, 359(6381), 1259–1263. Available from: <https://doi.org/10.1126/science.aan6042>.
- Flammersfeld, A., Lang, C., Flieger, A. & Pradel, G. (2018) Phospholipases during membrane dynamics in malaria parasites. *International Journal of Medical Microbiology : IJMM*, 308(1), 129–141. Available from: <https://doi.org/10.1016/j.ijmm.2017.09.015>.
- Flegg, J.A., Guerin, P.J., White, N.J. & Stepniewska, K. (2011) Standardizing the measurement of parasite clearance in falciparum malaria: the parasite clearance estimator. *Malaria Journal*, 10, 339. Available from: <https://doi.org/10.1186/1475-2875-10-339>.
- Foth, B.J., Goedecke, M.C. & Soldati, D. (2006) New insights into myosin evolution and classification. *Proceedings of the National Academy of Sciences of the United States of America*, 103(10), 3681–3686. Available from: <https://doi.org/10.1073/pnas.0506307103>.
- Foth, B.J., Zhang, N., Chaal, B.K., Sze, S.K., Preiser, P.R. & Bozdech, Z. (2011) Quantitative time-course profiling of parasite and host cell proteins in the human malaria parasite Plasmodium falciparum. *Molecular & Cellular Proteomics : MCP*, 10(8), M110.006411. Available from: <https://doi.org/10.1074/mcp.M110.006411>.
- Fowkes, F.J.I., Boeuf, P. & Beeson, J.G. (2016) Immunity to malaria in an era of declining malaria transmission. *Parasitology*, 143(2), 139–153. Available from: <https://doi.org/10.1017/S0031182015001249>.
- Franchini (1927) *Su di un plasmodio pigmentato di una scimmia*.
- Francis, S.E., Sullivan, D.J. & Goldberg, D.E. (1997) Hemoglobin metabolism in the malaria parasite Plasmodium falciparum. *Annual Review of Microbiology*, 51, 97–123. Available from: <https://doi.org/10.1146/annurev.micro.51.1.97>.
- Frevert, U., Usynin, I., Baer, K. & Klotz, C. (2006) Nomadic or sessile: can Kupffer cells function as portals for malaria sporozoites to the liver? *Cellular Microbiology*, 8(10), 1537–1546. Available from: <https://doi.org/10.1111/j.1462-5822.2006.00777.x>.
- Fry, M. & Pudney, M. (1992) Site of action of the antimalarial hydroxynaphthoquinone, 2-[trans-4-(4'-chlorophenyl) cyclohexyl]-3- hydroxy-1,4-naphthoquinone (566C80). *Biochemical pharmacology*, 43(7), 1545–1553. Available from: [https://doi.org/10.1016/0006-2952\(92\)90213-3](https://doi.org/10.1016/0006-2952(92)90213-3).

- Furukawa, M., He, Y.J., Borchers, C. & Xiong, Y. (2003) Targeting of protein ubiquitination by BTB-Cullin 3-Roc1 ubiquitin ligases. *Nature Cell Biology*, 5(11), 1001–1007. Available from: <https://doi.org/10.1038/ncb1056>.
- Gallup, J.L. & Sachs, J.D. (2001) The economic burden of malaria. *The American Journal of Tropical Medicine and Hygiene*, 64(1-2 Suppl), 85–96. Available from: <https://doi.org/10.4269/ajtmh.2001.64.85>.
- Garnham, P., Bird, R., Baker, J. & Bray, R. (1961) Electron microscope studies of motile stages of malaria parasites II. The fine structure of the sporozoite of *Laverania* (= *Plasmodium*) *falcipara*. *Transactions of the Royal Society of Tropical Medicine and Hygiene*, 55(1), 98–102. Available from: [https://doi.org/10.1016/0035-9203\(61\)90046-3](https://doi.org/10.1016/0035-9203(61)90046-3).
- Garoff, H. & Ansorge, W. (1981) Improvements of DNA sequencing gels. *Analytical Biochemistry*, 115(2), 450–457. Available from: [https://doi.org/10.1016/0003-2697\(81\)90031-2](https://doi.org/10.1016/0003-2697(81)90031-2).
- Gautret, P. & Motard, A. (1999) Periodic infectivity of *Plasmodium* gametocytes to the vector. A review. *Parasite (Paris, France)*, 6(2), 103–111. Available from: <https://doi.org/10.1051/parasite/1999062103>.
- Gething, P.W., Elyazar, I.R.F., Moyes, C.L., Smith, D.L., Battle, K.E. & Guerra, C.A. et al. (2012) A long neglected world malaria map: *Plasmodium vivax* endemicity in 2010. *PLoS Neglected Tropical Diseases*, 6(9), e1814. Available from: <https://doi.org/10.1371/journal.pntd.0001814>.
- Giao, P.T., Binh, T.Q., Kager, P.A., Long, H.P., van Thang, N. & van Nam, N. et al. (2001) Artemisinin for treatment of uncomplicated *falciparum* malaria: is there a place for monotherapy? *The American Journal of Tropical Medicine and Hygiene*, 65(6), 690–695. Available from: <https://doi.org/10.4269/ajtmh.2001.65.690>.
- Gibson, D.G., Young, L., Chuang, R.-Y., Venter, J.C., Hutchison, C.A. & Smith, H.O. (2009) Enzymatic assembly of DNA molecules up to several hundred kilobases. *Nature Methods*, 6(5), 343–345. Available from: <https://doi.org/10.1038/nmeth.1318>.
- Gilberger, T.-W., Thompson, J.K., Reed, M.B., Good, R.T. & Cowman, A.F. (2003) The cytoplasmic domain of the *Plasmodium falciparum* ligand EBA-175 is essential for invasion but not protein trafficking. *The Journal of Cell Biology*, 162(2), 317–327. Available from: <https://doi.org/10.1083/jcb.200301046>.
- Gilles, H. (1993) *Bruce-Chwatt's essential malariology.*, 3rd edition. E. Arnold Distributed in the Americas by Little Brown: London, Boston, Boston.
- Gilson, P.R. & Crabb, B.S. (2009) Morphology and kinetics of the three distinct phases of red blood cell invasion by *Plasmodium falciparum* merozoites. *International Journal for Parasitology*, 39(1), 91–96. Available from: <https://doi.org/10.1016/j.ijpara.2008.09.007>.
- Ginsburg, H. (1990) Some reflections concerning host erythrocyte-malarial parasite interrelationships. *Blood Cells*, 16(2-3), 225–235. Available from: <https://pubmed.ncbi.nlm.nih.gov/2257312/>.
- Glunt, K.D., Abílio, A.P., Bassat, Q., Bulo, H., Gilbert, A.E. & Huijben, S. et al. (2015) Long-lasting insecticidal nets no longer effectively kill the highly resistant *Anopheles funestus* of southern Mozambique. *Malaria Journal*, 14, 298. Available from: <https://doi.org/10.1186/s12936-015-0807-z>.
- Gluzman, I.Y., Francis, S.E., Oksman, A., Smith, C.E., Duffin, K.L. & Goldberg, D.E. (1994) Order and specificity of the *Plasmodium falciparum* hemoglobin degradation pathway. *The Journal of Clinical Investigation*, 93(4), 1602–1608. Available from: <https://doi.org/10.1172/JCI117140>.
- Goel, N., Dhiman, K., Kalidas, N., Mukhopadhyay, A., Ashish & Bhattacharjee, S. (2021) *Plasmodium falciparum* Kelch13 and its artemisinin-resistant mutants assemble as hexamers in solution: a SAXS data driven shape restoration study. *BioRxiv*, 2021.02.07.430181. Available from: <https://doi.org/10.1101/2021.02.07.430181>.
- Goldberg, D.E. (1993) Hemoglobin degradation in *Plasmodium*-infected red blood cells. *Seminars in Cell Biology*, 4(5), 355–361. Available from: <https://doi.org/10.1006/scel.1993.1042>.

- Goldberg, D.E. (2005) Hemoglobin degradation. *Current Topics in Microbiology and Immunology*, 295, 275–291. Available from: [https://doi.org/10.1007/3-540-29088-5\\_11](https://doi.org/10.1007/3-540-29088-5_11).
- Goldberg, D.E. (2013) Complex nature of malaria parasite hemoglobin degradation corrected. *Proceedings of the National Academy of Sciences*, 110(14), 5283–5284. Available from: <https://doi.org/10.1073/pnas.1303299110>.
- Goldberg, D.E., Slater, A.F., Cerami, A. & Henderson, G.B. (1990) Hemoglobin degradation in the malaria parasite *Plasmodium falciparum*: an ordered process in a unique organelle. *Proceedings of the National Academy of Sciences of the United States of America*, 87(8), 2931–2935. Available from: <https://doi.org/10.1073/pnas.87.8.2931>.
- Gosling, R.D., Gesase, S., Mosha, J.F., Carneiro, I., Hashim, R. & Lemnge, M. et al. (2009) Protective efficacy and safety of three antimalarial regimens for intermittent preventive treatment for malaria in infants: a randomised, double-blind, placebo-controlled trial. *The Lancet*, 374(9700), 1521–1532. Available from: [https://doi.org/10.1016/S0140-6736\(09\)60997-1](https://doi.org/10.1016/S0140-6736(09)60997-1).
- Götte, M. (2012) The distinct contributions of fitness and genetic barrier to the development of antiviral drug resistance. *Current Opinion in Virology*, 2(5), 644–650. Available from: <https://doi.org/10.1016/j.coviro.2012.08.004>.
- Gould, S.B., Tham, W.-H., Cowman, A.F., McFadden, G.I. & Waller, R.F. (2008) Alveolins, a new family of cortical proteins that define the protist infrakingdom Alveolata. *Molecular Biology and Evolution*, 25(6), 1219–1230. Available from: <https://doi.org/10.1093/molbev/msn070>.
- Greenwood, B. (2010) Anti-malarial drugs and the prevention of malaria in the population of malaria endemic areas. *Malaria Journal*, 9 Suppl 3(Suppl 3), S2. Available from: <https://doi.org/10.1186/1475-2875-9-S3-S2>.
- Greenwood, B.M., Fidock, D.A., Kyle, D.E., Kappe, S.H.I., Alonso, P.L. & Collins, F.H. et al. (2008) Malaria: progress, perils, and prospects for eradication. *The Journal of Clinical Investigation*, 118(4), 1266–1276. Available from: <https://doi.org/10.1172/JCI33996>.
- Grotendorst, C.A., Kumar, N., Carter, R. & Kaushal, D.C. (1984) A surface protein expressed during the transformation of zygotes of *Plasmodium gallinaceum* is a target of transmission-blocking antibodies. *Infection and Immunity*, 45(3), 775–777. Available from: <https://doi.org/10.1128/iai.45.3.775-777.1984>.
- Grüring, C., Heiber, A., Kruse, F., Ungefehr, J., Gilberger, T.-W. & Spielmann, T. (2011) Development and host cell modifications of *Plasmodium falciparum* blood stages in four dimensions. *Nature Communications*, 2, 165. Available from: <https://doi.org/10.1038/ncomms1169>.
- Grützke, J., Rindte, K., Goosmann, C., Silvie, O., Rauch, C. & Heuer, D. et al. (2014) The spatiotemporal dynamics and membranous features of the *Plasmodium* liver stage tubovesicular network. *Traffic (Copenhagen, Denmark)*, 15(4), 362–382. Available from: <https://doi.org/10.1111/tra.12151>.
- Guerra, C.A., Gikandi, P.W., Tatem, A.J., Noor, A.M., Smith, D.L. & Hay, S.I. et al. (2008) The limits and intensity of *Plasmodium falciparum* transmission: implications for malaria control and elimination worldwide. *PLoS Medicine*, 5(2), e38. Available from: <https://doi.org/10.1371/journal.pmed.0050038>.
- Gwadz, R.W. (1976) Successful immunization against the sexual stages of *Plasmodium gallinaceum*. *Science (New York, N.Y.)*, 193(4258), 1150–1151. Available from: <https://doi.org/10.1126/science.959832>.
- Haase, S. & Koning-Ward, T.F. de (2010) New insights into protein export in malaria parasites. *Cellular Microbiology*, 12(5), 580–587. Available from: <https://doi.org/10.1111/j.1462-5822.2010.01455.x>.
- Hamusse, S.D., Balcha, T.T. & Belachew, T. (2012) The impact of indoor residual spraying on malaria incidence in East Shoa Zone, Ethiopia. *Global Health Action*, 5, 11619. Available from: <https://doi.org/10.3402/gha.v5i0.11619>.

- Hanahan, D. (1983) Studies on transformation of *Escherichia coli* with plasmids. *Journal of Molecular Biology*, 166(4), 557–580. Available from: [https://doi.org/10.1016/S0022-2836\(83\)80284-8](https://doi.org/10.1016/S0022-2836(83)80284-8).
- Hanssen, E., Sougrat, R., Frankland, S., Deed, S., Klonis, N. & Lippincott-Schwartz, J. et al. (2008) Electron tomography of the Maurer's cleft organelles of *Plasmodium falciparum*-infected erythrocytes reveals novel structural features. *Molecular Microbiology*, 67(4), 703–718. Available from: <https://doi.org/10.1111/j.1365-2958.2007.06063.x>.
- Hargreaves, K., Hunt, R.H., Brooke, B.D., Mthembu, J., Weeto, M.M. & Awolola, T.S. et al. (2003) *Anopheles arabiensis* and *An. quadriannulatus* resistance to DDT in South Africa. *Medical and Veterinary Entomology*, 17(4), 417–422. Available from: <https://doi.org/10.1111/j.1365-2915.2003.00460.x>.
- Hargreaves, K., Koekemoer, L.L., Brooke, B.D., Hunt, R.H., Mthembu, J. & Coetzee, M. (2000) *Anopheles funestus* resistant to pyrethroid insecticides in South Africa. *Medical and Veterinary Entomology*, 14(2), 181–189. Available from: <https://doi.org/10.1046/j.1365-2915.2000.00234.x>.
- Hartgers, F.C. & Yazdanbakhsh, M. (2006) Co-infection of helminths and malaria: modulation of the immune responses to malaria. *Parasite Immunology*, 28(10), 497–506. Available from: <https://doi.org/10.1111/j.1365-3024.2006.00901.x>.
- Hartman, M.A. & Spudich, J.A. (2012) The myosin superfamily at a glance. *Journal of Cell Science*, 125(Pt 7), 1627–1632. Available from: <https://doi.org/10.1242/jcs.094300>.
- Haruki, H., Nishikawa, J. & Laemmli, U.K. (2008) The anchor-away technique: rapid, conditional establishment of yeast mutant phenotypes. *Molecular Cell*, 31(6), 925–932. Available from: <https://doi.org/10.1016/j.molcel.2008.07.020>.
- Hasson, T. (2003) Myosin VI: two distinct roles in endocytosis. *Journal of Cell Science*, 116(Pt 17), 3453–3461. Available from: <https://doi.org/10.1242/jcs.00669>.
- Hawking, F., Wilson, M.E. & Gammage, K. (1971) Evidence for cyclic development and short-lived maturity in the gametocytes of *Plasmodium falciparum*. *Transactions of the Royal Society of Tropical Medicine and Hygiene*, 65(5), 549–559. Available from: [https://doi.org/10.1016/0035-9203\(71\)90036-8](https://doi.org/10.1016/0035-9203(71)90036-8).
- HEGNER, R. (1938) RELATIVE FREQUENCY OF RING-STAGE PLASMODIA IN RETICULOCYTES AND MATURE ERYTHROCYTES IN MAN AND MONKEY. *American Journal of Epidemiology*, 27(3), 690–718. Available from: <https://doi.org/10.1093/oxfordjournals.aje.a118422>.
- Heiber, A., Kruse, F., Pick, C., Grüring, C., Flemming, S. & Oberli, A. et al. (2013) Identification of new PNEPs indicates a substantial non-PEXEL exportome and underpins common features in *Plasmodium falciparum* protein export. *PLoS Pathogens*, 9(8), e1003546. Available from: <https://doi.org/10.1371/journal.ppat.1003546>.
- Heintzelman, M.B. (2004) Actin and myosin in *Gregarina polymorpha*. *Cell Motility and the Cytoskeleton*, 58(2), 83–95. Available from: <https://doi.org/10.1002/cm.10178>.
- Heintzelman, M.B. & Schwartzman, J.D. (1997) A novel class of unconventional myosins from *Toxoplasma gondii*. *Journal of Molecular Biology*, 271(1), 139–146. Available from: <https://doi.org/10.1006/jmbi.1997.1167>.
- Heintzelman, M.B. & Schwartzman, J.D. (2001) Myosin Diversity in Apicomplexa. *The Journal of parasitology*, 87(2), 429–432. Available from: [https://doi.org/10.1645/0022-3395\(2001\)087\[0429:MDIA\]2.0.CO;2](https://doi.org/10.1645/0022-3395(2001)087[0429:MDIA]2.0.CO;2).
- Helms, M.J., Ambit, A., Appleton, P., Tetley, L., Coombs, G.H. & Mottram, J.C. (2006) Bloodstream form *Trypanosoma brucei* depend upon multiple metacaspases associated with RAB11-positive endosomes. *Journal of Cell Science*, 119(Pt 6), 1105–1117. Available from: <https://doi.org/10.1242/jcs.02809>.
- Henrici, R.C. & Sutherland, C.J. (2018) Alternative pathway to reduced artemisinin susceptibility in *Plasmodium falciparum*. *Proceedings of the National Academy of Sciences*, 115(50), 12556–12558. Available from: <https://doi.org/10.1073/pnas.1818287115>.

- Henrici, R.C., van Schalkwyk, D.A. & Sutherland, C.J. (2019) Modification of pfap2 $\mu$  and pfubp1 Markedly Reduces Ring-Stage Susceptibility of Plasmodium falciparum to Artemisinin In Vitro. *Antimicrobial Agents and Chemotherapy*, 64(1). Available from: <https://doi.org/10.1128/AAC.01542-19>.
- Henriques, G., Hallett, R.L., Beshir, K.B., Gadalla, N.B., Johnson, R.E. & Burrow, R. et al. (2014) Directional selection at the pfmdr1, pfcr1, pfubp1, and pfap2mu loci of Plasmodium falciparum in Kenyan children treated with ACT. *The Journal of Infectious Diseases*, 210(12), 2001–2008. Available from: <https://doi.org/10.1093/infdis/jiu358>.
- Henriques, G., Martinelli, A., Rodrigues, L., Modrzynska, K., Fawcett, R. & Houston, D.R. et al. (2013) Artemisinin resistance in rodent malaria--mutation in the AP2 adaptor  $\mu$ -chain suggests involvement of endocytosis and membrane protein trafficking. *Malaria Journal*, 12, 118. Available from: <https://doi.org/10.1186/1475-2875-12-118>.
- Henriques, G., van Schalkwyk, D.A., Burrow, R., Warhurst, D.C., Thompson, E. & Baker, D.A. et al. (2015) The Mu subunit of Plasmodium falciparum clathrin-associated adaptor protein 2 modulates in vitro parasite response to artemisinin and quinine. *Antimicrobial Agents and Chemotherapy*, 59(5), 2540–2547. Available from: <https://doi.org/10.1128/AAC.04067-14>.
- Hettmann, C., Herm, A., Geiter, A., Frank, B., Schwarz, E. & Soldati, T. et al. (2000) A dibasic motif in the tail of a class XIV apicomplexan myosin is an essential determinant of plasma membrane localization. *Molecular Biology of the Cell*, 11(4), 1385–1400. Available from: <https://doi.org/10.1091/mbc.11.4.1385>.
- Hien, T.T., Thuy-Nhien, N.T., Phu, N.H., Boni, M.F., Thanh, N.V. & Nha-Ca, N.T. et al. (2012) In vivo susceptibility of Plasmodium falciparum to artesunate in Binh Phuoc Province, Vietnam. *Malaria Journal*, 11(1), 355. Available from: <https://doi.org/10.1186/1475-2875-11-355>.
- Hiller, N.L., Bhattacharjee, S., van Ooij, C., Liolios, K., Harrison, T. & Lopez-Estraño, C. et al. (2004) A host-targeting signal in virulence proteins reveals a secretome in malarial infection. *Science (New York, N.Y.)*, 306(5703), 1934–1937. Available from: <https://doi.org/10.1126/science.1102737>.
- Hogan, B., Eibach, D., Krumkamp, R., Sarpong, N., Dekker, D. & Kreuels, B. et al. (2018) Malaria Coinfections in Febrile Pediatric Inpatients: A Hospital-Based Study From Ghana. *Clinical Infectious Diseases : an Official Publication of the Infectious Diseases Society of America*, 66(12), 1838–1845. Available from: <https://doi.org/10.1093/cid/cix1120>.
- Høgh, B., Clarke, P.D., Camus, D., Nothdurft, H.D., Overbosch, D. & Günther, M. et al. (2000) Atovaquone-proguanil versus chloroquine-proguanil for malaria prophylaxis in non-immune travellers: a randomised, double-blind study. *The Lancet*, 356(9245), 1888–1894. Available from: [https://doi.org/10.1016/s0140-6736\(00\)03260-8](https://doi.org/10.1016/s0140-6736(00)03260-8).
- Hopkins, J., Fowler, R., Krishna, S., Wilson, I., Mitchell, G. & Bannister, L. (1999) The Plastid in Plasmodium falciparum Asexual Blood Stages: a Three-Dimensional Ultrastructural Analysis. *Protist*, 150(3), 283–295. Available from: [https://doi.org/10.1016/S1434-4610\(99\)70030-1](https://doi.org/10.1016/S1434-4610(99)70030-1).
- Hoshen, M.B., Heinrich, R., Stein, W.D. & Ginsburg, H. (2000) Mathematical modelling of the within-host dynamics of Plasmodium falciparum. *Parasitology*, 121 (Pt 3), 227–235. Available from: <https://doi.org/10.1017/s0031182099006368>.
- Hott, A., Tucker, M.S., Casandra, D., Sparks, K. & Kyle, D.E. (2015) Fitness of artemisinin-resistant Plasmodium falciparum in vitro. *The Journal of Antimicrobial Chemotherapy*, 70(10), 2787–2796. Available from: <https://doi.org/10.1093/jac/dkv199>.
- Hunt, P., Afonso, A., Creasey, A., Culleton, R., Sidhu, A.B.S. & Logan, J. et al. (2007) Gene encoding a deubiquitinating enzyme is mutated in artesunate- and chloroquine-resistant rodent malaria parasites. *Molecular Microbiology*, 65(1), 27–40. Available from: <https://doi.org/10.1111/j.1365-2958.2007.05753.x>.

- Hunt, P., Martinelli, A., Modrzynska, K., Borges, S., Creasey, A. & Rodrigues, L. et al. (2010a) Experimental evolution, genetic analysis and genome re-sequencing reveal the mutation conferring artemisinin resistance in an isogenic lineage of malaria parasites. *BMC Genomics*, 11, 499. Available from: <https://doi.org/10.1186/1471-2164-11-499>.
- Hunt, P., Martinelli, A., Modrzynska, K., Borges, S., Creasey, A. & Rodrigues, L. et al. (2010b) Experimental evolution, genetic analysis and genome re-sequencing reveal the mutation conferring artemisinin resistance in an isogenic lineage of malaria parasites. *BMC Genomics*, 11(1), 499. Available from: <https://doi.org/10.1186/1471-2164-11-499>.
- Imwong, M., Suwannasin, K., Kunasol, C., Sutawong, K., Mayxay, M. & Rekol, H. et al. (2017) The spread of artemisinin-resistant *Plasmodium falciparum* in the Greater Mekong subregion: a molecular epidemiology observational study. *The Lancet Infectious Diseases*, 17(5), 491–497. Available from: [https://doi.org/10.1016/S1473-3099\(17\)30048-8](https://doi.org/10.1016/S1473-3099(17)30048-8).
- Ismail, H.M., Barton, V., Phanchana, M., Charoensutthivarakul, S., Wong, M.H.L. & Hemingway, J. et al. (2016) Artemisinin activity-based probes identify multiple molecular targets within the asexual stage of the malaria parasites *Plasmodium falciparum* 3D7. *Proceedings of the National Academy of Sciences*, 113(8), 2080–2085. Available from: <https://doi.org/10.1073/pnas.1600459113>.
- Jacot, D., Daher, W. & Soldati-Favre, D. (2013) Toxoplasma gondii myosin F, an essential motor for centrosomes positioning and apicoplast inheritance. *The EMBO Journal*, 32(12), 1702–1716. Available from: <https://doi.org/10.1038/emboj.2013.113>.
- Jeffries, T.R., Dove, S.K., Michell, R.H. & Parker, P.J. (2004) PtdIns-specific MPR pathway association of a novel WD40 repeat protein, WIPI49. *Molecular Biology of the Cell*, 15(6), 2652–2663. Available from: <https://doi.org/10.1091/mbc.e03-10-0732>.
- Jiang, D.Q., Tempel, W., Loppnau, P., Graslund, S., He, H. & Ravichandran, M. et al. (2015) *Crystal Structure Analysis of Kelch protein from Plasmodium falciparum*.
- Joice, R., Nilsson, S.K., Montgomery, J., Dankwa, S., Egan, E. & Morahan, B. et al. (2014) *Plasmodium falciparum* transmission stages accumulate in the human bone marrow. *Science Translational Medicine*, 6(244), 244re5. Available from: <https://doi.org/10.1126/scitranslmed.3008882>.
- Jonscher, E., Flemming, S., Schmitt, M., Sabitzki, R., Reichard, N. & Birnbaum, J. et al. (2019) PfVPS45 Is Required for Host Cell Cytosol Uptake by Malaria Blood Stage Parasites. *Cell Host & Microbe*, 25(1), 166–173.e5. Available from: <https://doi.org/10.1016/j.chom.2018.11.010>.
- Josling, G.A. & Llinás, M. (2015) Sexual development in *Plasmodium* parasites: knowing when it's time to commit. *Nature Reviews Microbiology*, 13(9), 573–587. Available from: <https://doi.org/10.1038/nrmicro3519>.
- Juliano, J.J., Porter, K., Mwapasa, V., Sem, R., Rogers, W.O. & Ariey, F. et al. (2010) Exposing malaria in-host diversity and estimating population diversity by capture-recapture using massively parallel pyrosequencing. *Proceedings of the National Academy of Sciences*, 107(46), 20138–20143. Available from: <https://doi.org/10.1073/pnas.1007068107>.
- Kadlecova, Z., Spielman, S.J., Loerke, D., Mohanakrishnan, A., Reed, D.K. & Schmid, S.L. (2017) Regulation of clathrin-mediated endocytosis by hierarchical allosteric activation of AP2. *Journal of Cell Biology*, 216(1), 167–179. Available from: <https://doi.org/10.1083/jcb.201608071>.
- Kafsack, B.F.C., Rovira-Graells, N., Clark, T.G., Bancells, C., Crowley, V.M. & Campino, S.G. et al. (2014) A transcriptional switch underlies commitment to sexual development in malaria parasites. *Nature*, 507(7491), 248–252.
- Kaksonen, M. & Roux, A. (2018) Mechanisms of clathrin-mediated endocytosis. *Nature Reviews. Molecular Cell Biology*, 19(5), 313–326. Available from: <https://doi.org/10.1038/nrm.2017.132>.

- Kamau, E., Campino, S., Amenga-Etego, L., Drury, E., Ishengoma, D. & Johnson, K. et al. (2015) K13-propeller polymorphisms in *Plasmodium falciparum* parasites from sub-Saharan Africa. *The Journal of Infectious Diseases*, 211(8), 1352–1355. Available from: <https://doi.org/10.1093/infdis/jiu608>.
- Kamya, M.R., Yeka, A., Bukirwa, H., Lugemwa, M., Rwakimari, J.B. & Staedke, S.G. et al. (2007) Artemether-lumefantrine versus dihydroartemisinin-piperaquine for treatment of malaria: a randomized trial. *PLoS Clinical Trials*, 2(5), e20. Available from: <https://doi.org/10.1371/journal.pctr.0020020>.
- Kara, U.A., Stenzel, D.J., Ingram, L.T. & Kidson, C. (1988) The parasitophorous vacuole membrane of *Plasmodium falciparum*: demonstration of vesicle formation using an immunoprobe. *European Journal of Cell Biology*, 46(1), 9–17. Available from: <https://pubmed.ncbi.nlm.nih.gov/3294009/>.
- Kaviratne, M., Khan, S.M., Jarra, W. & Preiser, P.R. (2002) Small variant STEVOR antigen is uniquely located within Maurer's clefts in *Plasmodium falciparum*-infected red blood cells. *Eukaryotic Cell*, 1(6), 926–935. Available from: <https://doi.org/10.1128/EC.1.6.926-935.2002>.
- Kawamoto, F., Liu, Q., Ferreira, M.U. & Tantular, I.S. (1999) How Prevalant are *Plasmodium ovale* and *P. malariae* in East Asia? *Parasitology today (Personal ed.)*, 15(10), 422–426. Available from: [https://doi.org/10.1016/s0169-4758\(99\)01511-2](https://doi.org/10.1016/s0169-4758(99)01511-2).
- Kayiba, N.K., Yobi, D.M., Tshibangu-Kabamba, E., Tuan, V.P., Yamaoka, Y. & Devleeschauwer, B. et al. (2021) Spatial and molecular mapping of Pfk13 gene polymorphism in Africa in the era of emerging *Plasmodium falciparum* resistance to artemisinin: a systematic review. *The Lancet Infectious Diseases*, 21(4), e82–e92. Available from: [https://doi.org/10.1016/S1473-3099\(20\)30493-X](https://doi.org/10.1016/S1473-3099(20)30493-X).
- Keeley, A. & Soldati, D. (2004) The glideosome: a molecular machine powering motility and host-cell invasion by Apicomplexa. *Trends in Cell Biology*, 14(10), 528–532. Available from: <https://doi.org/10.1016/j.tcb.2004.08.002>.
- Kilejian, A. (1979) Characterization of a protein correlated with the production of knob-like protrusions on membranes of erythrocytes infected with *Plasmodium falciparum*. *Proceedings of the National Academy of Sciences of the United States of America*, 76(9), 4650–4653. Available from: <https://doi.org/10.1073/pnas.76.9.4650>.
- Kinga Modrzynska, K., Creasey, A., Loewe, L., Cezard, T., Trindade Borges, S. & Martinelli, A. et al. (2012) Quantitative genome re-sequencing defines multiple mutations conferring chloroquine resistance in rodent malaria. *BMC Genomics*, 13, 106. Available from: <https://doi.org/10.1186/1471-2164-13-106>.
- Klemba, M., Gluzman, I. & Goldberg, D.E. (2004) A *Plasmodium falciparum* dipeptidyl aminopeptidase I participates in vacuolar hemoglobin degradation. *The Journal of Biological Chemistry*, 279(41), 43000–43007. Available from: <https://doi.org/10.1074/jbc.M408123200>.
- Klemenčič, M. & Funk, C. (2018a) Structural and functional diversity of caspase homologues in non-metazoan organisms. *Protoplasma*, 255(1), 387–397. Available from: <https://doi.org/10.1007/s00709-017-1145-5>.
- Klemenčič, M. & Funk, C. (2018b) Type III metacaspases: calcium-dependent activity proposes new function for the p10 domain. *New Phytologist*, 218(3), 1179–1191. Available from: <https://doi.org/10.1111/nph.14660>.
- Klonis, N., Creek, D.J. & Tilley, L. (2013) Iron and heme metabolism in *Plasmodium falciparum* and the mechanism of action of artemisinins. *Current Opinion in Microbiology*, 16(6), 722–727. Available from: <https://doi.org/10.1016/j.mib.2013.07.005>.
- Klonis, N., Crespo-Ortiz, M.P., Bottova, I., Abu-Bakar, N., Kenny, S. & Rosenthal, P.J. et al. (2011) Artemisinin activity against *Plasmodium falciparum* requires hemoglobin uptake and digestion. *Proceedings of the National Academy of Sciences*, 108(28), 11405–11410. Available from: <https://doi.org/10.1073/pnas.1104063108>.

- Knowles, R. & Gupta, B.M.D. (1932) A Study of Monkey-Malaria, and Its Experimental Transmission to Man. *The Indian Medical Gazette*, 67(6), 301–320.
- Koning-Ward, T.F. de, Dixon, M.W.A., Tilley, L. & Gilson, P.R. (2016) Plasmodium species: master renovators of their host cells. *Nature Reviews. Microbiology*, 14(8), 494–507. Available from: <https://doi.org/10.1038/nrmicro.2016.79>.
- Koning-Ward, T.F. de, Gilson, P.R., Boddey, J.A., Rug, M., Smith, B.J. & Papenfuss, A.T. et al. (2009) A newly discovered protein export machine in malaria parasites. *Nature*, 459(7249), 945–949. Available from: <https://doi.org/10.1038/nature08104>.
- Korenromp, E.L., Williams, B.G., Vlas, S.J. de, Gouws, E., Gilks, C.F. & Ghys, P.D. et al. (2005) Malaria attributable to the HIV-1 epidemic, sub-Saharan Africa. *Emerging Infectious Diseases*, 11(9), 1410–1419. Available from: <https://doi.org/10.3201/eid1109.050337>.
- Kriek, N., Tilley, L., Horrocks, P., Pinches, R., Elford, B.C. & Ferguson, D.J.P. et al. (2003) Characterization of the pathway for transport of the cytoadherence-mediating protein, PfEMP1, to the host cell surface in malaria parasite-infected erythrocytes. *Molecular Microbiology*, 50(4), 1215–1227. Available from: <https://doi.org/10.1046/j.1365-2958.2003.03784.x>.
- Krishnan, A. & Soldati-Favre, D. (2021) Amino Acid Metabolism in Apicomplexan Parasites. *Metabolites*, 11(2). Available from: <https://doi.org/10.3390/metabo11020061>.
- Krugliak, M., Zhang, J. & Ginsburg, H. (2002) Intraerythrocytic Plasmodium falciparum utilizes only a fraction of the amino acids derived from the digestion of host cell cytosol for the biosynthesis of its proteins. *Molecular and Biochemical Parasitology*, 119(2), 249–256. Available from: [https://doi.org/10.1016/s0166-6851\(01\)00427-3](https://doi.org/10.1016/s0166-6851(01)00427-3).
- Kyaw, M.P., Nyunt, M.H., Chit, K., Aye, M.M., Aye, K.H. & Lindegardh, N. et al. (2013) Reduced susceptibility of Plasmodium falciparum to artesunate in southern Myanmar. *PLoS One*, 8(3), e57689. Available from: <https://doi.org/10.1371/journal.pone.0057689>.
- Kyle, D.E. (1996) *Postantibiotic effect of quinine and dihydroartemisinin derivatives on Plasmodium falciparum in vitro: implications for a mechanism of recrudescence.*
- Kyle, D.E., Teja-Isavadharm, P., Li, Q. & Leo, K. (1998) Pharmacokinetics and pharmacodynamics of qinghaosu derivatives: how do they impact on the choice of drug and the dosage regimens? *Medecine Tropicale : Revue Du Corps De Sante Colonial*, 58(3 Suppl), 38–44. Available from: <https://pubmed.ncbi.nlm.nih.gov/10212896/>.
- LaCrue, A.N., Scheel, M., Kennedy, K., Kumar, N. & Kyle, D.E. (2011) Effects of artesunate on parasite recrudescence and dormancy in the rodent malaria model Plasmodium vinckei. *PLoS One*, 6(10), e26689. Available from: <https://doi.org/10.1371/journal.pone.0026689>.
- Ladda, R., Arnold, J. & Martin, D. (1966) Electron microscopy of Plasmodium falciparum 1. The structure of trophozoites in erythrocytes of human volunteers. *Transactions of the Royal Society of Tropical Medicine and Hygiene*, 60(3), 369–375. Available from: [https://doi.org/10.1016/0035-9203\(66\)90302-6](https://doi.org/10.1016/0035-9203(66)90302-6).
- Laemmli, U.K. (1970) Cleavage of structural proteins during the assembly of the head of bacteriophage T4. *Nature*, 227(5259), 680–685. Available from: <https://doi.org/10.1038/227680a0>.
- LaFleur, M.D., Kumamoto, C.A. & Lewis, K. (2006) Candida albicans biofilms produce antifungal-tolerant persister cells. *Antimicrobial Agents and Chemotherapy*, 50(11), 3839–3846. Available from: <https://doi.org/10.1128/AAC.00684-06>.
- Lamarque, M., Besteiro, S., Papoin, J., Roques, M., Vulliez-Le Normand, B. & Morlon-Guyot, J. et al. (2011) The RON2-AMA1 interaction is a critical step in moving junction-dependent invasion by apicomplexan parasites. *PLoS Pathogens*, 7(2), e1001276. Available from: <https://doi.org/10.1371/journal.ppat.1001276>.

- Lambros, C. & Vanderberg, J.P. (1979) Synchronization of *Plasmodium falciparum* erythrocytic stages in culture. *The Journal of Parasitology*, 65(3), 418–420. Available from: <https://pubmed.ncbi.nlm.nih.gov/383936/>.
- Langreth, S.G., Jensen, J.B., Reese, R.T. & Trager, W. (1978) Fine structure of human malaria in vitro. *The Journal of Protozoology*, 25(4), 443–452. Available from: <https://doi.org/10.1111/j.1550-7408.1978.tb04167.x>.
- Lanzer, M., Wickert, H., Krohne, G., Vincensini, L. & Braun Breton, C. (2006) Maurer's clefts: a novel multi-functional organelle in the cytoplasm of *Plasmodium falciparum*-infected erythrocytes. *International Journal for Parasitology*, 36(1), 23–36. Available from: <https://doi.org/10.1016/j.ijpara.2005.10.001>.
- Lauer, S.A., Rathod, P.K., Ghori, N. & Haldar, K. (1997) A membrane network for nutrient import in red cells infected with the malaria parasite. *Science (New York, N.Y.)*, 276(5315), 1122–1125. Available from: <https://doi.org/10.1126/science.276.5315.1122>.
- Lazarus, M.D., Schneider, T.G. & Taraschi, T.F. (2008) A new model for hemoglobin ingestion and transport by the human malaria parasite *Plasmodium falciparum*. *Journal of Cell Science*, 121(11), 1937–1949. Available from: <https://doi.org/10.1242/jcs.023150>.
- Lebrun, M., Michelin, A., El Hajj, H., Poncet, J., Bradley, P.J. & Vial, H. et al. (2005) The roptry neck protein RON4 re-localizes at the moving junction during *Toxoplasma gondii* invasion. *Cellular Microbiology*, 7(12), 1823–1833. Available from: <https://doi.org/10.1111/j.1462-5822.2005.00646.x>.
- Lee, R.E.C., Brunette, S., Puente, L.G. & Megeney, L.A. (2010) Metacaspase Yca1 is required for clearance of insoluble protein aggregates. *Proceedings of the National Academy of Sciences*, 107(30), 13348–13353. Available from: <https://doi.org/10.1073/pnas.1006610107>.
- Lee, R.S., Waters, A.P. & Brewer, J.M. (2018) A cryptic cycle in haematopoietic niches promotes initiation of malaria transmission and evasion of chemotherapy. *Nature Communications*, 9(1), 1689. Available from: <https://doi.org/10.1038/s41467-018-04108-9>.
- Lee, Y.-R., Yuan, W.-C., Ho, H.-C., Chen, C.-H., Shih, H.-M. & Chen, R.-H. (2010) The Cullin 3 substrate adaptor KLHL20 mediates DAPK ubiquitination to control interferon responses. *The EMBO Journal*, 29(10), 1748–1761. Available from: <https://doi.org/10.1038/emboj.2010.62>.
- Lew, A.E., Dluzewski, A.R., Johnson, A.M. & Pinder, J.C. (2002) Myosins of *Babesia bovis*: molecular characterisation, erythrocyte invasion, and phylogeny. *Cell Motility and the Cytoskeleton*, 52(4), 202–220. Available from: <https://doi.org/10.1002/cm.10046>.
- Lew, V.L., Macdonald, L., Ginsburg, H., Krugliak, M. & Tiffert, T. (2004) Excess haemoglobin digestion by malaria parasites: a strategy to prevent premature host cell lysis. *Blood Cells, Molecules & Diseases*, 32(3), 353–359. Available from: <https://doi.org/10.1016/j.bcmed.2004.01.006>.
- Lew, V.L., Tiffert, T. & Ginsburg, H. (2003) Excess hemoglobin digestion and the osmotic stability of *Plasmodium falciparum*-infected red blood cells. *Blood*, 101(10), 4189–4194. Available from: <https://doi.org/10.1182/blood-2002-08-2654>.
- Li, G.-Q., Guo, X.-B., Fu, L.-C., Jian, H.-X. & Wang, X.-H. (1994) Clinical trials of artemisinin and its derivatives in the treatment of malaria in China. *Transactions of the Royal Society of Tropical Medicine and Hygiene*, 88, 5–6. Available from: [https://doi.org/10.1016/0035-9203\(94\)90460-x](https://doi.org/10.1016/0035-9203(94)90460-x).
- Li, J. & Zhou, B. (2010) Biological actions of artemisinin: insights from medicinal chemistry studies. *Molecules (Basel, Switzerland)*, 15(3), 1378–1397. Available from: <https://doi.org/10.3390/molecules15031378>.
- Liu, J., Istvan, E.S., Gluzman, I.Y., Gross, J. & Goldberg, D.E. (2006) *Plasmodium falciparum* ensures its amino acid supply with multiple acquisition pathways and redundant proteolytic enzyme systems. *Proceedings of the National Academy of Sciences of the United States of America*, 103(23), 8840–8845. Available from: <https://doi.org/10.1073/pnas.0601876103>.

- Looareesuwan, S., Viravan, C., Vanijanonta, S., Wilairatana, P., Suntharasamai, P. & Charoenlarp, P. et al. (1992) Randomised trial of artesunate and mefloquine alone and in sequence for acute uncomplicated falciparum malaria. *The Lancet*, 339(8797), 821–824. Available from: [https://doi.org/10.1016/0140-6736\(92\)90276-9](https://doi.org/10.1016/0140-6736(92)90276-9).
- Lumb, V., Das, M.K., Singh, N., Dev, V., Khan, W. & Sharma, Y.D. (2011) Multiple origins of Plasmodium falciparum dihydropteroate synthetase mutant alleles associated with sulfadoxine resistance in India. *Antimicrobial Agents and Chemotherapy*, 55(6), 2813–2817. Available from: <https://doi.org/10.1128/AAC.01151-10>.
- Maccallum, W.G. (1897) ON THE FLAGELLATED FORM OF THE MALARIAL PARASITE. *The Lancet*, 150(3872), 1240–1241. Available from: [https://doi.org/10.1016/S0140-6736\(00\)46556-6](https://doi.org/10.1016/S0140-6736(00)46556-6).
- Maier, A.G., Cooke, B.M., Cowman, A.F. & Tilley, L. (2009) Malaria parasite proteins that remodel the host erythrocyte. *Nature Reviews Microbiology*, 7(5), 341–354. Available from: <https://doi.org/10.1038/nrmicro2110>.
- Maier, A.G., Rug, M., O'Neill, M.T., Brown, M., Chakravorty, S. & Szestak, T. et al. (2008) Exported proteins required for virulence and rigidity of Plasmodium falciparum-infected human erythrocytes. *Cell*, 134(1), 48–61. Available from: <https://doi.org/10.1016/j.cell.2008.04.051>.
- Maiga, A.W., Fofana, B., Sagara, I., Dembele, D., Dara, A. & Traore, O.B. et al. (2012) No evidence of delayed parasite clearance after oral artesunate treatment of uncomplicated falciparum malaria in Mali. *The American Journal of Tropical Medicine and Hygiene*, 87(1), 23–28. Available from: <https://doi.org/10.4269/ajtmh.2012.12-0058>.
- MalariaGEN, Ahouidi, A., Ali, M., Almagro-Garcia, J., Amambua-Ngwa, A. & Amaratunga, C. et al. (2021) An open dataset of Plasmodium falciparum genome variation in 7,000 worldwide samples. *Wellcome Open Research*, 6, 42. Available from: <https://doi.org/10.12688/wellcomeopenres.16168.2>.
- MalariaGEN Plasmodium falciparum Community Project (2016) Genomic epidemiology of artemisinin resistant malaria. *eLife Sciences Publications, Ltd*, 2016. Available from: <https://elifesciences.org/articles/08714> [Accessed 15 July 2021].
- Malleret, B., Claser, C., Ong, A.S.M., Suwanarusk, R., Sriprawat, K. & Howland, S.W. et al. (2011) A rapid and robust tri-color flow cytometry assay for monitoring malaria parasite development. *Scientific Reports*, 1, 118. Available from: <https://doi.org/10.1038/srep00118>.
- Malleret, B., Li, A., Zhang, R., Tan, K.S.W., Suwanarusk, R. & Claser, C. et al. (2015) Plasmodium vivax: restricted tropism and rapid remodeling of CD71-positive reticulocytes. *Blood*, 125(8), 1314–1324. Available from: <https://doi.org/10.1182/blood-2014-08-596015>.
- MAP (2021) *The Malaria Atlas Project*. Available from: <https://malariaatlas.org/> [Accessed 14 July 2021].
- Marti, M., Good, R.T., Rug, M., Knuepfer, E. & Cowman, A.F. (2004) Targeting malaria virulence and remodeling proteins to the host erythrocyte. *Science (New York, N.Y.)*, 306(5703), 1930–1933. Available from: <https://doi.org/10.1126/science.11102452>.
- Martin, R.E. & Kirk, K. (2004) The malaria parasite's chloroquine resistance transporter is a member of the drug/metabolite transporter superfamily. *Molecular Biology and Evolution*, 21(10), 1938–1949. Available from: <https://doi.org/10.1093/molbev/msh205>.
- Martine Zilversmit & Daniel L. Hartl (2014) Evolutionary History and Population Genetics of Human Malaria Parasites. In: *Molecular Approaches to Malaria*. John Wiley & Sons, Ltd, pp. 95–109.
- Mathieu, L.C., Cox, H., Early, A.M., Mok, S., Lazrek, Y. & Paquet, J. et al. (2020) Local emergence in Amazonia of Plasmodium falciparum k13 C580Y mutants associated with in vitro artemisinin resistance. *eLife Sciences Publications, Ltd*, 12 May. Available from: <https://elifesciences.org/articles/51015> [Accessed 16 July 2021].

- Matthews, K., Kalanon, M., Chisholm, S.A., Sturm, A., Goodman, C.D. & Dixon, M.W.A. et al. (2013) The Plasmodium translocon of exported proteins (PTEX) component thioredoxin-2 is important for maintaining normal blood-stage growth. *Molecular Microbiology*, 89(6), 1167–1186. Available from: <https://doi.org/10.1111/mmi.12334>.
- Matuschewski, K., Mota, M.M., Pinder, J.C., Nussenzweig, V. & Kappe, S.H. (2001) Identification of the class XIV myosins Pb-MyoA and Py-MyoA and expression in Plasmodium sporozoites. *Molecular and Biochemical Parasitology*, 112(1), 157–161. Available from: [https://doi.org/10.1016/s0166-6851\(00\)00360-1](https://doi.org/10.1016/s0166-6851(00)00360-1).
- Matz, J.M., Matuschewski, K. & Kooij, T.W.A. (2013) Two putative protein export regulators promote Plasmodium blood stage development in vivo. *Molecular and Biochemical Parasitology*, 191(1), 44–52. Available from: <https://doi.org/10.1016/j.molbiopara.2013.09.003>.
- Mbengue, A., Bhattacharjee, S., Pandharkar, T., Liu, H., Estiu, G. & Stahelin, R.V. et al. (2015) A molecular mechanism of artemisinin resistance in Plasmodium falciparum malaria. *Nature*, 520(7549), 683–687. Available from: <https://doi.org/10.1038/nature14412>.
- McFadden, G.I., Reith, M.E., Munholland, J. & Lang-Unnasch, N. (1996) Plastid in human parasites. *Nature*, 381(6582), 482. Available from: <https://doi.org/10.1038/381482a0>.
- McHugh, E., Batinovic, S., Hanssen, E., McMillan, P.J., Kenny, S. & Griffin, M.D.W. et al. (2015) A repeat sequence domain of the ring-exported protein-1 of Plasmodium falciparum controls export machinery architecture and virulence protein trafficking. *Molecular Microbiology*, 98(6), 1101–1114. Available from: <https://doi.org/10.1111/mmi.13201>.
- McIntosh, H.M. & Olliaro, P. (2000) Artemisinin derivatives for treating uncomplicated malaria. *The Cochrane Database of Systematic Reviews*, (2), CD000256. Available from: <https://doi.org/10.1002/14651858.CD000256>.
- McIntosh, M. (2001) Two classes of plant-like vacuolar-type H<sup>+</sup>-pyrophosphatases in malaria parasites. *Molecular and Biochemical Parasitology*, 114(2), 183–195. Available from: [https://doi.org/10.1016/s0166-6851\(01\)00251-1](https://doi.org/10.1016/s0166-6851(01)00251-1).
- McMahon, H.T. & Boucrot, E. (2011) Molecular mechanism and physiological functions of clathrin-mediated endocytosis. *Nature Reviews. Molecular Cell Biology*, 12(8), 517–533. Available from: <https://doi.org/10.1038/nrm3151>.
- McMillan, P.J., Millet, C., Batinovic, S., Maiorca, M., Hanssen, E. & Kenny, S. et al. (2013) Spatial and temporal mapping of the PfEMP1 export pathway in Plasmodium falciparum. *Cellular Microbiology*, 15(8), 1401–1418. Available from: <https://doi.org/10.1111/cmi.12125>.
- Medica, D.L. & Sinnis, P. (2005) Quantitative dynamics of Plasmodium yoelii sporozoite transmission by infected anopheline mosquitoes. *Infection and Immunity*, 73(7), 4363–4369. Available from: <https://doi.org/10.1128/IAI.73.7.4363-4369.2005>.
- Meis, J.F., Jap, P.H., Verhave, J.P. & Meuwissen, J.H. (1983) Ultrastructural studies of a vesicle system associated with endoplasmic reticulum in exo-erythrocytic forms of Plasmodium berghei. *The Journal of Protozoology*, 30(1), 111–114. Available from: <https://doi.org/10.1111/j.1550-7408.1983.tb01042.x>.
- Ménard, D., Khim, N., Beghain, J., Adegnika, A.A., Shafiu-Alam, M. & Amodu, O. et al. (2016) A Worldwide Map of Plasmodium falciparum K13-Propeller Polymorphisms. *The New England Journal of Medicine*, 374(25), 2453–2464. Available from: <https://doi.org/10.1056/NEJMoa1513137>.
- Meshnick, S.R. (2002) Artemisinin: mechanisms of action, resistance and toxicity. *International journal for parasitology*, 32(13), 1655–1660. Available from: [https://doi.org/10.1016/s0020-7519\(02\)00194-7](https://doi.org/10.1016/s0020-7519(02)00194-7).

- Meshnick, S.R., Taylor, T.E. & Kamchonwongpaisan, S. (1996) Artemisinin and the antimalarial endoperoxides: from herbal remedy to targeted chemotherapy. *Microbiological Reviews*, 60(2), 301–315. Available from: <https://doi.org/10.1128/mr.60.2.301-315.1996>.
- Meslin, B., Barnadas, C., Boni, V., Latour, C., Monbrison, F. de & Kaiser, K. et al. (2007) Features of apoptosis in *Plasmodium falciparum* erythrocytic stage through a putative role of PfMCA1 metacaspase-like protein. *The Journal of Infectious Diseases*, 195(12), 1852–1859. Available from: <https://doi.org/10.1086/518253>.
- Meslin, B., Beavogui, A.H., Fasel, N. & Picot, S. (2011) *Plasmodium falciparum* metacaspase PfMCA-1 triggers a z-VAD-fmk inhibitable protease to promote cell death. *PloS One*, 6(8), e23867. Available from: <https://doi.org/10.1371/journal.pone.0023867>.
- Meslin, B., Zalila, H., Fasel, N., Picot, S. & Bienvenu, A.-L. (2011) Are protozoan metacaspases potential parasite killers? *Parasites & Vectors*, 4, 26. Available from: <https://doi.org/10.1186/1756-3305-4-26>.
- Metzger, W.G., Sulyok, Z., Theurer, A. & Köhler, C. (2020) Entwicklung von Impfstoffen gegen Malaria – aktueller Stand. *Bundesgesundheitsblatt - Gesundheitsforschung - Gesundheitsschutz*, 63(1), 45–55. Available from: <https://doi.org/10.1007/s00103-019-03070-1>.
- Meunier, B. & Robert, A. (2010) Heme as trigger and target for trioxane-containing antimalarial drugs. *Accounts of Chemical Research*, 43(11), 1444–1451. Available from: <https://doi.org/10.1021/ar100070k>.
- Miller, L.H., Baruch, D.I., Marsh, K. & Doumbo, O.K. (2002) The pathogenic basis of malaria. *Nature*, 415(6872), 673–679. Available from: <https://doi.org/10.1038/415673a>.
- Miotto, O., Almagro-Garcia, J., Manske, M., Maclinnis, B., Campino, S. & Rockett, K.A. et al. (2013) Multiple populations of artemisinin-resistant *Plasmodium falciparum* in Cambodia. *Nature Genetics*, 45(6), 648–655. Available from: <https://doi.org/10.1038/ng.2624>.
- Miotto, O., Amato, R., Ashley, E.A., Maclinnis, B., Almagro-Garcia, J. & Amaratunga, C. et al. (2015) Genetic architecture of artemisinin-resistant *Plasmodium falciparum*. *Nature Genetics*, 47(3), 226–234. Available from: <https://doi.org/10.1038/ng.3189>.
- Miotto, O., Sekihara, M., Tachibana, S.-I., Yamauchi, M., Pearson, R.D. & Amato, R. et al. (2020) Emergence of artemisinin-resistant *Plasmodium falciparum* with kelch13 C580Y mutations on the island of New Guinea. *PLoS Pathogens*, 16(12), e1009133. Available from: <https://doi.org/10.1371/journal.ppat.1009133>.
- Mita, T., Tachibana, S.-I., Hashimoto, M. & Hirai, M. (2016) *Plasmodium falciparum* kelch 13: a potential molecular marker for tackling artemisinin-resistant malaria parasites. *Expert Review of Anti-Infective Therapy*, 14(1), 125–135. Available from: <https://doi.org/10.1586/14787210.2016.1106938>.
- MMV Medicines for Malaria Venture (2021) *Medicines for Malaria Venture | Developing antimalarials to save lives*. Available from: <https://www.mmv.org/> [Accessed 15 July 2021].
- Mok, S., Ashley, E.A., Ferreira, P.E., Zhu, L., Lin, Z. & Yeo, T. et al. (2015) Drug resistance. Population transcriptomics of human malaria parasites reveals the mechanism of artemisinin resistance. *Science*, 347(6220), 431–435. Available from: <https://doi.org/10.1126/science.1260403>.
- Moon, R.W., Hall, J., Rangkuti, F., Ho, Y.S., Almond, N. & Mitchell, G.H. et al. (2013) Adaptation of the genetically tractable malaria pathogen *Plasmodium knowlesi* to continuous culture in human erythrocytes. *Proceedings of the National Academy of Sciences*, 110(2), 531–536. Available from: <https://doi.org/10.1073/pnas.1216457110>.
- Moore, R.B., Oborník, M., Janouskovec, J., Chrudimský, T., Vancová, M. & Green, D.H. et al. (2008) A photosynthetic alveolate closely related to apicomplexan parasites. *Nature*, 451(7181), 959–963. Available from: <https://doi.org/10.1038/nature06635>.

- Moorthy, V.S., Newman, R.D., Duclos, P., Okwo-Bele, J.M. & Smith, P.G. (2013) Assessment of the RTS,S/AS01 malaria vaccine. *The Lancet Infectious Diseases*, 13(4), 280–282. Available from: [https://doi.org/10.1016/S1473-3099\(13\)70047-1](https://doi.org/10.1016/S1473-3099(13)70047-1).
- Morrison, D.A. (2008) Prospects for elucidating the phylogeny of the Apicomplexa. *Parasite (Paris, France)*, 15(3), 191–196. Available from: <https://doi.org/10.1051/parasite/2008153191>.
- Moser, K.A., Madebe, R.A., Aydemir, O., Chiduo, M.G., Mandara, C.I. & Rumisha, S.F. et al. (2021) Describing the current status of Plasmodium falciparum population structure and drug resistance within mainland Tanzania using molecular inversion probes. *Molecular Ecology*, 30(1), 100–113. Available from: <https://doi.org/10.1111/mec.15706>.
- Mota, M.M., Pradel, G., Vanderberg, J.P., Hafalla, J.C., Frevert, U. & Nussenzweig, R.S. et al. (2001) Migration of Plasmodium sporozoites through cells before infection. *Science (New York, N.Y.)*, 291(5501), 141–144.
- Mugittu, K., Abdulla, S., Falk, N., Masanja, H., Felger, I. & Mshinda, H. et al. (2005) Efficacy of sulfadoxine-pyrimethamine in Tanzania after two years as first-line drug for uncomplicated malaria: assessment protocol and implication for treatment policy strategies. *Malaria Journal*, 4, 55. Available from: <https://doi.org/10.1186/1475-2875-4-55>.
- Mukherjee, A., Bopp, S., Magistrado, P., Wong, W., Daniels, R. & Demas, A. et al. (2017) Artemisinin resistance without pfcy10 mutations in Plasmodium falciparum isolates from Cambodia. *Malaria journal*, 16(1). Available from: <https://doi.org/10.1186/s12936-017-1845-5>.
- Mundwiler-Pachlatko, E. & Beck, H.-P. (2013) Maurer's clefts, the enigma of Plasmodium falciparum. *Proceedings of the National Academy of Sciences*, 110(50), 19987–19994. Available from: <https://doi.org/10.1073/pnas.1309247110>.
- Mutabingwa, T.K., Anthony, D., Heller, A., Hallett, R., Ahmed, J. & Drakeley, C. et al. (2005) Amodiaquine alone, amodiaquine+sulfadoxine-pyrimethamine, amodiaquine+artesunate, and artemether-lumefantrine for outpatient treatment of malaria in Tanzanian children: a four-arm randomised effectiveness trial. *The Lancet*, 365(9469), 1474–1480. Available from: [https://doi.org/10.1016/S0140-6736\(05\)66417-3](https://doi.org/10.1016/S0140-6736(05)66417-3).
- Mwangi, T.W., Bethony, J.M. & Brooker, S. (2006) Malaria and helminth interactions in humans: an epidemiological viewpoint. *Annals of Tropical Medicine and Parasitology*, 100(7), 551–570. Available from: <https://doi.org/10.1179/136485906X118468>.
- Nadal, E. de, Ammerer, G. & Posas, F. (2011) Controlling gene expression in response to stress. *Nature Reviews. Genetics*, 12(12), 833–845. Available from: <https://doi.org/10.1038/nrg3055>.
- Nair, S., Li, X., Arya, G.A., McDew-White, M., Ferrari, M. & Nosten, F. et al. (2018) Fitness Costs and the Rapid Spread of kelch13-C580Y Substitutions Conferring Artemisinin Resistance. *Antimicrobial Agents and Chemotherapy*, 62(9). Available from: <https://doi.org/10.1128/AAC.00605-18>.
- Nakazawa, S., Maoka, T., Uemura, H., Ito, Y. & Kanbara, H. (2002) Malaria parasites giving rise to recrudescence in vitro. *Antimicrobial Agents and Chemotherapy*, 46(4), 958–965. Available from: <https://doi.org/10.1128/AAC.46.4.958-965.2002>.
- Ndwiga, L., Kimenyi, K.M., Wamae, K., Osoti, V., Akinyi, M. & Omedo, I. et al. (2021) A review of the frequencies of Plasmodium falciparum Kelch 13 artemisinin resistance mutations in Africa. *International Journal for Parasitology. Drugs and Drug Resistance*, 16, 155–161. Available from: <https://doi.org/10.1016/j.ijpddr.2021.06.001>.
- Nguyen, D.S., Dao, B.H., Nguyen, P.D., Nguyen, V.H., Le, N.B. & Mai, V.S. et al. (1993) Treatment of malaria in Vietnam with oral artemisinin. *The American Journal of Tropical Medicine and Hygiene*, 48(3), 398–402. Available from: <https://pubmed.ncbi.nlm.nih.gov/8470777/>.

- Niaré, K., Paloque, L., Ménard, S., Tor, P., Ramadani, A.P. & Augereau, J.-M. et al. (2018) Multiple Phenotypic and Genotypic Artemisinin Sensitivity Evaluation of Malian Plasmodium falciparum Isolates. *The American Journal of Tropical Medicine and Hygiene*, 98(4), 1123–1131. Available from: <https://doi.org/10.4269/ajtmh.17-0798>.
- Niz, M. de, Burda, P.-C., Kaiser, G., Del Portillo, H.A., Spielmann, T. & Frischknecht, F. et al. (2017) Progress in imaging methods: insights gained into Plasmodium biology. *Nature Reviews Microbiology*, 15(1), 37–54. Available from: <https://doi.org/10.1038/nrmicro.2016.158>.
- Niz, M. de, Meibalan, E., Mejia, P., Ma, S., Brancucci, N.M.B. & Agop-Nersesian, C. et al. (2018) Plasmodium gametocytes display homing and vascular transmigration in the host bone marrow. *Science Advances*, 4(5), eaat3775. Available from: <https://doi.org/10.1126/sciadv.aat3775>.
- NobelPrize.org (2015) *The Nobel Prize in Physiology or Medicine 2015*. Available from: <https://www.nobelprize.org/prizes/medicine/2015/summary/> [Accessed 15 July 2021].
- Noedl, H., Se, Y., Schaecher, K., Smith, B.L., Socheat, D. & Fukuda, M.M. (2008) Evidence of artemisinin-resistant malaria in western Cambodia. *The New England Journal of Medicine*, 359(24), 2619–2620. Available from: <https://doi.org/10.1056/NEJMc0805011>.
- Nyalwidhe, J. & Lingelbach, K. (2006) Proteases and chaperones are the most abundant proteins in the parasitophorous vacuole of Plasmodium falciparum-infected erythrocytes. *Proteomics*, 6(5), 1563–1573. Available from: <https://doi.org/10.1002/pmic.200500379>.
- Obaldia, N., Meibalan, E., Sa, J.M., Ma, S., Clark, M.A. & Mejia, P. et al. (2018) Bone Marrow Is a Major Parasite Reservoir in Plasmodium vivax Infection. *MBio*, 9(3). Available from: <https://doi.org/10.1128/mBio.00625-18>.
- Ocan, M., Akena, D., Nsohya, S., Kanya, M.R., Senono, R. & Kinengyere, A.A. et al. (2019) K13-propeller gene polymorphisms in Plasmodium falciparum parasite population in malaria affected countries: a systematic review of prevalence and risk factors. *Malaria Journal*, 18(1), 60. Available from: <https://doi.org/10.1186/s12936-019-2701-6>.
- Olliaro, P.L. & Goldberg, D.E. (1995) The Plasmodium digestive Vacuole: Metabolic Headquarters and Choice Drug Target. *Parasitology Today*, 11(8), 294–297. Available from: [https://doi.org/10.1016/0169-4758\(95\)80042-5](https://doi.org/10.1016/0169-4758(95)80042-5).
- Olshina, M.A., Angrisano, F., Marapana, D.S., Riglar, D.T., Bane, K. & Wong, W. et al. (2015) Plasmodium falciparum coronin organizes arrays of parallel actin filaments potentially guiding directional motility in invasive malaria parasites. *Malaria Journal*, 14, 280. Available from: <https://doi.org/10.1186/s12936-015-0801-5>.
- O'Neill, P.M., Barton, V.E. & Ward, S.A. (2010) The molecular mechanism of action of artemisinin—the debate continues. *Molecules (Basel, Switzerland)*, 15(3), 1705–1721. Available from: <https://doi.org/10.3390/molecules15031705>.
- Osborne, A.R., Speicher, K.D., Tamez, P.A., Bhattacharjee, S., Speicher, D.W. & Haldar, K. (2010) The host targeting motif in exported Plasmodium proteins is cleaved in the parasite endoplasmic reticulum. *Molecular and Biochemical Parasitology*, 171(1), 25–31. Available from: <https://doi.org/10.1016/j.molbiopara.2010.01.003>.
- Ouattara, A., Kone, A., Adams, M., Fofana, B., Maiga, A.W. & Hampton, S. et al. (2015) Polymorphisms in the K13-propeller gene in artemisinin-susceptible Plasmodium falciparum parasites from Bougoula-Hameau and Bandiagara, Mali. *The American Journal of Tropical Medicine and Hygiene*, 92(6), 1202–1206. Available from: <https://doi.org/10.4269/ajtmh.14-0605>.
- Pagola, S., Stephens, P.W., Bohle, D.S., Kosar, A.D. & Madsen, S.K. (2000) The structure of malaria pigment beta-haematin. *Nature*, 404(6775), 307–310. Available from: <https://doi.org/10.1038/35005132>.

- PATH's Malaria Vaccine Initiative (2015) *Malaria vaccine roadmap*. Available from: <https://www.malariavaccine.org/malaria-and-vaccines/malaria-vaccine-roadmap> [Accessed 15 July 2021].
- Payne, D. (1987) Spread of chloroquine resistance in *Plasmodium falciparum*. *Parasitology Today*, 3(8), 241–246. Available from: [https://doi.org/10.1016/0169-4758\(87\)90147-5](https://doi.org/10.1016/0169-4758(87)90147-5).
- Periz, J., Whitelaw, J., Harding, C., Gras, S., Mario Igor Del Rosario Minina & Latorre-barragan, F. et al. (2017) *Toxoplasma gondii* F-actin forms an extensive filamentous network required for material exchange and parasite maturation. *eLife Sciences Publications, Ltd*, 21 March. Available from: <https://elifesciences.org/articles/24119> [Accessed 16 July 2021].
- Phan, G.T., Vries, P.J. de, Tran, B.Q., Le, H.Q., Nguyen, N.V. & Nguyen, T.V. et al. (2002) Artemisinin or chloroquine for blood stage *Plasmodium vivax* malaria in Vietnam. *Tropical Medicine & International Health : TM & IH*, 7(10), 858–864. Available from: <https://doi.org/10.1046/j.1365-3156.2002.00948.x>.
- Phyo, A.P., Nkhoma, S., Stepniewska, K., Ashley, E.A., Nair, S. & McGready, R. et al. (2012) Emergence of artemisinin-resistant malaria on the western border of Thailand: a longitudinal study. *The Lancet*, 379(9830), 1960–1966. Available from: [https://doi.org/10.1016/S0140-6736\(12\)60484-X](https://doi.org/10.1016/S0140-6736(12)60484-X).
- Picot, S., Burnod, J., Bracchi, V., Chumpitazi, B. & Ambroise-Thomas, P. (1997) Apoptosis related to chloroquine sensitivity of the human malaria parasite *Plasmodium falciparum*. *Transactions of the Royal Society of Tropical Medicine and Hygiene*, 91(5), 590–591. Available from: [https://doi.org/10.1016/s0035-9203\(97\)90039-0](https://doi.org/10.1016/s0035-9203(97)90039-0).
- Picot, S., Olliaro, P., Monbrison, F. de, Bienvenu, A.-L., Price, R.N. & Ringwald, P. (2009) A systematic review and meta-analysis of evidence for correlation between molecular markers of parasite resistance and treatment outcome in *falciparum* malaria. *Malaria Journal*, 8, 89. Available from: <https://doi.org/10.1186/1475-2875-8-89>.
- Plewes, K., Leopold, S.J., Kingston, H.W.F. & Dondorp, A.M. (2019) Malaria: What's New in the Management of Malaria? *Infectious Disease Clinics of North America*, 33(1), 39–60. Available from: <https://doi.org/10.1016/j.idc.2018.10.002>.
- Poumerol, G. & Wilder-Smith, A. (2012) *International travel and health: Situation as on January 2012*. World Health Organization: Geneva.
- Pradel, G. & Frevert, U. (2001) Malaria sporozoites actively enter and pass through rat Kupffer cells prior to hepatocyte invasion. *Hepatology (Baltimore, Md.)*, 33(5), 1154–1165. Available from: <https://doi.org/10.1053/jhep.2001.24237>.
- Preiser, P., Kaviratne, M., Khan, S., Bannister, L. & Jarra, W. (2000) The apical organelles of malaria merozoites: host cell selection, invasion, host immunity and immune evasion. *Microbes and Infection*, 2(12), 1461–1477. Available from: [https://doi.org/10.1016/S1286-4579\(00\)01301-0](https://doi.org/10.1016/S1286-4579(00)01301-0).
- Proikas-Cezanne, T., Ruckerbauer, S., Stierhof, Y.-D., Berg, C. & Nordheim, A. (2007) Human WIPI-1 puncta-formation: a novel assay to assess mammalian autophagy. *FEBS Letters*, 581(18), 3396–3404. Available from: <https://doi.org/10.1016/j.febslet.2007.06.040>.
- Prudêncio, M., Rodriguez, A. & Mota, M.M. (2006) The silent path to thousands of merozoites: the *Plasmodium* liver stage. *Nature Reviews. Microbiology*, 4(11), 849–856. Available from: <https://doi.org/10.1038/nrmicro1529>.
- Przyborski, J.M., Miller, S.K., Pfahler, J.M., Henrich, P.P., Rohrbach, P. & Crabb, B.S. et al. (2005) Trafficking of STEVOR to the Maurer's clefts in *Plasmodium falciparum*-infected erythrocytes. *The EMBO Journal*, 24(13), 2306–2317. Available from: <https://doi.org/10.1038/sj.emboj.7600720>.
- Qinghaosu Antimalaria Coordinating Research Group (1979) Antimalaria studies on Qinghaosu. *Chinese Medical Journal*, 92(12), 811–816. Available from: <https://pubmed.ncbi.nlm.nih.gov/117984/>.

- Radloff, P., Philips, J., Nkeyi, M., Kremsner, P. & Hutchinson, D. (1996) Atovaquone and proguanil for *Plasmodium falciparum* malaria. *The Lancet*, 347(9014), 1511–1514. Available from: [https://doi.org/10.1016/S0140-6736\(96\)90671-6](https://doi.org/10.1016/S0140-6736(96)90671-6).
- Ralph, S.A., van Dooren, G.G., Waller, R.F., Crawford, M.J., Fraunholz, M.J. & Foth, B.J. et al. (2004) Tropical infectious diseases: metabolic maps and functions of the *Plasmodium falciparum* apicoplast. *Nature Reviews. Microbiology*, 2(3), 203–216. Available from: <https://doi.org/10.1038/nrmicro843>.
- Raposo, G., Cordonnier, M.N., Tenza, D., Menichi, B., Dürrbach, A. & Louvard, D. et al. (1999) Association of myosin I alpha with endosomes and lysosomes in mammalian cells. *Molecular Biology of the Cell*, 10(5), 1477–1494. Available from: <https://doi.org/10.1091/mbc.10.5.1477>.
- Rathore, S., Datta, G., Kaur, I., Malhotra, P. & Mohammed, A. (2015) Disruption of cellular homeostasis induces organelle stress and triggers apoptosis like cell-death pathways in malaria parasite. *Cell Death & Disease*, 6(7), e1803. Available from: <https://doi.org/10.1038/cddis.2015.142>.
- Rayner, J.C., Vargas-Serrato, E., Huber, C.S., Galinski, M.R. & Barnwell, J.W. (2001) A *Plasmodium falciparum* homologue of *Plasmodium vivax* reticulocyte binding protein (PvRBP1) defines a trypsin-resistant erythrocyte invasion pathway. *The Journal of Experimental Medicine*, 194(11), 1571–1581. Available from: <https://doi.org/10.1084/jem.194.11.1571>.
- Reed, M.B., Saliba, K.J., Caruana, S.R., Kirk, K. & Cowman, A.F. (2000) Pgh1 modulates sensitivity and resistance to multiple antimalarials in *Plasmodium falciparum*. *Nature*, 403(6772), 906–909. Available from: <https://doi.org/10.1038/35002615>.
- Richie, D.L., Miley, M.D., Bhabhra, R., Robson, G.D., Rhodes, J.C. & Askew, D.S. (2007) The *Aspergillus fumigatus* metacaspases CasA and CasB facilitate growth under conditions of endoplasmic reticulum stress. *Molecular Microbiology*, 63(2), 591–604. Available from: <https://doi.org/10.1111/j.1365-2958.2006.05534.x>.
- Richie, T.L., Billingsley, P.F., Sim, B.K.L., James, E.R., Chakravarty, S. & Epstein, J.E. et al. (2015) Progress with *Plasmodium falciparum* sporozoite (PfSPZ)-based malaria vaccines. *Vaccine*, 33(52), 7452–7461. Available from: <https://doi.org/10.1016/j.vaccine.2015.09.096>.
- Riglar, D.T., Richard, D., Wilson, D.W., Boyle, M.J., Dekiwadia, C. & Turnbull, L. et al. (2011) Super-resolution dissection of coordinated events during malaria parasite invasion of the human erythrocyte. *Cell Host & Microbe*, 9(1), 9–20. Available from: <https://doi.org/10.1016/j.chom.2010.12.003>.
- Robinson, M.S., Sahlender, D.A. & Foster, S.D. (2010) Rapid inactivation of proteins by rapamycin-induced rerouting to mitochondria. *Developmental Cell*, 18(2), 324–331. Available from: <https://doi.org/10.1016/j.devcel.2009.12.015>.
- Rocamora, F., Zhu, L., Liong, K.Y., Dondorp, A., Miotto, O. & Mok, S. et al. (2018) Oxidative stress and protein damage responses mediate artemisinin resistance in malaria parasites. *PLoS Pathogens*, 14(3), e1006930. Available from: <https://doi.org/10.1371/journal.ppat.1006930>.
- Rohrbach, P., Sanchez, C.P., Hayton, K., Friedrich, O., Patel, J. & Sidhu, A.B.S. et al. (2006) Genetic linkage of *pfmdr1* with food vacuolar solute import in *Plasmodium falciparum*. *The EMBO Journal*, 25(13), 3000–3011. Available from: <https://doi.org/10.1038/sj.emboj.7601203>.
- Rønn, A.M., Msangeni, H.A., Mhina, J., Wernsdorfer, W.H. & Bygbjerg, I.C. (1996) High level of resistance of *Plasmodium falciparum* to sulfadoxine-pyrimethamine in children in Tanzania. *Transactions of the Royal Society of Tropical Medicine and Hygiene*, 90(2), 179–181. Available from: [https://doi.org/10.1016/s0035-9203\(96\)90129-7](https://doi.org/10.1016/s0035-9203(96)90129-7).
- Roode, J.C. de, Culleton, R., Bell, A.S. & Read, A.F. (2004) Competitive release of drug resistance following drug treatment of mixed *Plasmodium chabaudi* infections. *Malaria Journal*, 3, 33. Available from: <https://doi.org/10.1186/1475-2875-3-33>.

- Roode, J.C. de, Read, A.F., Chan, B.H.K. & Mackinnon, M.J. (2003) Rodent malaria parasites suffer from the presence of conspecific clones in three-clone *Plasmodium chabaudi* infections. *Parasitology*, 127(Pt 5), 411–418. Available from: <https://doi.org/10.1017/s0031182003004001>.
- Roper, C., Pearce, R., Nair, S., Sharp, B., Nosten, F. & Anderson, T. (2004) Intercontinental spread of pyrimethamine-resistant malaria. *Science (New York, N.Y.)*, 305(5687), 1124. Available from: <https://doi.org/10.1126/science.1098876>.
- Rosenthal, P.J. (2013) The interplay between drug resistance and fitness in malaria parasites. *Molecular Microbiology*, 89(6), 1025–1038. Available from: <https://doi.org/10.1111/mmi.12349>.
- Ross, R. (1898) THE RÔLE OF THE MOSQUITO IN THE EVOLUTION OF THE MALARIAL PARASITE. *The Lancet*, 152(3912), 488–490. Available from: [https://doi.org/10.1016/S0140-6736\(01\)81400-8](https://doi.org/10.1016/S0140-6736(01)81400-8).
- RTS, S.C.T.P. (2014) Efficacy and safety of the RTS,S/AS01 malaria vaccine during 18 months after vaccination: a phase 3 randomized, controlled trial in children and young infants at 11 African sites. *PLoS Medicine*, 11(7), e1001685. Available from: <https://doi.org/10.1371/journal.pmed.1001685>.
- RTS, S.C.T.P. (2015) Efficacy and safety of RTS,S/AS01 malaria vaccine with or without a booster dose in infants and children in Africa: final results of a phase 3, individually randomised, controlled trial. *The Lancet*, 386(9988), 31–45. Available from: [https://doi.org/10.1016/S0140-6736\(15\)60721-8](https://doi.org/10.1016/S0140-6736(15)60721-8).
- Rudzinska, M.A., Trager, W. & Bray, R.S. (1965) Pinocytotic uptake and the digestion of hemoglobin in malaria parasites. *The Journal of Protozoology*, 12(4), 563–576. Available from: <https://doi.org/10.1111/j.1550-7408.1965.tb03256.x>.
- Rug, M., Prescott, S.W., Fernandez, K.M., Cooke, B.M. & Cowman, A.F. (2006) The role of KAHRP domains in knob formation and cytoadherence of *P. falciparum*-infected human erythrocytes. *Blood*, 108(1), 370–378. Available from: <https://doi.org/10.1182/blood-2005-11-4624>.
- Rump, A., Scholz, T., Thiel, C., Hartmann, F.K., Uta, P. & Hinrichs, M.H. et al. (2011) Myosin-1C associates with microtubules and stabilizes the mitotic spindle during cell division. *Journal of Cell Science*, 124(Pt 15), 2521–2528. Available from: <https://doi.org/10.1242/jcs.084335>.
- Russo, I., Babbitt, S., Muralidharan, V., Butler, T., Oksman, A. & Goldberg, D.E. (2010) Plasmeprin V licenses *Plasmodium* proteins for export into the host erythrocyte. *Nature*, 463(7281), 632–636. Available from: <https://doi.org/10.1038/nature08726>.
- Sachs, J. & Malaney, P. (2002) The economic and social burden of malaria. *Nature*, 415(6872), 680–685. Available from: <https://doi.org/10.1038/415680a>.
- Sagara, I., Beavogui, A.H., Zongo, I., Soulama, I., Borghini-Fuhrer, I. & Fofana, B. et al. (2018) Pyronaridine–artesunate or dihydroartemisinin–piperazine versus current first-line therapies for repeated treatment of uncomplicated malaria: a randomised, multicentre, open-label, longitudinal, controlled, phase 3b/4 trial. *The Lancet*, 391(10128), 1378–1390. Available from: [https://doi.org/10.1016/S0140-6736\(18\)30291-5](https://doi.org/10.1016/S0140-6736(18)30291-5).
- Salas-Cortes, L., Ye, F., Tenza, D., Wilhelm, C., Theos, A. & Louvard, D. et al. (2005) Myosin Ib modulates the morphology and the protein transport within multi-vesicular sorting endosomes. *Journal of Cell Science*, 118(Pt 20), 4823–4832. Available from: <https://doi.org/10.1242/jcs.02607>.
- Saliba, K.J., Allen, R.J.W., Zisis, S., Bray, P.G., Ward, S.A. & Kirk, K. (2003) Acidification of the malaria parasite's digestive vacuole by a H<sup>+</sup>-ATPase and a H<sup>+</sup>-pyrophosphatase. *The Journal of Biological Chemistry*, 278(8), 5605–5612. Available from: <https://doi.org/10.1074/jbc.M208648200>.
- Sam-Yellowe, T.Y. (1996) Rhoptry organelles of the apicomplexa: Their role in host cell invasion and intracellular survival. *Parasitology Today*, 12(8), 308–316. Available from: [https://doi.org/10.1016/0169-4758\(96\)10030-2](https://doi.org/10.1016/0169-4758(96)10030-2).

- Sam-Yellowe, T.Y., Shio, H. & Perkins, M.E. (1988) Secretion of Plasmodium falciparum rhostry protein into the plasma membrane of host erythrocytes. *Journal of Cell Biology*, 106(5), 1507–1513. Available from: <https://doi.org/10.1083/jcb.106.5.1507>.
- Sánchez-valdéz, F.J., Padilla, A., Wang, W., Orr, D. & Tarleton, R.L. (2018) Spontaneous dormancy protects Trypanosoma cruzi during extended drug exposure. *eLife Sciences Publications, Ltd*, 26 March. Available from: <https://elifesciences.org/articles/34039#references> [Accessed 17 July 2021].
- Sargeant, T.J., Marti, M., Caler, E., Carlton, J.M., Simpson, K. & Speed, T.P. et al. (2006) Lineage-specific expansion of proteins exported to erythrocytes in malaria parasites. *Genome Biology*, 7(2), R12. Available from: <https://doi.org/10.1186/gb-2006-7-2-r12>.
- Schofield, L. & Grau, G.E. (2005) Immunological processes in malaria pathogenesis. *Nature Reviews. Immunology*, 5(9), 722–735. Available from: <https://doi.org/10.1038/nri1686>.
- Schumacher, F.-R., Sorrell, F.J., Alessi, D.R., Bullock, A.N. & Kurz, T. (2014) Structural and biochemical characterization of the KLHL3-WNK kinase interaction important in blood pressure regulation. *Biochemical Journal*, 460(2), 237–246. Available from: <https://doi.org/10.1042/BJ20140153>.
- Seed, T.M., Sterling, C.R., Aikawa, M. & Rabbege, J. (1976) Plasmodium simium: Ultrastructure of erythrocytic phase. *Experimental parasitology*, 39(2), 262–276. Available from: [https://doi.org/10.1016/0014-4894\(76\)90126-0](https://doi.org/10.1016/0014-4894(76)90126-0).
- Sellers, J.R. (2000) Myosins: a diverse superfamily. *Biochimica et Biophysica Acta (BBA) - Molecular Cell Research*, 1496(1), 3–22. Available from: [https://doi.org/10.1016/s0167-4889\(00\)00005-7](https://doi.org/10.1016/s0167-4889(00)00005-7).
- Shafik, S.H., Cobbold, S.A., Barkat, K., Richards, S.N., Lancaster, N.S. & Llinás, M. et al. (2020) The natural function of the malaria parasite's chloroquine resistance transporter. *Nature Communications*, 11(1), 3922. Available from: <https://doi.org/10.1038/s41467-020-17781-6>.
- Sharma, A.I., Demas, A.R., Hartl, D.L. & Wirth, D.F. (2019) Reply to Velavan et al.: Polymorphisms of pfcoronin in natural populations: Implications for functional significance. *Proceedings of the National Academy of Sciences*, 116(26), 12613–12614. Available from: <https://doi.org/10.1073/pnas.1907920116>.
- Sharma, A.I., Shin, S.H., Bopp, S., Volkman, S.K., Hartl, D.L. & Wirth, D.F. (2020) Genetic background and PfKelch13 affect artemisinin susceptibility of PfCoronin mutants in Plasmodium falciparum. *PLoS Genetics*, 16(12), e1009266. Available from: <https://doi.org/10.1371/journal.pgen.1009266>.
- Sherling, E.S. & van Ooij, C. (2016) Host cell remodeling by pathogens: the exomembrane system in Plasmodium-infected erythrocytes. *FEMS Microbiology Reviews*, 40(5), 701–721. Available from: <https://doi.org/10.1093/femsre/fuw016>.
- Shi, X., Xiang, S., Cao, J., Zhu, H., Yang, B. & He, Q. et al. (2019) Kelch-like proteins: Physiological functions and relationships with diseases. *Pharmacological Research*, 148, 104404. Available from: <https://doi.org/10.1016/j.phrs.2019.104404>.
- Shrestha, A. & Megeney, L.A. (2012) The non-death role of metacaspase proteases. *Frontiers in Oncology*, 2, 78. Available from: <https://doi.org/10.3389/fonc.2012.00078>.
- Sibley, C.H., Hyde, J.E., Sims, P.F., Plowe, C.V., Kublin, J.G. & Mberu, E.K. et al. (2001) Pyrimethamine–sulfadoxine resistance in Plasmodium falciparum: what next? *Trends in parasitology*, 17(12), 582–588. Available from: [https://doi.org/10.1016/s1471-4922\(01\)02085-2](https://doi.org/10.1016/s1471-4922(01)02085-2).
- Siddiqui, G., Srivastava, A., Russell, A.S. & Creek, D.J. (2017) Multi-omics Based Identification of Specific Biochemical Changes Associated With PfKelch13-Mutant Artemisinin-Resistant Plasmodium falciparum. *The Journal of Infectious Diseases*, 215(9), 1435–1444. Available from: <https://doi.org/10.1093/infdis/jix156>.

- Siddiqui, W.A. (1977) An effective immunization of experimental monkeys against a human malaria parasite, *Plasmodium falciparum*. *Science (New York, N.Y.)*, 197(4301), 388–389. Available from: <https://doi.org/10.1126/science.406671>.
- Sigrist, C.J.A., Cerutti, L., Castro, E. de, Langendijk-Genevaux, P.S., Bulliard, V. & Bairoch, A. et al. (2010) PROSITE, a protein domain database for functional characterization and annotation. *Nucleic Acids Research*, 38(Database issue), D161-6. Available from: <https://doi.org/10.1093/nar/gkp885>.
- Simwela, N.V., Hughes, K.R., Roberts, A.B., Rennie, M.T., Barrett, M.P. & Waters, A.P. (2020) Experimentally Engineered Mutations in a Ubiquitin Hydrolase, UBP-1, Modulate In Vivo Susceptibility to Artemisinin and Chloroquine in *Plasmodium berghei*. *Antimicrobial Agents and Chemotherapy*, 64(7). Available from: <https://doi.org/10.1128/AAC.02484-19>.
- Sinden, R.E. (1974) Excystment by sporozoites of malaria parasites. *Nature*, 252(5481), 314. Available from: <https://doi.org/10.1038/252314a0>.
- Sinden, R.E. (1983) Sexual Development of Malarial Parasites. *Advances in parasitology*, 22, 153–216. Available from: [https://doi.org/10.1016/s0065-308x\(08\)60462-5](https://doi.org/10.1016/s0065-308x(08)60462-5).
- Sinden, R.E. (2015) The cell biology of malaria infection of mosquito: advances and opportunities. *Cellular Microbiology*, 17(4), 451–466. Available from: <https://doi.org/10.1111/cmi.12413>.
- Sinden, R.E., Canning, E.U., Bray, R.S. & Smalley, M.E. (1978) Gametocyte and gamete development in *Plasmodium falciparum*. *Proceedings of the Royal Society of London. Series B, Biological Sciences*, 201(1145), 375–399. Available from: <https://doi.org/10.1098/rspb.1978.0051>.
- Sinden, R.E., Canning, E.U. & Spain, B. (1976) Gametogenesis and fertilization in *Plasmodium yoelii nigeriensis*: a transmission electron microscope study. *Proceedings of the Royal Society of London. Series B, Biological Sciences*, 193(1110), 55–76. Available from: <https://doi.org/10.1098/rspb.1976.0031>.
- Singh, B. & Daneshvar, C. (2013) Human infections and detection of *Plasmodium knowlesi*. *Clinical Microbiology Reviews*, 26(2), 165–184. Available from: <https://doi.org/10.1128/CMR.00079-12>.
- Singh, B., Sung, L.K., Matusop, A., Radhakrishnan, A., Shamsul, S.S.G. & Cox-Singh, J. et al. (2004) A large focus of naturally acquired *Plasmodium knowlesi* infections in human beings. *The Lancet*, 363(9414), 1017–1024. Available from: [https://doi.org/10.1016/S0140-6736\(04\)15836-4](https://doi.org/10.1016/S0140-6736(04)15836-4).
- Sinha, A., Hughes, K.R., Modrzynska, K.K., Otto, T.D., Pfander, C. & Dickens, N.J. et al. (2014) A cascade of DNA-binding proteins for sexual commitment and development in *Plasmodium*. *Nature*, 507(7491), 253–257. Available from: <https://doi.org/10.1038/nature12970>.
- Slomianny, C. (1990) Three-dimensional reconstruction of the feeding process of the malaria parasite. *Blood Cells*, 16(2-3), 369–378. Available from: <https://pubmed.ncbi.nlm.nih.gov/2096983/>.
- Smalley, M.E. & Sinden, R.E. (1977) *Plasmodium falciparum* gametocytes: their longevity and infectivity. *Parasitology*, 74(1), 1–8. Available from: <https://doi.org/10.1017/s0031182000047478>.
- Spielmann, T. & Gilberger, T.-W. (2010) Protein export in malaria parasites: do multiple export motifs add up to multiple export pathways? *Trends in Parasitology*, 26(1), 6–10. Available from: <https://doi.org/10.1016/j.pt.2009.10.001>.
- Spielmann, T., Gras, S., Sabitzki, R. & Meissner, M. (2020) Endocytosis in *Plasmodium* and *Toxoplasma* Parasites. *Trends in Parasitology*, 36(6), 520–532. Available from: <https://doi.org/10.1016/j.pt.2020.03.010>.
- Spielmann, T., Hawthorne, P.L., Dixon, M.W.A., Hannemann, M., Klotz, K. & Kemp, D.J. et al. (2006) A cluster of ring stage-specific genes linked to a locus implicated in cytoadherence in *Plasmodium falciparum* codes for PEXEL-negative and PEXEL-positive proteins exported into the host cell. *Molecular Biology of the Cell*, 17(8), 3613–3624. Available from: <https://doi.org/10.1091/mbc.E06-04-0291>.

- Spielmann, T., Montagna, G.N., Hecht, L. & Matuschewski, K. (2012) Molecular make-up of the Plasmodium parasitophorous vacuolar membrane. *International Journal of Medical Microbiology : IJMM*, 302(4-5), 179–186. Available from: <https://doi.org/10.1016/j.ijmm.2012.07.011>.
- Spycher, C., Klonis, N., Spielmann, T., Kump, E., Steiger, S. & Tilley, L. et al. (2003) MAHRP-1, a novel Plasmodium falciparum histidine-rich protein, binds ferriprotoporphyrin IX and localizes to the Maurer's clefts. *The Journal of Biological Chemistry*, 278(37), 35373–35383. Available from: <https://doi.org/10.1074/jbc.M305851200>.
- Srinivasan, P., Baldeviano, G.C., Miura, K., Diouf, A., Ventocilla, J.A. & Leiva, K.P. et al. (2017) A malaria vaccine protects Aotus monkeys against virulent Plasmodium falciparum infection. *Npj Vaccines*, 2. Available from: <https://doi.org/10.1038/s41541-017-0015-7>.
- Srinivasan, P., Beatty, W.L., Diouf, A., Herrera, R., Ambroggio, X. & Moch, J.K. et al. (2011) Binding of Plasmodium merozoite proteins RON2 and AMA1 triggers commitment to invasion. *Proceedings of the National Academy of Sciences*, 108(32), 13275–13280. Available from: <https://doi.org/10.1073/pnas.1110303108>.
- Staines, H.M., Ellory, J.C. & Kirk, K. (2001) Perturbation of the pump-leak balance for Na(+) and K(+) in malaria-infected erythrocytes. *American Journal of Physiology. Cell Physiology*, 280(6), C1576-87. Available from: <https://doi.org/10.1152/ajpcell.2001.280.6.C1576>.
- Stewart, M.J. & Vanderberg, J.P. (1988) Malaria sporozoites leave behind trails of circumsporozoite protein during gliding motility. *The Journal of Protozoology*, 35(3), 389–393. Available from: <https://doi.org/10.1111/j.1550-7408.1988.tb04115.x>.
- Stirmimann, C.U., Petsalaki, E., Russell, R.B. & Müller, C.W. (2010) WD40 proteins propel cellular networks. *Trends in Biochemical Sciences*, 35(10), 565–574. Available from: <https://doi.org/10.1016/j.tibs.2010.04.003>.
- Stokes, B.H., Rubiano, K., Dhingra, S.K., Mok, S., Straimer, J. & Gnädig, N.F. et al. (2021) *P. falciparum* K13 mutations present varying degrees of artemisinin resistance and reduced fitness in African parasites.
- Straimer, J., Gnädig, N.F., Stokes, B.H., Ehrenberger, M., Crane, A.A. & Fidock, D.A. (2017) Plasmodium falciparum K13 Mutations Differentially Impact Ozonide Susceptibility and Parasite Fitness In Vitro. *mBio*, 8(2). Available from: <https://doi.org/10.1128/mBio.00172-17>.
- Straimer, J., Gnädig, N.F., Witkowski, B., Amaratunga, C., Duru, V. & Ramadani, A.P. et al. (2015) Drug resistance. K13-propeller mutations confer artemisinin resistance in Plasmodium falciparum clinical isolates. *Science*, 347(6220), 428–431. Available from: <https://doi.org/10.1126/science.1260867>.
- Struck, N.S., Souza Dias, S. de, Langer, C., Marti, M., Pearce, J.A. & Cowman, A.F. et al. (2005) Re-defining the Golgi complex in Plasmodium falciparum using the novel Golgi marker PfGRASP. *Journal of Cell Science*, 118(Pt 23), 5603–5613. Available from: <https://doi.org/10.1242/jcs.02673>.
- Stump, A.D., Atieli, F.K., Vulule, J.M. & Besansky, N.J. (2004) Dynamics of the pyrethroid knockdown resistance allele in western Kenyan populations of Anopheles gambiae in response to insecticide-treated bed net trials. *The American Journal of Tropical Medicine and Hygiene*, 70(6), 591–596. Available from: <https://pubmed.ncbi.nlm.nih.gov/15210997/>.
- Sturm, A. (2006) Manipulation of Host Hepatocytes by the Malaria Parasite for Delivery into Liver Sinusoids. *Science (New York, N.Y.)*, 313(5791), 1287–1290.
- Sullivan, D.J. (2002) Theories on malarial pigment formation and quinoline action. *International journal for parasitology*, 32(13), 1645–1653. Available from: [https://doi.org/10.1016/s0020-7519\(02\)00193-5](https://doi.org/10.1016/s0020-7519(02)00193-5).
- Sultan, A.A., Thathy, V., Frevert, U., Robson, K.J., Crisanti, A. & Nussenzweig, V. et al. (1997) TRAP Is Necessary for Gliding Motility and Infectivity of Plasmodium Sporozoites. *Cell*, 90(3), 511–522. Available from: [https://doi.org/10.1016/s0092-8674\(00\)80511-5](https://doi.org/10.1016/s0092-8674(00)80511-5).

- Szallies, A., Kubata, B.K. & Duszenko, M. (2002) A metacaspase of *Trypanosoma brucei* causes loss of respiration competence and clonal death in the yeast *Saccharomyces cerevisiae*. *FEBS Letters*, 517(1-3), 144–150. Available from: [https://doi.org/10.1016/S0014-5793\(02\)02608-X](https://doi.org/10.1016/S0014-5793(02)02608-X).
- Tan, K.R., Katalenich, B.L., Mace, K.E., Nambozi, M., Taylor, S.M. & Meshnick, S.R. et al. (2014) Efficacy of sulphadoxine-pyrimethamine for intermittent preventive treatment of malaria in pregnancy, Mansa, Zambia. *Malaria Journal*, 13, 227. Available from: <https://doi.org/10.1186/1475-2875-13-227>.
- Tavares, J., Formaglio, P., Thiberge, S., Mordelet, E., van Rooijen, N. & Medvinsky, A. et al. (2013) Role of host cell traversal by the malaria sporozoite during liver infection. *The Journal of Experimental Medicine*, 210(5), 905–915.
- Tawk, L., Chicanne, G., Dubremetz, J.-F., Richard, V., Payrastre, B. & Vial, H.J. et al. (2010) Phosphatidylinositol 3-phosphate, an essential lipid in *Plasmodium*, localizes to the food vacuole membrane and the apicoplast. *Eukaryotic Cell*, 9(10), 1519–1530. Available from: <https://doi.org/10.1128/EC.00124-10>.
- Taylor, S.M., Parobek, C.M., DeConti, D.K., Kayentao, K., Coulibaly, S.O. & Greenwood, B.M. et al. (2015) Absence of putative artemisinin resistance mutations among *Plasmodium falciparum* in Sub-Saharan Africa: a molecular epidemiologic study. *The Journal of Infectious Diseases*, 211(5), 680–688. Available from: <https://doi.org/10.1093/infdis/jiu467>.
- Taylor, W.R.J., Hanson, J., Turner, G.D.H., White, N.J. & Dondorp, A.M. (2012) Respiratory manifestations of malaria. *Chest*, 142(2), 492–505. Available from: <https://doi.org/10.1378/chest.11-2655>.
- Tebar, F., Sorkina, T., Sorkin, A., Ericsson, M. & Kirchhausen, T. (1996) Eps15 is a component of clathrin-coated pits and vesicles and is located at the rim of coated pits. *The Journal of Biological Chemistry*, 271(46), 28727–28730. Available from: <https://doi.org/10.1074/jbc.271.46.28727>.
- Teuscher, F., Gatton, M.L., Chen, N., Peters, J., Kyle, D.E. & Cheng, Q. (2010) Artemisinin-induced dormancy in *Plasmodium falciparum*: duration, recovery rates, and implications in treatment failure. *The Journal of Infectious Diseases*, 202(9), 1362–1368. Available from: <https://doi.org/10.1086/656476>.
- Tilley, L., Sougrat, R., Lithgow, T. & Hanssen, E. (2008) The twists and turns of Maurer's cleft trafficking in *P. falciparum*-infected erythrocytes. *Traffic (Copenhagen, Denmark)*, 9(2), 187–197. Available from: <https://doi.org/10.1111/j.1600-0854.2007.00684.x>.
- Tilley, L., Straimer, J., Gnädig, N.F., Ralph, S.A. & Fidock, D.A. (2016) Artemisinin Action and Resistance in *Plasmodium falciparum*. *Trends in Parasitology*, 32(9), 682–696. Available from: <https://doi.org/10.1016/j.pt.2016.05.010>.
- Tirrell, A.R., Vendrely, K.M., Checkley, L.A., Davis, S.Z., McDew-White, M. & Cheeseman, I.H. et al. (2019) Pairwise growth competitions identify relative fitness relationships among artemisinin resistant *Plasmodium falciparum* field isolates. *Malaria Journal*, 18(1), 295. Available from: <https://doi.org/10.1186/s12936-019-2934-4>.
- Toenhake, C.G., Fraschka, S.A.-K., Vijayabaskar, M.S., Westhead, D.R., van Heeringen, S.J. & Bártfai, R. (2018) Chromatin Accessibility-Based Characterization of the Gene Regulatory Network Underlying *Plasmodium falciparum* Blood-Stage Development. *Cell Host & Microbe*, 23(4), 557-569.e9. Available from: <https://doi.org/10.1016/j.chom.2018.03.007>.
- Tonkin, C.J., van Dooren, G.G., Spurck, T.P., Struck, N.S., Good, R.T. & Handman, E. et al. (2004) Localization of organellar proteins in *Plasmodium falciparum* using a novel set of transfection vectors and a new immunofluorescence fixation method. *Molecular and Biochemical Parasitology*, 137(1), 13–21. Available from: <https://doi.org/10.1016/j.molbiopara.2004.05.009>.
- Torii, M., Matsumoto, Y., Kamboj, K.K., Maracic, M., Guo, S.Q. & Nussenzweig, R.S. et al. (1989) Association of microneme antigens of *Plasmodium brasilianum* merozoites with knobs and other parasite-induced

- structures in host erythrocytes. *Infection and Immunity*, 57(2), 596–601. Available from: <https://doi.org/10.1128/iai.57.2.596-601.1989>.
- Towbin, H., Staehelin, T. & Gordon, J. (1979) Electrophoretic transfer of proteins from polyacrylamide gels to nitrocellulose sheets: procedure and some applications. *Proceedings of the National Academy of Sciences of the United States of America*, 76(9), 4350–4354. Available from: <https://doi.org/10.1073/pnas.76.9.4350>.
- Trager, W. & Jensen, J.B. (1976) Human malaria parasites in continuous culture. *Science (New York, N.Y.)*, 193(4254), 673–675. Available from: <https://doi.org/10.1126/science.781840>.
- Trager, W., Rozario, C., Shio, H., Williams, J. & Perkins, M.E. (1992) Transfer of a dense granule protein of *Plasmodium falciparum* to the membrane of ring stages and isolation of dense granules. *Infection and Immunity*, 60(11), 4656–4661. Available from: <https://doi.org/10.1128/iai.60.11.4656-4661.1992>.
- Tseng, L.A. & Bixby, J.L. (2011) Interaction of an intracellular pentraxin with a BTB-Kelch protein is associated with ubiquitylation, aggregation and neuronal apoptosis. *Molecular and Cellular Neurosciences*, 47(4), 254–264. Available from: <https://doi.org/10.1016/j.mcn.2011.04.005>.
- Tsiatsiani, L., van Breusegem, F., Gallois, P., Zavialov, A., Lam, E. & Bozhkov, P.V. (2011) Metacaspases. *Cell Death and Differentiation*, 18(8), 1279–1288. Available from: <https://doi.org/10.1038/cdd.2011.66>.
- Tu, Y. (2011) The discovery of artemisinin (qinghaosu) and gifts from Chinese medicine. *Nature Medicine*, 17(10), 1217–1220. Available from: <https://doi.org/10.1038/nm.2471>.
- Tu, Y.Y., Ni, M.Y., Zhong, Y.R., Li, L.N., Cui, S.L. & Zhang, M.Q. et al. (1981) Studies on the constituents of *Artemisia annua* L. (author's transl). *Yao xue xue bao = Acta pharmaceutica Sinica*, 16(5), 366–370. Available from: <https://pubmed.ncbi.nlm.nih.gov/7246183/>.
- Uren, A. (2000) Identification of Paracaspases and Metacaspases Two Ancient Families of Caspase-like Proteins, One of which Plays a Key Role in MALT Lymphoma. *Molecular cell*, 6(4), 961–967. Available from: [https://doi.org/10.1016/s1097-2765\(00\)00094-0](https://doi.org/10.1016/s1097-2765(00)00094-0).
- Uwimana, A., Legrand, E., Stokes, B.H., Ndikumana, J.-L.M., Warsame, M. & Umulisa, N. et al. (2020) Emergence and clonal expansion of in vitro artemisinin-resistant *Plasmodium falciparum* kelch13 R561H mutant parasites in Rwanda. *Nature Medicine*, 26(10), 1602–1608. Available from: <https://doi.org/10.1038/s41591-020-1005-2>.
- Uwimana, A., Umulisa, N., Venkatesan, M., Svirgel, S.S., Zhou, Z. & Munyaneza, T. et al. (2021) Association of *Plasmodium falciparum* kelch13 R561H genotypes with delayed parasite clearance in Rwanda: an open-label, single-arm, multicentre, therapeutic efficacy study. *The Lancet Infectious Diseases*. Available from: [https://doi.org/10.1016/S1473-3099\(21\)00142-0](https://doi.org/10.1016/S1473-3099(21)00142-0).
- Vaidya, A.B. & Mather, M.W. (2000) Atovaquone resistance in malaria parasites. *Drug Resistance Updates : Reviews and Commentaries in Antimicrobial and Anticancer Chemotherapy*, 3(5), 283–287. Available from: <https://doi.org/10.1054/drup.2000.0157>.
- Valette, F.M., Olivier, C., Lézot, F., Oliver, L., Cochonneau, D. & Lalier, L. et al. (2019) Dormant, quiescent, tolerant and persister cells: Four synonyms for the same target in cancer. *Biochemical Pharmacology*, 162, 169–176. Available from: <https://doi.org/10.1016/j.bcp.2018.11.004>.
- van Wye, J., Ghori, N., Webster, P., Mitschler, R.R., Elmendorf, H.G. & Haldar, K. (1996) Identification and localization of rab6, separation of rab6 from ERD2 and implications for an 'unstacked' Golgi, in *Plasmodium falciparum*. *Molecular and Biochemical Parasitology*, 83(1), 107–120. Available from: [https://doi.org/10.1016/s0166-6851\(96\)02759-4](https://doi.org/10.1016/s0166-6851(96)02759-4).
- Vandana, Dixit, R., Tiwari, R., Katyal, A. & Pandey, K.C. (2019) Metacaspases: Potential Drug Target Against Protozoan Parasites. *Frontiers in Pharmacology*, 10, 790. Available from: <https://doi.org/10.3389/fphar.2019.00790>.

- Vandana, Shankar, S., Prasad, K.M., Kashif, M., Kalia, I. & Rai, R. et al. (2020) A nonpeptidyl molecule modulates apoptosis-like cell death by inhibiting *P. falciparum* metacaspase-2. *Biochemical Journal*, 477(7), 1323–1344. Available from: <https://doi.org/10.1042/BCJ20200050>.
- Vandana, Singh, A.P., Singh, J., Sharma, R., Akhter, M. & Mishra, P.K. et al. (2018) Biochemical characterization of unusual cysteine protease of *P. falciparum*, metacaspase-2 (MCA-2). *Molecular and Biochemical Parasitology*, 220, 28–41. Available from: <https://doi.org/10.1016/j.molbiopara.2018.01.001>.
- Vaughan, A.M., O'Neill, M.T., Tarun, A.S., Camargo, N., Phuong, T.M. & Aly, A.S.I. et al. (2009) Type II fatty acid synthesis is essential only for malaria parasite late liver stage development. *Cellular Microbiology*, 11(3), 506–520. Available from: <https://doi.org/10.1111/j.1462-5822.2008.01270.x>.
- Velavan, T.P., Nderu, D., Agbenyega, T., Ntoumi, F. & Kremsner, P.G. (2019) An alternative dogma on reduced artemisinin susceptibility: A new shadow from east to west. *Proceedings of the National Academy of Sciences*, 116(26), 12611–12612. Available from: <https://doi.org/10.1073/pnas.1907142116>.
- Vercammen, D., van de Cotte, B., Jaeger, G. de, Eeckhout, D., Casteels, P. & Vandepoele, K. et al. (2004) Type II metacaspases Atmc4 and Atmc9 of *Arabidopsis thaliana* cleave substrates after arginine and lysine. *The Journal of Biological Chemistry*, 279(44), 45329–45336. Available from: <https://doi.org/10.1074/jbc.M406329200>.
- VEuPathDB (2021) *PlasmoDB*. Available from: <https://plasmodb.org/plasmo/app> [Accessed 16 July 2021].
- Wall, R.J., Zeeshan, M., Katris, N.J., Limenitakis, R., Rea, E. & Stock, J. et al. (2019) Systematic analysis of *Plasmodium* myosins reveals differential expression, localisation, and function in invasive and proliferative parasite stages. *Cellular Microbiology*, 21(10), e13082. Available from: <https://doi.org/10.1111/cmi.13082>.
- Waller, R.F. & McFadden, G.I. (2005) The apicoplast: a review of the derived plastid of apicomplexan parasites. *Current Issues in Molecular Biology*, 7(1), 57–79. Available from: <https://pubmed.ncbi.nlm.nih.gov/15580780/>.
- Waller, R.F., Reed, M.B., Cowman, A.F. & McFadden, G.I. (2000) Protein trafficking to the plastid of *Plasmodium falciparum* is via the secretory pathway. *The EMBO Journal*, 19(8), 1794–1802. Available from: <https://doi.org/10.1093/emboj/19.8.1794>.
- Walliker, D., Hunt, P. & Babiker, H. (2005) Fitness of drug-resistant malaria parasites. *Acta Tropica*, 94(3), 251–259. Available from: <https://doi.org/10.1016/j.actatropica.2005.04.005>.
- Walliker, D., Quakyi, I.A., Wellem, T.E., McCutchan, T.F., Szarfman, A. & London, W.T. et al. (1987) Genetic analysis of the human malaria parasite *Plasmodium falciparum*. *Science (New York, N.Y.)*, 236(4809), 1661–1666. Available from: <https://doi.org/10.1126/science.3299700>.
- Wamae, P.M., Githeko, A.K., Otieno, G.O., Kabiru, E.W. & Duombia, S.O. (2015) Early biting of the *Anopheles gambiae* s.s. and its challenges to vector control using insecticide treated nets in western Kenya highlands. *Acta Tropica*, 150, 136–142. Available from: <https://doi.org/10.1016/j.actatropica.2015.07.008>.
- Wang, J., Zhang, C.-J., Chia, W.N., Loh, C.C.Y., Li, Z. & Lee, Y.M. et al. (2015) Haem-activated promiscuous targeting of artemisinin in *Plasmodium falciparum*. *Nature Communications*, 6(1), 10111. Available from: <https://doi.org/10.1038/ncomms10111>.
- Wangdi, K., Banwell, C., Gatton, M.L., Kelly, G.C., Namgay, R. & Clements, A.C.A. (2016) Malaria burden and costs of intensified control in Bhutan, 2006–14: an observational study and situation analysis. *The Lancet Global Health*, 4(5), e336–e343. Available from: [https://doi.org/10.1016/S2214-109X\(16\)00083-8](https://doi.org/10.1016/S2214-109X(16)00083-8).
- Wangdi, K., Furuya-Kanamori, L., Clark, J., Barendregt, J.J., Gatton, M.L. & Banwell, C. et al. (2018) Comparative effectiveness of malaria prevention measures: a systematic review and network meta-analysis. *Parasites & Vectors*, 11(1), 210. Available from: <https://doi.org/10.1186/s13071-018-2783-y>.
- Wargo, A.R. & Kurath, G. (2012) Viral fitness: definitions, measurement, and current insights. *Current Opinion in Virology*, 2(5), 538–545. Available from: <https://doi.org/10.1016/j.coviro.2012.07.007>.

- Wassmer, S.C., Taylor, T.E., Rathod, P.K., Mishra, S.K., Mohanty, S. & Arevalo-Herrera, M. et al. (2015) Investigating the Pathogenesis of Severe Malaria: A Multidisciplinary and Cross-Geographical Approach. *The American Journal of Tropical Medicine and Hygiene*, 93(3 Suppl), 42–56. Available from: <https://doi.org/10.4269/ajtmh.14-0841>.
- Watermeyer, J.M., Hale, V.L., Hackett, F., Clare, D.K., Cutts, E.E. & Vakonakis, I. et al. (2016) A spiral scaffold underlies cytoadherent knobs in Plasmodium falciparum-infected erythrocytes. *Blood*, 127(3), 343–351. Available from: <https://doi.org/10.1182/blood-2015-10-674002>.
- Watts, R.E., Ouedra, A., Marquart, L., Webb, L., Abd-Rahman, A.N. & Cascales, L. et al. (2020) Safety and parasite clearance of artemisinin-resistant Plasmodium falciparum infection: A pilot and a randomised volunteer infection study in Australia. *PLOS Medicine*, 17(8), e1003203. Available from: <https://doi.org/10.1371/journal.pmed.1003203>.
- Weiss, G.E., Gilson, P.R., Taechalerpaisarn, T., Tham, W.-H., Jong, N.W.M. de & Harvey, K.L. et al. (2015) Revealing the sequence and resulting cellular morphology of receptor-ligand interactions during Plasmodium falciparum invasion of erythrocytes. *PLoS Pathogens*, 11(2), e1004670. Available from: <https://doi.org/10.1371/journal.ppat.1004670>.
- Wellems, T.E. & Plowe, C.V. (2001) Chloroquine-resistant malaria. *The Journal of Infectious Diseases*, 184(6), 770–776. Available from: <https://doi.org/10.1086/322858>.
- Wellems, T.E., Sá, J.M., Su, X.-Z., Connelly, S.V. & Ellis, A.C. (2020) 'Artemisinin Resistance': Something New or Old? Something of a Misnomer? *Trends in Parasitology*, 36(9), 735–744. Available from: <https://doi.org/10.1016/j.pt.2020.05.013>.
- White, M.T., Verity, R., Griffin, J.T., Asante, K.P., Owusu-Agyei, S. & Greenwood, B. et al. (2015) Immunogenicity of the RTS,S/AS01 malaria vaccine and implications for duration of vaccine efficacy: secondary analysis of data from a phase 3 randomised controlled trial. *The Lancet Infectious Diseases*, 15(12), 1450–1458. Available from: [https://doi.org/10.1016/S1473-3099\(15\)00239-X](https://doi.org/10.1016/S1473-3099(15)00239-X).
- White, N.J. (1997) Assessment of the pharmacodynamic properties of antimalarial drugs in vivo. *Antimicrobial Agents and Chemotherapy*, 41(7), 1413–1422. Available from: <https://doi.org/10.1128/AAC.41.7.1413>.
- White, N.J. (2005) Intermittent presumptive treatment for malaria. *PLoS Medicine*, 2(1), e3. Available from: <https://doi.org/10.1371/journal.pmed.0020003>.
- White, N.J. (2008a) Plasmodium knowlesi: the fifth human malaria parasite. *Clinical Infectious Diseases : an Official Publication of the Infectious Diseases Society of America*, 46(2), 172–173. Available from: <https://doi.org/10.1086/524889>.
- White, N.J. (2008b) Qinghaosu (artemisinin): the price of success. *Science (New York, N.Y.)*, 320(5874), 330–334. Available from: <https://doi.org/10.1126/science.1155165>.
- White, N.J. (2011a) Determinants of relapse periodicity in Plasmodium vivax malaria. *Malaria Journal*, 10, 297. Available from: <https://doi.org/10.1186/1475-2875-10-297>.
- White, N.J. (2011b) The parasite clearance curve. *Malaria Journal*, 10(1), 278. Available from: <https://doi.org/10.1186/1475-2875-10-278>.
- White, N.J. (2013) Pharmacokinetic and pharmacodynamic considerations in antimalarial dose optimization. *Antimicrobial Agents and Chemotherapy*, 57(12), 5792–5807. Available from: <https://doi.org/10.1128/AAC.00287-13>.
- WHO (2006) Indoor residual spraying: Use of indoor residual spraying for scaling up global malaria control and elimination.
- WHO (2014) *Status report on artemisinin resistance*. Geneva.
- WHO (2015) *Guidelines for the treatment of malaria*. World Health Organization: Geneva.

- WHO (2017a) *Safety monitoring of the RTS,S vaccine*. Available from: <https://www.who.int/groups/global-advisory-committee-on-vaccine-safety/topics/malaria-vaccines/safety-rt-s> [Accessed 15 July 2021].
- WHO (2017b) *Status report on artemisinin and ACT resistance*. Geneva.
- WHO (2017c) WHO recommendations for achieving universal coverage with long-lasting insecticidal nets in malaria control.
- WHO (2018) *Status report on artemisinin resistance and ACT efficacy*. Geneva.
- WHO (2019a) *Status report on artemisinin resistance and ACT efficacy*. Geneva.
- WHO (2019b) WHO Model list essential medicines, 21st list.
- WHO (2020a) *Report on antimalarial drug efficacy, resistance and response: 10 years of surveillance (2010-2019)*. Geneva.
- WHO (2020b) World malaria report 2020. *World Health Organization*, 30 November. Available from: <https://www.who.int/publications/i/item/9789240015791> [Accessed 14 July 2021].
- Wickham, M.E., Rug, M., Ralph, S.A., Klonis, N., McFadden, G.I. & Tilley, L. et al. (2001) Trafficking and assembly of the cytoadherence complex in *Plasmodium falciparum*-infected human erythrocytes. *The EMBO Journal*, 20(20), 5636–5649. Available from: <https://doi.org/10.1093/emboj/20.20.5636>.
- Witkowski, B., Amaratunga, C., Khim, N., Sreng, S., Chim, P. & Kim, S. et al. (2013) Novel phenotypic assays for the detection of artemisinin-resistant *Plasmodium falciparum* malaria in Cambodia: in-vitro and ex-vivo drug-response studies. *The Lancet Infectious Diseases*, 13(12), 1043–1049. Available from: [https://doi.org/10.1016/S1473-3099\(13\)70252-4](https://doi.org/10.1016/S1473-3099(13)70252-4).
- Witkowski, B., Khim, N., Chim, P., Kim, S., Ke, S. & Kloeung, N. et al. (2013) Reduced artemisinin susceptibility of *Plasmodium falciparum* ring stages in western Cambodia. *Antimicrobial Agents and Chemotherapy*, 57(2), 914–923. Available from: <https://doi.org/10.1128/AAC.01868-12>.
- Woolner, S., O'Brien, L.L., Wiese, C. & Bement, W.M. (2008) Myosin-10 and actin filaments are essential for mitotic spindle function. *Journal of Cell Biology*, 182(1), 77–88. Available from: <https://doi.org/10.1083/jcb.200804062>.
- World Health Organization (2017) *Status report on artemisinin and ACT resistance Status report on artemisinin and ACT resistance*.
- WorldWide Antimalarial Resistance Network (WWARN) Lumefantrine PK/PD Study Group (2015) Artemether-lumefantrine treatment of uncomplicated *Plasmodium falciparum* malaria: a systematic review and meta-analysis of day 7 lumefantrine concentrations and therapeutic response using individual patient data. *BMC Medicine*, 13(1), 227. Available from: <https://doi.org/10.1186/s12916-015-0456-7>.
- WWARN K13 Genotype-Phenotype Study Group (2019) Association of mutations in the *Plasmodium falciparum* Kelch13 gene (Pf3D7\_1343700) with parasite clearance rates after artemisinin-based treatments—a WWARN individual patient data meta-analysis. *BMC Medicine*, 17(1), 1. Available from: <https://doi.org/10.1186/s12916-018-1207-3>.
- Xie, S.C., Dogovski, C., Hanssen, E., Chiu, F., Yang, T. & Crespo, M.P. et al. (2016) Haemoglobin degradation underpins the sensitivity of early ring stage *Plasmodium falciparum* to artemisinins. *Journal of Cell Science*, 129(2), 406–416. Available from: <https://doi.org/10.1242/jcs.178830>.
- Xu, T., Johnson, C.A., Gestwicki, J.E. & Kumar, A. (2010) Conditionally controlling nuclear trafficking in yeast by chemical-induced protein dimerization. *Nature Protocols*, 5(11), 1831–1843. Available from: <https://doi.org/10.1038/nprot.2010.141>.
- Yang, T., Yeoh, L.M., Tutor, M.V., Dixon, M.W., McMillan, P.J. & Xie, S.C. et al. (2019) Decreased K13 Abundance Reduces Hemoglobin Catabolism and Proteotoxic Stress, Underpinning Artemisinin Resistance. *Cell Reports*, 29(9), 2917-2928.e5. Available from: <https://doi.org/10.1016/j.celrep.2019.10.095>.

- Yeh, E. & DeRisi, J.L. (2011) Chemical rescue of malaria parasites lacking an apicoplast defines organelle function in blood-stage *Plasmodium falciparum*. *PLoS Biology*, 9(8), e1001138. Available from: <https://doi.org/10.1371/journal.pbio.1001138>.
- Yeka, A., Banek, K., Bakyaite, N., Staedke, S.G., Kanya, M.R. & Talisuna, A. et al. (2005) Artemisinin versus nonartemisinin combination therapy for uncomplicated malaria: randomized clinical trials from four sites in Uganda. *PLoS Medicine*, 2(7), e190. Available from: <https://doi.org/10.1371/journal.pmed.0020190>.
- Yeka, A., Dorsey, G., Kanya, M.R., Talisuna, A., Lugemwa, M. & Rwakimari, J.B. et al. (2008) Artemether-lumefantrine versus dihydroartemisinin-piperazine for treating uncomplicated malaria: a randomized trial to guide policy in Uganda. *PLoS One*, 3(6), e2390. Available from: <https://doi.org/10.1371/journal.pone.0002390>.
- Yeka, A., Kigozi, R., Conrad, M.D., Lugemwa, M., Okui, P. & Katureebe, C. et al. (2016) Artesunate/Amodiaquine Versus Artemether/Lumefantrine for the Treatment of Uncomplicated Malaria in Uganda: A Randomized Trial. *The Journal of Infectious Diseases*, 213(7), 1134–1142. Available from: <https://doi.org/10.1093/infdis/jiv551>.
- Yeka, A., Wallender, E., Mulebeke, R., Kibuuka, A., Kigozi, R. & Bosco, A. et al. (2019) Comparative Efficacy of Artemether-Lumefantrine and Dihydroartemisinin-Piperazine for the Treatment of Uncomplicated Malaria in Ugandan Children. *The Journal of Infectious Diseases*, 219(7), 1112–1120. Available from: <https://doi.org/10.1093/infdis/jiy637>.
- Yoon, H.S., Grant, J., Tekle, Y.I., Wu, M., Chaon, B.C. & Cole, J.C. et al. (2008) Broadly sampled multigene trees of eukaryotes. *BMC Evolutionary Biology*, 8, 14. Available from: <https://doi.org/10.1186/1471-2148-8-14>.
- Young, J.A., Fivelman, Q.L., Blair, P.L., La Vega, P. de, Le Roch, K.G. & Zhou, Y. et al. (2005) The *Plasmodium falciparum* sexual development transcriptome: a microarray analysis using ontology-based pattern identification. *Molecular and Biochemical Parasitology*, 143(1), 67–79. Available from: <https://doi.org/10.1016/j.molbiopara.2005.05.007>.
- Yu, M., Kumar, T.R.S., Nkrumah, L.J., Coppi, A., Retzlaff, S. & Li, C.D. et al. (2008) The fatty acid biosynthesis enzyme FabI plays a key role in the development of liver-stage malarial parasites. *Cell Host & Microbe*, 4(6), 567–578. Available from: <https://doi.org/10.1016/j.chom.2008.11.001>.
- Zhang, D.D., Lo, S.-C., Cross, J.V., Templeton, D.J. & Hannink, M. (2004) Keap1 is a redox-regulated substrate adaptor protein for a Cul3-dependent ubiquitin ligase complex. *Molecular and Cellular Biology*, 24(24), 10941–10953. Available from: <https://doi.org/10.1128/MCB.24.24.10941-10953.2004>.
- Zhang, Y., Huang, C., Kim, S., Golkaram, M., Dixon, M.W.A. & Tilley, L. et al. (2015) Multiple stiffening effects of nanoscale knobs on human red blood cells infected with *Plasmodium falciparum* malaria parasite. *Proceedings of the National Academy of Sciences*, 112(19), 6068–6073. Available from: <https://doi.org/10.1073/pnas.1505584112>.
- Zhao, L., Pi, L., Qin, Y., Lu, Y., Zeng, W. & Xiang, Z. et al. (2020) Widespread resistance mutations to sulfadoxine-pyrimethamine in malaria parasites imported to China from Central and Western Africa. *International Journal for Parasitology. Drugs and Drug Resistance*, 12, 1–6. Available from: <https://doi.org/10.1016/j.ijpddr.2019.11.002>.
- Zhu, G., Marchewka, M.J. & Keithly, J.S. (2000) *Cryptosporidium parvum* appears to lack a plastid genome. *Microbiology (Reading, England)*, 146 (Pt 2), 315–321. Available from: <https://doi.org/10.1099/00221287-146-2-315>.
- Zhu, L., Tripathi, J., Rocamora, F.M., Miotto, O., van der Pluijm, R. & Voss, T.S. et al. (2018) The origins of malaria artemisinin resistance defined by a genetic and transcriptomic background. *Nature Communications*, 9(1), 5158. Available from: <https://doi.org/10.1038/s41467-018-07588-x>.

## Danksagung

Zuallererst möchte ich mich ganz herzlich bei Dr. Tobias Spielmann für die tolle Möglichkeit bedanken, meine Doktorarbeit in seiner Arbeitsgruppe zu schreiben. Ich bin dir sehr dankbar für die große Unterstützung, die du mir über all die Jahre gegeben hast und du immer mit Rat und Tat zur Stelle warst. Deine Begeisterung für die Wissenschaft und das wissenschaftliche Arbeiten sind wirklich mitreißend und es hat mir sehr großen Spaß gemacht von dir zu lernen. Ich könnte mir keinen besseren Betreuer für meine Doktorarbeit vorstellen.

Ich möchte mich auch bei Prof. Tim-Wolf Gilberger, sowie bei Prof. Jürgen May und Dr. Paul-Christian Burda für die Co-Betreuung der Promotion bedanken. Die neuen Ideen und Anregungen, die durch die Gespräche mit euch entstanden sind, haben das gesamte Projekt unterstützt. Bei Herrn Prof. May möchte ich mich auch nochmals ganz herzlich für die finanzielle Unterstützung bedanken und die Möglichkeit, dass ich in Zusammenarbeit mit seiner Arbeitsgruppe einen Auslandsaufenthalt in Ghana am KCCR erleben durfte.

Desweiteren möchte ich mich bei Dr. Oumou Maiga-Ascofaré für die schöne Zusammenarbeit und Unterstützung bedanken. Du hast mich nicht nur hinsichtlich des Promotionsprojekts betreut, sondern hast mich auch während der Zeit in Ghana unterstützt und in deine Familie aufgenommen. Das war für mich ein sehr schönes, einmaliges Erlebnis.

Ein großer Dank geht auch an Birgit Förster, die die Amplifikation und Sequenzierung der Patientenproben durchgeführt hat und mich damit tatkräftig unterstützt hat.

Ich möchte mich bei allen ehemaligen und aktuellen Mitgliedern der AG Spielmann und AG Gilberger für die wunderbare Zeit bedanken und die wertvollen Freundschaften, die dadurch entstanden sind. Unsere Zeit im Labor, aber vor allem auch unsere gemeinsamen Ausflüge und Unternehmungen sind unvergesslich und haben mir riesigen Spaß gemacht. Ohne euch wäre meine Promotion nicht die geworden, die sie ist.

Und zu guter Letzt möchte ich mich noch für die enorme Unterstützung durch meine Familie und meinem Freund Stefan bedanken. Ich bin sehr glücklich, dass ich euch habe und ich so viele schöne Momente mit euch erleben darf. Danke, dass ich mich zu jeder Zeit auf euch verlassen kann und ihr immer für mich da seid.

## List of publications

Behrens, H., **Schmidt, S.**, Spielmann, T. (2021) *The newly discovered role of endocytosis in artemisinin resistance*. Medicinal Research Reviews, DOI: 10.1002/med.21848

Birnbaum, J.\* , Scharf, S.\* , **Schmidt, S.**, Jonscher, E., Hoeijmakers, W. A. M., Flemming, S., Toenhake, C. G., Schmitt, M., Sabitzki, R., Bergmann, B., Fröhlke, U., Mesén-Ramírez, P., Blancke Soares, A., Herrmann, H., Bártfai, R., Spielmann, T. (2020) *A Kelch13-defined endocytosis pathway mediates artemisinin resistance in malaria parasites*. Science, Vol. 367, Issue 6473, pp. 51 – 59. DOI: 10.1126/science.aax4735

Hoeijmakers, W. A. M., Miao, J., **Schmidt, S.**, Toenhake, C. G., Shrestha, S., Venhuizen, J., Henderson, R., Birnbaum, J., Ghidelli-Disse, S., Drewes, G., Cui, L., Stunnenberg, H. G., Spielmann, T., Bártfai, R. (2019) *Epigenetic reader complexes of the human malaria parasite, Plasmodium falciparum*. Nucleic Acids Research, Vol. 47, Issue 22, pp. 11574 – 11588

## Appendix

### Appendix A

#### Appendix A.1 Determination of relative position of MCA2<sup>wt</sup>-3xHA and K13.

Relative localization MCA2/K13	Date	Image	MCA2 foci	K13 foci	Co-loc	partial co-loc	no co-loc
	02.12.2020	DAPI61ed	1	1	1	0	0
		DAPI60ed	1	2	0	1	0
		DAPI60ed	1	1	0	1	0
		DAPI59ed	1	2	0	0	1
		DAPI58ed2	1	2	0	0	1
		DAPI58ed	1	4	1	0	0
		DAPI57ed	1	1	1	0	0
		DAPI57ed	2	5	1	0	1
		DAPI56ed	1	5	1	0	0
	04.12.2020	DAPI59ed4	2	2	1	0	1
		DAPI59ed3	1	2	0	1	0
		DAPI59ed	6	3	0	2	4
		DAPI58ed2	2	4	2	0	0
		DAPI58ed	1	1	0	1	0
		DAPI57ed	3	3	2	0	1
		DAPI56ed2	2	4	0	1	1
		DAPI65ed	3	3	0	1	2
		DAPI64ed	3	6	1	1	1
		DAPI63ed	2	3	1	0	1
		DAPI62ed3	2	2	2	0	0
		DAPI62ed2	1	4	1	0	0
		DAPI62ed	1	3	1	0	0
		DAPI73ed	2	2	2	0	0
		DAPI73ed	1	2	1	0	0
		DAPI72ed	1	4	1	0	0
		DAPI70ed	1	1	0	0	1
		DAPI69ed	2	2	1	1	0
		DAPI68ed2	1	3	1	0	0
		DAPI68ed	2	3	0	2	0
		DAPI66ed	1	1	0	0	1
Summe		30	50	81	22	12	16
Proportion					44	24	32

**Appendix A.2** Determination of relative position of MCA2<sup>Y1344Stop</sup>-GFP and K13.

Relative location MCA2/K13 (Tropfen)	Date	Image	MCA2 (Y1344.)	Kelch13	Co-loc	partial co-loc	no co-loc
	29.05.2020	Alexa09ed2	2	2	1	1	0
	12.06.2020	Alexa10ed	3	6	2	1	0
		Alexa11ed	3	4	3	0	0
		Alexa12ed	2	1	1	0	1
		GFP07ed	2	3	1	1	0
		GFP07ed2	5	6	4	0	1
	01.07.2020	Alexa04ed	1	2	0	0	1
		Alexa04ed2	2	2	1	0	1
		Alexa09ed	2	1	1	0	1
		Alexa12ed	1	1	0	1	0
		Alexa14ed	2	2	2	0	0
		Alexa20ed3	1	2	1	0	0
		Alexa31ed	1	1	1	0	0
		Alexa31ed2	2	2	1	1	0
		Alexa32ed	2	1	1	0	1
		GFP05ed	1	1	1	0	0
		GFP07ed	1	1	1	0	0
		GFP07ed2	2	3	2	0	0
		GFP11ed2	1	1	1	0	0
		GFP11ed2	1	1	1	0	0
		GFP11ed2	1	1	1	0	0
		GFP11ed2	1	1	1	0	0
		GFP12ed2	2	2	0	2	0
		GFP14ed	1	1	0	1	0
		GFP16ed	1	1	1	0	0
		GFP18ed	1	1	1	0	0
		GFP18ed2	1	1	1	0	0
		GFP19ed	1	1	0	0	1
		GFP22ed2	1	1	0	0	1
		GFP23ed	1	1	1	0	0
		GFP24ed2	2	1	0	0	2
		GFP25ed	1	1	1	0	0
		GFP25ed3	3	2	0	2	1
		GFP29ed2	1	1	1	0	0
		GFP29ed4	1	1	0	1	0
		GFP30ed2	1	1	0	0	1
		GFP30ed3	3	3	3	0	0
		GFP35ed	1	1	1	0	0
		GFP35ed2	1	1	0	1	0
	17.08.2020	Alexa06ed	1	1	1	0	0
		GFP10ed	1	1	1	0	0
		GFP10ed2	1	1	0	1	0
		GFP11ed	1	1	0	0	1
		GFP12ed	3	3	2	1	0
		GFP12ed2	1	1	0	0	1
		GFP13ed	1	1	0	0	1
<b>Summe</b>		n=46	71	75	42	14	15
Co-loc MCA2/K13					59		
Partial Co-loc						20	
no co-loc							21

### Appendix A.3 Determination of relative position of MCA2<sup>Y1344Stop</sup> and K13 in smears.

Relative location MCA2/K13 (Smear)	Date	Image	MCA2 (Y1344.)	Kelch13	Co-loc	partial co-loc	no co-loc
	27.07.2020	GFP76ed	2	1	1	0	1
		GFP79ed	2	1	1	0	1
		GFP79ed	2	2	2	0	0
		GFP79ed2	1	1	1	0	0
		GFP81ed	1	1	1	0	0
		GFP82ed2	2	2	2	0	0
		GFP83ed	1	2	1	0	0
		GFP86ed	1	1	1	0	0
		GFP89ed2	2	1	1	0	1
		GFP93ed	1	2	1	0	0
		GFP94ed	2	1	1	0	1
		GFP94ed	1	1	1	0	0
	17.08.2020	GFP17ed	1	1	1	0	0
		GFP18ed	2	1	1	0	1
		GFP19ed	3	1	1	0	2
		GFP19ed2	2	2	1	0	1
		GFP20ed	3	2	2	0	1
		GFP22ed	3	3	3	0	0
		GFP25ed	2	1	1	0	1
		GFP27ed	2	2	2	0	0
Summe		n=20	36	29	26	0	10
Co-loc MCA2/K13					72		
Partial Co-loc						0	
no co-loc							28

## Appendix B

### Appendix B.1 Determination of relative position of MyoF<sup>wt</sup>-3xHA and K13 (acetone IFA).

MyosinF (3xHA) + K13mCh									
ACETON									
Date	Image	Stage	mCherry # of MyoF foci	GFP # of Kelch foci	# co-loc	# partial co-loc	# close foci	no co-loc	remarks
Aceton IFA (vom 26.06.2020)	DAP19ed2	R	2	5	1	0	1	0	no hemozine
	DAP19ed3	R	1	1	0	0	1	0	no hemozine
	DAP19ed4	T	1	2	0	0	1	0	0 Kelch foci close to hemozine but not MyoF
	DAP19ed6	R	2	2	1	0	1	0	no hemozine
	DAP19ed7	R	3	1	0	1	2	0	no hemozine
	DAP19ed8 (1)	R	2	3	0	1	1	0	no hemozine
	DAP19ed8 (2)	R	1	3	0	0	1	0	no hemozine
	DAP19ed10 (1)	T	1	2	0	0	1	0	0 Kelch foci close to hemozine but not MyoF
	DAP19ed10 (2)	R	1	2	0	0	1	0	no hemozine
	DAP19ed11	T	2	3	1	0	1	0	0 1 MyoF focus close to FV
	DAP120ed2	R	3	2	1	0	2	0	no hemozine
	DAP120ed3	R	1	1	0	0	1	0	no hemozine
	DAP121ed	R	1	3	0	0	1	0	no hemozine
	DAP121ed2	R	2	1	0	0	2	0	no hemozine
	DAP121ed3	R	1	2	0	1	0	0	no hemozine
	DAP121ed5	R	2	1	0	0	2	0	no hemozine
	DAP122ed2	R	1	1	0	1	0	0	no hemozine
	DAP122ed3	R	5	4	3	1	1	0	no hemozine
	DAP123ed	T	1	2	0	1	0	0	no hemozine
	DAP123ed2	R	2	1	0	0	2	0	no hemozine
	DAP123ed5	T	3	1	0	0	3	0	0 1 MyoF focus close to FV
	DAP124ed	T	3	2	0	0	2	1	2 MyoF foci close to FV
	DAP125ed4	T	2	2	0	0	2	0	0 2 MyoF foci close to FV
	DAP125ed5	T	2	3	0	1	1	0	0 1 MyoF focus close to FV
	DAP125ed7	R	1	1	0	0	1	0	no hemozine
	DAP125ed8	R	3	1	0	1	2	0	no hemozine
	DAP125ed11	T	1	2	1	0	0	0	0 1 MyoF focus close to FV
	DAP126ed (1)	T	2	3	0	2	0	0	0 2 MyoF foci close to FV
	DAP126ed (2)	T	2	3	0	1	1	0	0 1 MyoF focus close to FV
	DAP126ed2	R	1	1	0	0	1	0	no hemozine
	DAP126ed3	R	2	2	1	0	1	0	no hemozine
SUMME		31	57	63	9	11	36	1	
Co-loc MyoF(3xHA)/K13					16				
Partial co-loc MyoF(3xHA)/K13						19			
Close foci MyoF(3xHA)/K13							63		
No co-loc MyoF(3xHA)/K13								2	
Co-loc MyoF/K13 at FV					2				
MyoF foci at FV									11
Co-loc at FV [%]		18							

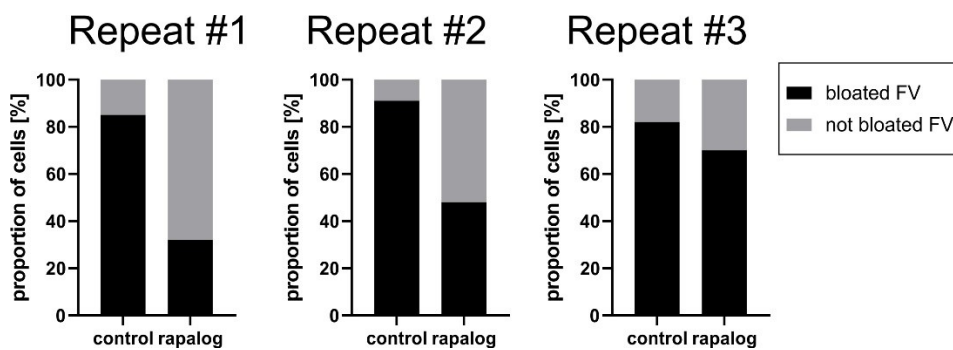
## Appendix B.2 Determination of relative position of MyoF<sup>wt</sup>-3xHA and K13 (formaldehyde/glutaraldehyde IFA).

MyosinF (3xHA) + K13mCh										
FORMALDEHYDE/GLUTARALDEHYDE										
Date	Image	Stage	mCherry # of MyoF foci	GFP # of Kelch foci	# co-loc	# partial co-loc	# close foci	no co-loc	remarks	
In solution IFA (vom 26.06.2020)	DAPI51ed	R	3	1	1	0	0	0	2	no hemozoin
	DAPI54ed2	R	3	1	0	0	0	0	3	no hemozoin
	DAPI57ed	T	1	4	0	0	1	0	1	MyoF focus close to FV
	DAPI58ed	T	2	4	0	1	1	0	0	MyoF apart of FV at cell periphery
	DAPI59ed	T	2	6	1	1	0	0	1	MyoF focus close to FV
	DAPI59ed2	R	4	1	1	0	0	0	3	no hemozoin
	DAPI62ed	T	1	3	0	1	0	0	1	MyoF focus close to FV
	DAPI63ed	T	1	6	1	0	0	0	1	MyoF focus close to FV
	GFP26ed	T	5	6	0	0	4	0	3	MyoF foci close FV
	GFP26ed2	T	7	5	1	0	4	0	2	MyoF foci close FV
<b>SUMME</b>	<b>10</b>		<b>29</b>	<b>37</b>	<b>5</b>	<b>3</b>	<b>10</b>	<b>11</b>		
Co-loc MyoF(3xHA)/K13					17					
Partial co-loc MyoF(3xHA)/K13						10				
Close foci MyoF(3xHA)/K13							34			
No co-loc MyoF(3xHA)/K13								38		
MyoF in trophs										7
MyoF in trophs at FV										6
MyoF near FV [%]										86
Co-loc MyoF/K13 in rings [%]					20					
Co-loc MyoF/K13 in trophs [%]					16					
Co-loc MyoF/K13 in trophs at FV [%]					30					

## Appendix B.3 Determination of relative position of MyoF<sup>wt</sup>-2x2 and K13.

MyosinF (2x2FKBP) + K13mCh										
Date	Image	Stage	GFP # of MyoF foci	mCherry # of Kelch foci	# co-loc	# partial co-loc	# close foci	no co-loc	remarks	
16.11.2020 (63x)	Alexa11ed	ET	2	1	0	2	0	0	2	MyoF foci close to FV
	Alexa11ed3	LT	2	1	0	0	0	2	2	MyoF foci close to FV
	Alexa11ed4	ER	1	2	0	0	0	1	0	no hemozoin
	Alexa12ed	ET	2	1	0	0	0	2	2	MyoF foci close to FV
	Alexa12ed2	LT	3	1	0	0	2	1	3	MyoF foci close to FV
	GFP54ed	LT	1	2	0	0	1	0	1	MyoF focus close to FV
	GFP55ed	ET	1	1	0	0	1	0	0	MyoF apart of FV
16.11.2020 (100x)	GFP60ed	ET	1	1	1	0	0	0	1	MyoF apart of FV
	GFP61ed	LR	1	1	0	0	0	1	1	MyoF focus close to FV
	GFP62ed	LT	2	1	0	0	2	0	2	MyoF foci close to FV
02.10.2020	Alexa07ed	ET	4	2	0	1	1	2	2	MyoF foci close to FV
23.11.2020	GFP77ed	LT	1	1	0	0	0	1	1	MyoF apart of FV
	GFP81ed	LT	2	3	0	0	2	0	0	MyoF apart of FV
	GFP82ed	LT	2	1	1	0	0	1	1	MyoF focus close to FV
<b>SUMME</b>	<b>14</b>		<b>25</b>	<b>19</b>	<b>2</b>	<b>3</b>	<b>9</b>	<b>11</b>		
Co-loc MyoF(2x2)/K13					8					
Partial co-loc MyoF(2x2)/K13						12				
Close foci MyoF(2x2)/K13							36			
No co-loc MyoF(2x2)/K13								44		
Total MyoF in late ring and trophs										24
MyoF in late ring and trophs at FV										16
MyoF near FV [%]										67
Co-loc MyoF/K13 in late rings and trophs at FV [%]					13					

## Appendix B.4 Independent replications of bloated food vacuole assay performed with MyoF<sup>wt</sup>-2x2+1xNLS.



**Appendix B.5** Assessment of relative position of MyoF<sup>wt</sup>-2x2 and K13 in the presence of 10  $\mu$ M Cytochalasin D at two different time points. *green* (ET) early trophozoite; *orange* (LT), late trophozoite; *blue* (ER), early ring (rings were excluded from calculations).

Zeitpunkt	Bild	Stadium	Foci K13	Foci MyosinF	Co-loc	Partial co-loc	No co-loc
Start	GFP21ed	LT	2	4	1	0	3
	GFP21ed2	ET	1	1	0	0	1
	GFP18ed	LT	1	4	1	0	3
	GFP17ed	LT	2	1	0	0	1
	GFP15ed	ET	2	2	1	0	1
	GFP12ed2	ET	1	1	0	0	1
	GFP12ed	ET	1	1	0	0	1
	GFP11ed3	ET	1	1	0	0	1
	GFP11ed	LT	1	3	1	0	2
	GFP09ed	ET	1	2	1	0	1
	GFP15ed2	ET	1	1	0	1	0
	GFP15ed3	ET	1	1	0	0	1
	GFP16ed	ET	1	1	0	0	1
	GFP13ed3	ET	1	1	0	1	0
	GFP13ed3	LT	1	1	0	0	1
	GFP19ed2	ET	1	3	0	0	3
	GFP17ed2	ET	2	3	1	0	2
<b>Summe</b>	<b>n=17 cells</b>						
Summe foci (ET)			14	18	3	2	13
Co-loc MyoF(2x2)/K13					17		
Partial co-loc MyoF(2x2)/K13						11	
No co-loc MyoF(2x2)/K13							72
Summe foci (LT)			7	13	3	0	10
Co-loc MyoF (2x2)					23		
Partial co-loc MyoF (2x2)						0	
No co-loc MyoF (2x2)							77

Zeitpunkt	Bild	Stadium	Foci K13	Foci MyosinF	Co-loc	Partial co-loc	No co-loc
Kontrolle	GFP54ed	ET	1	2	1	0	1
1h nach Start	GFP53ed	LT	1	3	1	0	2
	GFP52ed	LT	1	2	0	0	2
	GFP51ed	ET	1	1	0	0	1
	GFP48ed	ET	1	1	0	0	1
	GFP47ed	ET	1	2	1	0	1
	GFP46ed	ET	1	3	0	0	3
	GFP44ed	ET	2	1	0	1	0
	GFP43ed	ET	1	4	1	0	3
	GFP42ed	LT	1	2	1	0	1
	GFP50ed2	ET	1	2	1	0	1
	GFP50ed	ET	1	1	0	0	1
	GFP49ed	LT	2	3	1	0	2
	<b>Summe</b>	<b>n=13 cells</b>					
Summe foci (ET)			10	17	4	1	12
Co-loc MyoF(2x2)/K13					24		
Partial co-loc MyoF(2x2)/K13						6	
No co-loc MyoF(2x2)/K13							71
Summe foci (LT)			5	10	3	0	7
Co-loc MyoF (2x2)					30		
Partial co-loc MyoF (2x2)						0	
No co-loc MyoF (2x2)							70

Zeitpunkt	Bild	Stadium	Foci K13	Foci MyosinF	Co-loc	Partial co-loc	No co-loc
mit CytD (10µM)	GFP41ed	LT	1	3	0	1	2
1h nach Start	GFP40ed2	LT	5	8	3	0	5
	GFP39ed	LT	1	4	1	0	3
	GFP39ed2	LT	1	2	0	1	1
	GFP39ed3	LT	2	2	1	0	1
	GFP37ed	ET	1	1	0	0	1
	GFP36ed	ET	1	2	0	0	2
	GFP33ed2	ET	1	1	0	1	0
	GFP30ed	LT	1	2	1	0	1
	GFP28ed	LT	1	1	0	1	0
	GFP27ed	ET	1	1	0	1	0
	GFP26ed	LT	4	5	2	0	3
	GFP25ed	LT	2	1	0	0	1
	GFP24ed	LT	1	1	0	0	1
	GFP22ed (1)	LT	1	2	0	0	2
	GFP22ed (2)	ET	2	2	0	0	2
	GFP31ed2 (1)	LT	1	2	0	0	2
	GFP31ed2 (2)	LT	1	1	0	0	1
	GFP31ed	LT	1	2	1	0	1
	GFP40ed3	ER	1	1	0	1	0
<b>Summe</b>	<b>n=20 cells</b>						
Summe foci (ET)			6	7	0	2	5
Co-loc MyoF(2x2)/K13					0		
Partial co-loc MyoF(2x2)/K13						29	
No co-loc MyoF(2x2)/K13							71
Summe foci (LT)			23	36	9	3	24
Co-loc MyoF (2x2)					25		
Partial co-loc MyoF (2x2)						8	
No co-loc MyoF (2x2)							67

**Appendix B.6** Assessment of relative position of MyoF<sup>wt</sup>-2x2 and P40PX in the presence of rapalog. at four different time points. Color code represents different time points. *FV*, food vacuole; *V*, vesicles

	Timepoint	Treatment	Image	MyoF (FV)	MyoF (V)	Co-Loc (FV)	Co-loc (V)	close foci (FV)	close foci (V)	no co-loc	
	Start	control	Alexa17ed	1	0	0	0	1	0	0	
			Alexa16ed	1	0	0	0	1	0	0	
			GFP04ed	1	0	0	0	0	1	0	
			Alexa13ed	2	0	0	0	2	0	0	
			Alexa06ed	1	0	1	0	0	0	0	
			Alexa10ed	2	0	0	0	2	0	0	
			Alexa12ed2	2	0	2	0	0	0	0	
	2 h	control	Alexa36ed	1	0	1	0	0	0	0	
			Alexa35ed2	2	0	0	0	1	1	0	
			Alexa34ed	1	0	0	1	0	0	0	
			Alexa33ed	0	1	0	0	0	1	0	
			Alexa32ed	2	1	0	0	2	0	1	
			Alexa30ed	3	0	0	0	3	0	0	
		rapalog	Alexa29ed	1	1	1	1	0	0	0	
			Alexa28ed	1	0	1	0	0	0	0	
			Alexa27ed	1	0	1	0	0	0	0	
			Alexa26ed	1	2	1	1	0	1	0	
			Alexa24ed	2	0	2	0	0	0	0	
			Alexa22ed	1	0	1	0	0	0	0	
			Alexa21ed	1	0	1	0	0	0	0	
			Alexa18ed	1	0	1	0	0	0	0	
			Alexa23ed	2	0	2	0	0	0	0	
			Alexa25ed	2	0	2	0	0	0	0	
			Alexa26ed2	2	0	2	0	0	0	0	
			Alexa28ed2	1	1	1	0	0	1	0	
			Alexa20ed	2	0	2	0	0	0	0	
	4 h	control	Alexa57ed	2	0	2	0	0	0	0	
			Alexa56ed	2	0	0	0	2	0	0	
			Alexa54ed	2	0	2	0	0	0	0	
			Alexa53ed	2	0	1	0	1	0	0	
		rapalog	Alexa52ed	1	0	1	0	0	0	0	
			Alexa51ed	1	0	1	0	0	0	0	
			Alexa50ed	1	0	1	0	0	0	0	
			Alexa49ed	1	1	1	1	0	0	0	
			Alexa47ed	1	0	1	0	0	0	0	
			Alexa46ed2	1	0	1	0	0	0	0	
			Alexa44ed	2	0	1	0	1	0	0	
			Alexa42ed	1	0	1	0	0	0	0	
			Alexa41ed	1	0	0	0	1	0	0	
			Alexa45ed	1	1	1	1	0	0	0	
			Alexa46ed	1	0	1	0	0	0	0	
	24 h	control	Alexa25ed2	2	0	1	0	1	0	0	
			Alexa24ed	1	0	1	0	0	0	0	
			Alexa22ed	1	1	1	0	0	1	0	
			Alexa21ed	1	0	0	0	1	0	0	
			Alexa20ed	1	0	1	0	0	0	0	
			Alexa19ed	1	0	1	0	0	0	0	
			Alexa18ed	2	0	0	0	0	0	2	
			Alexa15ed	1	0	1	0	0	0	0	
			Alexa15ed2	2	0	2	0	0	0	0	
			Alexa17ed	1	0	1	0	0	0	0	
			Alexa25ed	2	0	2	0	0	0	0	
		rapalog	Alexa13ed	2	0	2	0	0	0	0	
			Alexa11ed	2	0	2	0	0	0	0	
			Alexa10ed	1	0	1	0	0	0	0	
			Alexa08ed	1	1	1	1	0	0	0	
			Alexa07ed	1	0	1	0	0	0	0	
			Alexa06ed	1	0	0	0	1	0	0	
			Alexa14ed	2	0	2	0	0	0	0	
	Timepoint	Treatment	Image	MyoF (FV)	MyoF (V)	Co-Loc (FV)	Co-loc (V)	close foci (FV)	close foci (V)	no co-loc (FV)	no co-loc (V)
<b>Summe</b>	Start	control	n=7	10	0	3	0	6	1	0	
	2 h	control	n=6	9	2	1	1	6	2	1	
		rapalog	n=13	18	4	18	2	0	2	0	
	4 h	control	n=4	8	0	5	0	3	0	0	
		rapalog	n=11	12	2	10	2	2	0	0	
	24 h	control	n=11	15	1	11	0	2	1	2	
		rapalog	n=7	10	1	9	1	1	0	0	
	Timepoint	Treatment	Image	MyoF (gesamt)		Co-Loc (gesamt)		close foci (gesamt)		no co-loc	
<b>Summe</b>	Start	control		10		3		7			
<b>Gesamtauswertung</b>	2 h	control		11		2		8			
		rapalog		22		20		2			
	4 h	control		8		5		3			
		rapalog		14		12		2			
	24 h	control		16		11		3			
		rapalog		11		10		1			
<b>Prozentualer Anteil</b>	Start	control				30		70		0	
<b>Gesamtauswertung</b>	2 h	control				18		73		9	
		rapalog				91		9		0	
	4 h	control				63		38		0	
		rapalog				86		14		0	
	24 h	control				69		19		13	
		rapalog				91		9		0	

## Appendix C

Primers used for cloning and sequencing of DNA samples from Ghanain field isolate

#	Oligo Name	Sequence 5' to 3'
1	1 Kelch13 (PF3D7_1343700) fwd	GGCGTAAATATTCGTGTTATAATTTCTCCAAG
2	1 Kelch13 (PF3D7_1343700) rev	GTGCATGAAAATAAATATTAAGAAG
3	2 Formin2 (PF3D7_1025000) fwd	GAAAAAGATATATACTAAATTTCTACAC
4	2 Formin2 (PF3D7_1025000) rev	CACCATTTTATCATCATTTTCTTCGTCGTCTCC
5	3 Formin2 (PF3D7_1025000) fwd	GCATCTAGGAGAAGAGGAAGAAGAAAATGAAAAG
6	3 Formin2 (PF3D7_1025000) rev	CAAACAAAGGAATATAAAAATAATATATAGGG
7	4 UBP1 (PF3D7_0104300) fwd	CGAAAGAAGAAAATAATAATAATTAATAAAAAGG
8	4 UBP1 (PF3D7_0104300) rev	GGTATATTACTTTCTATAATTTTCATATCACTACTAC
9	5 UBP1 (PF3D7_0104300) fwd	CAATGATAATAATATGAACAGTAATAAACAAC
10	5 UBP1 (PF3D7_0104300) rev	CATAATTGTTTTGTTATCATCATCTTTTGG
11	6 UBP1 (PF3D7_0104300) fwd	GGGTTCAACAAGAAATAGTATAAAAAGGGAGG
12	6 UBP1 (PF3D7_0104300) rev	CTATTGGATATTAATCATCATCGTCACTATC
13	7 UBP1 (PF3D7_0104300) fwd	GATGATAATTTAGGAAATAATATTTCCATCC
14	7 UBP1 (PF3D7_0104300) rev	GTTTAATTTTGTTCGCTATTCTTG
15	8 MyosinC (PF3D7_1329100) fwd	TTTTATTAATATATAAACAATTTAGGGCG
16	8 MyosinC (PF3D7_1329100) rev	CCTCATTGTTGTTGGTTGTATCTTGC
17	9 MyosinC (PF3D7_1329100) fwd	GGCCAATTTTATACTCTCCAGTTTATATGTAAC
18	9 MyosinC (PF3D7_1329100) rev	GTTCACTGTGTTGATTAGGAGGTACAGAGG
19	10 MyosinC (PF3D7_1329100) fwd	GATATATGATATAGTAAATAATTATGC
20	10 MyosinC (PF3D7_1329100) rev	CATAGGAATATATTCAAATGTATACAC
21	11 KB19 (PF3D7_0813000) fwd	GGAAAAAAGAAAGAAGAAATTGTACATAATAAATAAG
22	11 KB19 (PF3D7_0813000) rev	GATACACACATGATATCATACATAAGGC
23	12 Unknown (PF3D7_0609700) fwd	CCATTTTATTAACAACCTTAGATAC
24	12 Unknown (PF3D7_0609700) rev	CTTTCATGTTTGTTCCTTTTCTTTCCCG
25	13 Unknown (PF3D7_0609700) fwd	GTTAATTTTGATGAAATAAATCCTAATGG
26	13 Unknown (PF3D7_0609700) rev	GTAATAATTCGTATTTACTACAATTCGAC
27	14 Unknown (PF3D7_0609700) fwd	CGAATGTAAGGAATATAACCATATG
28	14 Unknown (PF3D7_0609700) rev	GGTGAAAAATATAGAAAATCTAATATTCG

33	1a Kelch13 (PF3D7_1343700) fwd	CCATTGATATGAGTGTATTAGATTGGAAC
34	1b Kelch13 (PF3D7_1343700) fwd	CGGAATTAAGTGATGCTAGTGATTTTG
35	1c Kelch13 (PF3D7_1343700) fwd	GAGAATGATAAAAAAAAAAATTGTTGATGC
36	1d Kelch13 (PF3D7_1343700) fwd	CGATGGAATTATTAGATATTAGTCAAC
37	1e Kelch13 (PF3D7_1343700) fwd	GGGGATATGATGGCTCTTCTATTATACCG
38	1f Kelch13 (PF3D7_1343700) fwd	CATATTAGATTCCGTTGAACAATATCAACC
39	2a Formin2 (PF3D7_1025000) fwd	CGGCCTCTTCTTTCTTCAGAATTCGGG
40	2b Formin2 (PF3D7_1025000) fwd	GTTGTCGCTTGTGCTCATGCTCAGAATGG
41	2c Formin2 (PF3D7_1025000) fwd	CCCCTTTGTTTACCCAGCTTCGATATTGTTAG
42	2d Formin2 (PF3D7_1025000) fwd	CCCTCTTCTGTACCCATGGAGTTGTTAC
43	3a Formin2 (PF3D7_1025000) fwd	CGTCAAGGACATGTTGTGGATAAGGATTTA
44	3b Formin2 (PF3D7_1025000) fwd	GAAGATGCACGGTAAGGGTATGATG
45	3c Formin2 (PF3D7_1025000) fwd	GAAGAGATAAATAGAAAATTGAAGAAGAAAT
46	3d Formin2 (PF3D7_1025000) fwd	GATGAAAAAATCTTATCATTTTGAAAAATATG
47	3e Formin2 (PF3D7_1025000) fwd	GCCTATCGACAATTATGTTTTGTGAACGC
48	3f Formin2 (PF3D7_1025000) fwd	GGTGATAGCGTAGATATTTTTTCAAGCCTTG
49	4a UBP1 (PF3D7_0104300) fwd	CGACTCGTTCAGCTTATCTAATACG
50	4b UBP1 (PF3D7_0104300) fwd	CCATAGCGATAGTATTAATAATAGTATTA
51	4c UBP1 (PF3D7_0104300) fwd	GATGATAATATGGATGACGATGATGATG
52	4d UBP1 (PF3D7_0104300) fwd	GATACCATAGATGATGTTTTTAAAAATAAAG
53	4e UBP1 (PF3D7_0104300) fwd	CATCAAATAGTATGTATAAAGATTATTCG
54	4f UBP1 (PF3D7_0104300) fwd	GCACATGAGGGGTTGTCAAAAAAATGTTG
55	4g UBP1 (PF3D7_0104300) fwd	GATGATATGGAAGAAATGACAAGATTTAG
56	5a UBP1 (PF3D7_0104300) fwd	GGTCTTTCATGAAGATCTTTTAAAGAAG
57	5b UBP1 (PF3D7_0104300) fwd	CATCTTAATAATCATGAGAGTGATGAC
58	5c UBP1 (PF3D7_0104300) fwd	GAACGATTCAGGTGATTTTGCGGTGG
59	5d UBP1 (PF3D7_0104300) fwd	CGCCTTTTACACAATAAACATTTTAAAG
60	5e UBP1 (PF3D7_0104300) fwd	CGAAAAATATGACAAATATGACAAATATG
61	5f UBP1 (PF3D7_0104300) fwd	GAGTGTTTTGATAGAAGAAAATAAGTATG
62	5g UBP1 (PF3D7_0104300) fwd	GGTGGTATAAGAATCGTCGTAATAATTTT
63	5h UBP1 (PF3D7_0104300) fwd	GCTGATGATTTAGTATACTTGTTTAATG
64	6a UBP1 (PF3D7_0104300) fwd	GACGATGATGATAGTATCAACGCTCATC
65	6b UBP1 (PF3D7_0104300) fwd	GGATAAATAAAAAAGATGATTTAC

66	6c UBP1 (PF3D7_0104300) fwd	GTAAATAGAGACATGAGAGAAATCATG
67	6d UBP1 (PF3D7_0104300) fwd	GCATGTCGAATATATCTTTGGCTGgtgag
68	6e UBP1 (PF3D7_0104300) fwd	GAAGAAAGATTA AAAAGGAGAGGAGGTG
69	6f UBP1 (PF3D7_0104300) fwd	CCTCTAATCAAATGCTTCCGGGTGATC
70	6g UBP1 (PF3D7_0104300) fwd	GTTTTCAAAGTTTGAATTGTAATAGAACG
71	7a UBP1 (PF3D7_0104300) fwd	CATCAGAAAAATTTAATGTA AAAAG
72	7b UBP1 (PF3D7_0104300) fwd	GGATTCAAAAAAGTATTATCTCAAAAAA
73	7c UBP1 (PF3D7_0104300) fwd	CGCAAAATAGAATATCCGATCAAATGG
74	7d UBP1 (PF3D7_0104300) fwd	GAATCATGCAAACCGTGTGAGTCCC
75	7e UBP1 (PF3D7_0104300) fwd	GTAACTACAGATAAGTCATATATATC
76	7f UBP1 (PF3D7_0104300) fwd	GTGGAATGAAATTATATCCCTCCTTGTG
77	7g UBP1 (PF3D7_0104300) fwd	GGAGCAATAATACATGGTGGGATATCAGC
78	8a MyosinC (PF3D7_1329100) fwd	CGGATGAATTTTATCTTCGAAATTTAG
79	8b MyosinC (PF3D7_1329100) fwd	GCATGAGGCATCCATATTACATAGTTTG
80	8c MyosinC (PF3D7_1329100) fwd	GAAGCATTGGTAATGCTCGAACATTAAG
81	8d MyosinC (PF3D7_1329100) fwd	CCTAGTACATCAAAATTTAGAAATCTGG
82	8e MyosinC (PF3D7_1329100) fwd	CCATAGTGGCGAATAACGAACATTACAAAAACC
83	8f MyosinC (PF3D7_1329100) fwd	CCTTATGGTGTATTTTGTATGTTAGATG
84	8g MyosinC (PF3D7_1329100) fwd	CCTTATGGTGTATTTTGTATGTTAGATG
85	9a MyosinC (PF3D7_1329100) fwd	CGAAGTTTAAAGCCATTGTTATTGAG
86	9b MyosinC (PF3D7_1329100) fwd	GGAAGAGTATATTAGCTAGAAAAACAATTG
87	9c MyosinC (PF3D7_1329100) fwd	GGATAGTATGGAAATTATGAGTATCCAAGG
88	9d MyosinC (PF3D7_1329100) fwd	GGGACAGATCAAAGATACAAATAATAATG
89	9e MyosinC (PF3D7_1329100) fwd	GTACGTTTAGGTGATGAAGATAATTTAGG
90	10a MyosinC (PF3D7_1329100) fw	CGAAACGAGGAGACATAGGCAAAAAATAAT
91	10b MyosinC (PF3D7_1329100) fw	GTGTTTTAGGACTAGTTTGGAGTTAAAAATG
92	10c MyosinC (PF3D7_1329100) fw	GGGAAGTGTCAACAGGTTTTTTATTA AAAAG
93	10d MyosinC (PF3D7_1329100) fw	CATCACCAGCAATCATTGTA AATTCATGTG
94	11a KBI9 (PF3D7_0813000) fwd	CGAAATCAAAAAATCGACGCTCATCAACTAG
95	11b KBI9 (PF3D7_0813000) fwd	CGATAATAATTTAATGAATTCGATGGGAATC
96	11c KBI9 (PF3D7_0813000) fwd	GCTATGGATAATGCAAATTATTATAACACC
97	11d KBI9 (PF3D7_0813000) fwd	GTGGTTCAGGATTATTACACTCAGGCAATA
98	12a Unknown (PF3D7_0609700) fw	CCCCTTGGATTAGTTTCGTATTATCGTTGTACGG

99	12b Unknown (PF3D7_0609700) fw	CCGCGTGTGGTATTACCAGTTTGAAAGGG
100	12c Unknown (PF3D7_0609700) fw	GAAAATGAGGATGATGAAGAATATGATAG
101	12d Unknown (PF3D7_0609700) fw	CGATAATTATAAGCAGCTACCGTTATG
102	12e Unknown (PF3D7_0609700) fw	GTGATGAGAGTTATCACCACAGTGATAATC
103	12f Unknown (PF3D7_0609700) fw	GAAATTGAAGAAATGAAGAAAAGGTTTAGC
104	12g Unknown (PF3D7_0609700) fw	CATCAAATTCATGTGATGATGATTTTTTTCG
105	13a Unknown (PF3D7_0609700) fw	GAGTACGAAAGAAAAATGACATTGTGG
106	13b Unknown (PF3D7_0609700) fw	CAGAGGATATTATAGGTGATAACCATGTG
107	13c Unknown (PF3D7_0609700) fw	GTATAAAAATGTGCGAGATGATGAGGAAAA
108	13d Unknown (PF3D7_0609700) fw	CATTTGTCCTTTAACCCTTATGAAATATA
109	14a Unknown (PF3D7_0609700) fw	GAGTCATAAATTTGCTCAAATAAATAATTATC
110	14b Unknown (PF3D7_0609700) fw	GATTGTGATGATAATCAAATTGATTGTGG
111	14c Unknown (PF3D7_0609700) fw	CATTATCGATGAAAATTTAAAACGAATTC
112	14d Unknown (PF3D7_0609700) fw	CCACTGTGAGTTGTGTGATGCAACTTATTC
113	1n Kelch13 fw	TTATTTATTCATTATTATTATGTTTTTG
114	1n Kelch13 rv	TATAAAAATAAGAACATTTAAAATTTCTTC
115	2n Formin2 fw	GATATATACTAAATATTTCTACACATATAAT
116	2n Formin2 rv	CCTTTTTACCTTTCATAAAAGGTGTCTTAC
117	3n Formin2 fw	GGAATATGATTTTTTTGAATTTAACAAAGATG
118	3n Formin2 rv	GGGAAAAATAATAAATAAATAAATAAATGATTAAC
119	4n UBP1 fw	GAAGAAAATAATAAATAATAAAAAGGAAAA
120	4n UBP1 rv	GTTGTTATTACTGTTCATATTATTATC
121	5n UBP1 fw	GATAATAATGAACAGTAATAAACAAC
122	5n UBP1 rv	CTGCCATGACACTTTGATCAGCATACATATTGC
123	6n UBP1 fw	CAGCAATATGATGCTGATCAAAGTGCATG
124	6n UBP1 rv	CTAAACATATCATCATATGAAATATAATG
125	7n UBP1 fw	GATGAATTTATTGGATCTTTTTAAAAATAATTC
126	8n MyosinC rv	CTTGAGGAAAGCTTTCCAAAAATTTATTTTCC
127	9n MyosinC fw	GAAATACAAGAAATATAAATAATCTAAAG
128	9n MyosinC rv	GTAATTACAATTATTATGAGTATTATCCAAG
129	10n MyosinC fw	CTTTACATTCTAATTTCTTGGATAATAC
130	10n MyosinC rv	CACATATATATATATATATATATGAACAAAATTTACAATATC
131	UBP1(wt)-3xHA-T2A-Neo fwd	gctatttagtgacactatagaactcaagctgcgccgcTAACCTTTTTAAAAATATGTTAACTACAG
132	UBP1(wt)-3xHA-T2A-Neo rev	GCGTAATCTGGAACATCGTATGGGTACATGGTGGTACCAAAGTACAAATCTGGAGATATGGGTGC
133	UBP1(R3138H)-3xHA-T2A-Neo fw	GGCTCCAATTAGCCCTGACCTTTATTTCCctaggACCATGTACCCATACGATGTTCCAGATTACG
136	UBP1(mutant)-3xHA-T2A-Neo rev	GTTAATAAACTTCCTCTTCTCCTCGTCGACAGCATAAATCTGGAACATCATATGGATACATAG
137	Kelch13 codon ad fw	CTGCTGCTGGTCTGGAGGTGCAGGTAGACCTAGGATGGAGGGTGAGAAGGTTAAGACTAAAAG
138	Kelch13 codon ad rv	CTGCCATATCCCTCGAGTCATAATAACTTCGTATAATGTATGCTATACGAAGTTATAGGCCCTTCAAATGTTAGCAATCAATACTG
141	K13(V520A) mutant fw	CGACAGGTTGAGGGACGTTTGGTACGCTAGTTCAAACCTGAACATCCAAGGAGGAACAACCTGCGG

142	K13(V520A) mutant rv	CCTTGGAATGTTCAAGTTTGAAGTACGCTACCAAACGTCCTCAACCTGTCGTATACCTC
147	UBP1(mutant) Neo rev	GAAAAACGAACATTAAGCTGCCATATCCCTCGAGTTAGAAGAACTCGTCAAGAAGGCGATAG
148	1a Kelch13 rev	GTTCGAATCTAATACACTCATATCAATGG
149	11n KBI9 fw	GAAAGAAGAAATTGTACATAATAAATAAGTAAAA
150	11n KBI9 rv	GATATTACAAATGTATATATAATTTTACTGG
152	UBP1(mut)-3xHA KpnI fw	GCGAGCGTCAGAACAAGAAGAAGTCAAGCTGGTACCAGATGAACGACAGTGTGTTACTAAGG
153	UBP1(mut)-3xHA Sall rv 1	CGGGTACATCGTAGCGTAATCTGGAACATCGTATGGGTACATGGTCCTAGGAAAAAAGGTCAGGGCTAATT GGAG
154	UBP1(mut)-3xHA Sall rv 2	CATGTTAATAAACTTCTCTTCTCTCCGTCGACAGCATAATCTGGAACATCATATGGATACATAGTCGCGTAG TCCGGCACGTCGTACGGGTACATCGTAGCGTAATCTGGA
155	12n Unknown (PF3D7_0609700) rv	CATCGTTATTTTTGTTCCCTCACCACC
156	13n Unknown (PF3D7_0609700) fw	CCACTTTTCTGATGAAAAGGATGAATC
157	13n Unknown (PF3D7_0609700) rv	GTGATGAATTTCTCAATATATCTATAATG
158	14n Unknown (PF3D7_0609700) fw	CTTATTAATGATTAATGAATATAAAC
159	2e Formin2 rev	CAACTTACGAATGGAATCATTTC
160	2f Formin2 rev	CATTTGTTGAATTTAAATCCTTATC
161	3g Formin2 rev	GTATATTTAGGCGTTTGTTTG
162	4h UBP1 rev	CATATGAGATGTAATGTCG
163	4i UBP1 rev	CTCCTTCATAATTATCTGGAAGAG
164	4j UBP1 rev	GTATTCAAATGATTCAAGATCATC
165	6h UBP1 rev	CCTTTTAAACTTGATGAGACGTTG
166	6i UBP1 rev	GGTATAAAATATACTAATAATAATATG
167	6j UBP1 rev	CTATTGGATATATTACTATCATCG
168	8h MyosinC rev	GCTATTAATAAAAAATCCACATAGACC
169	8i MyosinC rev	CCTAAATAAGCACTATTTGAAGTAGC
170	9f MyosinC rev	GCTTTTAAACTTCGAAGATCACTTC
171	10h MyosinC rev	CCTTTAACATATATATCTTTATC
172	10i MyosinC fwd	CCAAATTATCAGGTCATAAAAAGG
173	10k MyosinC rev	GTGTATACATTTGAATATATTCC
174	11e UB/9 rev	GTTTACTTCTATATGAACATTTG
175	11f UB/9 rev	CATTGGATTAATAATCATCTG
176	11g UB/9 rev	GGTGAATAATTATTATTTAAGG
177	KBI5 HR fwd	GCTATTTAGTGACACTATAGAATACTCGCGCCGCTAAGCTATATGTAAGGCAAATATAAAAATGC
178	KBI5 HR rev	GTTCTCTCTATTGAAGTAACTTTCCGAAATAAGTTGCAAATTTTTATTTTTCTTC
179	KBI5 codon adj (mut) fwd	GGAAAAAATAAAAAATTTGCAACTTATTTTCGAAACGTTACTTCAATAGAGAGGAAC
180	KBI5 codon adj (mut) rev	GCACCAGCAGCAGCACCTCTAGCACGCGTTGCTTCGTGCTTTTTATGCATTAACCTATAAGG
181	KBI6 HR fwd	GCTATTTAGTGACACTATAGAATACTCGCGCCGCTAAAAGAACGTTAAACAAAATTTTCAAATTTTAGAG
182	KBI6 HR rev	CTTAATACTACGTTAATCTCTGTGCTTACCTAAAAAGAACAAGGAGCGGAAAATTTGACAGC
183	KBI6 codon adj (mut)1 fwd	GCTGTCAATTTTCCGCTCCTTTTGTCTTTTAGGTAAGCACAGAGATTAACCGTAGTATTAAG
184	KBI6 codon adj (mut)1 rev	GGTGGTAAAGTGACTCCTTATCAAGAAGAC
185	KBI6 codon adj (mut)2 fwd	GAACAGTCAGATAGCAAACAGTCTTCTTGATAAGGAGTCACTTTACCACC
186	KBI6 codon adj (mut)2 rev	CCTCCAGCACCAGCAGCAGCACCTCTAGCACGCGTAAGAATCTGTTTGAAAAGGTTTATTGCG
187	KBI9 HR fwd	GGTGACACTATAGAATACTCGCGCCGCTAATCGTCAGCAACACAATTGGGTATATCAG
188	KBI9 HR rev	GCTTGAGTCAGTAACAACCTCAACGTGCTTTCTAGTTGATGAGCGTCGATTTTTGATTTCG
189	KBI9 codon adj (mut) fwd	CGAAATCAAAAAATCGACGCTCATCAACTAGAAAGCACGTTGAGGTTGTTACTGACTCAAGC
190	KBI9 codon adj (mut) rev	GCACCTCCAGCACCAGCAGCAGCACCTCTAGCACGCGTGAACCTTCTTACTGTCGAATACTGGG

191	KBI1 HR fwd	GGTGACACTATAGAATACTCGCGCCGCTAAACTAATGTTAATAATAATATGAAC
192	KBI1 HR rev	CTTACTTACAACGTTGTTCTTAGCCTTGAAGTTATATAGGAATTATTTAAATATCAG
193	KBI1 codon adj (mut) fwd	CTGATAATTTTAAATAATTCCTATATAACTTCAAGTCTAAGAACAACGTTGTAAGTAAG
194	KBI1 codon adj (mut) rev	GCACCAGCAGCAGCACCTCTAGCACGCGTTTCATTCATGAATATCTTAAAGTTGC
195	KBI2 HR fwd	GGTGACACTATAGAATACTCGCGCCGCTAAGTTAGCGACACAAAATCCGAGGATAG
196	KBI2 HR rev	GGTTAATCTGTGCTTTTAAATAAATCAATCAACTTTAATAAATTTTGTATTTTTATTTTCATTTTGC
197	KBI2 codon adj (mut) fwd	GCAAAATGAAAATAAAAATACAAAATTTATTAAGTTGATTGATTTATTAAGCACAGATTAACC
198	KBI2 codon adj (mut) rev	GCACCAGCAGCAGCACCTCTAGCACGCGTACGTACAACCTGCTTAAAGAAGGTAG
205	KBI11 HR fwd	GGTGACACTATAGAATACTCGCGCCGCTAACAGAATAACAATGCAGTGAATATAG
206	KBI11 HR rev	CTTATTCTGATTCTGATTCTGATTAGCTCTCATAATTTCACTCTGAAATTTTATATTATCGC
207	KBI11 codon adj (mut)1 fwd	GCGATAATATAAAAATTCAGAGTGAATTTATGAGAGCTAATCAGAATCAGAATCAGAATAAG
208	KBI11 codon adj (mut)1 rev	CCTTCTTCTCCATATTCTTCTTCTTCTCG
209	KBI11 codon adj (mut)2 fwd	GCCTATATATTTGAACGAGAAGAAGAATATGGAGAAGAAGG
210	KBI11 codon adj (mut)2 rev	GCACCAGCAGCAGCACCTCTAGCACGCGTGTATGTTAATCTTCTCAAGTGAATATTGC
211	Formin2 HR fwd	GGTGACACTATAGAATACTCGCGCCGCTAAGTTAATAATAATATATGGTCATCCG
212	Formin2 HR rev	GGTAGTTCTCCTTCTCACGACTACGTAACCTCCATTTTAAACTTCTTCCATATTTCG
213	Formin2 codon adj (mut) fwd	CGAATATGGAAGGAAGTTTAAATGGAAGTTACGTAGTCGTGAGAAGGAGAAGTACC
214	Formin2 codon adj (mut) rev	GCACCAGCAGCAGCACCTCTAGCACGCGTTGATGAGTTGTCTACTGATTTAAGTG
215	UBP1 HR fwd	GGTGACACTATAGAATACTCGCGCCGCTAATTAATGAAAAATAGATTTTAGATATGC
216	UBP1 HR rev	CTTGTGGTTCTGAATGAATATCTTACTATATTTTTAATTCATTTTCATCTATC
217	UBP1 codon adj S (mut) fwd	TATATATTATATTTGATAGATGAAAATGAATTAATAATATATAGTAAGATATTCATTCCAGAACCAC
218	UBP1 codon adj S (mut) rev	GGTACTTCTTAATCTTTACACCACCCATGCGAATGTCTTCTATGTTGTTGGTGAAC
219	UBP1 codon adj J (mut) fwd	CGCTAATAGAGTTTCCACAAACAACATAGAAGCATTGCGATGGGTGGTGAAGATTAAGAAGTACC
220	UBP1 codon adj J (mut) rev	CCAGCACCAGCAGCAGCACCTCTAGCACGCGTAAATAAAGGTCAGGGCTAATTGG
221	KBI7 cod adj SEQ 1 fw	ATATACCATTCTTATTACTGAAATTAGAC
222	KBI7 cod adj SEQ 2 fw	GAGTTCCGTAACAAAACACTACATGAGCTGC
223	KBI1 cod adj SEQ 1 fw	GCCCAAAGGAGAACATAAAGAAGAACCAC
224	KBI1 cod adj SEQ 2 fw	CTCAGGGAAAGGAGAACGCATACAAG
225	KBI5 mut SEQ fw	CAATGACAAGAGTGACCAGAATGAGAAGC
226	KBI1 cod adj SEQ 3 rev	CGTTGTCCATGTGGTTAACGTAGTCATAACC
227	KBI11 SEQ 1 fw	CGACAAGAACATACACAACAATAACAAC
228	KBI11 SEQ 2 fw	GCCTTATAGGATGCATTTTCATGCATGTACG
229	KBI11 SEQ 3 fw	GCAAGACAAGTGCCACGTAGACATGGAGTG
230	Formin2 SEQ 1 fw	TTTGAATGATAAATTTGATAATCAATACATAG
231	Formin2 SEQ 2 rev	CTTAATATACTACCCTCAATACGCTCCTCG
232	Formin2 SEQ 3 fw	GAGTTGAACACTACAAGTACAAAGACAAGGAC
233	KBI6 SEQ 1 fw	CGTTAACATTTTCATAACAATTAAGAGC
234	KBI6 SEQ 2 fw	CCAGTTCTCAAACACTTCAACAACATGCC
235	KBI6 SEQ 3 fw	GAAGCACAAGCATAAAGAGATAAACGAGTAC
236	KBI6 SEQ 4 fw	CCACAGTTCAATGACTAACAAGCAGAAAAC
240	Formin2 SEQ 4 rv	CTAATGTTCCAAATCTGCATAAGTTCCG
241	5'UTR KBI2 mut intcheck fw	ATTTACATTTGTGTTGCATAATTTGAAATC
242	KBI2 mut cod adj intcheck rv	CGTTACGAAGCTTGAAGTCAACTCCATC
243	3'UTR KBI2 mut intcheck rv	GTCGTGTACCCATTTATATATTTCTCTGG
244	5'UTR KBI5 mut intcheck fw	GATATATAATATTTATTTATTTTGAATTTGTTT
245	KBI5 mut cod adj intcheck rv	GGTACTCGCACTCCCTACTAAGTATGTTCC
246	3'UTR KBI5 mut intcheck rv	ATATTCACATTCTCGTGATAAAATATTTTCG

247	5'UTR KBI9 mut intcheck fw	TACATCTGCTTTAGGAAAAAGAAAGAAG
248	KBI9 mut cod adj intcheck rv	CTTCTCGTCGATTCACTGTCGCTTGAG
249	3'UTR KBI9 mut intcheck rv	TTTCATCATACTCTGAATCAGAACTATCTG
253	5'UTR KBI11 mut intcheck fw	AAGAAAAAAGAAAAATAATGTAAGAAATATAAG
254	KBI11 mut cod adj intcheck rv	ATTCTGATTCTTATTCTGATTCTTATTCTG
255	3'UTR KBI11 mut intcheck rv	GGTTTTGTTTTGGTTTTGTTTTGGTTTTGG
256	5'UTR KBI1 mut intcheck fw	CCCCCTCTTTTTTTTTTAATGTTTCATGTG
257	KBI1 mut cod adj intcheck rv	CAGCATCGCACTTGTATGATCCACTTTAC
258	3'UTR KBI1 mut intcheck rv	TATTTCTGCGTCACATTATAACTCCCCG
259	5'UTR Form2 mut intcheck fw	GGAACAATGAATAAAGCTTTAAGGATATG
260	Form2 mut cod adj intcheck rv	CTTAATGTCAAGACTCTGAAAATACGCTGG
261	3'UTR Form2 mut intcheck rv	CTATTCTTTCTTATTTTTATATCCAATG
262	KBI11 SEQ 4 fw	CCAGAAGGGTATAATATTCGACATTAACGAGG
267	15 Ap2mu (PF3D7_1218300) fw	GTAAACACGATTAGCGTCATTTGTTCTTCCG
268	15 Ap2mu (PF3D7_1218300) rv	TTTGTTGTTCTTGTGTTGAAGTAACACCCG
269	15n Ap2mu (PF3D7_1218300) fw	GTTCTCCGTTTTATCAATAGATTTG
270	15n Ap2mu (PF3D7_1218300) rv	CCTTGTTTGAAGTAACACCCGATTG
271	15a Ap2mu (PF3D7_1218300) fw	GAAATATGTGATGAAATAATAGATTATGG
272	15b Ap2mu (PF3D7_1218300) rv	TTTTAATATATTCACCTCTAATGTTGTGG
273	15c Ap2mu (PF3D7_1218300) fw	TTTAATTATATAACAGGTAATTGTACATGG
274	15d Ap2mu (PF3D7_1218300) fw	GATAATGAAGAAATAATTATTGATAATTGC
275	15e Ap2mu (PF3D7_1218300) fw	AATGTTCAAGTTAAATATAAATCCATAGGC
276	MyoC(wt)-3xHA-T2A-Neo fw	gctatttagtgacactatagaataactcaagctgcgccgcTAATCTCAGAAGATAAAATTATTTTCATCATC
277	MyoC(wt)-3xHA-T2A-Neo rv	CGTAATCTGGAACATCGTATGGGTACATGGTGTACCTACAAAAGACCTGCGCCAGAAAACATG
278	MyoC(N277S) HR fw	gctatttagtgacactatagaataactcaagctgcgccgcTAAGAAGGTGCAAATAAATGTGTACATAGGAAC
279	MyoC(N277S) HR rv	CGTTGTTTGACATTATACTGTTGTCAACTATACTTGCCCTTTTACAGCTTTACAAAAGTTGG
280	MyoC(N277S) cod adj fw	CATATTTTTACCAACTTTGTAAAGCTGTAAGAGGCAAGTATAGTTGACAACAGTATAATGTCAAAACAACG
281	MyoC(N277S) cod adj rv	GCGTAATCTGGAACATCGTATGGGTACATGGTGTACCAACGAAGCTACGTCTCCAAAATACAATATTACCC
282	MyoC(S969P) HR fw	ttagtgacactatagaataactcaagctgcgccgcTAATTGTTACATAGTAAGAATACATATGTATCCC
283	MyoC(S969P) HR rv	CGTTTACGTATAATGTAAGTGTATATGTAGGACAAATCAACTTTTTCAGCTTCTGTCTTTTTAATTTTC
284	MyoC(S969P) cod adj fw	GAAATTAAGACAAGAAGCTGAAAGTTGATTTGTCCTACATATACACTTACATTATACGTAACG
285	MyoC(S969P) cod adj rv	GTAATCTGGAACATCGTATGGGTACATGGTGTACCAACGAAGCTACGTCTCCAAAATACAATATTACCC
286	MyoC(S1457L) HR fw	gctatttagtgacactatagaataactcaagctgcgccgcTAAATATAAACAAGAAGAAAAATAAAGAAC
287	MyoC(S1457L) HR rv	GAAAAGACTCTCCTCAACGTTCTTGTACTAAGATATCCCAATCTACAATTTTTATTGGGAAC
288	MyoC(S1457L) cod adj fw	GTTCCCAATAAAAATTGTAGATTGTGGATATCTTAGTAACAAGAAGCTGAGGAGAGTCTTTTC
289	MyoC(S1457L) cod adj rv	CTGGAACATCGTATGGGTACATGGTGTACCAACGAAGCTACGTCTCCAAAATACAATATTACCC
290	MyoC S969P SEQ1 fw	CCCGTTTTGGTGATGCTAATGAAGAAGAGG
291	MyoC S969P SEQ2 fw	GGTGATTTGAAGATACGTAACACTATTCTGTAACG
292	MyoC S969P SEQ3 fw	CGCAACAAGATTACACTTCACAGCAACTAC
293	MyoC S969P SEQ4 fw	AGTCATCATCAATAATGAGTCTTAAAAACG
294	MCA2(wt)-3xHA-T2A-Neo fw	ggtgacactatagaataactcaagctgcgccgcTAATGAGTACTACCAGATGACATCAAATTTTTATCAC
295	MCA2(wt)-3xHA-T2A-Neo rv	CTGGAACATCGTATGGGTACATGGTGTACCGGAAACACATTTAATATTCAAATCGATAATACC
296	MyoC(D500G) HR fw	gacactatagaataactcaagctgcgccgcTAAGAATCAACAAAATATGTTATGAAATTTTTAGC

297	MyoC(D500G) HR rv	GTCAAGAACTCCGCAGAAAAGGTTAATGCCTTTTATATATCCTATAGATTCAATTTGTTCTTTCAACC
298	MyoC(D500G) cod adj fw	GAAAGAACAATGAATCTATAGGATATATAAAAGGCATTAACCTTTTCTCGGGAGTCTTGACATATTCG
299	MyoC(Q635H) HR fw	gglgacactatagaataactcaagctgcggcgcTAAGATCATATAGAAAATAACATTTGTGAGGAACCC
300	MyoC(Q635H) HR rv	CTCTAAGAATCCTGTGCTGTTGTAAACTACGTGCCAGCAAATGTACAATAATAAACTACTAG
301	MyoC(Q635H) cod adj fw	GTAGTTTTATTATTGTACATTTTGTGGGCACGTAGTTTACAACAGCACAGGATTCTTAGAGAAG
302	MCA2 (Y1334.)-GFP fwd	gglgacactatagaataactcaagctgcggcgcTAAATAATTTTAGCAAACCAATTTTTAGATAAATTTTTTATG
303	MCA2 (Y1334.)-GFP rev	CAGCACCAGCAGCAGCACCTCTAGCacgctTTTTTTAATTGTTTCATATAACTTTTTATTTTTGGTC
304	MCA2(Y1344.)-3xHA fw	gglgacactatagaataactcaagctgcggcgcTAAATAATTTTAGCAAACCAATTTTTAGATAAATTTTTTATG
305	MCA2(Y1344.)-3xHA rv	CTGGAACATCGTATGGGTACATGGTGGTACCTTTTTTAATTGTTTCATATAACTTTTTATTTTTGGTC
306	UBP1 mut SEQ1 fw	CGTTCATTTATAAAAATTAATATTTAATTGG
307	UBP1 mut SEQ2 fw	CATTCCTTTCTTCAAGAAGTACTACTTCC
308	UBP1 mut SEQ3 fw	CTTCAACGTTAAGGACTTCATTACTAACC
309	UBP1 mut SEQ4 fw	GGACGCAGTTAACTCAGTTAACCACGTTAAC
310	Intcheck UB1(wt)-3xHA fw	GTCAAATGCATCAAGAGAATACGAATAGTG
311	Intcheck UB1(wt)-3xHA rv	GCCTATACAATATTTATGTTTAAATTTTTGTTTCGC
312	16 Ap2a (PF3D7_0617100) fw	GTAACCAATAATTTATATAATAATAAAAGACACAAC
313	16 Ap2a (PF3D7_0617100) rv	GATCTGATAAATATCTATAACACTTCATAGC
314	17 Ap2a (PF3D7_0617100) fw	GAAAGTAACAATAGTAATAATAATAGCAAC
315	17 Ap2a (PF3D7_0617100) rv	TAAAATATTACAATAATAAAAAGAGAACAG
316	16n Ap2a (PF3D7_0617100) fw	TAAATAAAAGACACAACAATAATTACAC
317	16n Ap2a (PF3D7_0617100) rv	CACTTCATAGCTGCATAAGTTTGTACTTTC
318	17n Ap2a (PF3D7_0617100) fw	GTAATAATAATAGCAACAATAATAACAACAAC
319	17n Ap2a (PF3D7_0617100) rv	CAATAATAAAAAGAGAACAGATGTTATAGATTG
320	16a Ap2a (PF3D7_0617100) rv	CATTATTTTTATATCTGCTTTTATGGTAC
321	16b Ap2a (PF3D7_0617100) fw	GAGTCAATGTATTATTATATAAAAAAGGAAG
322	16c Ap2a (PF3D7_0617100) fw	CATTGAATATGGTATTATTATGAATGTTCC
323	17a Ap2a (PF3D7_0617100) fw	tatlttcagACATGCCGTTATTGACTTTAACG
324	17b Ap2a (PF3D7_0617100) fw	CTCACTGTATCAGACATCTTTTACAATATACCC
325	17c Ap2a (PF3D7_0617100) fw	ttgglagATTGGAATGCTCATATGCGCATC
326	18 MCA2 (PF3D7_1438400) fw	CATTGATGTTTCTCTAGGGAGAATTTCTTCC
327	18 MCA2 (PF3D7_1438400) rv	GTATTACTACTAGGTAAGAAAACGCCACTGTTTGG
328	18n MCA2 (PF3D7_1438400) fw	GAATTTCTCCAACATGATATTCAAAATACAATC
329	18n MCA2 (PF3D7_1438400) rv	GATTTAAAATATTAATATTATTCAAAGTTTTCTCATTATCC
330	18a MCA2 (PF3D7_1438400) fw	CTTGATATAACACAAAATGAAAACCAAACGC
331	18b MCA2 (PF3D7_1438400) rv	GTACGAATCTTTCATAGTGAATAGGAACCCG
332	MyoC mut HR fwd	gclatttagtgacactatagaataactcaagctgcggcgcTAAATAATCGAGTGTATATGAATTAATGAAG
333	MyoC mut HR rev	CTTCTCTCTCTCGTTTGCCTGTCGCATACGGGATCATATACAATATCTTTCATATTATTATTATTGTTCC G
334	MyoC mut cod adj (mut) fwd	CGAACAATAATAATAATATGAAAGATATTGTATATGATCCCGTATGCGACGACGCAACGAGGAGGAAGAG

335	MyoC mut cod adj (mut) rev	GCACCAGCAGCAGCACCTCTAGCacgcgtAACGAAGCTACGTCTCCAAAATACAATATTACCC
336	MCA2 mut HR fwd	gctatttagtgacactatagaactcgcggccgctaaAATAGTATGAACACATATTCGCCCTTTATATAGTTCC
337	MCA2 mut HR rev	GCTGGTTAATCTCGTAAGGAAGCTCGTTGTATAAGTAATTCCTAATTAACATATCAGCTGACC
338	MCA2 mut cod adj (mut) fwd	GGTCAGCTGATATGTTAATTAGGAATTACTTATACAACGAGCTTCCTTACGAGATTAAACCAGC
339	MCA2 mut cod adj (mut) rev	CAGCACCAGCAGCAGCACCTCTAGCacgcgtACTTACGCACCTTATGTTAAGGTCTATTATTCC
340	MyoC S1457L SEQ1 fw	GAATAGTGGATATTCTGTATGTGGACCAAGG
341	K13 (V589I) mut rv	GTTCAACCTTTCTCCGTTTGTACCTCCTATAATGTATATCTTGTTCGAATGCTACGCACATTGC
342	K13 (V589I) mut fw	CAATGTGCGTAGCATTGCAACAAGATATACATTATAGGAGGTACAAACGGAGAAAGGTTGAAC
343	Kelch13 SEQ1 fw	CTTGAACATTCCAAGGAGGAACAACCTGCGG
344	K13 (E612K) mut rv	CCTTGCCTCCAACAATGCGTAAGGGAAGTCTTCCACTTGTTCATCTTCTCCTCGTAAACCTC
345	K13 (E612K) mut fw	GAGGTTTACGAGGAGAAGATGAACAAGTGAAGCAGTTCCCTTACGCATTGTTGGAGGCAAGG
346	5' MyoC(S969P) intcheck fw	CTACTGTTTTCTTGAATAAATAAGGATCAG
347	3' MyoC(S969P) intcheck rv	CAGCAATTTCTTTTATGTAATAAATCTCTTTC
348	MyoC (S969P) intcheck ca rv	GCCTGAATCTTTGAAGCGTAGTAGTTCTGACGG
349	5'UTR UBP1 mut intcheck fw	GAAATCTTTGAAAAATATTTTAATGCTGATG
350	UBP1 mut cod adj intcheck rv	GAACGTGTTGAAGTTAATCTTGTGTTCTG
351	3'UTR UBP1 mut intcheck rv	CCCAAAATAATATACACATAATATTCATATAG
360	MyoC mut SEQ 1 fwd	GTAAAATTATAAGTAAGCATACATCGAGTAG
361	MyoC mut SEQ 2 fwd	GAACATTAAGCAAAAAAAGAACAACAAGGAG
362	MyoC mut SEQ 3 fwd	CTTCGTAAGAACAAAAAGTTAGTTAAACAACG
363	MyoC mut SEQ 4 fwd	GGAATACAGAAGTCAAAACAAAAAACCCAGC
364	MyoC mut SEQ 5 fwd	GTCTTCTTAGGATTGTTAACCTTAACTCAGG
365	5'UTR MyoC mut intcheck fw	GAAAATAGATTTTACAGATTTTAAAGAACATGTAC
366	MyoC mut cod adj intcheck rv	GCTCCAATAAAAAGGTTATTCTTCTCTCC
367	3'UTR MyoC mut intcheck rv	GAATAAATTGTTTTTTTCTCTTCTCATTAGC
368	AP2a-16d-fw	GTATTTAGATATAATAAAATTGATAAGTAG
369	AP2a-16e-rev	CATTGACTCATATTTTGAATAATTA
370	AP2a-16f-rev	CTACTTTTATTGTTATTATTATAATC
371	AP2a-16g-rev	CAATTTCTTCAATATTAATGTACACTC
372	AP2a-17d-rev	GTATATGCATTTATGTGTTTGC
373	AP2a-17e-rev	CATATATATATATATATATTATCC
374	AP2a-17f-rev	CTATATTATTCTTATTTATGAACATTATG
375	AP2a-17f-fw	CATAAATGTTCAATAAAGAATAATATAG
376	AP2a-17g-rev	CAATACACTTTAAATATTTTAAACTTG
377	AP2a-17h-fw	GATCTATATAAAAATACCATATTATAC
382	Eps15 HR mut C-term fw	glgacactatagaactcgcggccgctaagACGATGTAACCTTTTCGACAGAATGCTGATG
383	Eps15 HR mut C-term rv	CGTTGTCGTTGTTGTTGTCGTAAGTGTGTTATTATTATTATCATATGATTATTATTATTATTATCATATG
384	Eps15 CA (mut C-term) fw	GATAATAATAATAATAATAATACATATGATAATAATAATAAACAACACTTACGACAACAACAACGACAACG
385	Eps15 CA (mut C-term) rv	GCACCAGCAGCAGCACCTCTAGCacgcgtTGATGAGTTGCTACTGATTTAAGTGAGTTG
386	Eps15 mut SEQ5 fw	GAGATAAAAATAAAAAGAAGATGCACGGTAAGGG
387	Eps15 mut SEQ6 fw	CATGATTGACTACCTTAAGAAGCAGAAGCAGCG
388	5'UTR Eps15 mut intcheck fw	cattttattcaattattatccctcc
389	Eps15 mut CA intcheck rv	GTCAACCATTCGTTGTCGTTGTTGTTGTCG
390	3'UTR Eps15 mut intcheck rv	CAAATGGAAATCTTTATCCACCATACCATTATC
391	K13(V520I) mutant rv	CCTCCTTGGAATGTTCAAGTTTGAACCTTATGTACCAACGTCCTCAACCTGTCGTATACC
392	K13(V520I) mutant fw	GGTATACGACAGGTTGAGGGACGTTTGGTACATAAGTTCAAACCTTGAACATTTCAAGGAGGAAC
395	Myo N277S SEQ1 fw	GCTTTACATGGAGGAGGAATAAGGTGGGACCC

396	Myo N277S SEQ2 fw	GTAAAAAGAATAAGAAGATGCAGGACACTACAAC
397	Myo N277S SEQ3 fw	GAAATCAATTCTTGCACGTAAGCAGCTTCGTCG
398	Myo N277S SEQ4 fw	TATTAGAGAAGGTTCCGGTGTGTGATCAAC
399	Myo (S1457L) Blpl fw	ACAGGACAACATTAACAAAACTACACTTTGCTTAGCGTTGGTTGCAAAGACGGAGTAATTTAC
400	Myo D500G SEQ1 fw	TGGATGTTTTATTTTTAAAAGTGGTTGAAAG
401	MCA2 mut SEQ1 fw	ccttatattatataatgttgccattgtgaac
402	MCA2 mut SEQ2 fw	GTGAATAATATGAATAATATGAATAATGTG
403	MCA2 mut SEQ3 fw	GAAAAACAGTAATCGTGCAGTAGTTATGCC
404	MCA2 mut SEQ4 fw	GTAATAACGTAGACAAGAAGAACAACGACG
405	MCA2 mut SEQ5 fw	GAGAACAGTTTGTACAACCTCACTACTCACC
406	MCA2 mut SEQ6 fw	CTATACAATGAAGGACAGTTATATTAGTAGTC
407	MCA2 mut SEQ7 fw	AAGAAGCTTCAGGTTGTAAGCAGCTTTGC
408	Intcheck 5UTR MCA2 wt fw	GGAATATAATTTGAAATATGTAAAAATTTAACTGTCC
409	Intcheck 3UTR MCA2 wt rv	CATAAACACAAAAATTTAAAGATGGAGTGG
410	Intcheck 5UTR MyoF wt fw	CAAATTATCAGGTCATAAAAAGGCAATAACATG
411	Intcheck 3UTR MyoF wt rv	ATATATATATATATGAACAAAATTTACAATATC
412	Intcheck 5UTR MyoF 277 fw	AAAAATTTTATTTAATATATAACAAAATTTGATAGGG
413	Intcheck 3UTR MyoF 277 rv	CATTTTCATTATTACTCATAATTGAATTATCC
414	Intcheck MyoF 277 CA rv	GTTCTCAACATCGTCGTTCTCGTTGTTGAC
416	Intcheck 5UTR MCA2 (Y1344.) fw	ATCCATAACAATAATAATAATATTGAGTGG
417	Intcheck 3UTR MCA2 (Y1344.) rv	AACTTTTTTGTGTTTGGTATCTTTGTCAAGC
418	Intcheck 5UTR MyoF (S1457L) fw	CGAATGAGTGTATTTCCCGAGGCATGTATC
419	Intcheck 3UTR MyoF (S1457L) rv	GTAGCATCAAATACTACAATTATACATATTG
420	Intcheck MyoF 1457 CA rv	GTTCTTAATGTAGTTGAAAAGACTCTCCTC
421	Intcheck 5UTR MyoF (Q635H) fw	CGAAAATTATGTAATTATAAATGTGATGAAG
422	Intcheck 3UTR MyoF (Q635H) rv	TTTTTTCAAGAAAACCAGTAGAATTATACAC
423	Intcheck MyoF 635 CA rv	CTTGTCTCTCTCTAAGAACTCTGTGCTGTTG
424	Intcheck 5UTR MyoF (D500G) fw	CAAACAATATTAATTAGTGGTGAATCAGGTGC
425	Intcheck 3UTR MyoF (D500G) rv	GATTCAAATCCAAGATATCTAATACACCAC
426	Intcheck MyoF 500 CA rv	CTCGAAACCGAATATGTCAAGAACTCCGCAG
428	HR MyoF wt (N-term) fw	gglgacactatagaataactcgccgcTAAGAAGGTGCAAATAAATGTGTATAGGAACAAAG
429	HR MyoF wt (N-term) rv	CCTCTTCTGATATTAACCTCTGCTGTTAAACCTGAAGGAGCAGACAACCCTCGAATCAAATAAG
432	1g Kelch13 (PF3D7_1343700) rv	CAAATAAAGCCTTATAATCATAGTTATTACCACC
433	5UTR KBI6 mut intcheck fw	GATTTGATTATAAAATAGATCTTATAACCAGG
434	KBI6 mut cod adj intcheck rv	CTCGAATAACTTAATACTACGGTTAATCTC
435	3UTR KBI6 mut intcheck rv	CTTACGGTACCATCTTTTTGTGTTCTCTCTC
437	Intcheck 3' MyoF 277 rv neu	CATCACATTTATAATTTACATAATTTTCGACGTC
439	5UTR KBI11 mut intcheck fw neu	TTTTTTTTTGATGTACAATAATTAAGAG
440	3UTR KBI11 mut intcheck rv neu	GATGACTATTATTAATATTGTTGTTGATGTTG
441	5 intcheck MyoF (Q635H) fw neu	CAATTATGAGTAATAATGAAAATGATGACGTCG
442	3UTR intcheck MyoF (Q635H) rv neu	CAATTTCTGTGCATCTAAGATAACTGATCC

443	MCA2 mut SEQ8 rv	GGTTTGAGTTATAGTACTGCATTATGTTACGG
444	MCA2 mut HR NEU fwd	gctatttagtgacactatagaactactcgccgcccgttaaAGTGAAAATGATAGAAACGAATCTATACAG
445	MCA2 mut CA SnaBI rev	GCAGCCCTAGTAATGTTTGAAGTTTTTACTACGTAGTCATTATACGGTTGTTGTTTGAATATATCTTC

## Appendix D

**Appendix D.1** Mutations found in the different candidates by sequencing of field isolate DNA obtained from the Fever without source study in Ghana (PCR and sequencing was kindly performed by Birgit Förster) [Hogan *et al.* 2018]. Prevalence (%) is indicated in case, they were already listed in MalariaGEN (*Pf* Community Project).

Candidate	Mutation	Type	Base exchange	West Africa	Central Africa	East Africa	South Asia	SEA (West)	SEA (East)
Kelch13 (PF3D7_1343700)	no mutation found								
UBP1 (PF3D7_0104300)	N1710S	non-syn	AAC/AGC						
	K1914N	non-syn	AAA/AAC						
	E1915K	non-syn	GAA/AAA						
	1283F	syn	TTT/TTC	99,8	99,7	100	100	100	100
MyosinF (PF3D7_1329100)	N277S	non-syn	AAC/AGC	32,9	38,6	41,5	71,4	67	54,8
	I568V	non-syn	ATA/GTA	79,7	70,9	72,4	90,4	99,7	100
	C1196S	non-syn	TGC/AGC	99,9	100	100	100	100	100
	H1587R	non-syn	CAT/CGT						
	N1615K	non-syn	AAC/AAA						
	M1872L	non-syn	ATG/CTG	93,2	91,6	94,7	84,8	99	94,3
	T1930S	non-syn	ACA/TCA	94,5	93,8	95,9	86,7	99	94,9
	1896S	syn	TCA/TCT	93,2	92,2	95,5	87	99	94,9
	1728S	syn	TCC/TCT	87,8	89,8	89,9	98,6	100	100
1870S	syn	AGC/AGT	93,2	91,6	94,7	84,5	99	94,3	
KIC6 (PF3D7_0609700)	Y1215C	non-syn	TAT/TGT	34,6	27,7	31,4	51,6	82,9	96,8
	D1651N	non-syn	GAT/AAT						
	K1652Q	non-syn	AAA/CAA						
	D1658N	non-syn	GAT/AAT						
	K1659Q	non-syn	AAA/CAA						
	D1672N	non-syn	GAT/AAT						
	D1675N	non-syn	GAT/AAT						
	1848N	syn	AAT/AAC	39,7	36,3	38,6	11,7	1,5	3,5
1671D	syn	GAT/GAC							
KIC7 (PF3D7_0813000)	no mutations found								

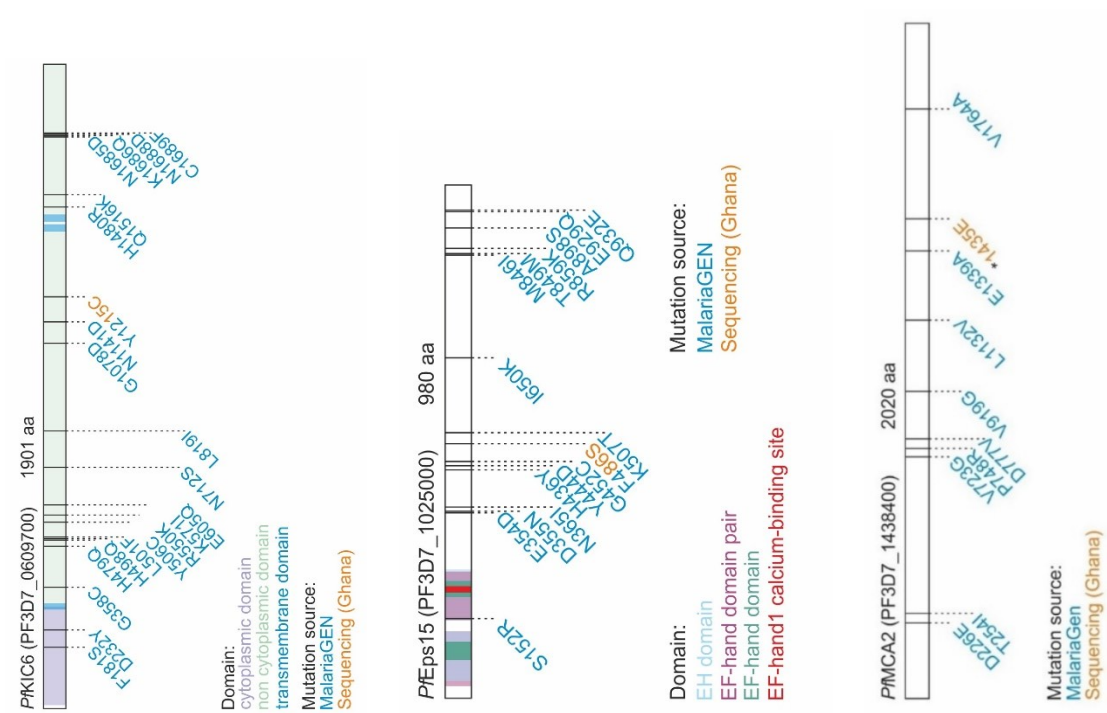
Ap2 $\mu$ (PF3D7_1218300)	no mutations found								
Ap2a (PF3D7_0617100)	709N	syn	AAT/AAC						
MCA2 (PF3D7_1438400)	1435E	syn	GAG/GAA	21	14,9	14,8	50,4	75,3	71,2
Eps15 (PF3D7_1025000)	<b>F486S</b>	non- syn	TTT/TCT	90,7	92,5	93,3	97,5	99,1	98,9

**Appendix D.2** Prepared multipools that were not finished until the end of the thesis. Recodonized sequence was ordered and produced by GenScript®.

Candidate	Mutation	Reference
<i>PKIC6</i> (PF3D7_0609700)	C1689F	MalariaGen
	D232Y	MalariaGen
	E605Q	MalariaGen
	F181S	MalariaGen
	G1078D	MalariaGen
	G358C	MalariaGen
	H1480R	MalariaGen
	H479Q	MalariaGen
	H498Q	MalariaGen
	K1686Q	MalariaGen
	K571I	MalariaGen
	L501F	MalariaGen
	L819I	MalariaGen
	N1141D	MalariaGen
	N1685D	MalariaGen
	N1688D	MalariaGen
	N712S	MalariaGen
	Q1516K	MalariaGen
	R550K	MalariaGen
	Y1215C	MalariaGen & Sequencing Ghana
Y506C	MalariaGen	
<i>PEps15</i> (PF3D7_1025000)	S152R	MalariaGen
	E354D	MalariaGen
	D355N	MalariaGen
	N365I	MalariaGen
	H436Y	MalariaGen
	Y444D	MalariaGen
	G452C	MalariaGen
	F486S	MalariaGen & Sequencing Ghana
	K507T	MalariaGen
	I650K	MalariaGen
	M846I	MalariaGen
	T849M	MalariaGen
	R859K	MalariaGen

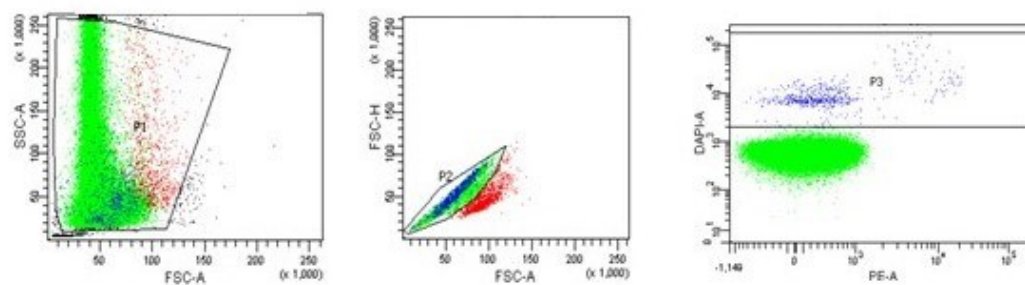
	A898S	MalariaGen
	E929Q	MalariaGen
	Q932E	MalariaGen
PMCA2 (PF3D7_1438400)	D226E	MalariaGen
	T254I	MalariaGen
	V723G	MalariaGen
	P748R	MalariaGen
	D777V	MalariaGen
	V919G	MalariaGen
	L1132V	MalariaGen
	E1339A	MalariaGen
	V1764A	MalariaGen

### Appendix D.3 Schemes of multipools corresponding to Appendix D.2.

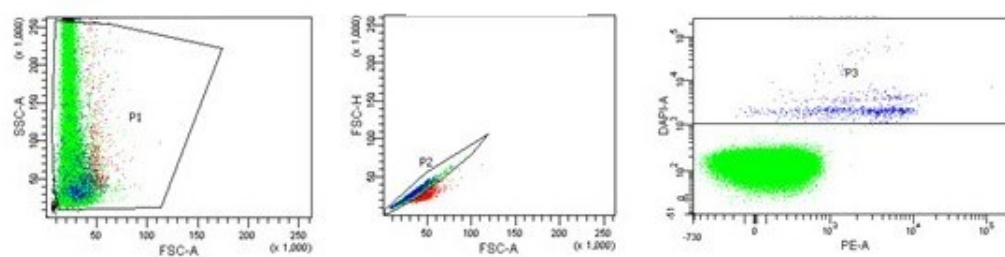


## Appendix E

### Appendix E.1 Gating strategy growth curve (FACSDiva Version 6.1.3).

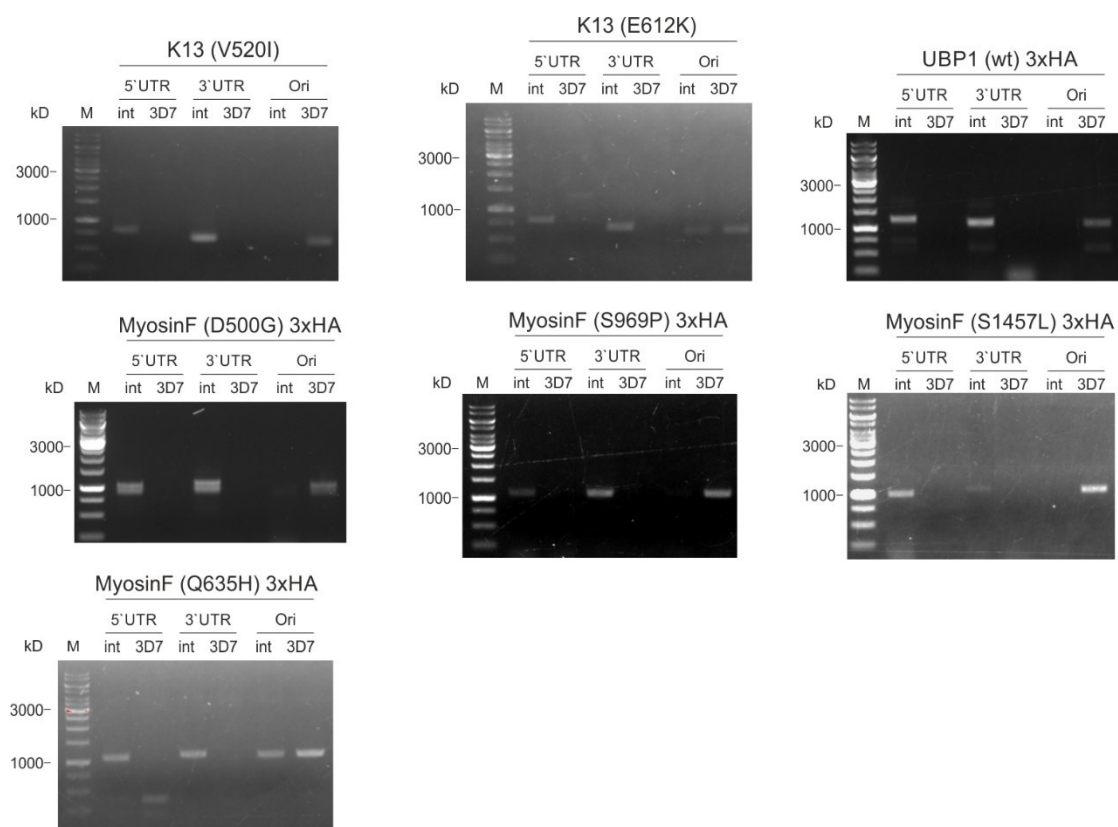


### Appendix E.2 Gating strategy fitness assay (FACSDiva Version 6.1.3).

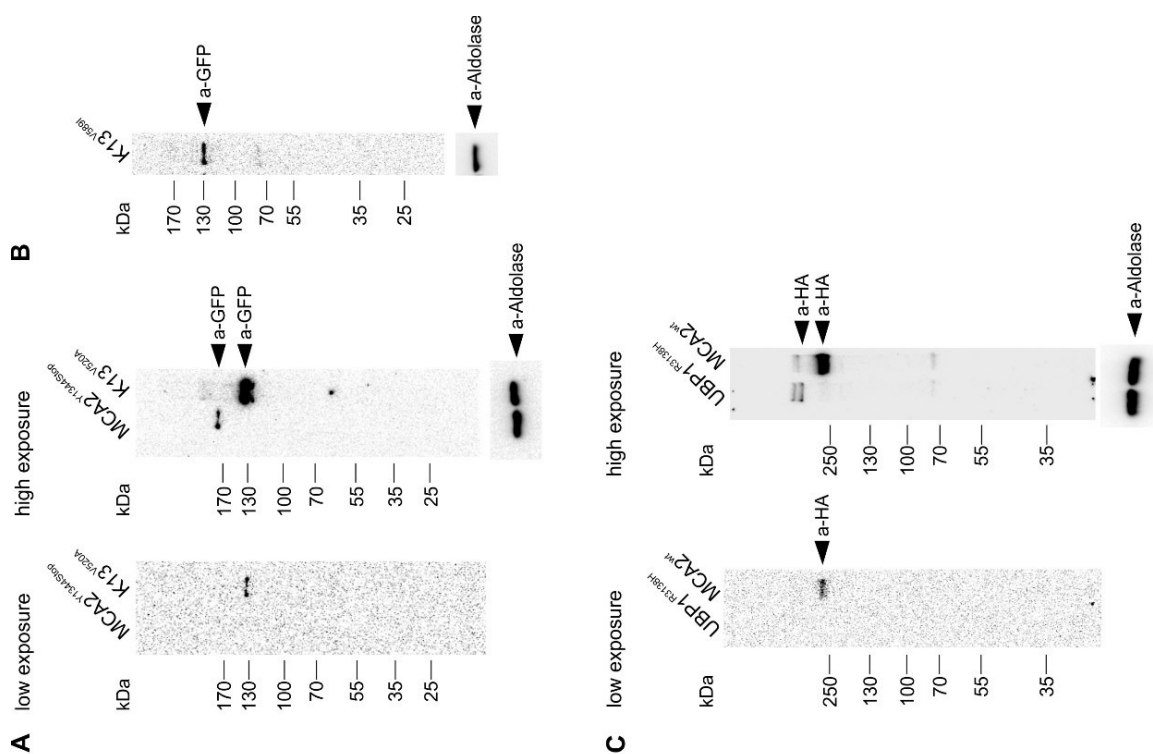


## Appendix F

## Appendix F.1 Integration checks of cell lines transfected with SLI-plasmids.

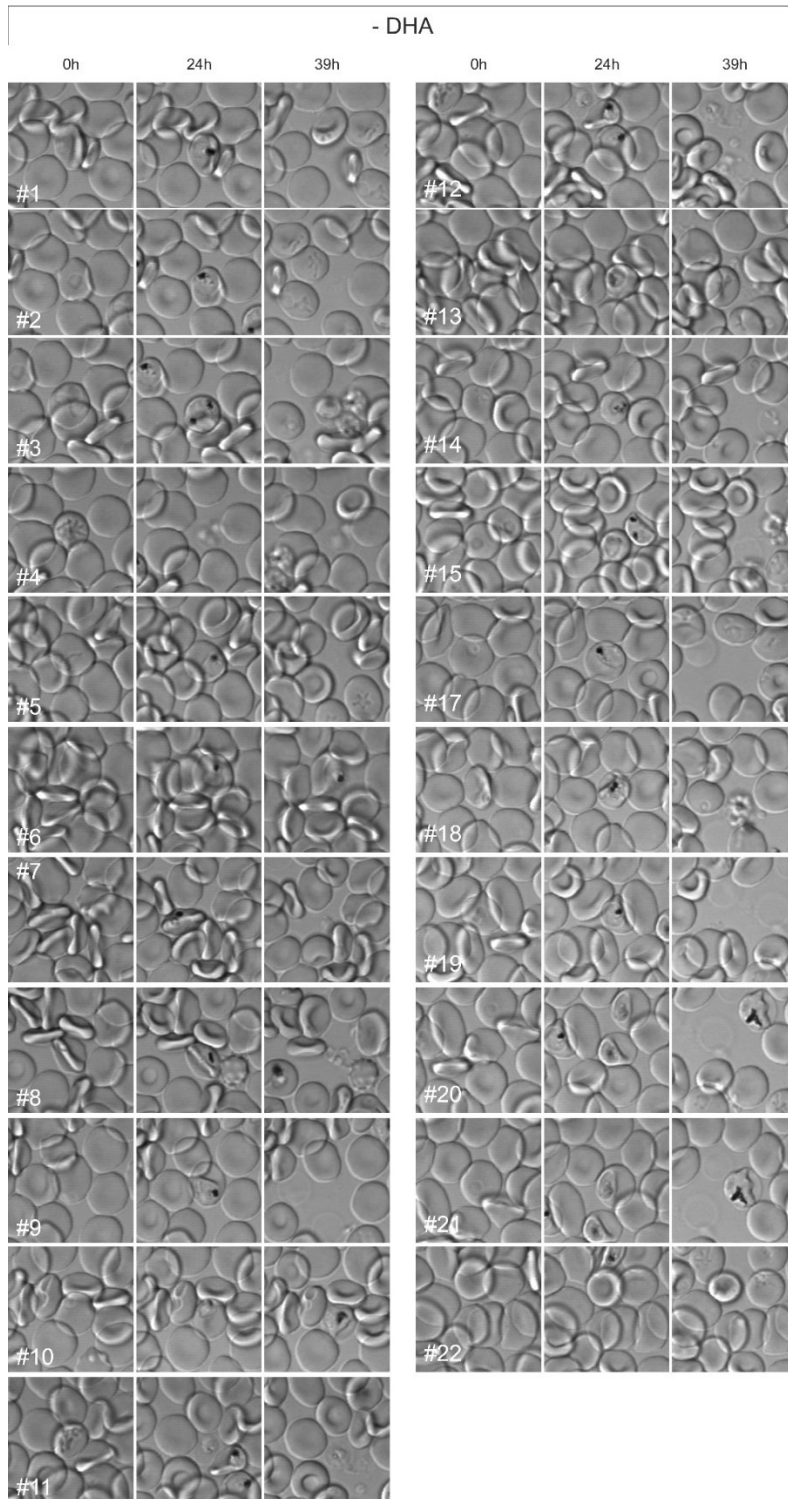


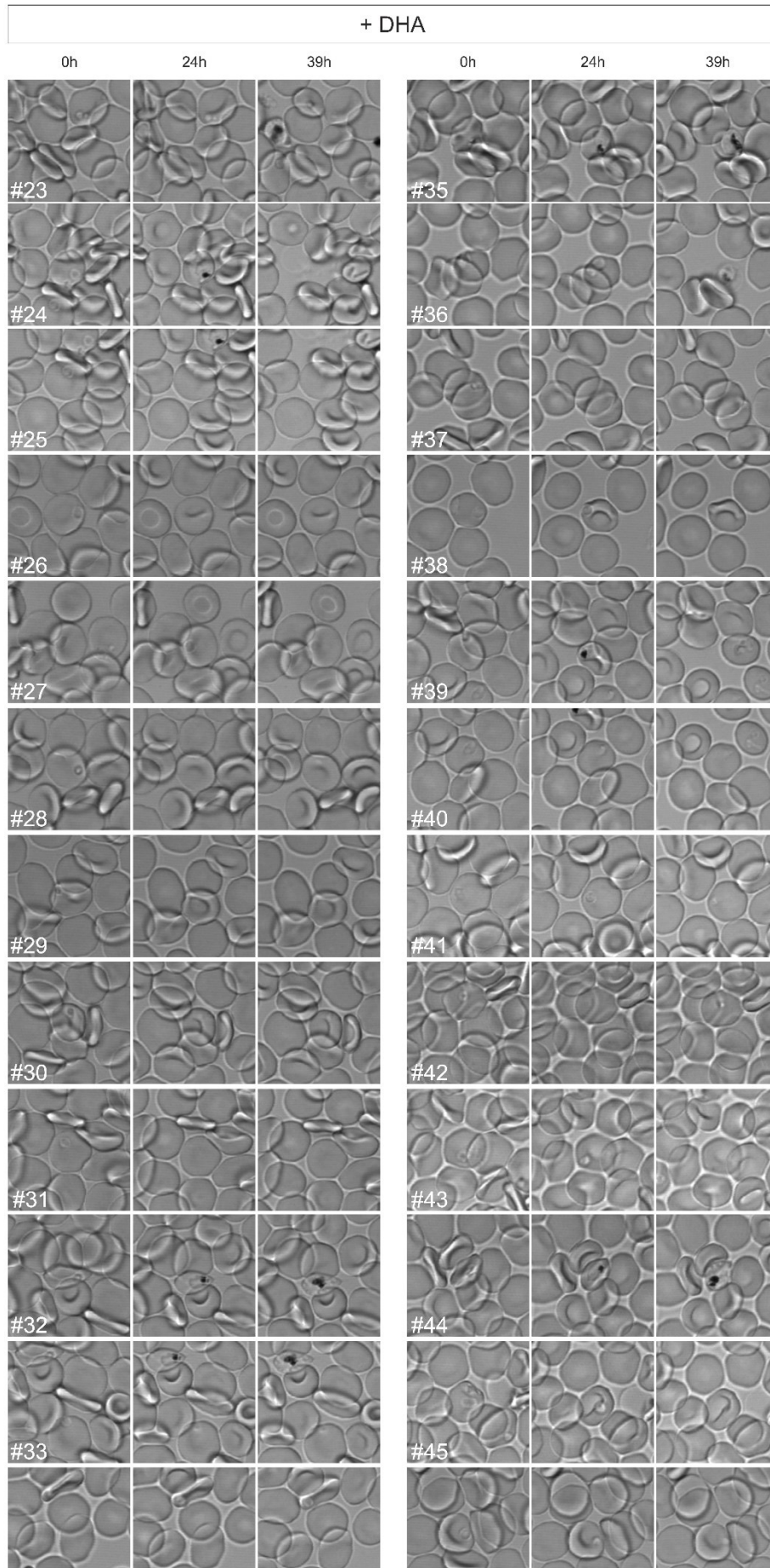
## Appendix F.2 Western blot analysis of different mutants obtained via SLI.

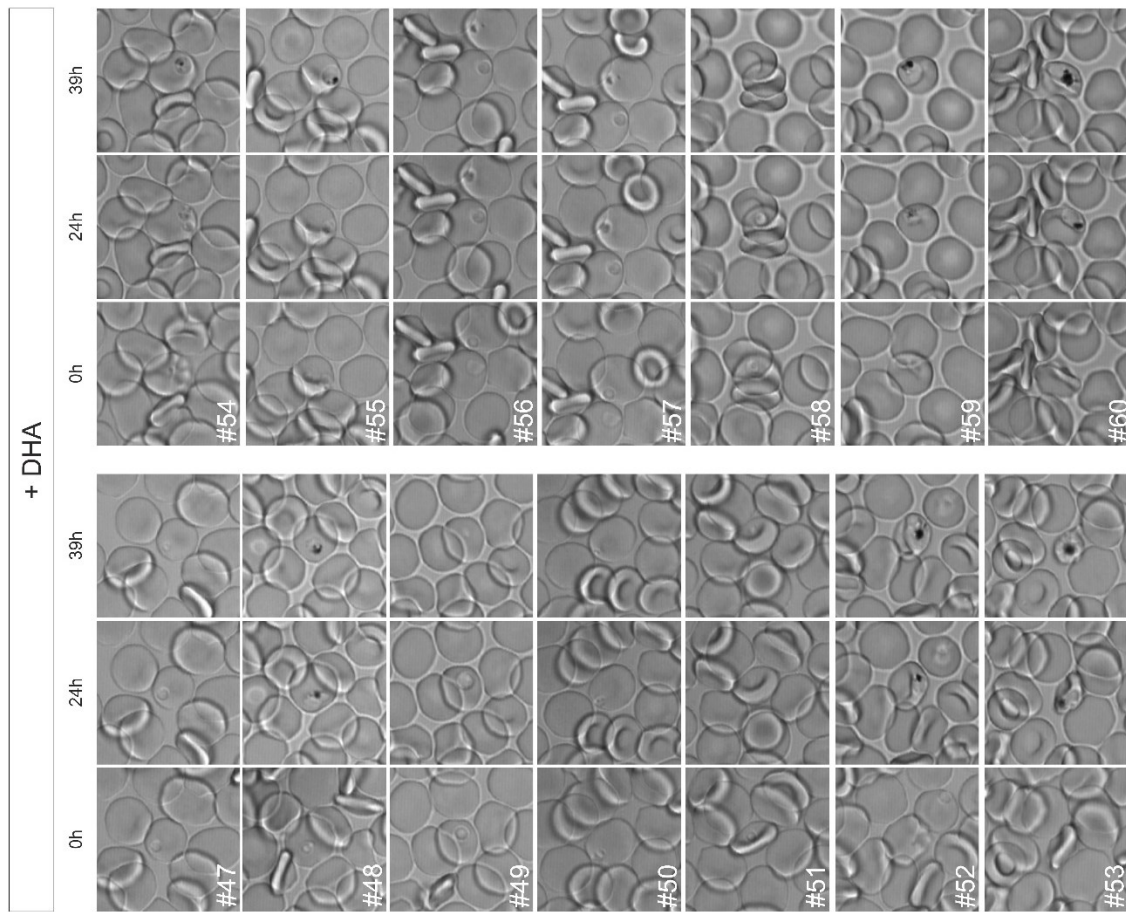


## Appendix G

**Appendix G.1** Confocal microscopy images of K13C580Y parasites after DHA removal in RSA. Three different time points were imaged, and development of cells was followed-up. Corresponding calculations are listed in Appendix G.2.







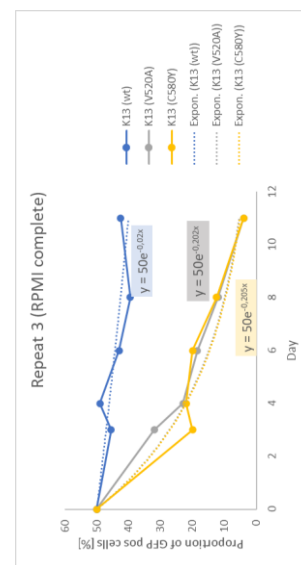
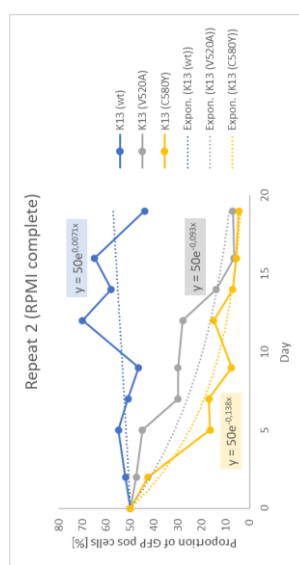
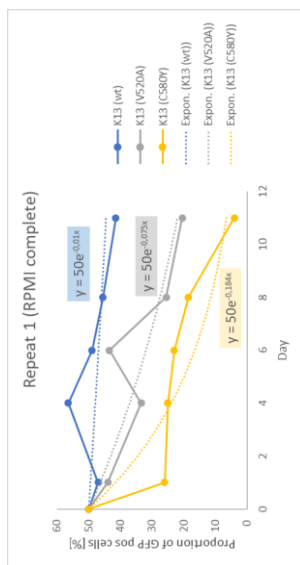
**Appendix G.2** Assessment of development of K13<sup>C580Y</sup> parasites after DHA removal. Three different timepoints were imaged by confocal microscopy (see Appendix G.1).

	Treatment	Parasite (K13 <sup>C580Y</sup> )	39 h after DHA removal			24 h after DHA removal			follow-up of parasites (measured area at 24h)	remarks
			reinvasion	delayed growth	dead	area [ $\mu\text{m}^2$ ]	Min	Max		
	control	#1	1	0	0	23,875	25	164	reinvasion	
		#2	1	0	0	25,203	29	191	reinvasion	
		#3	1	0	0	17,25	27	183	reinvasion	
		#4	1	0	0	1,078	92	111	reinvasion	cell destroyed by method after 39h
		#5	1	0	0	17,594	41	155	reinvasion	
		#6	1	0	0	17,094	31	149	reinvasion	cell destroyed by method after 39h
		#7	1	0	0	22,078	25	182	reinvasion	
		#8	1	0	0	26,031	32	200	reinvasion	
		#9	1	0	0	25,25	30	150	reinvasion	cell destroyed by method after 39h
		#10	0	1	0	10,172	53	145	late schizont	
		#11	0	0	1	8,125	75	133	reinvasion	cell destroyed by method after 39h
		#12	1	0	0	20,516	31	130	reinvasion	
		#13	1	0	0	14,531	57	172	reinvasion	
		#14	1	0	0	11,375	44	144	reinvasion	
		#15	1	0	0	14,5	34	216	reinvasion	
		#16	1	0	0	3,219	76	136	reinvasion	parasite dead after 24h
		#17	1	0	0	17,453	27	169	reinvasion	
		#18	1	0	0	28,703	37	193	reinvasion	
		#19	1	0	0	19,141	32	166	reinvasion	
		#20	1	0	0	15,719	62	220	reinvasion	
		#21	0	1	0	13,641	77	159	late schizont	
		#22	1	0	0	11,828	36	225	reinvasion	
	<b>Summe (39h)</b>	<b>17</b>	<b>15</b>	<b>2</b>	<b>0</b>	<b>Summe (24h)</b>	<b>17</b>	<b>18</b>		
	Reinvasion [%]		88							
	Troph/schizont [%]			12						
	Dead [%]				0					

Treatment	Parasite (K13 <sup>CS80Y</sup> )	39 h after ART removal			24 h after DHA removal			follow-up of parasites (measured area at 24h)	remarks
		reinvasion	delayed growth	dead	area [ $\mu\text{m}^2$ ]	Min	Max		
DHA	#23	0		1	0	11,016	74	157	late schizont
	#24					12,438	26	153	cell destroyed by method after 39h
	#25	0	0	1		0,312	139	154	parasite dead after 24h
	#26	0	0	1		0,953	89	116	parasite dead after 24h
	#27	0	0	1		4,391	75	132	dying ring
	#28	0	0	1		0,156	100	106	parasite dead after 24h
	#29	0	0	1		0,266	116	144	parasite dead after 24h
	#30	0	0	1		0,203	104	110	parasite dead after 24h
	#31	0	0	1		0,188	96	100	parasite dead after 24h
	#32	0	1	0		9,688	28	127	late schizont
	#33	0	0	1		0,75	93	123	parasite dead after 24h
	#34	0	1	0		3,859	83	192	arrest in ring
	#35	0	1	0		12,688	38	142	late schizont
	#36					4,281	78	140	cell destroyed by method after 39h
	#37	0	0	1		0,219	99	107	parasite dead after 24h
	#38	0	0	1		3,531	79	128	dying ring
	#39	1	0	0		15,5	27	212	reinvasion
	#40	0	0	1		1,688	104	135	parasite dead after 24h
	#41	0	0	1		4,781	101	136	dying ring
	#42	0	0	1		0,328	112	122	parasite dead after 24h
	#43	0	0	1		4,719	95	172	dying ring
	#44	0	1	0		12,328	41	174	late schizont
	#45	0	0	1		5,859	80	183	dying ring
	#46	0	0	1		1,156	102	131	parasite dead after 24h
	#47	0	0	1		3,828	109	147	dying ring
	#48	0	0	1		14,141	46	143	dying trophozoite
	#49	0	0	1		9,562	93	158	dying ring
	#50	0	0	1		2,312	76	118	dying ring
	#51	0	0	1		0,719	94	107	parasite dead after 24h
	#52	0	1	0		8,422	28	144	late schizont
	#53	0	1	0		11,734	39	147	late schizont
	#54	0	1	0		5,219	73	115	young trophozoite
	#55	0	1	0		7,828	66	155	young trophozoite
	#56	0	1	0		4,484	95	135	arrest in ring
	#57	0	0	1		0,391	80	133	parasite dead after 24h
	#58	0	0	1		4,953	73	152	dying ring
	#59	0	1	0		8,125	52	130	young trophozoite
	#60	0	0	1		13,109	34	142	late schizont
Summe (39h)	36	1	12	23	Summe (24h)	36	8		
Reinvasion [%]		3							
Troph/schizont [%]			33						
Dead [%]				64					
					Late schizont	7	19		
					Dying ring	9	25		
					arrest in ring	2	6		
					reinvasion	1	3		
					dying troph	1	3		
					young troph	3	8		
					dead	13	36		
					Summe	36	[%]		

## Appendix H

**Appendix H.1** Raw curves of three independent fitness assays performed in RPMI complete medium. Corresponding calculations are listed in Appendix H.2.



## Appendix H.2 Calculation of fitness costs per generation of different mutations grown in RPMI complete medium. Corresponding raw curves are listed in Appendix H.1

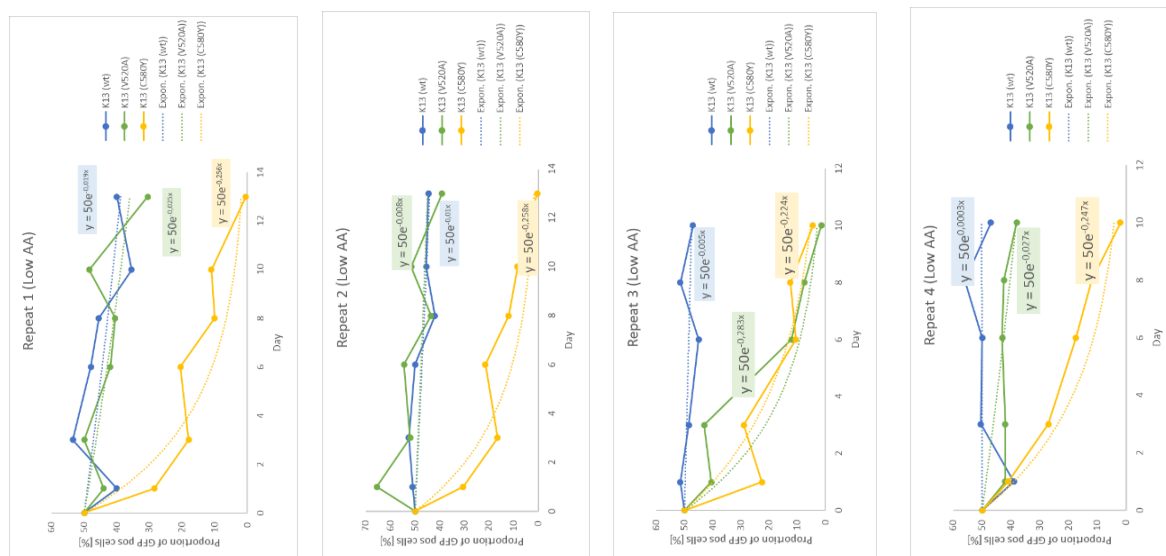
Repeat 1	Factor from trend line	retained growth per day	% loss per day	factor per generation	retained growth /generation
WT	-0,010	0,990	0,995	-0,02	0,980198673
520	-0,075	0,928	7,226	-0,15	0,860707976
580	-0,184	0,832	16,806	-0,368	0,692117182

Repeat 2	Factor from trend line	retained growth per day	% loss per day	factor per generation	retained growth /generation
WT	0,0071	1,007	-0,713	0,0142	1,014301299
520	-0,093	0,911	8,881	-0,186	0,830273595
580	-0,138	0,871	12,890	-0,276	0,758812931

Repeat 3	Factor from trend line	retained growth per day	% loss per day	factor per generation	retained growth /generation
WT	-0,02	0,980	1,980	-0,04	0,960789439
520	-0,202	0,817	18,291	-0,404	0,667644121
580	-0,205	0,815	18,535	-0,41	0,66365025

Repeat	growth factor /day			Repeat	growth factor/generation*		
	WT	V520A	C580Y		WT	V520A	C580Y
1	0,990	0,928	0,832	1	0,980	0,861	0,692
2	1,007	0,911	0,871	2	1,014	0,830	0,759
3	0,980	0,817	0,815	3	0,961	0,668	0,664
mean	<b>0,992</b>	<b>0,885</b>	<b>0,839</b>	mean	<b>0,985</b>	<b>0,786</b>	<b>0,705</b>
sd	0,011	0,049	0,024	sd	0,022	0,085	0,040
*assumption: 1 generation=2 days							
Repeat	fitness cost per generation						
	WT	V520A	C580Y				
1	0,020	0,139	0,308				
2	-0,014	0,170	0,241				
3	0,039	0,332	0,336				
mean	<b>0,015</b>	<b>0,214</b>	<b>0,295</b>				
sd	0,022	0,085	0,040				

## Appendix H.3 Raw curves of three independent fitness assays performed in low AA medium. Corresponding calculations are listed in Appendix H.4.



**Appendix H.4** Calculation of fitness costs per generation of different mutations grown in low AA medium. Corresponding raw curves are listed in Appendix H.3

Repeat 1	Factor from trend line	retained growth per day	% loss per day	factor per generation	retained growth /generation
WT	-0,019	0,981	1,9	-0,04	0,96
520	-0,025	0,975	2,5	-0,05	0,95
580	-0,256	0,774	22,6	-0,51	0,60

Repeat 2	Factor from trend line	growth factor /day	% loss per day	factor per generation	retained growth /generation
WT	-0,01	0,990	1,0	-0,02	0,98
520	-0,008	0,992	0,8	-0,02	0,98
580	-0,258	0,773	22,7	-0,52	0,60

Repeat 3	Factor from trend line	growth factor /day	% loss per day	factor per generation	retained growth /generation
WT	-0,005	0,995	0,5	0,0	0,99
520	-0,283	0,754	24,6	-0,6	0,57
580	-0,224	0,799	20,1	-0,4	0,64

Repeat 4	Factor from trend line	growth factor /day	% loss per day	factor per generation	retained growth /generation
WT	0,0003	1,000	0,0	0,00	1,00
520	-0,027	0,973	2,7	-0,05	0,95
580	-0,247	0,781	21,9	-0,49	0,61

Repeat	growth factor /day			Repeat	growth factor/generation*		
	WT	V520A	C580Y		WT	V520A	C580Y
1	0,981	0,975	0,774	1	0,96	0,95	0,60
2	0,990	0,992	0,773	2	0,98	0,98	0,60
3	0,995	0,754	0,799	3	0,99	0,57	0,64
4	1,000	0,973	0,781	4	1,00	0,95	0,61
average	<b>0,992</b>	<b>0,924</b>	<b>0,782</b>	average	<b>0,983</b>	<b>0,863</b>	<b>0,611</b>
sd	0,007	0,098	0,011	sd	0,014	0,171	0,017
fitness cost/day	0,008	0,076	0,218	*assumption: 1 generation=2 days			
					fitness cost per generation		
				Repeat	WT	V520A	C580Y
				1	0,037	0,049	0,401
				2	0,020	0,016	0,403
				3	0,010	0,432	0,361
				4	-0,001	0,053	0,390
				average	<b>0,017</b>	<b>0,137</b>	<b>0,389</b>
				sd	0,014	0,171	0,017